Analysis and Control of Degradation in Covalent Adaptable Networks

by

JUAN J. HERNANDEZ

B.S., Massachusetts Institute of Technology, 2015

M.S., University of Colorado Boulder, 2020

A thesis submitted to the

Faculty of the Graduate School of the

University of Colorado in partial fulfillment

of the requirement for the degree of

Doctor of Philosophy

Department of Chemical and Biological Engineering

2022

Committee Members:

Christopher N. Bowman

Timothy J. White

Jeffrey W. Stansbury

Andrew P. Goodwin

Yifu Ding

ABSTRACT

Hernandez, Juan Jose (Ph.D., Chemical and Biological Engineering)

Analysis and Control of Covalent Adaptable Network Degradation

Thesis directed by Professor Christopher N. Bowman

This thesis explores polymer degradation within covalent adaptable networks (CANs), focusing on degradation and properties controlled by the thiol-thioester exchange, the thiol-thioaminal exchange, and the thioaminal scission reactions. By comparing mass loss profiles and mechanical property changes to theoretical models developed herein, this work explores the degree to which polymer network structure and reaction kinetics tune the degradation process.

The first part of this thesis focuses on the base-catalyzed thiol-thioester exchange reaction and how this reaction was used to degrade thioester-containing CANs. Statistical models quantitatively depicted the degradation process where these models incorporated the thiol-thioester exchange reaction kinetics, polymer structure, and mass gained from the exchanging thiol. A single reaction rate constant (*k)* fit experimental mass loss profiles to model predictions, and only varied from 0.0024 – 0.0051 $M^{-1}min^{-1}$ throughout all degradation conditions studied including changing crosslinking density, reactant concentration, oligomer lengths, and oligomer distributions. Using these parameters, degradation within thioesters networks could be tuned to occur on timescales from 2.5 h to near infinity, shift the degradation mechanism from surface to bulk, enable > 90 % selective recovery of fillers, and mediate controlled mass release.

The second part of this thesis focuses on how thioaminal groups enable degradation within CANs. First, the thiol-thioaminal exchange reaction was explored as a new, reversible-exchange CAN chemistry. The exchange reaction was monitored by a small molecule system, showing the

choice of thiol impacted four kinetic parameters (k_f, k_r, K_{eq}, $t_{1/2,eq}$). Meanwhile, thioaminal-containing networks were found to stress relax (10 s at 95 °C), degrade rapidly when exposed to neat excess thiol (from 4 – 380 min), and exhibit temperature-independent crosslink density. Second, the thioaminal scission reaction was used as a means to create constructing-then-destructing CANs. Exposing thioaminal small molecules to photoradicals probed polymerization and scission reactions and found the exposure resulted in thioamide formation. Increasing thiol substitution (1^o – 3^o) resulted in greater extent of scission (5 – 39 %), with scission occurring semi-orthogonally to the thiol-ene polymerization reaction. Constructing-then-destructing CANs that depended on total light dose exposure were created, switching between construction and destruction at a light dose of 2 J/cm^2 under the selected conditions.

DEDICATION

To everyone who started their Ph.D.…

and realized that everything they thought they knew was wrong.

ACKNOWLEDGEMENTS

This journey would have been impossible without the support and mentorship of so many people in my life. First, I thank my advisor Dr. Christopher Bowman for his guidance throughout these years. From the jubilation to depression you have helped me live the phrase "you do not *get* a Ph.D., you *become* a Ph.D." Additionally, I thank the rest of my committee members, Dr. Jeffrey Stansbury, Dr. Andrew Goodwin, Dr. Yifu Ding, and particularly Dr. Timothy White who co-advised me in the early part of my Ph.D. program.

I am indebted to all the members of the Bowman Lab and the RPM lab for showing how to conduct research day after day. From my direct mentors (Chen, Kim, Katie, Parag) to my mentees (Sean, Claire, Cassie) I could not have achieved this without all of you. I also thank all my collaborators, because without your time and effort I could not be here today.

Outside of academic guidance, I am indebted to Dr. Leslie Blood and Dr. Elizabeth Parsons. Despite my best efforts, Leslie taught me that having consistent routines does not mean less freedom but instead frees up more energy. Meanwhile, Beth taught me that anxiety can in fact be helpful, and I will continue to refine and pass on those therapy skills for the rest of my life.

Lastly, I want to express my gratitude towards all the friendships that sustained me and family members who supported me day after day. I am humbled by everyone who bought me groceries, gave me pep-talks, and even put their lives on hold while I recovered from a broken hip. I am happy to say that my family's sacrifice in emigrating to the United States, along with dad's patient wisdom and mom's stress-induced pacing, have more than paid off.

Thank you all so much. With much love,

Dr. Juan Jose Hernandez

Table of Contents

LIST OF TABLES

LIST OF SCHEMES

LIST OF FIGURES

Chapter 1: Introduction

1.1 Research Motivation

Crosslinked polymers, also referred to as thermosets, contain irreversible crosslinks that connect polymer chains, and this grants these materials the benefits of increased dimensional stability, temperature resistance, and chemical resistance.[1,2] These combined benefits make thermosets highly valuable in the creation of engineering-grade plastics,[3] shape-memory materials,[4,5] robotic actuators,[6–8] and medical gels.[9,10] However, these irreversible links also make thermosets difficult to reprocess or degrade by conventional thermally-triggered means.[11–13] Reprocessing and degradation of thermosets is crucial for the continued development of smart materials as this enables material recycling / upcycling,[14,15] post-manufacturing modification,[16–18] on-demand drug release,[19,20] and controlled breakdown into environmentally-friendly components.[21,22]

Of the current methods to reprocess thermosets, including pyrolysis[23,24] and mechanical forces,[25,26] dynamic rearrangement of the covalent bonds within thermosets shows particular promise, creating a new subset of polymers termed covalent adaptable networks (CANs). When triggered, the dynamic bonds within the CANs rearrange via typically mild chemical reactions, allowing these materials to access the benefits of polymer crosslinking while still allowing the material reprocessing nascent to thermoplastics.[27–29] A number of stimuli have been developed to trigger dynamic rearrangement within CANs, including temperature,[12,30,31] pH,[32,33] light,[34,35] and mechanical forces,[36,37] leading to rapid growth in the development of reprocessable and degradable thermosets. As the field continues to expand, several quantitative models have been developed to characterize CAN-specific degradation processes,[38–40] but nevertheless there is still a need to

continue improving these models along with a need to broaden the library of chemical groups available to create CANs.

This thesis investigates polymer degradation within CANs, developing models to quantitively describe an already established CAN chemistry while also exploring new uses of chemical reactions to create novel CANs. These studies specifically focus on the thiol-thioester exchange, the thiol-thioaminal exchange, and the thioaminal scission reactions and how each of these reactions may lead to CAN degradation. Studying these reactions not only directly contributed to the knowledge of thioester and thioaminal based CANs, but also created chemistry agnostic models that apply to numerous degrading systems.

1.2 Polymer Degradation

1.2.1 Thermosets

Polymer degradation refers to the irreversible process through which functionality or material mass is lost.[41,42] Degradation results from chemical changes and may be triggered by a number of different stimuli including light,[43,44] temperature,[23,24] chemical scission,[45,46] electricity,[47,48] and mechanical agitation.[49,50] While loss of functionality via degradation, such as discoloration in paints[42] or conductivity losses in organic solar cells,[51] impacts the functional purpose of a material, it does not necessarily lead to mass loss. Degradation mediated by mass lass, however, results in fragments of a material leaving the structure, and eventually leads to mechanical failures including crazing, cracking, or erosion,[52] **Figure 1.1a**. With the increasing demand to design dynamic materials with multi-stage control[6,8,53] and to reduce plastic pollution,[54,55] mass loss degradation remains an important field of study and as such is the focus of this thesis.

A number of quantitative methods have been developed to describe polymeric mass loss degradation including mathematical models,[56,57] experimental procedures,[10,58,59] and computer simulations.[60] Within the mathematical models, mass loss may generally be considered to occur through two different extremes: surface degradation or bulk degradation[61] as seen in **Figure 1.1b**. Surface degradation is a diffusion or a solubility-limited process, in which mass is lost from the surface of a polymeric object and the structure shrinks until all mass is consumed.[61–63] Bulk degradation is a reaction-limited process, in which the bonds connecting the polymer are progressively cleaved throughout the entire polymer, until reverse gelation is reached and any remaining material dissolves. These two mechanisms result in different mass loss profiles, with surface degradation resulting in linear mass loss versus time[53,64] while bulk degradation results in an initially slow mass loss followed by a sudden burst.[65] Often times, mass loss from degradation occurs as a mix of these two extremes with components such as sample geometry, diffusion time, reaction time, and polymer structure all impacting the specific degradation process.[42,52]

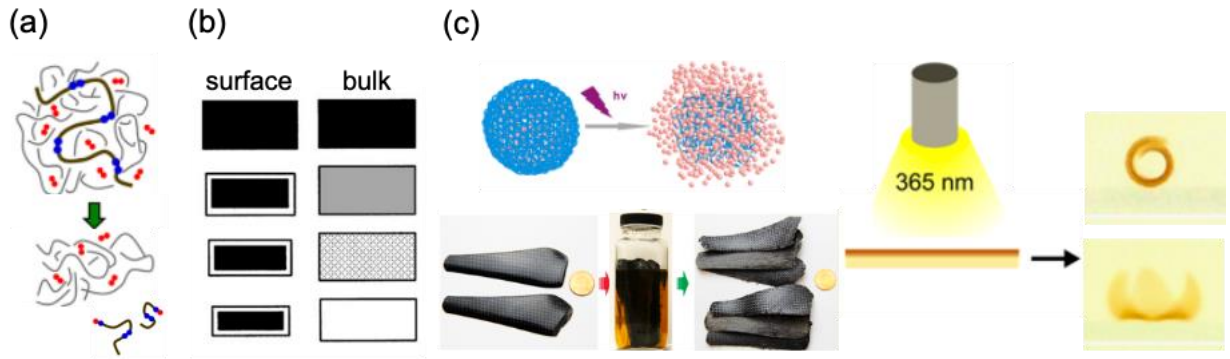

Figure 1.1. (a) Mass loss resulting from polymer degradation.[40] (b) Surface (*left*) versus bulk (*right*) degradation mechanisms, where lighter color represents a lower crosslinking density.[61] (c) Thermoset degradation used for drug release (*top left*),[64] part recycling (*bottom left*),[65] and shape-changing actuators (*right*).[66]

Within thermosets, degradation cleaves polymer crosslinks and creates detached segments that diffuse out of the network.[42] Degradation proceeds by reactions that either directly cleave polymer

bonds, *e.g.* hydrolysis cleavage of esters in poly-lactic acid chains,[45,69] or initiate a secondary reaction that cleaves these bonds, *e.g.* photodeprotection of acids and bases via NPPOC or o-NBE.[70,71] By controlling these triggers and the structure of the thermoset, degradation may be tuned from surface to bulk processes,[60,61] and this wide range has shown promise in the fields of material recycling,[32,72] actuation,[73] 4-D printing,[17,18] and drug release.[19,20] Nevertheless, even with this tunability, thermoset degradation has proven difficult due to the typically irreversible crosslinks that comprise these materials, which is why current research has focused on the development of degradable CANs.

1.2.2 Covalent Adaptable Networks

CANs are thermosets with dynamic bonds that allow topological rearrangements, combining the mechanical property benefits of thermosets with the reprocessability of thermoplastics.[27] Unlike degradation of traditional thermosets, CANs degrade via reversible reactions that occur through either a reversible addition or reversible exchange process,[28,74] **Figure 1.2** . Reversible addition CANs rearrange chemical groups by disconnecting covalent bonds through a dissociated transition state, leading to a reverse gelation temperature at which the retro reaction dominates, the CAN hits reverse gelation, and the polymer degrades.[75,76] Diels-Alder,[77,78] urea,[79] and imine reactions[80] have all been used to create reversible addition CANs that readily degrade at temperatures even below 150 °C. Conversely, reversible exchange CANs rearrange chemical groups by connecting covalent bonds through an associated transition state, leading to no reverse gelation temperature as crosslink density never decreases.[29] Instead, degradation in reversible exchange CANs proceeds by reacting the network with an excess of terminal monomers,[67,81] and

the transesterification[74] and thioester[82] chemistries have shown these networks may even be repolymerized upon addition of more crosslinking units.

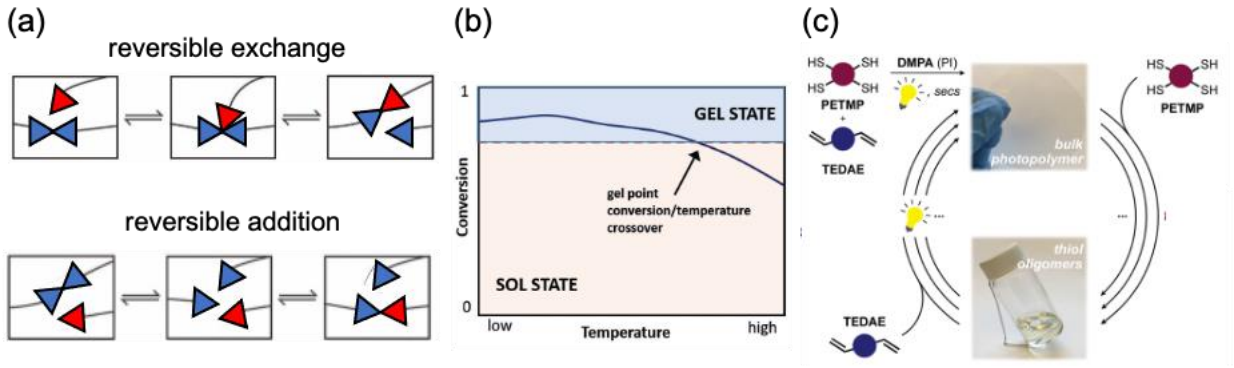

Figure 1.2. (a) Reversible addition versus reversible exchange mechanisms for CANs.[27] (b) Reversible addition CANs exhibit a reverse-gelation temperature.[28] (c) Reversible exchange CANs degrade by addition of excess monomer.[80]

Of the two types of CANs, reversible exchange CANs grants increased dimensional stability and solvent resistance because the crosslink density of these materials does not change with temperature.[83,84] Due to these benefits, quantitative models that consider diffusion, chemical reactions, and mass transfer have been developed to specifically characterize degradation of reversible exchange CANs, with a recent focus on the transesterification,[40,85] boronic-ester exchange,[39] and thiol-thioester exchange[86,87] reactions. While these models establish a solid foundation for this field, fundamental questions still remain as to how reversible exchange reactions lead to degradation different from traditional thermoset and there is much left to explore.

1.3 Exchange Reactions

Exchange reactions replace the functional groups between two chemical moieties via a linked transition state, resulting in a 2nd order process similar to S_N2 reactions.[27,88] Transesterification,[89]

transimination,[90,91] and transiloxanification[92] are all viable exchange reactions which have shown promise in the fields of organic synthesis,[89] enzyme alteration,[93] tissue engineering,[94] and covalent organic frameworks.[90] Within polymers, chemical moieties that are introduced into thermosets and may undergo exchange reactions form reversible exchange covalent adaptable networks (CANs), also known as vitrimers,[29] which allow rearrangement of network topology via these reactions,[28,88] **Figure 1.3**. When triggered within polymers, these exchange reactions have been shown to reduce stress,[34] degrade networks,[95] and enable material reprocessing.[13,96]

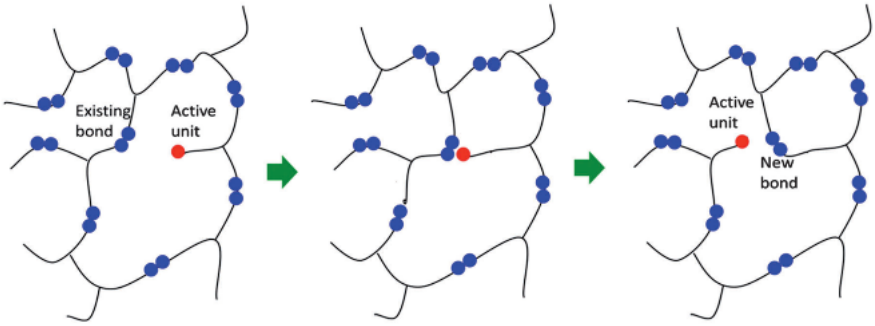

Figure 1.3. Reversible exchange in CANs leads to topology rearrangement via a connected transition state.[86]

Thiol-X exchange reactions are a versatile subset of exchange reactions where one of the components is a thiol. Thiol-thioester,[97] thiol-thioaminal,[98] and thiol-disulfide[99,100] exchange have all shown the versatility of this reaction class, which arises from the increased nucleophilicity of the thiolate group.[100] With applications in aqueous media synthesis,[97] oligomer post-functionalization,[99] and forming chemical libraries[101] thiol-X exchange continues to broaden the impact of exchange reactions. Within the subset of polymers, the thiol-thioester and thiol-thioaminal exchange reactions show particular promise.

1.3.1 Thiol-Thioester Exchange

The thiol-thioester exchange reaction replaces the functional groups attached to a thiol and a thioester, as seen in **Figure 1.4**. Thiol-thioester exchange has been studied due to its rapid kinetics,[35] selective reaction,[97] and ability to be triggered under mild conditions.[102] It may proceed through uncatalyzed[97] or catalyzed[103,104] pathways. A number of methods have been explored to tune the thiol-thioester exchange reaction including the impact of solvent,[102] pKa,[87] substitution,[103] steric hindrance,[105] and temperature.[106] This wide range of research has enabled thiol-thioester exchange to contribute to numerous fields including cyclic peptide formation[107] and dynamic lipid bilayers.[106]

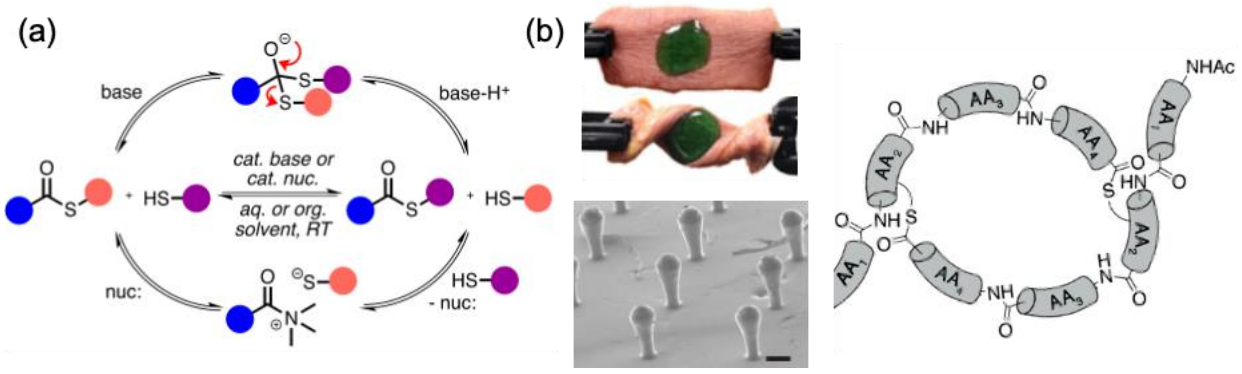

Figure 1.4. (a) Mechanism for the thiol-thioester exchange reaction as catalyzed by a base (*top*) or nucleophile (*bottom*).[35] (b) Thiol-thioester exchange in CANs used for washable gels (*top left*),[106] sacrificial 3-D printed organoids (*bottom left*),[33] and cyclic peptides (*right*).[105]

Within the context of polymer networks, adding the thiol-thioester exchange reaction into the network forms thioester reversible exchange CANs. In the presence of excess thiol and an appropriate trigger, these CANs rearrange topology through the thiol-thioester exchange reaction and have found applications in washable wound sealants,[108] side-chain modification,[109] tunable microparticles,[110] bistable phase materials,[35] repolymerizable networks,[82] and self-immolating

oligonucleotides.[111] Recent work in quantitatively degrading these CANs[33,82,87] has shown degradation in these networks may be tuned, offering an effective probe into the degradation processes of reversible exchange CANs.

1.3.2 Thiol-Thioaminal Exchange

The thiol-thioaminal exchange reaction replaces the functional groups attached to a thiol and a thioaminal moiety, as seen in **Figure 1.5**. Thiol-thioaminal exchange has been studied due to its selective exchange,[112] biocompatibility,[113] and self-catalysis[16] which arises from interactions between the thioaminal and thiol groups. Thioaminals, also referred to as *N,S*-acetals[114] or thiomethylamine[115,116] groups, are the *N,S* analogue of acetals and catalyze thiol-thioaminal exchange by using its nucleophilic nitrogen to deprotonate thiols, forming the thiolates needed to mediate the reaction.[16] The thiol-thioaminal exchange reaction has been used for biological chemistry including altering cell expression[98] and pharmaceutical synthesis[117] but is still relatively understudied compared to other exchange reactions. In the context of polymers, Wojtecki and co-workers have shown thiol-thioaminal exchange may be used to create dynamic linear polymers, post-functionalizable oligomers at temperatures below 100 °C,[16] and have proposed the formation of thioaminal networks for lithography.[118] However, despite these promising results little work has continued to develop the understanding of thiol-thioaminal exchange, and a need arises to explore this exchange chemistry in CANs.

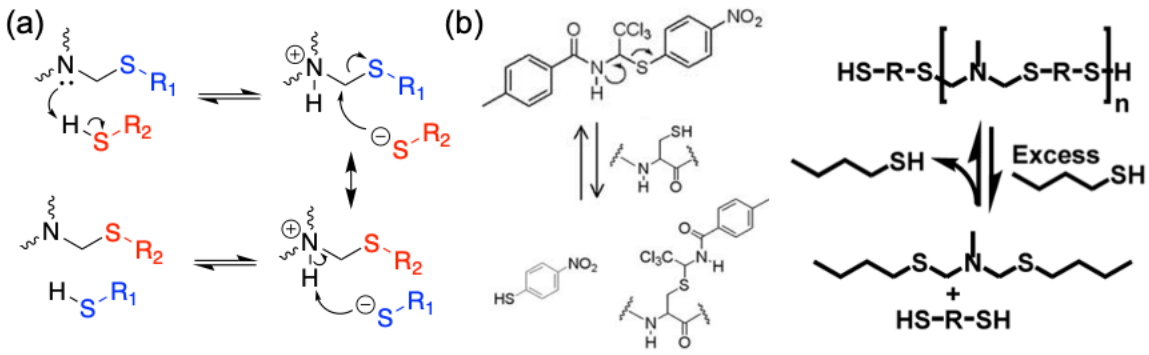

Figure 1.5. (a) Mechanism for the thiol-thioaminal exchange reaction showing self-catalysis.[16] (b) Thiol-thioaminal exchange used for biological switches (*left*)[96] and depolymerization (*right*).[16]

1.4 Photomediated Scission

Photomediated scission reactions cleave covalent bonds, with light showing promise over other triggers due to its spatiotemporal control[119] and ability to tune reaction kinetics and equilibria via irradiation parameters.[20] Within polymers photomediated scission reactions result in disconnected polymer chains[120–122] and scission may occur through either reversible photoreactions; including azobenzenes,[123] coumarins,[124] and other cyclo-additions;[125] or irreversible photoreactions; including ortho-nitrobenzyl esters,[71,126] vinyl ketones,[127] radical formation,[119] and high-power ablation.[120] The polymer chain disconnection itself may occur through two means, either the scission reaction directly disconnects chains or the scission reaction deprotects secondary groups that later disconnect chains.[35,70,119]

The location of the photolabile groups in the polymer structure impacts polymer design. Photolabile groups in pendant side chains alter polymer functionality, such as changing hydrophilicity,[128] while photolabile groups in main chains alter molecular weight.[66] Combining all of these advantages, photomediated scission in polymers has been used for micropatterning,[126]

burst-release capsules,[121,129] selective cell harvesting,[130] shape-changing actuators,[68] and triggered degradation.[131]

Acetals, the -O-C-O- chemical group, offer particularly interesting photomediated scission because these groups readily cleave by a number of means including hydrolysis,[132,133] temperature,[134] mechanical agitation,[49] and light.[130] As such, light may be used to directly cleave acetals[130] or light may be used to trigger one of these secondary reactions that cleaves acetals.[135] Given that a number of acetal adjacent chemistries, including thioacetals (S,O), dithioacetals (S,S), aminals (N,N) and thioaminals (S,N), have shown similar propensities toward scission[114,136–138] exploring scission within the acetal family group offers the chance to expand the library of light induced degradation.

1.5 Research Outline

This thesis focuses on the analysis and control of polymer degradation within covalent adaptable networks (CANs), exploring how dynamic reactions within CANs cleave bonds and induce mass loss. The thiol-thioester exchange, the thiol-thioaminal exchange, and the thioaminal scission reactions were chosen as the chemistries with which to explore degradation and a combination of mass loss, mechanical property changes, and theoretical model predictions were used to study these reactions. The first part of this thesis, Chapters 3 and 4, explore how the thiol-thioester exchange reaction results in network degradation. The effects of network structure and reaction kinetics are explored, showing model predictions matched well with experiments and indicate these two parameters may be used to tune the time scale and mechanism of degradation. The second part of this thesis, Chapters 5 and 6, explores how thioaminal groups may be used to create two new types of CANs. Chapter 5 explores the creation of reversible exchange CANs that

rearrange under near-ambient conditions by means of the thiol-thioaminal exchange reaction, while Chapter 6 explores how to develop constructing-then-destructing CANs via the newly discovered thioaminal scission reaction. Lastly, major findings and suggested future work are summarized in the Conclusions section of this thesis, offering guidance to future researches continuing to explore this field.

Chapter 3 investigates how the thiol-thioester exchange reaction results in the degradation of thioester-containing networks. To study this transition, a statistical kinetic model was created that quantitatively predicted the bulk degradation of thioester networks via base-catalyzed thiol-thioester exchange. Reaction kinetics, polymer structure, and mass gain were all accounted for by the model and theoretical predictions were subsequently compared to experimental degradation of thioester networks via mass loss studies. These studies showed a single reaction rate constant, *k*, could accurately match model predictions to experiments results, with *k* only ranging from 0.0039 to 0.0051 $M^{-1}min^{-1}$ throughout all the parameters studied. Altering the concentration of thiol and base in the degrading solution, or changing the crosslink density of the thioester network, resulted in tunable degradation timescales that varied from 2.5 h to theoretical infinity. Lastly, degradation was explored within 3-D printed thioester composites, with mass loss studies showing that 3-D printed thioester networks completely dissolved within 12 h while 3-D printed thioester composites experienced complete matrix resolution but still enabled 91 % recovery of the inert composite filler.

Chapter 4 investigates how tuning oligomer structure within thioester CANs offers new ways to control network degradation that is mediated by the base-catalyzed thiol-thioester exchange reaction. A second statical kinetic model was developed which considered the impact of two oligomer structure components: the number thioester linkages within oligomers (N) and their

dispersity profiles. Model predictions showed the number of thioester linkages had a greater impact on the degradation process, impacting degradation time by tenfold as N increased from 2 to 50 while narrowing oligomer disperse only resulted in a twofold change. Thioester networks composed of oligomers containing 1 – 4 repeating thioester linkages were synthesized and submerged in a solution of 1 M butyl-3-mercaptopropionate, 0.3 M triethylamine, and acetone to track experimental mass loss. Experimental results matched model predictions, showing increasing thioester links in oligomers from 1 – 4 repeat units decreased mass loss time from 25 – 4 h and allowed proper data fitting when using only one fitting parameter, k, which ranged from 0.0024 to 0.0040 $M^{-1}min^{-1}$. Blended CANs, which were created by mixing N = 1 and N = 4 oligomers in various molar ratios, showed these mixed networks granted easy degradation control by simply tuning the mixing ratio. Lastly, mass release studies using the model dye, Nile Red, confirmed that thioester oligomers in CANs enable mass release that is quantifiable via the Beer-Lambert law.

Chapter 5 moves on to investigate the thiol-thioaminal exchange reaction and its ability to create CANs that not only rearrange rapidly at near-ambient conditions but do so without exogenous catalyst. First, a small molecule system studied the thiol-thioaminal exchange reaction between a thioaminal (DMTA) and one of three thiols (BMP, BTG, TP). Combining experimental results with an established literature model extracted kinetic parameters for the exchange reaction (k_f, k_r, K_{eq}, $t_{1/2,eq}$) and showed the choice of thiol most impacted the reverse reaction rate constant, with k_r ranging from 0.2 to 110 $mM^{-1}min^{-1}$. Thioaminal containing networks were then photocured via the thiol-ene photopolymerization reaction and stress relaxed, showing an activation energy ($E_{a,SR}$) of 87 $\pm$ 8 kJ/mol. Increasing the % excess thiol and the temperature resulted in networks that stress relaxed as quickly as 5 s at 95 °C. Frequency sweep experiments resulted in similar activation energies, $E_{a,FS}$, was 107 $\pm$ 8 kJ/mol, and confirmed that thiol-thioaminal exchange

produced reversible exchange type CANs. Submerging thioaminal films in one of four thiols (BMP, BTG, TP, HT) showed thiol-thioaminal exchange led to network degradation and the choice of thiol greatly impacted degradation speed (380 versus 4 min).

Chapter 6 finally investigates the radical-mediated thioaminal scission reaction as a new photodegradation process, and how this reaction may be used to achieve polymerizing-then-degrading networks under a single near-UV light source. Thioaminal small molecules with varying degrees of thiol-substitution ($1^o - 3^o$) were exposed to photoradicals and confirmed photo-activated thioaminals undergo scission to produce thioamide groups, identifiable by distinct NMR singles at 3.26 and 3.29 ppm and an FTIR peak around 1530 cm^{-1}. Increased thiol substitution on the thioaminal resulted in greater extent of scission, increasing from 5 ± 1 % to 39 ± 3 %. This thioaminal scission was found to occur semi-orthogonally to the radical-mediated thiol-ene reaction, with thiol-ene achieving near quantitative yield within 0.5 min while thioaminal scission required up to 15 min of exposure. Thioaminal networks were then synthesized and thioaminal scission triggered within to create two-stage polymerizing-then-degrading networks that transitioned depending on the total light dose. The polymerization and degradation regimes switched at 2 J/cm^2, plateaued at 13 J/cm^2 and could be exploited to create single materials that served as both positive and negative photoresists.

1.6 References

(1) Hiemenz, P. C.; Lodge, T. P. *Polymer Chemistry Second Edition*; CRC Press Taylor & Francis Group, 2007. https://doi.org/10.1201/9781420018271-4.

(2) Jin, Y.; Lei, Z.; Taynton, P.; Huang, S.; Zhang, W. Malleable and Recyclable Thermosets: The Next Generation of Plastics. *Matter* **2019**, *1* (6), 1456–1493. https://doi.org/10.1016/j.matt.2019.09.004.

(3) Ramon, E.; Sguazzo, C.; Moreira, P. M. G. P. A Review of Recent Research on Bio-Based Epoxy Systems for Engineering Applications and Potentialities in the Aviation Sector. *Aerospace* **2018**, *5* (4). https://doi.org/10.3390/aerospace5040110.

(4) Liu, C.; Qin, H.; Mather, P. T. Review of Progress in Shape-Memory Polymers. *J. Mater. Chem.* **2007**, *17* (16), 1543–1558. https://doi.org/10.1039/b615954k.

(5) Mao, Y.; Ding, Z.; Yuan, C.; Ai, S.; Isakov, M.; Wu, J.; Wang, T.; Dunn, M. L.; Qi, H. J. 3D Printed Reversible Shape Changing Components with Stimuli Responsive Materials. *Sci. Rep.* **2016**, *6* (January), 1–13. https://doi.org/10.1038/srep24761.

(6) Peng, X.; Wang, H. Shape Changing Hydrogels and Their Applications as Soft Actuators. *J. Polym. Sci. Part B Polym. Phys.* **2018**, *56* (19), 1314–1324. https://doi.org/10.1002/polb.24724.

(7) Hu, L.; Zhang, Q.; Li, X.; Serpe, M. J. Stimuli-Responsive Polymers for Sensing and Actuation. *Mater. Horizons* **2019**, *6* (9), 1774–1793. https://doi.org/10.1039/c9mh00490d.

(8) Whitesides, G. M. Soft Robotics. *Angewandte Chemie - International Edition*. April 9, 2018, pp 4258–4273. https://doi.org/10.1002/anie.201800907.

(9) Rosales, A. M.; Anseth, K. S. The Design of Reversible Hydrogels to Capture Extracellular Matrix Dynamics. *Nat. Rev. Mater.* **2016**, *1* (2), 1–15. https://doi.org/10.1038/natrevmats.2015.12.

(10) Holloway, J. L.; Ma, H.; Rai, R.; Burdick, J. A. Modulating Hydrogel Crosslink Density and Degradation to Control Bone Morphogenetic Protein Delivery and in Vivo Bone Formation. *J. Control. Release* **2014**, *191*, 63–70. https://doi.org/10.1016/j.jconrel.2014.05.053.

(11) Wölfel, B.; Seefried, A.; Allen, V.; Kaschta, J.; Holmes, C.; Schubert, D. W. Recycling and Reprocessing of Thermoplastic Polyurethane Materials towards Nonwoven Processing. *Polymers (Basel).* **2020**, *12* (9), 1–13. https://doi.org/10.3390/POLYM12091917.

(12) Röttger, M.; Domenech, T.; Van Der Weegen, R.; Breuillac, A.; Nicolaÿ, R.; Leibler, L. High-Performance Vitrimers from Commodity Thermoplastics through Dioxaborolane Metathesis. *Science (80-.).* **2017**, *356* (6333), 62–65. https://doi.org/10.1126/science.aah5281.

(13) Taplan, C.; Guerre, M.; Winne, J. M.; Du Prez, F. E. Fast Processing of Highly Crosslinked, Low-Viscosity Vitrimers. *Mater. Horizons* **2020**, *7* (1), 104–110. https://doi.org/10.1039/c9mh01062a.

(14) Pickering, S. J. Recycling Technologies for Thermoset Composite Materials-Current Status. *Compos. Part A Appl. Sci. Manuf.* **2006**, *37* (8), 1206–1215. https://doi.org/10.1016/j.compositesa.2005.05.030.

(15) Hakkarainen, M.; Xu, Y.; Odelius, K. Photocurable, Thermally Reprocessable, and Chemically Recyclable Vanillin-Based Imine Thermosets. *ACS Sustain. Chem. Eng.* **2020**, *8* (46), 17272–17279. https://doi.org/10.1021/acssuschemeng.0c06248.

(16) Wojtecki, R. J.; Jones, G. O.; Yuen, A. Y.; Chin, W.; Boday, D. J.; Nelson, A.; García, J.

M.; Yang, Y. Y.; Hedrick, J. L. Developments in Dynamic Covalent Chemistries from the Reaction of Thiols with Hexahydrotriazines. *J. Am. Chem. Soc.* **2015**, *137* (45), 14248–14251. https://doi.org/10.1021/jacs.5b08815.

(17) Ambulo, C. P.; Burroughs, J. J.; Boothby, J. M.; Kim, H.; Shankar, M. R.; Ware, T. H. Four-Dimensional Printing of Liquid Crystal Elastomers. *ACS Appl. Mater. Interfaces* **2017**, *9* (42), 37332–37339. https://doi.org/10.1021/acsami.7b11851.

(18) Cui, C.; An, L.; Zhang, Z.; Ji, M.; Chen, K.; Yang, Y.; Su, Q.; Wang, F.; Cheng, Y.; Zhang, Y. Reconfigurable 4D Printing of Reprocessable and Mechanically Strong Polythiourethane Covalent Adaptable Networks. *Adv. Funct. Mater.* **2022**, *32* (29), 1–9. https://doi.org/10.1002/adfm.202203720.

(19) Barba, A. A.; d'Amore, M.; Chirico, S.; Lamberti, G.; Titomanlio, G. A General Code to Predict the Drug Release Kinetics from Different Shaped Matrices. *Eur. J. Pharm. Sci.* **2009**, *36* (2–3), 359–368. https://doi.org/10.1016/j.ejps.2008.10.006.

(20) Bertrand, O.; Gohy, J. F. Photo-Responsive Polymers: Synthesis and Applications. *Polym. Chem.* **2017**, *8* (1), 52–73. https://doi.org/10.1039/c6py01082b.

(21) Zhu, Y.; Romain, C.; Williams, C. K. Sustainable Polymers from Renewable Resources. *Nature* **2016**, *540* (7633), 354–362. https://doi.org/10.1038/nature21001.

(22) Raquez, J. M.; Deléglise, M.; Lacrampe, M. F.; Krawczak, P. Thermosetting (Bio)Materials Derived from Renewable Resources: A Critical Review. *Prog. Polym. Sci.* **2010**, *35* (4), 487–509. https://doi.org/10.1016/j.progpolymsci.2010.01.001.

(23) Kazemi, M.; Faisal Kabir, S.; Fini, E. H. State of the Art in Recycling Waste Thermoplastics and Thermosets and Their Applications in Construction. *Resour. Conserv. Recycl.* **2021**, *174* (April), 105776. https://doi.org/10.1016/j.resconrec.2021.105776.

(24) Yang, P.; Zhou, Q.; Yuan, X. X.; Van Kasteren, J. M. N.; Wang, Y. Z. Highly Efficient Solvolysis of Epoxy Resin Using Poly(Ethylene Glycol)/NaOH Systems. *Polym. Degrad. Stab.* **2012**, *97* (7), 1101–1106. https://doi.org/10.1016/j.polymdegradstab.2012.04.007.

(25) Min, Y.; Huang, S.; Wang, Y.; Zhang, Z.; Du, B.; Zhang, X.; Fan, Z. Sonochemical Transformation of Epoxy-Amine Thermoset into Soluble and Reusable Polymers. *Macromolecules* **2015**, *48* (2), 316–322. https://doi.org/10.1021/ma501934p.

(26) Di, C.; Genua, A.; Rymarczyk, M.; Dobbels, C.; Malburet, S.; Graillot, A.; Mija, A. Chemical and Mechanical Reprocessed Resins and Bio-Composites Based on Five Epoxidized Vegetable Oils Thermosets Reinforced with Flax Fibers or PLA Woven. *Compos. Sci. Technol.* **2021**, *205* (September 2020), 108678. https://doi.org/10.1016/j.compscitech.2021.108678.

(27) Kloxin, C. J.; Bowman, C. N. Covalent Adaptable Networks: Smart, Reconfigurable and Responsive Network Systems. *Chem. Soc. Rev.* **2013**, *42* (17), 7161–7173. https://doi.org/10.1039/c3cs60046g.

(28) Podgórski, M.; Fairbanks, B. D.; Kirkpatrick, B. E.; McBride, M.; Martinez, A.; Dobson, A.; Bongiardina, N. J.; Bowman, C. N. Toward Stimuli-Responsive Dynamic Thermosets through Continuous Development and Improvements in Covalent Adaptable Networks (CANs). *Adv. Mater.* **2020**, *32* (20), 1–26. https://doi.org/10.1002/adma.201906876.

(29) Guerre, M.; Taplan, C.; Winne, J. M.; Du Prez, F. E. Vitrimers: Directing Chemical Reactivity to Control Material Properties. *Chem. Sci.* **2020**, *11* (19), 4855–4870. https://doi.org/10.1039/d0sc01069c.

(30) Liu, J.; Li, J.; Luo, Z.; Zhou, Y. Fast Room-temperature Self-healing Vitrimers Enabled by Accelerated Associative Exchange Kinetics. *Chem. Eng. J.* **2023**, *452* (P3), 139452.

https://doi.org/10.1016/j.cej.2022.139452.
(31) Podgórski, M.; Mavila, S.; Huang, S.; Spurgin, N.; Sinha, J.; Bowman, C. N. Thiol–Anhydride Dynamic Reversible Networks. *Angew. Chemie - Int. Ed.* **2020**, *59* (24), 9345–9349. https://doi.org/10.1002/anie.202001388.
(32) García, J. M.; Jones, G. O.; Virwani, K.; Mccloskey, B. D.; Boday, D. J.; Huurne, G. M.; Horn, H. W.; Coady, D. J.; Bintaleb, A. M.; Alabdulrahman, A. M. S.; Alsewailem, F.; Almegren, H. A. A.; Hedrick, J. L. Recyclable, Strong Thermosets and Organogels via Paraformaldehyde Condensation with Diamines. *Science (80-.).* **2014**, *13073* (May), 732–735. https://doi.org/10.1126/science.1251484.
(33) Carberry, B. J.; Hergert, J. E.; Yavitt, F. M.; Hernandez, J. J.; Speckl, K. F.; Bowman, C. N.; McLeod, R. R.; Anseth, K. S. 3D Printing of Sacrificial Thioester Elastomers Using Digital Light Processing for Templating 3D Organoid Structures in Soft Biomatrices. *Biofabrication* **2021**, *13* (4). https://doi.org/10.1088/1758-5090/ac1c98.
(34) Scott, T. F.; Schneider, A. D.; Cook, W. D.; Bowman, C. N. Chemistry: Photoinduced Plasticity in Cross-Linked Polymers. *Science (80-.).* **2005**, *308* (5728), 1615–1617. https://doi.org/10.1126/science.1110505.
(35) Worrell, B. T.; McBride, M. K.; Lyon, G. B.; Cox, L. M.; Wang, C.; Mavila, S.; Lim, C. H.; Coley, H. M.; Musgrave, C. B.; Ding, Y.; Bowman, C. N. Bistable and Photoswitchable States of Matter. *Nat. Commun.* **2018**, *9*, 1–7. https://doi.org/10.1038/s41467-018-05300-7.
(36) Fortman, D. J.; Brutman, J. P.; Cramer, C. J.; Hillmyer, M. A.; Dichtel, W. R. Mechanically Activated, Catalyst-Free Polyhydroxyurethane Vitrimers. *J. Am. Chem. Soc.* **2015**, *137* (44), 14019–14022. https://doi.org/10.1021/jacs.5b08084.
(37) De Alwis Watuthanthrige, N.; Ahammed, B.; Dolan, M. T.; Fang, Q.; Wu, J.; Sparks, J. L.; Zanjani, M. B.; Konkolewicz, D.; Ye, Z. Accelerating Dynamic Exchange and Self-Healing Using Mechanical Forces in Crosslinked Polymers. *Mater. Horizons* **2020**, *7* (6), 1581–1587. https://doi.org/10.1039/c9mh01938c.
(38) Kuang, X.; Roach, D. J.; Wu, J.; Hamel, C. M.; Ding, Z.; Wang, T.; Dunn, M. L.; Qi, H. J. Advances in 4D Printing: Materials and Applications. *Adv. Funct. Mater.* **2019**, *29* (2), 1–23. https://doi.org/10.1002/adfm.201805290.
(39) Marco-Dufort, B.; Willi, J.; Vielba-Gomez, F.; Gatti, F.; Tibbitt, M. W. Environment Controls Biomolecule Release from Dynamic Covalent Hydrogels. *Biomacromolecules* **2021**, *22* (1), 146–157. https://doi.org/10.1021/acs.biomac.0c00895.
(40) Yu, K.; Yang, H.; Dao, B. H.; Shi, Q.; Yakacki, C. M. Dissolution of Covalent Adaptable Network Polymers in Organic Solvent. *J. Mech. Phys. Solids* **2017**, *109*, 78–94. https://doi.org/10.1016/j.jmps.2017.08.006.
(41) Vohlidal, J. Polymer Degradation: A Short Review. *Chem. Teach. Int.* **2021**, *3* (2), 213–220. https://doi.org/10.1515/cti-2020-0015.
(42) Hawkins, W. L. *Polymer Degradation and Stabilization*; Polymers Properties and Applications; Springer Berlin Heidelberg: Berlin, Heidelberg, 1984; Vol. 8. https://doi.org/10.1007/978-3-642-69376-2.
(43) Decker, C.; Zahouily, K. Photodegradation and Photooxidation of Thermoset and UV-Cured Acrylate Polymers. *Polym. Degrad. Stab.* **1999**, *64*, 293–304. https://doi.org/10.1016/S0141-3910(98)00205-5.
(44) Armstrong, R. D.; Jenkins, A. T. A.; Johnson, B. W. An Investigation into the Uv Breakdown of Thermoset Polyester Coatings Using Impedance Spectroscopy. *Corros. Sci.* **1995**, *37* (10), 1615–1625. https://doi.org/10.1016/0010-938X(95)00063-P.

(45) Lazzari, S.; Codari, F.; Storti, G.; Morbidelli, M.; Moscatelli, D. Modeling the PH-Dependent PLA Oligomer Degradation Kinetics. *Polym. Degrad. Stab.* **2014**, *110*, 80–90. https://doi.org/10.1016/j.polymdegradstab.2014.08.012.
(46) Metters, A. T.; Anseth, K. S.; Bowman, C. N. Fundamental Studies of a Novel, Biodegradable PEG-b-PLA Hydrogel. *Polymer (Guildf).* **2000**, *41* (11), 3993–4004. https://doi.org/10.1016/S0032-3861(99)00629-1.
(47) Zakrevskii, V. A.; Sudar, N. T.; Zaopo, A.; Dubitsky, Y. A. Mechanism of Electrical Degradation and Breakdown of Insulating Polymers. *J. Appl. Phys.* **2003**, *93* (4), 2135–2139. https://doi.org/10.1063/1.1531820.
(48) Kim, J. S.; Ho, P. K. H.; Murphy, C. E.; Seeley, A. J. A. B.; Grizzi, I.; Burroughes, J. H.; Friend, R. H. Electrical Degradation of Triarylamine-Based Light-Emitting Polymer Diodes Monitored by Micro-Raman Spectroscopy. *Chem. Phys. Lett.* **2004**, *386* (1–3), 2–7. https://doi.org/10.1016/j.cplett.2003.12.124.
(49) Soars, S.; Kamps, J.; Fairbanks, B.; Bowman, C. Stimuli-Responsive Depolymerization of Poly(Phthalaldehyde) Copolymers and Networks. *Macromol. Chem. Phys.* **2021**, *222* (17), 1–7. https://doi.org/10.1002/macp.202100111.
(50) McBride, R. A.; Gillies, E. R. Kinetics of Self-Immolative Degradation in a Linear Polymeric System: Demonstrating the Effect of Chain Length. *Macromolecules* **2013**, *46* (13), 5157–5166. https://doi.org/10.1021/ma4009753.
(51) Jørgensen, M.; Norrman, K.; Krebs, F. C. Stability/Degradation of Polymer Solar Cells. *Sol. Energy Mater. Sol. Cells* **2008**, *92* (7), 686–714. https://doi.org/10.1016/j.solmat.2008.01.005.
(52) Singh, B.; Sharma, N. Mechanistic Implications of Plastic Degradation. *Polym. Degrad. Stab.* **2008**, *93* (3), 561–584. https://doi.org/10.1016/j.polymdegradstab.2007.11.008.
(53) Hopfenberg, H. B. Controlled Release from Erodible Slabs, Cylinders, and Spheres. In *Am Chem Soc Div Org Coat Plast Chem Prepr*; 1976; Vol. 36, pp 26–32. https://doi.org/10.1021/bk-1976-0033.ch003.
(54) Schneiderman, D. K.; Hillmyer, M. A. 50th Anniversary Perspective: There Is a Great Future in Sustainable Polymers. *Macromolecules* **2017**, *50* (10), 3733–3749. https://doi.org/10.1021/acs.macromol.7b00293.
(55) Browne, M. A.; Crump, P.; Niven, S. J.; Teuten, E.; Tonkin, A.; Galloway, T.; Thompson, R. Accumulation of Microplastic on Shorelines Woldwide: Sources and Sinks. *Environ. Sci. Technol.* **2011**, *45* (21), 9175–9179. https://doi.org/10.1021/es201811s.
(56) Khawam, A.; Flanagan, D. R. Solid-State Kinetic Models: Basics and Mathematical Fundamentals. *J. Phys. Chem. B* **2006**, *110* (35), 17315–17328. https://doi.org/10.1021/jp062746a.
(57) Han, X.; Pan, J. Polymer Chain Scission, Oligomer Production and Diffusion: A Two-Scale Model for Degradation of Bioresorbable Polyesters. *Acta Biomater.* **2011**, *7* (2), 538–547. https://doi.org/10.1016/j.actbio.2010.09.005.
(58) Metters, A. T.; Bowman, C. N.; Anseth, K. S. A Statistical Kinetic Model for the Bulk Degradation of PLA-b-PEG-b-PLA Hydrogel Networks. *J. Phys. Chem. B* **2000**, *104* (30), 7043–7049. https://doi.org/10.1021/jp000523t.
(59) Rydholm, A. E.; Reddy, S. K.; Anseth, K. S.; Bowman, C. N. Development and Characterization of Degradable Thiol-Allyl Ether Photopolymers. *Polymer (Guildf).* **2007**, *48* (15), 4589–4600. https://doi.org/10.1016/j.polymer.2007.05.063.
(60) Göpferich, A. Mechanisms of Polymer Degradation and Erosion. *Biomater. Silver Jubil.*

Compend. **1996**, *17* (2), 117–128. https://doi.org/10.1016/B978-008045154-1.50016-2.
(61) Burkersroda, F. Von; Schedl, L.; Göpferich, A. Why Degradable Polymers Undergo Surface Erosion or Bulk Erosion. *Biomaterials* **2002**, *23* (21), 4221–4231. https://doi.org/10.1016/S0142-9612(02)00170-9.
(62) Klose, D.; Siepmann, F.; Elkharraz, K.; Siepmann, J. PLGA-Based Drug Delivery Systems: Importance of the Type of Drug and Device Geometry. *Int. J. Pharm.* **2008**, *354* (1–2), 95–103. https://doi.org/10.1016/j.ijpharm.2007.10.030.
(63) Lu, L.; Garcia, C. A.; Mikos, A. G. In Vitro Degradation of Thin Poly(DL-Lactic-Co-Glycolic Acid) Films. *J. Biomed. Mater. Res.* **1999**, *46* (2), 236–244. https://doi.org/10.1002/(SICI)1097-4636(199908)46:2<236::AID-JBM13>3.0.CO;2-F.
(64) Sackett, C. K.; Narasimhan, B. Mathematical Modeling of Polymer Erosion: Consequences for Drug Delivery. *Int. J. Pharm.* **2011**, *418* (1), 104–114. https://doi.org/10.1016/j.ijpharm.2010.11.048.
(65) Kohrs, N. J.; Liyanage, T.; Venkatesan, N.; Najarzadeh, A.; Puleo, D. A. *Drug Delivery Systems and Controlled Release*; Elsevier, 2019; Vol. 1–3. https://doi.org/10.1016/B978-0-12-801238-3.11037-2.
(66) Lv, C.; Wang, Z.; Wang, P.; Tang, X. Photodegradable Polyurethane Self-Assembled Nanoparticles for Photocontrollable Release. *Langmuir* **2012**, *28* (25), 9387–9394. https://doi.org/10.1021/la301534h.
(67) Kuang, X.; Zhou, Y.; Shi, Q.; Wang, T.; Qi, H. J. Recycling of Epoxy Thermoset and Composites via Good Solvent Assisted and Small Molecules Participated Exchange Reactions. *ACS Sustain. Chem. Eng.* **2018**, *6* (7), 9189–9197. https://doi.org/10.1021/acssuschemeng.8b01538.
(68) Käpylä, E.; Delgado, S. M.; Kasko, A. M. Shape-Changing Photodegradable Hydrogels for Dynamic 3D Cell Culture. *ACS Appl. Mater. Interfaces* **2016**, *8* (28), 17885–17893. https://doi.org/10.1021/acsami.6b05527.
(69) Vu, D. T.; Kolah, A. K.; Asthana, N. S.; Peereboom, L.; Lira, C. T.; Miller, D. J. Oligomer Distribution in Concentrated Lactic Acid Solutions. *Fluid Phase Equilib.* **2005**, *236* (1–2), 125–135. https://doi.org/10.1016/j.fluid.2005.06.021.
(70) Zivic, N.; Kuroishi, P. K.; Dumur, F.; Gigmes, D.; Dove, A. P.; Sardon, H. Recent Advances and Challenges in the Design of Organic Photoacid and Photobase Generators for Polymerizations. *Angew. Chemie - Int. Ed.* **2019**, *58* (31), 10410–10422. https://doi.org/10.1002/anie.201810118.
(71) Romano, A.; Roppolo, I.; Rossegger, E.; Schlögl, S.; Sangermano, M. Recent Trends in Applying Ortho-Nitrobenzyl Esters for the Design of Photo-Responsive Polymer Networks. *Materials (Basel).* **2020**, *13* (12), 1–26. https://doi.org/10.3390/ma13122777.
(72) Kaminker, R.; Callaway, E. B.; Dolinski, N. D.; Barbon, S. M.; Shibata, M.; Wang, H.; Hu, J.; Hawker, C. J. Solvent-Free Synthesis of High-Performance Polyhexahydrotriazine (PHT) Thermosets. *Chem. Mater.* **2018**, *30* (22), 8352–8358. https://doi.org/10.1021/acs.chemmater.8b03926.
(73) Javed, M.; Tasmim, S.; Abdelrahman, M. K.; Ambulo, C. P.; Ware, T. H. Degradation-Induced Actuation in Oxidation-Responsive Liquid Crystal Elastomers. *Crystals* **2020**, *10* (5). https://doi.org/10.3390/cryst10050420.
(74) Zhang, Y.; Zhang, L.; Yang, G.; Yao, Y.; Wei, X.; Pan, T.; Wu, J.; Tian, M.; Yin, P. Recent Advances in Recyclable Thermosets and Thermoset Composites Based on Covalent Adaptable Networks. *J. Mater. Sci. Technol.* **2021**, *92*, 75–87.

https://doi.org/10.1016/j.jmst.2021.03.043.
(75) Scheutz, G. M.; Lessard, J. J.; Sims, M. B.; Sumerlin, B. S. Adaptable Crosslinks in Polymeric Materials: Resolving the Intersection of Thermoplastics and Thermosets. *J. Am. Chem. Soc.* **2019**, *141* (41), 16181–16196. https://doi.org/10.1021/jacs.9b07922.
(76) Ma, S.; Webster, D. C. Degradable Thermosets Based on Labile Bonds or Linkages: A Review. *Prog. Polym. Sci.* **2018**, *76*, 65–110. https://doi.org/10.1016/j.progpolymsci.2017.07.008.
(77) Reutenauer, P.; Buhler, E.; Boul, P. J.; Candau, S. J.; Lehn, J. M. Room Temperature Dynamic Polymers Based on Diels-Alder Chemistry. *Chem. - A Eur. J.* **2009**, *15* (8), 1893–1900. https://doi.org/10.1002/chem.200802145.
(78) Oehlenschlaeger, K. K.; Guimard, N. K.; Brandt, J.; Mueller, J. O.; Lin, C. Y.; Hilf, S.; Lederer, A.; Coote, M. L.; Schmidt, F. G.; Barner-Kowollik, C. Fast and Catalyst-Free Hetero-Diels-Alder Chemistry for on Demand Cyclable Bonding/Debonding Materials. *Polym. Chem.* **2013**, *4* (16), 4348–4355. https://doi.org/10.1039/c3py00476g.
(79) Ying, H.; Zhang, Y.; Cheng, J. Dynamic Urea Bond for the Design of Reversible and Self-Healing Polymers. *Nat. Commun.* **2014**, *5*. https://doi.org/10.1038/ncomms4218.
(80) Snyder, R. L.; Lidston, C. A. L.; De Hoe, G. X.; Parvulescu, M. J. S.; Hillmyer, M. A.; Coates, G. W. Mechanically Robust and Reprocessable Imine Exchange Networks from Modular Polyester Pre-Polymers. *Polym. Chem.* **2020**, *11* (33), 5346–5355. https://doi.org/10.1039/c9py01957j.
(81) Chao, A.; Negulescu, I.; Zhang, D. Dynamic Covalent Polymer Networks Based on Degenerative Imine Bond Exchange: Tuning the Malleability and Self-Healing Properties by Solvent. *Macromolecules* **2016**, *49* (17), 6277–6284. https://doi.org/10.1021/acs.macromol.6b01443.
(82) Wang, C.; Goldman, T. M.; Worrell, B. T.; McBride, M. K.; Alim, M. D.; Bowman, C. N. Recyclable and Repolymerizable Thiol-X Photopolymers. *Mater. Horizons* **2018**, *5* (6), 1042–1046. https://doi.org/10.1039/c8mh00724a.
(83) Denissen, W.; Winne, J. M.; Du Prez, F. E. Vitrimers: Permanent Organic Networks with Glass-like Fluidity. *Chem. Sci.* **2016**, *7* (1), 30–38. https://doi.org/10.1039/c5sc02223a.
(84) El-Zaatari, B. M.; Ishibashi, J. S. A.; Kalow, J. A. Cross-Linker Control of Vitrimer Flow. *Polym. Chem.* **2020**, *11* (33), 5339–5345. https://doi.org/10.1039/d0py00233j.
(85) Kuang, X.; Shi, Q.; Zhou, Y.; Zhao, Z.; Wang, T.; Qi, H. J. Dissolution of Epoxy Thermosets: Via Mild Alcoholysis: The Mechanism and Kinetics Study. *RSC Adv.* **2018**, *8* (3), 1493–1502. https://doi.org/10.1039/c7ra12787a.
(86) Hernandez, J. J.; Dobson, A. L.; Carberry, B. J.; Kuenstler, A. S.; Shah, P. K.; Anseth, K. S.; White, T. J.; Bowman, C. N. Controlled Degradation of Cast and 3-D Printed Photocurable Thioester Networks via Thiol–Thioester Exchange. *Macromolecules* **2022**, *55*, 1376–1385. https://doi.org/10.1021/acs.macromol.1c02459.
(87) Carberry, B. J.; Hernandez, J. J.; Dobson, A.; Bowman, C. N.; Anseth, K. S. Kinetic Analysis of Degradation in Thioester Cross-Linked Hydrogels as a Function of Thiol Concentration, p Ka, and Presentation. *Macromolecules* **2022**, *55* (6), 2123–2129. https://doi.org/10.1021/acs.macromol.1c02396.
(88) Yang, H.; Yu, K.; Mu, X.; Shi, X.; Wei, Y.; Guo, Y.; Qi, H. J. A Molecular Dynamics Study of Bond Exchange Reactions in Covalent Adaptable Networks. *Soft Matter* **2015**, *11* (31), 6305–6317. https://doi.org/10.1039/c5sm00942a.
(89) Lee, D. W.; Park, Y. M.; Lee, K. Y. Heterogeneous Base Catalysts for Transesterification

in Biodiesel Synthesis. *Catal. Surv. from Asia* **2009**, *13* (2), 63–77. https://doi.org/10.1007/s10563-009-9068-6.
(90) Vitaku, E.; Dichtel, W. R. Synthesis of 2D Imine-Linked Covalent Organic Frameworks through Formal Transimination Reactions. *J. Am. Chem. Soc.* **2017**, *139* (37), 12911–12914. https://doi.org/10.1021/jacs.7b06913.
(91) Layer, R. W. The Chemistry of Imines. *Chem. Rev.* **1963**, *63* (5), 489–510. https://doi.org/10.1021/cr60225a003.
(92) Zheng, P.; McCarthy, T. J. A Surprise from 1954: Siloxane Equilibration Is a Simple, Robust, and Obvious Polymer Self-Healing Mechanism. *J. Am. Chem. Soc.* **2012**, *134* (4), 2024–2027. https://doi.org/10.1021/ja2113257.
(93) Garrido-González, J. J.; Sánchez-Santos, E.; Habib, A.; Cuevas Ferreras, Á. V.; Sanz, F.; Morán, J. R.; Fuentes de Arriba, Á. L. Transesterification of Non-Activated Esters Promoted by Small Molecules Mimicking the Active Site of Hydrolases. *Angew. Chemie - Int. Ed.* **2022**, *61* (35). https://doi.org/10.1002/anie.202206072.
(94) CAMMARATA, P. S.; COHEN, P. P. The Scope of the Transamination Reaction in Animal Tissues. *J. Biol. Chem.* **1950**, *187* (1), 439–452.
(95) Melchor Bañales, A. J.; Larsen, M. B. Thermal Guanidine Metathesis for Covalent Adaptable Networks. *ACS Macro Lett.* **2020**, *9* (7), 937–943. https://doi.org/10.1021/acsmacrolett.0c00352.
(96) Podgórski, M.; Huang, S.; Bowman, C. N. Additive Manufacture of Dynamic Thiol-Ene Networks Incorporating Anhydride-Derived Reversible Thioester Links. *ACS Appl. Mater. Interfaces* **2021**, *13* (11), 12789–12796. https://doi.org/10.1021/acsami.0c18979.
(97) Bracher, P. J.; Snyder, P. W.; Bohall, B. R.; Whitesides, G. M. The Relative Rates of Thiol-Thioester Exchange and Hydrolysis for Alkyl and Aryl Thioalkanoates in Water. *Orig. Life Evol. Biosph.* **2011**, *41* (5), 399–412. https://doi.org/10.1007/s11084-011-9243-4.
(98) Chen, J.; Zhang, X. F.; Kort, M. E.; Huth, J. R.; Sun, C.; Miesbauer, L. J.; Cassar, S. C.; Neelands, T.; Scott, V. E.; Moreland, R. B.; Reilly, R. M.; Hajduk, P. J.; Kym, P. R.; Hutchins, C. W.; Faltynek, C. R. Molecular Determinants of Species-Specific Activation or Blockade of TRPA1 Channels. *J. Neurosci.* **2008**, *28* (19), 5063–5071. https://doi.org/10.1523/JNEUROSCI.0047-08.2008.
(99) Le Neindre, M.; Nicolaÿ, R. One-Pot Deprotection and Functionalization of Polythiol Copolymers via Six Different Thiol-X Reactions. *Polym. Int.* **2014**, *63* (5), 887–893. https://doi.org/10.1002/pi.4665.
(100) Houk, J.; Whitesides, G. M. Structure-Reactivity Relations for Thiol-Disulfide Interchange. *J. Am. Chem. Soc.* **1987**, *109* (22), 6825–6836. https://doi.org/10.1021/ja00256a040.
(101) Orrillo, A. G.; Furlan, R. L. E. Sulfur in Dynamic Covalent Chemistry. *Angew. Chemie - Int. Ed.* **2022**, *61* (26). https://doi.org/10.1002/anie.202201168.
(102) Worrell, B. T.; Mavila, S.; Wang, C.; Kontour, T. M.; Lim, C. H.; McBride, M. K.; Musgrave, C. B.; Shoemaker, R.; Bowman, C. N. A User's Guide to the Thiol-Thioester Exchange in Organic Media: Scope, Limitations, and Applications in Material Science. *Polym. Chem.* **2018**, *9* (36), 4523–4534. https://doi.org/10.1039/c8py01031e.
(103) Bongiardina, N. J.; Long, K. F.; Podgórski, M.; Bowman, C. N. Substituted Thiols in Dynamic Thiol-Thioester Reactions. *Macromolecules* **2021**, *54* (18), 8341–8351. https://doi.org/10.1021/acs.macromol.1c00649.
(104) Cargoët, M.; Diemer, V.; Snella, B.; Desmet, R.; Blanpain, A.; Drobecq, H.; Agouridas, V.; Melnyk, O. Catalysis of Thiol-Thioester Exchange by Water-Soluble Alkyldiselenols

Applied to the Synthesis of Peptide Thioesters and SEA-Mediated Ligation. *J. Org. Chem.* **2018**, *83* (20), 12584–12594. https://doi.org/10.1021/acs.joc.8b01903.

(105) Sun, X. H.; Yu, H. Z.; Pei, S. Q.; Dang, Z. M. Theoretical Investigations on the Thiol-Thioester Exchange Steps of Different Thioesters. *Chinese Chem. Lett.* **2015**, *26* (10), 1259–1264. https://doi.org/10.1016/j.cclet.2015.07.003.

(106) Konetski, D.; Mavila, S.; Wang, C.; Worrell, B.; Bowman, C. N. Production of Dynamic Lipid Bilayers Using the Reversible Thiol-Thioester Exchange Reaction. *Chem. Commun.* **2018**, *54* (58), 8108–8111. https://doi.org/10.1039/c8cc03471k.

(107) Ghosh, S.; Ingerman, L. A.; Frye, A. G.; Lee, S. J.; Gagné, M. R.; Waters, M. L. Dynamic Cyclic Thiodepsipeptide Libraries From Thiol-Thioester Exchange. *Org. Lett.* **2010**, *12* (8), 1860–1863. https://doi.org/10.1021/ol1004752.

(108) Ghobril, C.; Charoen, K.; Rodriguez, E. K.; Nazarian, A.; Grinstaff, M. W. A Dendritic Thioester Hydrogel Based on Thiol-Thioester Exchange as a Dissolvable Sealant System for Wound Closure. *Angew. Chemie - Int. Ed.* **2013**, *52* (52), 14070–14074. https://doi.org/10.1002/anie.201308007.

(109) Fila, K.; Goliszek, M.; Podkościelna, B.; Podgórski, M. Polymer Side-Chain Modification in Methacrylate and Styrene Copolymers through Thiol-Thioester Dynamic Exchange. *Eur. Polym. J.* **2020**, *136* (August), 109918. https://doi.org/10.1016/j.eurpolymj.2020.109918.

(110) Martinez, A. M.; Cox, L. M.; Darabi, A.; Bongiardina, N. J.; Bowman, C. N. Tunable Surfaces and Films from Thioester Containing Microparticles. *ACS Appl. Mater. Interfaces* **2022**, *14* (23), 27177–27186. https://doi.org/10.1021/acsami.2c05113.

(111) Mavila, S.; Culver, H. R.; Anderson, A. J.; Prieto, T. R.; Bowman, C. N. Athermal, Chemically Triggered Release of RNA from Thioester Nucleic Acids. *Angew. Chemie - Int. Ed.* **2022**, *61* (1), 1–5. https://doi.org/10.1002/anie.202110741.

(112) Saiz, C.; Wipf, P.; Manta, E.; Mahler, G. Reversible Thiazolidine Exchange: A New Reaction Suitable for Dynamic Combinatorial Chemistry. *Org. Lett.* **2009**, *11* (15), 3170–3173. https://doi.org/10.1021/ol901104a.

(113) Chang, H.-M.; Oakes, J.; Olsson, A.; Panaitescu, L.; Britt, B.; Kearney, C.; Kane, R. Synthesis and In Vitro Evaluation of Adenosine Deaminase Resistant N-6 Aminal and Thioaminal Prodrugs of Cordycepin. *Lett. Drug Des. Discov.* **2005**, *2* (2), 133–136. https://doi.org/10.2174/1570180053175151.

(114) Junjappa, H.; Ila, H.; Asokan, C. V. α-Oxoketene-S,S-, N,S- and N,N-Acetals: Versatile Intermediates in Organic Synthesis. *Tetrahedron* **1990**, *46* (16), 5423–5506. https://doi.org/10.1016/S0040-4020(01)87748-6.

(115) Beifuss, U.; Ledderhose, S. Intermolecular Polar [4π+ + 2π] Cycloadditions of Cationic 2-Azabutadienes from Thiomethylamines: A New and Efficient Method for the Regio- and Diastereo-Selective Synthesis of 1,2,3,4-Tetrahydroquinolines. *J. Chem. Soc. Chem. Commun.* **1995**, *1* (20), 2137–2138. https://doi.org/10.1039/C39950002137.

(116) Kim, J. K.; Souma, Y.; Beutow, N.; Ibbeson, C.; Caserio, M. C. Alkylation and Sulfenylation of Amino Thioethers. Tetrahydro-l,3-Thiazine and Related Compounds. *J. Org. Chem.* **1989**, *54* (7), 1714–1720. https://doi.org/10.1021/jo00268a039.

(117) Doss, G. A.; Baillie, T. A. Addressing Metabolic Activation as an Integral Component of Drug Design. *Drug Metab. Rev.* **2006**, *38* (4), 641–649. https://doi.org/10.1080/03602530600959466.

(118) Boday, D. J.; García, J. M.; Hedrick, J. L.; Wojtecki, R. J. POLY (THIOAMINAL) PROBE BASED LITHOGRAPHY. US 9 , 862 , 802 B2, 2018.

(119) Chatani, S.; Kloxin, C. J.; Bowman, C. N. The Power of Light in Polymer Science: Photochemical Processes to Manipulate Polymer Formation, Structure, and Properties. *Polym. Chem.* **2014**, *5* (7), 2187–2201. https://doi.org/10.1039/c3py01334k.
(120) Pasparakis, G.; Manouras, T.; Argitis, P.; Vamvakaki, M. Photodegradable Polymers for Biotechnological Applications. *Macromol. Rapid Commun.* **2012**, *33* (3), 183–198. https://doi.org/10.1002/marc.201100637.
(121) Wang, H. C.; Zhang, Y.; Possanza, C. M.; Zimmerman, S. C.; Cheng, J.; Moore, J. S.; Harris, K.; Katz, J. S. Trigger Chemistries for Better Industrial Formulations. *ACS Appl. Mater. Interfaces* **2015**, *7* (12), 6369–6382. https://doi.org/10.1021/acsami.5b00485.
(122) Manouras, T.; Vamvakaki, M. Field Responsive Materials: Photo-, Electro-, Magnetic- and Ultrasound-Sensitive Polymers. *Polym. Chem.* **2017**, *8* (1), 74–96. https://doi.org/10.1039/c6py01455k.
(123) Russew, M. M.; Hecht, S. Photoswitches: From Molecules to Materials. *Adv. Mater.* **2010**, *22* (31), 3348–3360. https://doi.org/10.1002/adma.200904102.
(124) Trenor, S. R.; Shultz, A. R.; Love, B. J.; Long, T. E. Coumarins in Polymers: From Light Harvesting to Photo-Cross-Linkable Tissue Scaffolds. *Chem. Rev.* **2004**, *104* (6), 3059–3077. https://doi.org/10.1021/cr030037c.
(125) Houck, H. A.; Blasco, E.; Du Prez, F. E.; Barner-Kowollik, C. Light-Stabilized Dynamic Materials. *J. Am. Chem. Soc.* **2019**, *141* (31), 12329–12337. https://doi.org/10.1021/jacs.9b05092.
(126) Li, L.; Deng, X. X.; Li, Z. L.; Du, F. S.; Li, Z. C. Multifunctional Photodegradable Polymers for Reactive Micropatterns. *Macromolecules* **2014**, *47* (14), 4660–4667. https://doi.org/10.1021/ma501019c.
(127) Reeves, J. A.; Allegrezza, M. L.; Konkolewicz, D. Rise and Fall: Poly(Phenyl Vinyl Ketone) Photopolymerization and Photodegradation under Visible and UV Radiation. *Macromol. Rapid Commun.* **2017**, *38* (13), 1–5. https://doi.org/10.1002/marc.201600623.
(128) Byambaa, B.; Konno, T.; Ishihara, K. Detachment of Cells Adhered on the Photoreactive Phospholipid Polymer Surface by Photoirradiation and Their Functionality. *Colloids Surfaces B Biointerfaces* **2013**, *103*, 489–495. https://doi.org/10.1016/j.colsurfb.2012.11.008.
(129) Han, D.; Tong, X.; Zhao, Y. Fast Photodegradable Block Copolymer Micelles for Burst Release. *Macromolecules* **2011**, *44* (3), 437–439. https://doi.org/10.1021/ma102778d.
(130) Pasparakis, G.; Manouras, T.; Selimis, A.; Vamvakaki, M.; Argitis, P. Laser-Induced Cell Detachment and Patterning with Photodegradable Polymer Substrates. *Angew. Chemie* **2011**, *123* (18), 4228–4231. https://doi.org/10.1002/ange.201007310.
(131) Yousif, E.; Haddad, R. Photodegradation and Photostabilization of Polymers, Especially Polystyrene: Review. *Springerplus* **2013**, *2* (1), 1–32. https://doi.org/10.1186/2193-1801-2-398.
(132) Cordes, E. H.; Bull, H. G. Mechanism and Catalysis for Hydrolysis of Acetals, Ketals, and Ortho Esters. *Chem. Rev.* **1974**, *74* (5), 581–603. https://doi.org/10.1021/cr60291a004.
(133) Fife, T. H. General Acid Catalysis of Acetal, Ketal, and Ortho Ester Hydrolysis. *Acc. Chem. Res.* **1972**, *5* (8), 264–272. https://doi.org/10.1021/ar50056a002.
(134) Zhang, X.; Chen, G.; Collins, A.; Jacobson, S.; Morganelli, P.; Dar, Y. L.; Musa, O. M. Thermally Degradable Maleimides for Reworkable Adhesives. *J. Polym. Sci. Part A Polym. Chem.* **2009**, *47* (4), 1073–1084. https://doi.org/10.1002/pola.23217.
(135) Walker, W. D.; Sandoz, M. J.; Roland, S.; Buster, T. M.; Newman, J. K.; Patton, D. L.

Command-Destruct Thermosets: Via Photoinduced Thiol-Catalyzed β-Scission of Acyclic Benzylidene Acetals. *Polym. Chem.* **2020**, *11* (43), 6873–6878. https://doi.org/10.1039/d0py01006e.

(136) Liu, B.; Thayumanavan, S. Mechanistic Investigation on Oxidative Degradation of ROS-Responsive Thioacetal/Thioketal Moieties and Their Implications. *Cell Reports Phys. Sci.* **2020**, *1* (12), 100271. https://doi.org/10.1016/j.xcrp.2020.100271.

(137) Kumhee, C. Acetal Copolymers: Synthesis, Chemical Modifications and Degradation Study, 1994.

(138) Fialho, D. M. Physical Organic Principles Governing the Spontaneous Prebiotic Emergence of Proto-Nucleic Acids, Georgia Institute of Technology, 2019.

Chapter 2: Objectives

This thesis focuses on polymer degradation within covalent adaptable networks (CANs), exploring how the thiol-thioester exchange, the thiol-thioaminal exchange, and the thioaminal scission reactions all lead to cleaved polymer connections. Within the various aspects of degradation, this thesis focuses on studying mass loss and mechanical property changes as degradation proceeds and investigates how these physical changes compare to theoretical model predictions. The overarching hypothesis of this thesis is that degradation within CANs may be precisely controlled by manipulating the bond-scission reaction chemistry and the polymer network structure, leading to predictable mass loss and material property changes.

Three chemical reactions were studied in the development of this thesis: the thiol-thioester exchange, the thiol-thioaminal exchange, and the thioaminal scission reaction. Exchange reactions are associative processes that replace the functional groups between two chemical moieties. When the exchange reaction replaces a terminal group with a crosslinked group the crosslink density of the network decreases and degradation ensues. Within exchange reactions, the thiol-thioester exchange switches the functional groups attached to the thiol and thioester moieties, and this reaction was investigated due to its high selectivity, rapid exchange rate, and ability to be catalyzed by mild bases. Meanwhile, the thiol-thioaminal exchange switches the functional groups attached to the thiol and thioaminal moieties, and thiol-thioaminal exchange was studied due to its high selectivity, self-catalysis, and even faster exchange rate, which when combined may unlock different degradation mechanisms. Unlike these exchange reactions, scission reactions decrease polymer connections by cleaving functional groups and increase the total number of polymer chains. The thioaminal scission reaction was found to cleave thioaminals via a radical-mediated process, resulting in the formation of thioamides. Thioaminal scission was investigated due to its

potential to selectively cleave thioaminal networks. By combining all three chemical routes discussed, this thesis offers unique ways to probe degradation within CANs.

To investigate the manner through which polymer degradation may be precisely controlled by manipulating reaction chemistry and polymer network structure, three aims were pursued.

Aim 1 - Investigate how small molecule thiol-thioester exchange translates to macroscopic degradation of thioester-containing networks.

Previous research on the degradation of polymer networks, both experimentally and computationally, has mostly focused on degradation induced by scission reactions. Only recently have researchers started building statistical models to describe the macroscopic degradation process induced by exchange reactions within CANs. To improve the knowledge of how exchange reactions lead to macroscopic degradation of networks, Aim 1 focused on studying the thiol-thioester exchange reaction. A statistical model was developed to quantitatively depict the degradation process of thioester-containing networks upon base-catalyzed thiol-thioester exchange. This model incorporated the exchange reaction kinetics, polymer structure, and mass gain resulting from bond exchange. These model predictions were then compared to experimental mass loss profiles measured for photopolymerized thioester-containing networks. Aim 1 is explored in Chapter 3 of this thesis.

Aim 2 - Investigate how oligomer structure of thioester-containing networks impacts degradation via thiol-thioester exchange.

Of the various approaches to controlling the degradation of polymer networks, modulating the network structure enables degradation control without having to change chemical degradation

conditions. Research on this avenue is being conducted both experimentally and theoretically to study the degradation of CANs, and placing oligomers with these CANs as a means to modulate network structure offers a promising way to control the degradation process. Aim 2 was to investigate the mass loss of networks constructed from different thioester-containing oligomers to understand the impact of the degradation process upon the thiol-thioester exchange. A statistical model taking into account the impact of two oligomer structural components, the number of thioester linkages within oligomers (N) and their dispersity, was developed. These model predictions were compared to experimental mass loss profiles measured for photocured thioester networks, and these networks were composed of various oligomers structures. Controlled degradation was then further explored by investigating how combining oligomers of different lengths into one CAN could tune the degradation profile, and how a model dye could guide controlled mass release within thioester networks. Aim 2 is explored in Chapter 4 of this thesis.

Aim 3 - Explore thioaminal groups as another possible route to create CANs. Specifically, Aim 3a - Investigate thiol-thioaminal exchange as a means to create CANs triggered under low temperature conditions.

With the increasing focus on recyclable thermosets there has been a push to design reversible exchange CANs that rearrange fast enough to be reprocessed by traditional thermoplastic techniques. Aim 3a contributes to this effort by exploring the thiol-thioaminal exchange reaction, offering the possibility to create reversible exchange CANs that rapidly relax under near-ambient conditions. A small molecule system was used to study the thiol-thioaminal exchange reaction between thioaminal DMTA and one of three thiols (BMP, BTG, TP). Thioaminal-containing networks were then photopolymerized and used to study stress relaxation of these materials, and

this data was combined with frequency sweep experiments to evaluate the proper characterization of these polymers as CANs. Lastly, to study degradation via exchange reactions, as is typical for reversible exchange CANs, the mass loss of thioaminal-containing networks was tracked as these networks were submerged in four thiol monomers (BMP, BTG, TP, HT). Aim 3a is explored in Chapter 5 of this thesis.

Aim 3b - Explore thioaminal scission as a novel radical-mediated approach to CAN degradation and investigate its potential to create constructing-then-destructing materials. While several research studies have investigated the integration of photopolymers with photoscission reactions to create constructing-then-destructing materials, few have explored the possibility of building the constructing-then-destructing materials by controlling the polymerization/photoscission reaction kinetics. Aim 3b explored the thioaminal scission reaction as a novel approach to creating a reaction-kinetics controlled system. Synthesis of three thioaminal small molecules with varying degrees of thiol-substitution (1^o – 3^o) investigated the speed, extent, and products of this scission reaction. The reaction was then compared to the thiol-ene polymerization reaction to identify its potential as semi-orthogonal, *i.e.* whether it occurred on a vastly different timescale. A thioaminal-containing network was then photopolymerized and its utility investigated as a light dose dependent system that could show distinct construction then destruction regimes. Aim 3b is explored in Chapter 6 of this thesis.

Successful completion of these Aims contributed to the field of polymer degradation by 1) developing models that accurately describe the mass loss of degrading networks mediated by thiol-thioester exchange reactions, 2) establishing thiol-thioaminal exchange as a new CAN chemistry,

and 3) establishing thioaminal scission as a novel radical-mediated approach to degradable CANs. In a broader sense, the models developed in Aim 1 and 2 may readily be adapted to other exchange chemistries as the structural components of these models are chemistry agnostic. Following similar logic, the kinetic parameters extracted from the small molecule study of the thiol-thioaminal exchange reaction in Aim 3a are not limited to polymers, and may be widely applied to any chemical system considering the use of thioaminals. Lastly, within Aim 3b the newly discovered thioaminal scission reaction is also not limited to polymers and future research may consider exploring thioaminal scission as a new multi-purpose phototrigger.

Chapter 3: Controlled Degradation of Cast and 3-D printed Photocurable Thioester Networks via Thiol-Thioester Exchange*

*Manuscript published under the same name in *Macromolecules*, **2022**, 55 (4), 1376-1385.

3.1 Abstract

This work examined and quantitatively predicted degradation of thioester-containing networks facilitated by base-catalyzed thiol-thioester exchange. A statistical model was developed that incorporated polymer structure, thiol-thioester exchange reaction kinetics, and mass gain resulting from dynamic bond exchange and this model was compared to mass loss studies. Experimental results matched model predictions, showing degradation times could be controlled from 2.5 to 12 hours with optimal conditions by varying the free thiol butyl 3-mercaptopropionate concentration from 0.0 M to 4.9 M and the base-catalyst triethylamine molar ratio from 0 to 40 mol%. Furthermore, thioester-based composite materials were formed by SLA 3-D printing and subsequently degraded, achieving 91% recovery of the composite filler. This work provides insight into thioester facilitated degradation and its future use in selective material release or encapsulated filler recovery applications.

3.2 Introduction

In recent years, waste from slowly-degrading polymers has driven the need to consider the wholistic lifecycle of manufactured plastics. Polymers which cannot degrade rapidly or be recycled pollute the environment,[1] leading to an increased focus on designing multi-use or on demand degradable plastics. Polymer composites that cannot degrade must be scrapped, leading to the loss

of both specially synthesized chemical components and valuable fillers used to make these composites.[2]

One subset of polymers, thermosets, are particularly difficult to degrade but have advantageous material properties. Thermosets are composed of covalent chemical crosslinks that enable dimensional stability, solvent resistance, and temperature resistance. However, the non-reconfigurability of these permanent crosslinks limits recyclability or reuse and further inhibits degradation. Covalent adaptable networks (CANs) offer an effective way to reuse thermoset polymers by having crosslinks with triggerable, dynamic bonds.[3] Rearrangement of these dynamic bonds allows reprocessing of thermosets, and different dynamic chemistries use different stimuli to induce network rearrangement, for example, by exposure to heat or light.[4] Past work has shown CANs enable thermoset degradation,[5–9] yet these studies are often empirical, and it remains a challenge to quantitatively predict degradation behavior, limiting their application in larger scale processes such as stereolithography (SLA) additive manufacturing. SLA uses light to cure liquid monomers layer-by-layer to form a 3-D object. While a variety of dynamic chemistries, such as transesterification,[10] disulfide metathesis,[11,12] and trithiocarbonate addition-fragmentation[13] have been SLA 3-D printed, little work has been done to explore the degradation process of these printed CAN-based polymers.

Degradation in CANs refers to the permanent cleavage of crosslinks in a network, which leads to the formation of detached monomers and a reduction in mass as the increasing sol fraction comprised of monomers and oligomers leaves the network.[14] This degradation process has two limiting extremes: surface and bulk degradation.[15] Surface degradation is a diffusion-limited process where crosslinks are cleaved only on the surface of a bulk polymeric object, gradually shrinking the material from the outside until the entire network dissolves into solution. Conversely,

bulk degradation is a reaction-limited process where crosslinks are cleaved throughout the entire polymer network simultaneously, until the reverse gelation point is reached and the material depolymerizes and fully dissolves into solution.[15] Often, degradation of a polymer network is a combination of both surface and bulk mechanisms.

Of the various dynamic chemistries, degradation studies on thioester-containing networks offer wider understanding of network architectures due to thioesters being compatible with existing thiol-x chemistries. Dynamic bond rearrangement in thioester-containing CANs comes from the thiol-thioester exchange reaction, which may occur through either a base- or a nucleophile-mediated pathway.[8,16] While other thiol-based dynamic chemistries have been used to create dynamic networks, such as Meldrum's acid systems[17,18] and thiol-yne systems,[19,20] thiol-thioester exchange is attractive due to its highly selective reactivity with thiols, efficiency with mild bases, stability in aqueous solutions, and inherent biocompatibility as a common biosynthetic pathway.[16,21–23] While past work has shown thioester networks degrade efficiently[8] (**Figure 3.1**) and may be SLA 3-D printed,[24] the process and time scale for degradation of these structures has yet to be investigated.

Past studies on the degradation process of other dynamic chemistries offer guidance on how to study thioester-based degradation. In ester crosslinked materials, mass loss resulting from transesterification-based CAN degradation is well described by models that combine surface and bulk degradation.[25–27] Recent work on boronic ester CAN degradation similarly created a surface degradation model that also matched mass loss studies.[28] However, a bulk degradation model for CANs is missing, and this model would more accurately capture the relevant degradation processes of CANs with thinner cross sectional areas, such as those formed in 3-D printed parts. Past work on understanding bulk degradation of thermosets has focused on studying degradation of

hydrogels,[5,29–33] and while these analyses provide insightful models, they are not applicable to more hydrophobic or more crosslinked bulk CANs which may experience significantly reduced swelling. To this end, a bulk degradation model of thioester-based CANs would both investigate the degradation processes particular to thiol-thioester exchange and also widen the scope of degradation models applicable to CAN chemistries.

This paper sought to investigate the degradation process and time scale that thiol-thioester exchange enables in cast and 3-D printed networks. As such, a statistical kinetic model for bulk degradation of thioester networks was generated which combined the thiol-thioester exchange reaction kinetics, mass gain resulting from thiol-thioester exchange, and the structure of the polymer network being degraded. Mass loss experiments verified model predictions for how the concentration of free thiol, relative mol percent of base catalyst, and monomer functionality all impacted mass loss rates. Lastly, 3-D printed and degraded thioester composites matched model predictions for degradation time of 3-D printed samples and showed the effectiveness of using thioester degradation to selectively recover composite fillers. The understanding of thiol-thioester facilitated degradation gained in this work enables the implementation of degradable thioester systems for recycling and selective material recovery applications in additive manufacturing specifically and in composite materials generally.

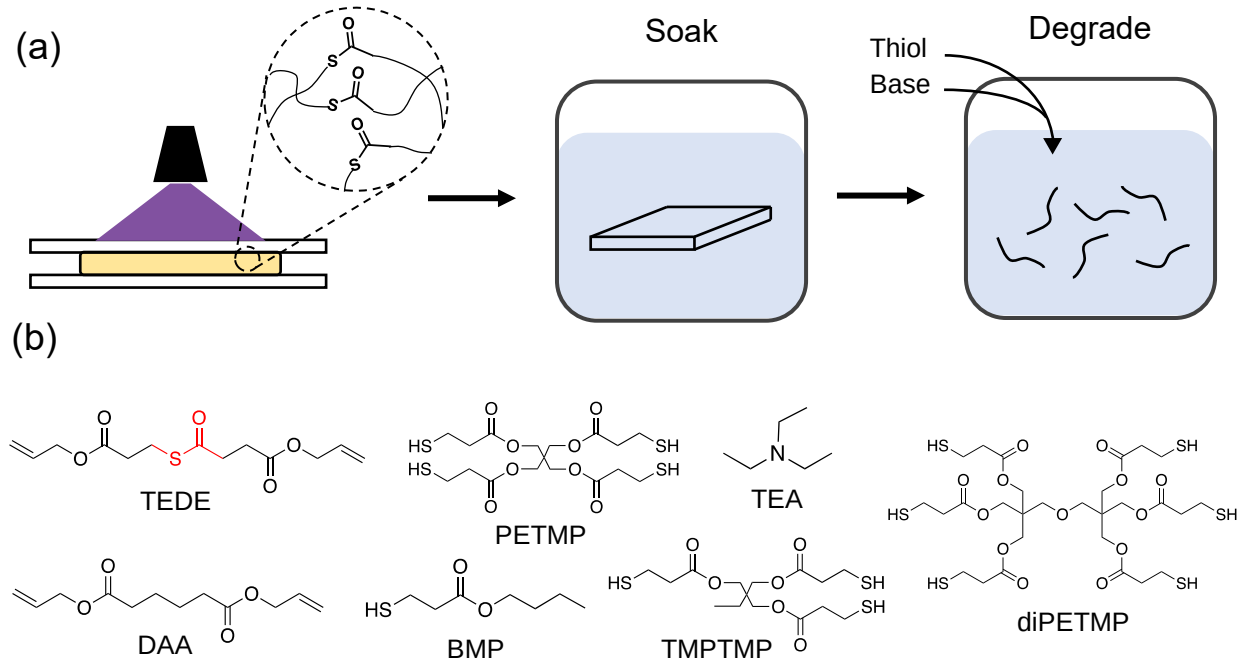

Figure 3.1. Addition of excess thiol and base-catalyst triggers degradation of thioester-containing thermosets via thiol-thioester exchange. (a) Thioester-containing networks were photocured via thiol-ene combination, swelled in acetone, and degraded by exposure to thiol and base. (b) Monomers, free thiol, and base-catalyst used to create networks and trigger thiol-thioester exchange.

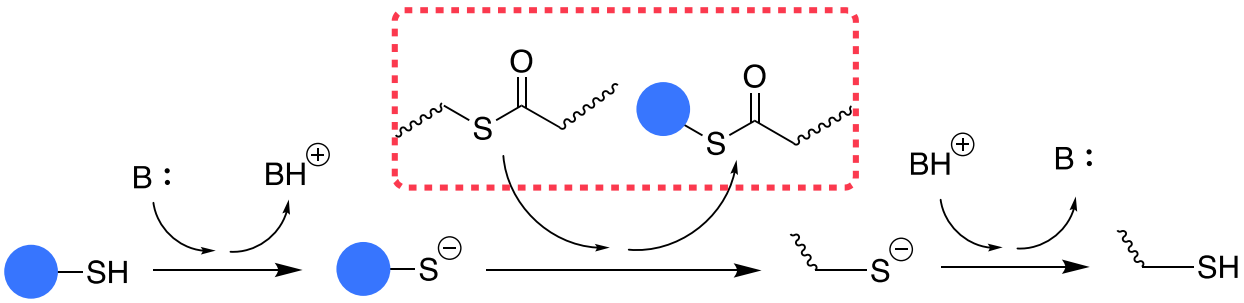

Scheme 3.1. Base-catalyzed thiol-thioester exchange swaps the group attached to a free thiol with the group attached to a thioester. In this work, the thioester groups were initially connected to the network and the exchange resulted in dangling ends (highlighted box).

3.3 Materials and Experimental Methods

3.3.1 Materials

A previously reported procedure was used to synthesize the thioester monomer TEDE.[34] All other materials used were purchased commercially and used without further purification. 3-mercaptopropionic acid (3-MPA), allyl alcohol (AA), butyl 3-mercaptopropionate (BMP), trimethylpropane tris(3-mercaptopropionate) (TMPTMP), p-toluenesulfonic acid (pTsOH), pentaerythritol tetrakis(3-mercaptopropionate) (PETMP), and crosslinked poly(styrene-co-divinylbenzene) microspheres (6-10 um) were purchased from Sigma Aldrich. Diallyl adipate (DAA) and succinic anhydride (SA) were purchased from TCI Chemicals. 4-dimethylamino-pyridine (DMAP) was purchased from Oakwood Chemical, dipentaerythritol hexakis(3-mercaptopropionate) (diPETMP) from Bruno Bock Chemische Fabric, and Irgacure 819 (I819) from IGM Resins.

3.3.2 Thin Film Preparation and Degradation

To prepare thioester films, one thiol and one ene monomer were combined with I-819 and pyrogallol in a molar ratio of 1 thiol: 1 ene: 0.5 wt% I819: 0.06 wt% pyrogallol, loaded between glass slides spaced 100 µm apart, and irradiated to complete conversion (405 nm, 30 mW/cm^2, 5 minutes). Samples were then trimmed to a length and width of 25 mm, with an average weight of 100 mg, and used for further experiments.

The initial mass of each film was recorded, m_o, then samples were allowed to swell in a solution of BMP and acetone overnight, with the concentration of BMP set by the degradation conditions. Films were then transferred to a constructed apparatus composed of a covered 100 x 50 mm Pyrex Petri dish, a stir bar spun at 400 RPM, and a steel grid which let degradation solution

flow above and below the films (**Figure S3.3** in the SI). TEA was added to initiate degradation, then films were removed at specific times and patted dry with a Kimwipe. Films were then soaked in acetone overnight, dried in a vacuum oven at 50 ºC for 24 hours, and weighed again to measure the final dry mass, m_{final}. Experimental mass loss was calculated by

$$ML_{exp} = \frac{m_o - m_{final}}{m_o} \quad (1)$$

3.3.3 3-D Printing and Filler Recovery

Samples were 3-D printed on a Prusa SL1 masked-SLA 3-D printer, washed with dichloromethane, and air dried for 30 minutes. Printed resins contained a molar ratio of 1 thiol: 1 ene: 0.5 wt% I819: 0.06 wt%. Thioester composites contained 80 wt% resin and 20 wt% poly(styrene-co-divinylbenzene) microspheres. Exposure times and E_cD_p values for 3-D printed parts are listed in **Table S3.1**.

3-D printed composites were placed in a solution of 2M BMP and 30 mol% TEA in acetone, and allowed to stir overnight to recover the microspheres. Acetone was added at twice the volume of the initial solution, and the mixture was centrifuged at 1000 RPM for 2 minutes. The settled microspheres were then redispersed in pure acetone, centrifuged again at 1000 RPM for 2 minutes, and dried in a vacuum oven at 50 °C for 24 hours.

3.3.4 Dynamic Mechanical Analysis

An RSA-G2, from TI Instruments, was used for dynamic mechanical analysis (DMA). Samples were heated from -50 °C to 50 °C, with a ramp rate of 3 °C / minute and a frequency of 1 Hz. Samples were run in tension with a strain of 0.03 % and a preload force of 0.34 N. The T_g was determined as the peak of the tan delta curve. The molecular weight between crosslinks, M_c, was calculated from DMA data via

$$M_c = \frac{3\rho R T_{min}}{E_{r,min}} \quad (2)$$

where ρ stands for polymer density and was assumed to be constant at 1,100 kg/m^3, R for the universal gas constant, $E_{r,min}$ for the minimum storage modulus value just as the polymer enters the rubbery plateau, and T_{min} for the temperature in Kelvin where $E_{r,min}$ is reached.[35]

3.3.5 Model Development

Modeling bulk degradation of an ideal step-growth polymer network containing thioester linkages required examination of the step-growth network structure and the reaction kinetics of thiol-thioester exchange. The approach used here was modified from Rydholm et al.,[32] which in turn was based on step-growth network formation equations first proposed by Macosko and Miller.[36] This model was derived with four primary assumptions: (i) the polymers under consideration were ideal networks; (ii) the reaction rate constant for the thiol-thioester exchange remained constant throughout the degrading process; (iii) cleaved segments diffused nearly immediately out of the thioester network; and (iv) no further thiol-thioester exchange reactions need be considered in cleaved segments because these segments rapidly diffused out of the network and did not have time for additional thiol-thioester exchange. These assumptions will not hold for all networks and may be of interest to explore in future studies. Past work suggests that cyclization occurs to varying extents,[32] reaction rate constants may depend on temperature and other conversion dependent network features,[26] networks with larger values of M_c will cleave into large oligomers with significant diffusion times,[37] and lastly networks containing multiple degradable thioester units between crosslinks will increase the likelihood of secondary thiol-thioester exchange reactions that may re-attach segments prior to their release.[29]

3.3.5.1 Structure Component of Model

For an ideal step-growth network with monomer functionality *Z*, each arm of the multifunctional monomer unit is detached from or attached to an infinite network with probability *y* or *1-y*, respectively. Detachment from the network can occur in two ways. The first is via cleavage of the thioester bond from an adjacent multifunctional monomer unit through the thiol-thioester exchange reaction. This occurs with a probability *P*, the fraction of thioester bonds that have been cleaved. The second is via detachment of an adjacent monomer unit. Given that the connecting thioester bond is not cleaved, an arm can be detached from the infinite network if the neighboring multifunctional monomer unit has all its remaining arms detached from the network. This provides an equation for the probability of arm detachment as a function of the thiol-thioester exchange and network connectivity:

$$y = P + (1 - P)y^{Z-1} \quad (3)$$

where *y* is the probability that an arm of a multifunctional monomer unit is detached from the network; *P* is the probability that a thioester bond has cleaved which is dictated by the thiol-thioester exchange kinetics; and *Z* is the number of functional groups on a monomer. Recognizing that $y = 1$ is always a solution to equation 3, the factor $y - 1$ can be removed from the equation, leaving a general equation in *y*, for $Z > 2$:

$$\sum_{k=1}^{Z-2} y^k = \frac{P}{1-P} \quad (4)$$

The general equation predicts a critical value for *P* (P_c) above which $y = 1$ and the polymer network shifts from an infinite network to finite, soluble components. This value of P_c corresponds to the point of reverse gelation, given by:

$$P_c = \frac{Z-2}{Z-1} \quad (5)$$

The value of P_c from equation 5 agrees exactly with the Flory prediction for reverse gelation of a stoichiometric reaction of monomers with functionality Z (SI Section 3.8.2.6).[38]

3.3.5.2 Mass loss from y, P, and network properties

Maximum percent mass loss in such a system is given by the sum of the mass fractions of all degradable units in the network multiplied by the fraction of those units that have separated from the network:

$$ML_{max} = \sum_i W_i F_i \quad (6)$$

where W_i is the mass fraction of degradable component i in the network and F_i is the fraction of those components that have separated from the network. In the ideal step-growth network examined, the entire mass of the network consists of one type of repeat unit: multifunctional monomer units with thioester linkers between them. This results in the mass fraction of these units in the network to be one, or $W_i = 1$. The fraction of these multifunctional monomer units that have detached from the infinite network is the fraction of units that have all arms, i.e. Z number of arms, detached. This results in a fractional mass loss equation for an ideal step-growth network:

$$ML_{max} = y^Z \quad (7)$$

where y^Z represents F_i, the proportion of multifunctional monomer units that have detached from the network.

Early in the degradation process, however, mass gain as a function of the degrading thiol molecular weight is expected. As thioesters become cleaved, there is a net mass gain of the excess monofunctional thiol used for degradation as these molecules add to the network (**Figure 3.2a** *middle*). This mass adds to the overall network until the arm containing that thioester is detached

from the network (**Figure 3.2a** *right*). To account for this effect, a parameter *q* is defined to be the fraction of thioesters that have been cleaved but are still attached to the network, where:

$$q = \frac{1}{2}P(1 - y^{Z-1}) \quad (8)$$

This relationship represents the probability that a thioester has cleaved (*P*) and that at least one of the other arms of the multifunctional monomer unit remains attached. The prefactor *1/2* is necessary because only half of the dangling ends formed via thioester cleavage contribute to the mass gain. A detailed derivation for equation 8 can be found in the Supporting Information Section 3.8.2.4.

From *q*, the total number of thioester bonds that have been cleaved but are still attached to the network can be calculated from the stoichiometry of network formation and the assumption that one molecule of excess thiol used for degradation reacts with one thioester bond. Combining the expression for *q* and knowledge of network stoichiometry provides the following equation for fractional mass gain:

$$MG = \frac{ZP(1-y^{Z-1})MW_{SH}}{2(2\,MW_M + Z \cdot MW_{diene})} \quad (9)$$

where *MG* is fractional mass gain, MW_{SH} is the molecular weight of the excess monofunctional thiol, MW_{diene} is the molecular weight of the thioester-containing diene, and MW_M is the molecular weight of the multifunctional monomer (SI Section 3.8.2.5). Combining the mass gain from equation 9 with the mass loss from equation 7 gives an expression for the net fractional mass loss:

$$ML_{Model} = y^z - \frac{ZP(1-y^{Z-1})MW_{SH}}{2(2\,MW_M + Z \cdot MW_{diene})} \quad (10)$$

3.3.5.3 Kinetic Component of Model

The kinetics of the thiol-thioester exchange reaction drive the degradation rate. As shown in **Scheme 3.1**, when thioesters are initially linked to a network, the exchange forms a new thioester with a dangling end, thereby reducing the number of crosslinks.

By setting the initial conditions of the thiol-thioester exchange to use a large excess of free thiol and base catalyst, the exchange can be tuned to behave as a pseudo first-order reaction. The initial concentration of free thiol and base govern the formation of unlinked thiolate (**Scheme 3.1** *left*). If the unlinked thiolate consumed by the thiol-thioester exchange is minimal (**Scheme 3.1** *middle*), then the formation of unlinked thiolate can be considered an acid-base reaction in equilibrium. Knowing the initial concentration of free thiol and base catalyst and the pKa of each component, the concentration of thiolate created is calculated using

$$10^{\Delta pKa} = \frac{[S^-]^2}{([SH]_0 - [S^-])([B]_0 - [S^-])} \quad (11)$$

where ΔpKa stands for the difference in pKa values between the free thiol and base, $[SH]_0$ stands for the initial concentration of free thiol, $[B]_0$ stands for the initial concentration of base, and $[S^-]$ stands for the concentration of unlinked thiolate. This produces a quadratic equation in $[S^-]$ that is readily solved.

The initial concentration of unlinked thiolate in all experiments of this study was more than 200x the initial concentration of thioesters linked to the network. As such, the consumption of the unlinked thiolate by the thiol-thioester exchange was minimal and equation 11 applied. Furthermore, the large excess of unlinked thiolate drove thiol-thioester exchange toward the reaction products consistent with Le Chatelier's principle. Thus, while the thiol-thioester exchange was a second order reaction, the effectively constant concentration of unlinked thiolate allowed the exchange to be treated as a pseudo-first order reaction modeled by

$$[TE] = [TE]_0 e^{-k[S^-]t} \quad (12)$$

where $[TE]$ refers to the current concentration of thioesters linked to the network and $[TE]_0$ refers to the initial concentration of thioesters linked to the network.

The network structure and kinetics portions of the model come together by relating the probability of cleaving a random thioester crosslink, *P*, to the concentration of linked thioesters via

$$P = \frac{[TE]_0 - [TE]}{[TE]_0} = 1 - e^{-k[S^-]t} \quad (13)$$

Equation 13 uses equation 12 to relate the probability P to the second-order rate constant *k*, the unlinked thiolate concentration $[S^-]$, and the time *t*. Combining equations 4, 10 and 13 gives a direct prediction for how the mass of a thioester-containing polymer will decrease with time due to thiol-thioester exchange.

3.4 Results and Discussion

3.4.1 Model results for mass loss

The derived model provides insight into how network structure and reaction kinetics impact bulk degradation of thioester networks. Inspection of equation 10 showed that *Z*, the functionality of the thiol monomer and a vital part of the network structure, impacts the net mass loss and mass gain. For $Z = 2$, a polymer consists entirely of linear polymer chains. In this case, $y = 1$ for all values of *P*, and the predicted net fractional mass loss is 1, indicating a crosslinked network is never formed. On the other extreme, as $Z \rightarrow \infty$, the value for net mass loss approaches $-\frac{P MW_{SH}}{2\, MW_{diene}}$ for $P < 1$. This value is a function of excess thiol molecular weight (from MW_{SH}), the number of thioester units in the network (from MW_{diene}), and the time allowed for degradation (from *P*). The

negative sign indicates that only mass gain is expected in such a system, as no monomer unit can leave until all thioester groups have been cleaved.

Figure 3.2b and **3.2c** used model systems of TMPTMP ($Z = 3$), PETMP ($Z = 4$), and di-PETMP ($Z = 6$) with BMP as the excess monothiol and TEDE as the thioester-containing diene to show the extreme and intermediate cases for Z. For the less crosslinked system ($Z = 3$), mass gain was predicted but was nearly balanced by mass loss (**Figure 3.2c**). For the more highly crosslinked systems ($Z = 4$ and $Z = 6$), however, mass gain had a significant overall effect. This outcome arose because a much higher P, which corresponded to a longer degradation time, was required before units could be freed from the network. The result of this was an approximately 3% and 7% net gain in mass for $Z = 4$ and $Z = 6$, respectively, before mass loss could counteract the effect of thiol addition to the network.

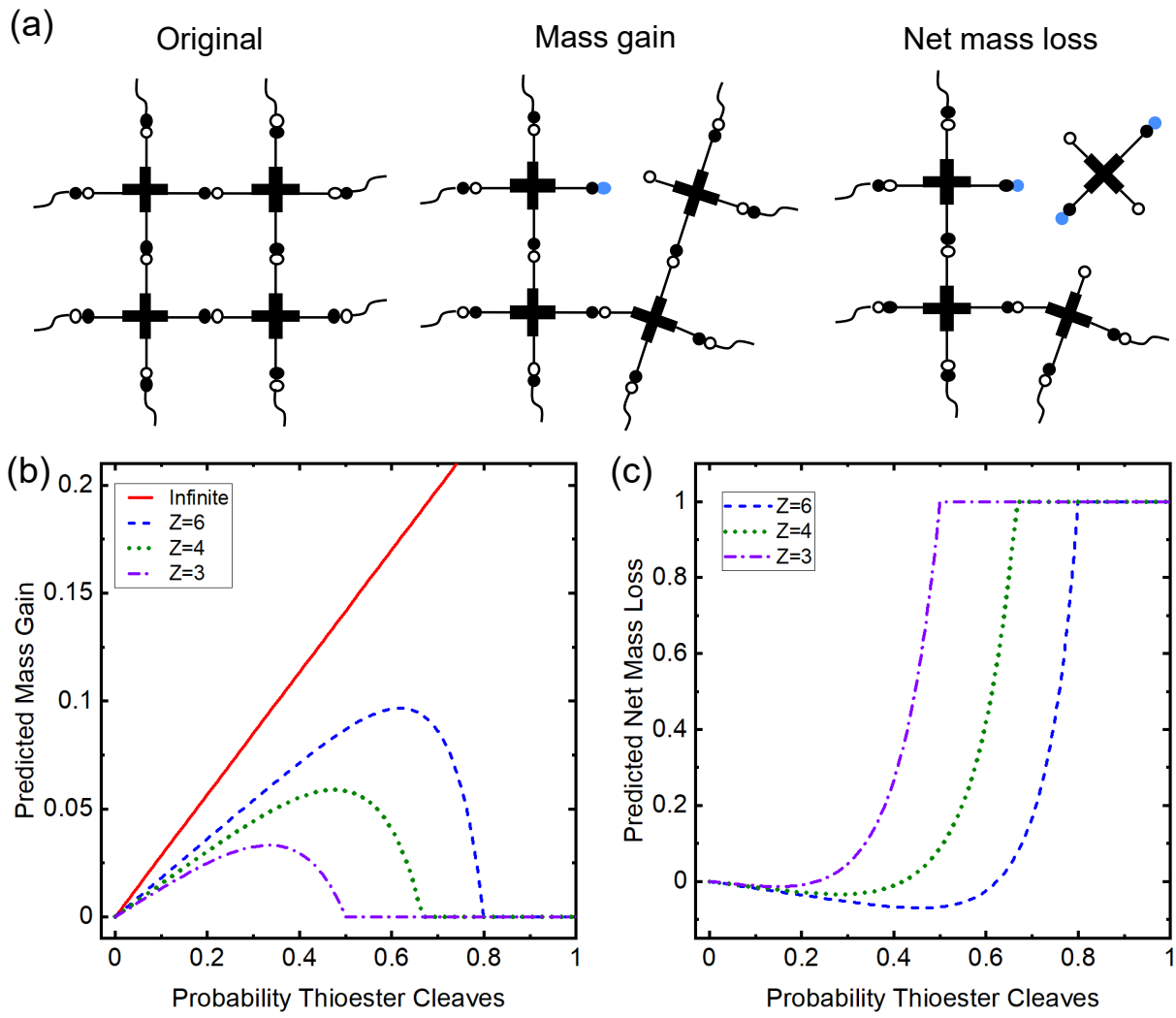

Figure 3.2. Degradation of thioester-containing networks is predicted to proceed first through a small amount of mass gain and then through net mass loss based on the derived model. (a) Thioesters (black circles) and thiols (white circles) underwent exchange with free thiol (blue circles). Net mass loss was achieved when all bonds of a repeat unit were cleaved (right). (b) Plot comparing predicted mass gain from thiol-thioester exchange versus probability a thioester crosslink cleaves, as was calculated by equation 9. (c) Plot comparing predicted net mass loss from thiol-thioester exchange versus probability a thioester crosslink cleaves, based on equation 10.

3.4.2 Verification of Bulk Degradation

To ensure that the thioester networks experimentally studied in this work underwent bulk rather than surface degradation, the molecular weight between crosslinks, M_c, and glass transition

temperature, T_g, of a model network were probed by DMA throughout the degradation process. Bulk degradation leads to a decrease in network connectivity throughout the entire polymer network, and as such all properties that depend on network connectivity, such as M_c and T_g, shift during degradation.[39] **Figure 3.3** shows that as degradation proceeded in photocured TEDE-PETMP films soaked in 2M BMP and 30 mol% TEA degrading solution, T_g dropped and M_c increased in ways that were characteristic of films experiencing bulk degradation. **Figure 3.3a** shows that with increasing degradation time, T_g decreased from – 12 °C to – 26 °C, and the rubbery plateau modulus decreased from 14 MPa to 1.5 MPa. **Figure 3.3b** shows that experimental data for M_c, as was calculated by equation 2, increased with degradation time and matched bulk degradation model predictions for M_c (equations S4-S5 in the SI). [31]

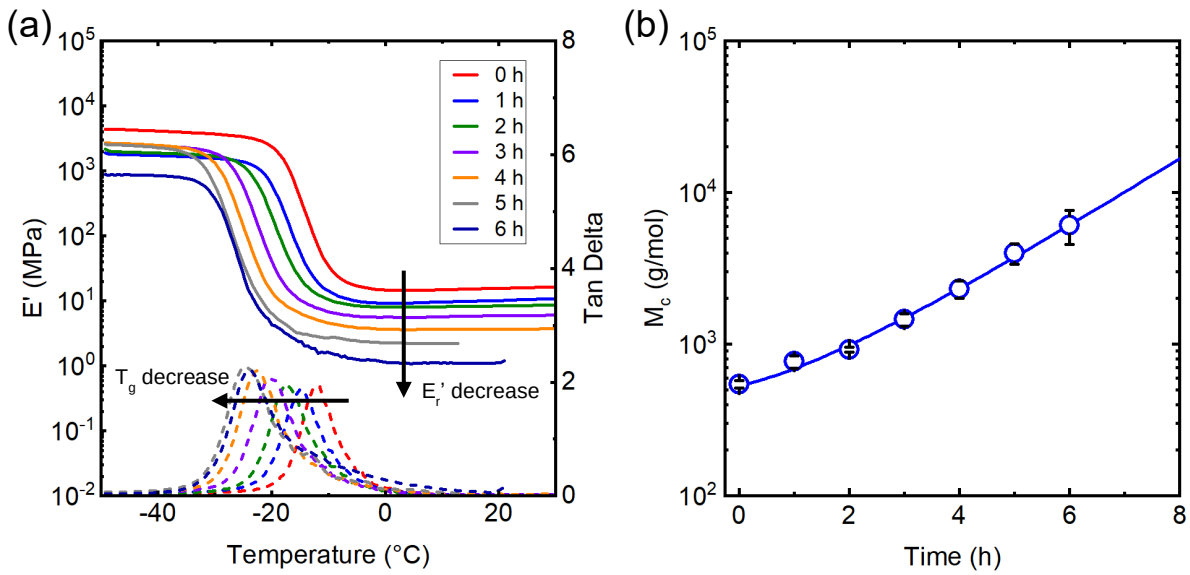

Figure 3.3. T_g and M_c measurements suggested thioester networks underwent bulk degradation. (a) Plot comparing storage modulus and tan delta with temperature, repeated for various film degradation times, shows increased degradation time lowered T_g and E_r' of films which was typical of bulk degradation. (b) Plot comparing $\boldsymbol{M_c}$ with film degradation time shows model prediction (line) matched experimental data (markers) well. The model prediction used equation S4 in the SI, for a $Z = 4$ network where rate constant $k = 0.0051 \pm 0.0001$ $M^{-1}min^{-1}$ including standard error.

Comparisons of characteristic reaction and diffusion times and mass swelling ratio of thin films also supported the claim that these thioester networks underwent bulk degradation. The characteristic reaction time was ≈100 times larger than diffusion time (420 minutes and 5 minutes, respectively) which suggested a reaction-limited process (SI Section 3.8.2.3). The mass swelling ratio of the thin films increased up to 20 during degradation, which also suggested cleavage of crosslinks within the polymer network as is characteristic of bulk degradation (**Figure S3.2** in the SI).

3.4.3 Verification of Model

To validate the derived bulk-degradation model, the predicted mass loss as a function of three process variables was compared to experiment: the initial free thiol concentration, the initial molar ratio of thiol to base, and the monomer functionality, *Z*. Changing the multifunctional thiol monomer used to create these networks allowed *Z* to range from 3 - 6 (**Figure 3.1b**).

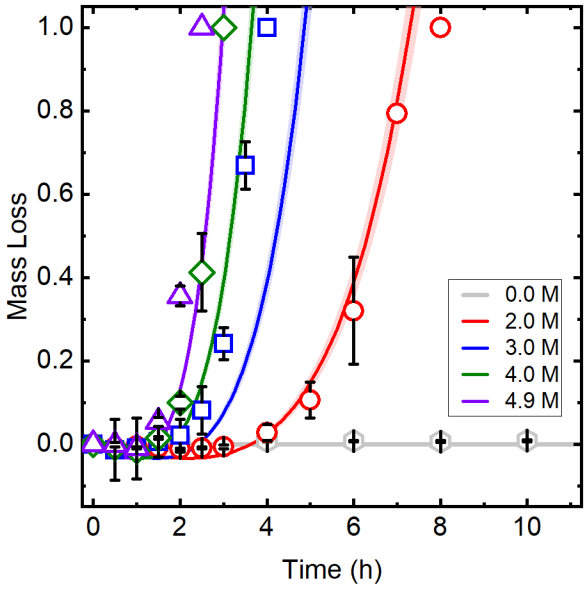

Figure 3.4. Higher concentration of thiol in the degrading solution led to faster mass loss. Mass loss plotted versus time shows model predictions (lines with error bands) and experimental data

(markers with error bars) matched well for BMP concentrations ranging from 0.0 M to 4.9 M. Rate constant value used for the model fit was $k = 0.0042 \pm 0.0001$ $M^{-1}min^{-1}$ including standard error. Error bands on model predictions are error propagated from standard error on k, and error bars on experimental data are standard deviation.

3.4.3.1 Free Thiol Concentration

As the initial concentration of free thiol increased, so too did the rate of mass loss. The data in **Figure 3.4** show how mass loss changed as a function of initial concentration of free thiol BMP, which ranged from 0.0M to 4.9M, at a constant ratio of 30 mol% TEA. The 0.0M sample served as a control with no free thiol added but TEA was included at a concentration that matched the TEA content of the 2.0M BMP sample in acetone. As thiol concentration increased, the total time for mass loss decreased from ≈8 h to ≈2.5 h for the 2.0M to 4.9M samples. Experimental data matched model predictions well, and as predicted at early degradation times, a small amount of mass gain was experimentally observed. Despite having different concentrations of BMP and thus different degradation times, the 2.0M to 4.9M samples all had a Z value of 4 and thus experienced the same net mass loss at the same probability of degradation, *P*, as shown in **Figure 3.2c**. Furthermore, the critical probability at which total mass loss was achieved, P_c, was 0.67 for all samples (equation 5). These model predictions are useful to determine the degradation conditions required to fully degrade a thioester network after a specific amount of time.

The second order reaction rate constant *k* was used as a fitting parameter to compare model predictions with experimental results. As such, k is not a function of thiolate concentration, and all experimental data were fit to a single value of k. **Figure 3.4** shows that a *k* value of 0.0042 ± 0.0001 $M^{-1}min^{-1}$, including standard error, predicted experimental mass loss well for all of the conditions assessed here. Model predictions for the 3.0 – 4.9 M samples deviated from experimental results more, likely due to the convolution of the measured reaction rate constant

with mass transport limitations of large oligomers diffusing out of the degrading polymer network. Nevertheless, the *k* value from **Figure 3.4** was similar to the **Figure 3.3b** value, 0.0042 versus 0.0051 $M^{-1}min^{-1}$, and lies closer to previously reported reaction rate constant values for uncatalyzed thiol-thioester exchange in small molecule aqueous systems ($k \approx 10^{-5}$ $M^{-1}min^{-1}$)[40] than to catalyzed exchange in small molecule systems ($k \approx 10^{3}$ $M^{-1}min^{-1}$).[41,42] This decrease was likely due to the limited mobility of thiolates in polymeric systems and the lack of a polar protic solvent to stabilize thiol-thioester exchange.[16]

3.4.3.2 Ratio of Base Catalyst

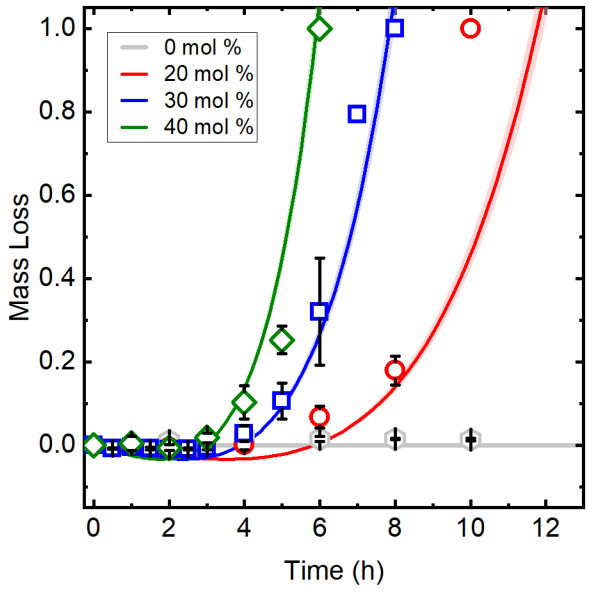

Figure 3.5. Higher molar ratio of base to thiol in the degrading solution led to faster mass loss. Mass loss plotted versus time shows model predictions (lines with error bands) and experimental data (markers with error bars) matched well as TEA molar ratio increased from 0 to 40 mol%. Rate constant value used for model fit was $k = 0.0039 \pm 0.0001$ $M^{-1}min^{-1}$ including standard error. Error bands on model predictions are error propagated from standard error on k, and error bars on experimental data are standard deviation.

As the ratio of base increased, the mass loss rate also increased. **Figure 3.5** shows data for how the mass loss changed as a function of the TEA mol ratio, going from 0 mol% to 40 mol%, while

keeping the BMP concentration at 2.0M. The 0 mol% sample served as a control: no TEA was added but 2.0M BMP in acetone was still included. As the ratio of base to thiol increased from 20 mol% to 40 mol%, the total time for polymer degradation decreased from ≈10 h to ≈6 h. Experimental data matched model predictions well, and similar to **Figure 3.4** at early degradation times a small amount of mass gain was observed. Also similar to **Figure 3.4**, even though the 20 to 40 mol% samples had varying amounts of TEA, all were $Z = 4$ networks and followed the same net mass loss profile depicted in **Figure 3.2c** and achieved total mass loss at $P_c = 0.67$ (equation 5). Lastly, fitting the model prediction to experimental data in **Figure 3.5** resulted in a rate constant k of 0.0039 ± 0.0001 $M^{-1}min^{-1}$ including standard error, which was similar in value to previous experiments as changing the molar ratio of base catalyst to free thiol should not impact the intrinsic reaction rate constant of thiol-thioester exchange.

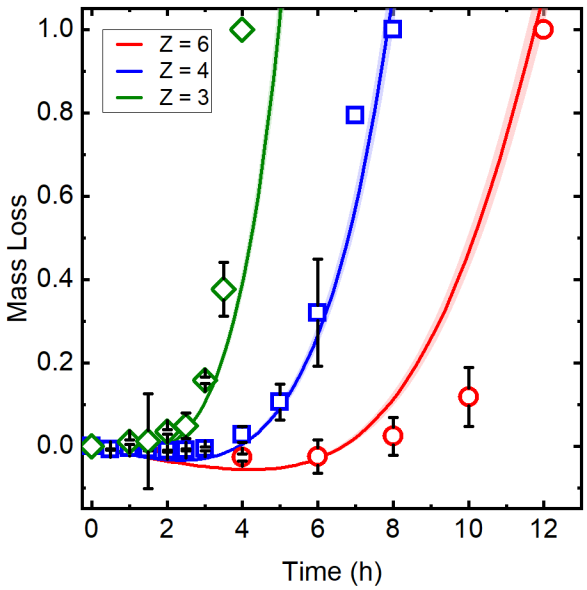

Figure 3.6. A greater number of functional groups in the network structure led to slower mass loss. Mass loss plotted versus time shows model predictions (lines with error bands) and experimental data (markers with error bars) matched well for monomer functionality Z when it ranged from 3 to 6. Rate constant value used for model fit was k = 0.0039 ± 0.0001 $M^{-1}min^{-1}$ including standard error. Error bands on model predictions are error propagated from standard error on k, and error bars on experimental data are standard deviation.

3.4.3.3 Monomer Functionality

Increasing monomer functionality, *Z*, resulted in slower mass loss. The data in **Figure 3.6** show how the mass loss changed as a function of *Z*, where *Z* ranged from 3 to 6, while using 2.0M BMP and 30 mol% TEA for the degradation solution. Each value of *Z* came from a different thiol-ene network, where TMPTMP (*Z* = 3), PETMP (*Z* = 4), or diPETMP (*Z* = 6) were reacted with TEDE to make these networks. As *Z* increased from 3 to 6, the total time for the polymer network to degrade increased from ≈4 h to ≈12 h. Experimental data matched model predictions well, and the *Z* = 6 sample experienced the most mass gain as predicted by the model, reaching approximately 3 %.

Unlike **Figures 3.4** and **3.5**, each sample in **Figure 6** was modelled by a different mass loss equation, as shown in **Figure 3.2c**. As such, each sample had a distinct value of P_c (equation 5): for *Z* = 3, 4, and 6 P_c equaled 0.5, 0.67, and 0.8, respectively. Larger values of Z resulted in higher P_c values because larger *Z* networks have a greater number of arms connected to each crosslink, and as such a higher fraction of thioester groups must cleave before crosslinks fully disconnect and a repeat unit leaves the network. Because of this, a *Z* = 3 network will achieve greater mass loss than a *Z* = 6 network when the same probability of thioester groups cleaving, *P*, is reached. Despite the variation in network structure, the model predictions for all samples yielded a similar value for rate constant *k*, 0.0039 ± 0.0001 $M^{-1}min^{-1}$ including standard error, suggesting that changes in the polymer network structure had little effect on the reaction rate constant of thiol-thioester exchange.

3.4.4 3-D Printing Thioesters

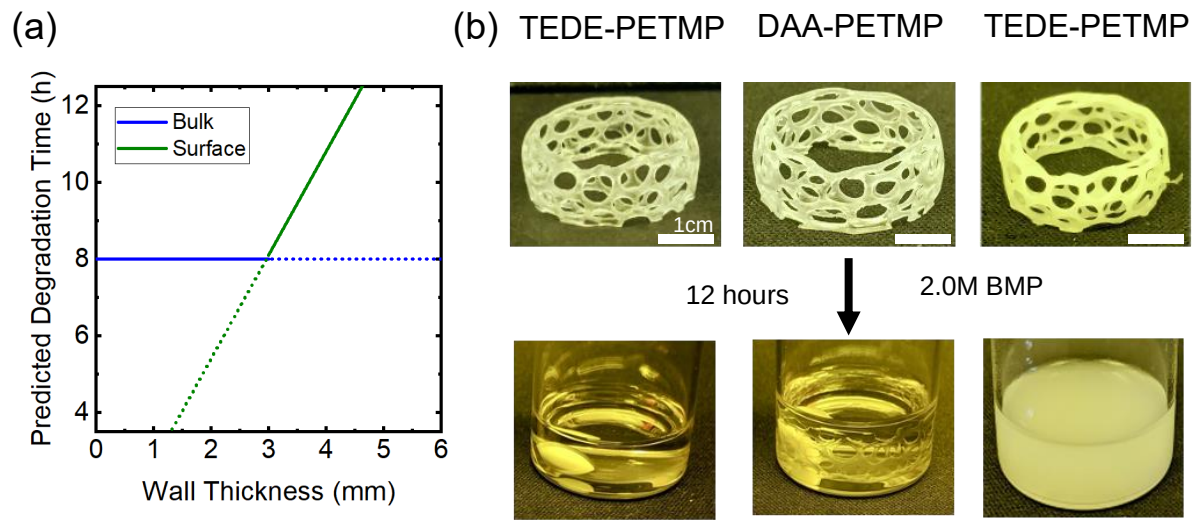

Figure 3.7. Selective degradation of a thioester network enabled recovery of fillers in 3-D printed thioester composites. (a) Predicted time for a thioester network to fully degrade plotted versus network thickness, using bulk and surface degradation models. Below 3 mm degradation time was predicted to be constant. (b) SLA 3-D printed rings composed of various polymer networks (*top*), with part thickness in the bulk degrading regime, were exposed to a degrading solution (*bottom*). The TEDE-PETMP composite contained 20 weight % of 6-10 μm poly(styrene-co-divinylbenzene) microspheres.

To broaden the scope of these thioester-containing CANs toward industrial applications, SLA 3-D printed thioester networks were investigated. As 3-D printed structures may vary in thickness, and thickness impacts characteristic diffusion time and thus the degradation process, the effect of wall thickness in degrading thioester CANs was studied.

Figure 3.7a shows model predictions for how time to achieve complete degradation varied with wall thickness when 3-D printed parts were soaked in 2.0M BMP, 30 mol% TEA degrading solution. Far below the 3 mm wall thickness, bulk degradation dominated as characteristic diffusion time was significantly lower than reaction time. Since bulk degradation occurs simultaneously throughout a polymer network, the time to reach complete degradation was independent of wall thickness and remained a constant 8 hours. Far above 3 mm wall thickness, surface degradation dominated as the characteristic reaction time was then significantly lower than

the diffusion time. Using the Hopfenberg model,[43] degradation time in the surface degrading regime was predicted to increase linearly with wall thickness, and this rate of increase was driven by the rate of height change of a 1-D polymer slab. Surface degradation carried out on 5 mm thick, 3-D printed slabs of TEDE-PETMP showed height decreases of 0.37 ± 0.02 mm / hour, meaning that in the surface degrading regime degradation time increased with wall thickness at a rate of 2.7 ± 0.15 hours / mm (**Figure S3.5** in the SI). At approximately 3 mm wall thickness, both models converged and network dissolution was a function of both bulk and surface degradation. Following the models described in **Figure 3.7a**, one may broaden the design of degradable thioester structures by combining the 3mm (or other) critical length scale with the two other parameters investigated by this work (i.e., the composition of the degrading solution and the polymer network structure). This approach would enable the creation of multi-stage degrading 3-D printed networks, where degradation regimes and time scales would be controlled by wall thickness, degradation conditions, and the network structure.

Using the degradation regime predictions from **Figure 3.7a**, network dissolution of 3-D printed thioester-containing and 3-D printed thioester-devoid chemistries in the bulk degrading regime were investigated. Voronoi-style lattice rings with strut lengths varying from 0.5 to 2.0 mm and with a consistent strut depth of 0.6 mm were SLA 3-D printed to exhibit the complex structures and rapid production times enabled by additive manufacturing. Since all struts were 0.6 mm deep, this value was used as wall thickness, which was well below the 3 mm threshold and ensured degradation in the bulk degrading regime. **Figure 3.7b** shows how the rings, composed of three different networks, behaved after a 12-hour soak in the degrading solution previously used for thin film studies (2.0M BMP, 30 mol% TEA). Networks that contained thioester groups readily dissolved, while networks without the thioester groups were unaffected. Thioester composites

containing 20 weight % of 6-10 μm poly(styrene-co-divinylbenzene) microspheres degraded similar to neat networks. Centrifuging the degraded composite solution allowed recovery of 91 ± 1.4% of the microspheres, showing efficient recovery of fillers in thioester composites. Unlike composite degradation via other CAN chemistries, thiol-thioester degradation occurred rapidly at room temperature within hours, not days,[44,45] and this dissolution time may be even further reduced through several means such as using a more basic catalyst (diazabicycloundec-7-ene), a more polar solvent (methanol), a more reactive monothiol (methyl thioglycolate), a lower Z monomer (Z = 3), or by increasing the temperature of the reaction above room temperature.[16] Beyond this work, one could explore the regions where both reaction and diffusion mechanisms are at play for degradation, and how 3-D printed multi-stage degrading parts may be used to investigate the models developed in this work or other mixed-mode models.[27,28]

3.5 Conclusions

This work investigated degradation kinetics based on thiol-thioester exchange for thioester-containing networks. By means of a theoretical model, derived from the reaction kinetics and the polymer network structure, mass gain from the thiol molecules adding into the network and net mass loss from crosslinks cleaving were predicted and experimentally verified by mass loss studies. Reaction rate constants, *k*, used as a fitting parameter for the derived model, were found to range from 0.0039 to 0.0051 $M^{-1}min^{-1}$ and fit within previously reported values. Further investigations on exchange kinetics and network structure found that increasing the concentration of free thiol, the ratio of base to thiol, or decreasing monomer functionality sped up the mass loss rate. Lastly, SLA 3-D printed thioester composites showed that thioester-containing CANs

selectively degraded to allow recovery of 91% of the filler in a composite, paving the way for thioester-facilitated filler recovery.

Beyond the degradation of thioester-containing CANs, the work herein expands the general understanding of dynamic bond-exchange based bulk degradation and the use of thermosetting polymers for material recovery. The model derived in this work presents a new method to account for mass gain due to reversible exchange during degradation and is anticipated to be applicable to various dynamic chemistries and CANs applications. The presented procedure to degrade 3-D printed composites establishes a new method to create degradable thermoset composites and controllably recover fillers from these thermosets on an industrial scale. Altogether, this work shows the versatility of CANs for selective degradation and material recovery applications.

3.6 Acknowledgements

This work was made possible by funding from the Graduate Assistance in Areas of National Need (GAANN) and a National Science Foundation's Grant DMR 1809841. A.S.K acknowledges support from an Arnold O. Beckman Postdoctoral Fellowship.

3.7 References

(1) Barnes, D. K. A.; Galgani, F.; Thompson, R. C.; Barlaz, M. Accumulation and Fragmentation of Plastic Debris in Global Environments. *Philos. Trans. R. Soc. B Biol. Sci.* **2009**, *364* (1526), 1985–1998. https://doi.org/10.1098/rstb.2008.0205.

(2) Pickering, S. J. Recycling Technologies for Thermoset Composite Materials-Current Status. *Compos. Part A Appl. Sci. Manuf.* **2006**, *37* (8), 1206–1215. https://doi.org/10.1016/j.compositesa.2005.05.030.

(3) Kloxin, C. J.; Bowman, C. N. Covalent Adaptable Networks: Smart, Reconfigurable and Responsive Network Systems. *Chem. Soc. Rev.* **2013**, *42* (17), 7161–7173. https://doi.org/10.1039/c3cs60046g.

(4) Podgórski, M.; Fairbanks, B. D.; Kirkpatrick, B. E.; McBride, M.; Martinez, A.; Dobson, A.; Bongiardina, N. J.; Bowman, C. N. Toward Stimuli-Responsive Dynamic Thermosets through Continuous Development and Improvements in Covalent Adaptable Networks (CANs). *Adv. Mater.* **2020**, *32* (20), 1–26. https://doi.org/10.1002/adma.201906876.

(5) Nimmo, C. M.; Owen, S. C.; Shoichet, M. S. Diels-Alder Click Cross-Linked Hyaluronic Acid Hydrogels for Tissue Engineering. *Biomacromolecules* **2011**, *12* (3), 824–830. https://doi.org/10.1021/bm101446k.

(6) Chao, A.; Negulescu, I.; Zhang, D. Dynamic Covalent Polymer Networks Based on Degenerative Imine Bond Exchange: Tuning the Malleability and Self-Healing Properties by Solvent. *Macromolecules* **2016**, *49* (17), 6277–6284. https://doi.org/10.1021/acs.macromol.6b01443.

(7) Kuang, X.; Zhou, Y.; Shi, Q.; Wang, T.; Qi, H. J. Recycling of Epoxy Thermoset and Composites via Good Solvent Assisted and Small Molecules Participated Exchange Reactions. *ACS Sustain. Chem. Eng.* **2018**, *6* (7), 9189–9197. https://doi.org/10.1021/acssuschemeng.8b01538.

(8) Wang, C.; Goldman, T. M.; Worrell, B. T.; McBride, M. K.; Alim, M. D.; Bowman, C. N. Recyclable and Repolymerizable Thiol-X Photopolymers. *Mater. Horizons* **2018**, *5* (6), 1042–1046. https://doi.org/10.1039/c8mh00724a.

(9) Melchor Bañales, A. J.; Larsen, M. B. Thermal Guanidine Metathesis for Covalent Adaptable Networks. *ACS Macro Lett.* **2020**, *9* (7), 937–943. https://doi.org/10.1021/acsmacrolett.0c00352.

(10) Shi, Q.; Yu, K.; Kuang, X.; Mu, X.; Dunn, C. K.; Dunn, M. L.; Wang, T.; Jerry Qi, H. Recyclable 3D Printing of Vitrimer Epoxy. *Mater. Horizons* **2017**, *4* (4), 598–607. https://doi.org/10.1039/c7mh00043j.

(11) Yu, K.; Xin, A.; Du, H.; Li, Y.; Wang, Q. Additive Manufacturing of Self-Healing Elastomers. *NPG Asia Mater.* **2019**, *11* (1). https://doi.org/10.1038/s41427-019-0109-y.

(12) Li, X.; Yu, R.; He, Y.; Zhang, Y.; Yang, X.; Zhao, X.; Huang, W. Self-Healing Polyurethane Elastomers Based on a Disulfide Bond by Digital Light Processing 3D Printing. *ACS Macro Lett.* **2019**, *8* (11), 1511–1516. https://doi.org/10.1021/acsmacrolett.9b00766.

(13) Bagheri, A.; Ling, H.; Bainbridge, C. W. A.; Jin, J. Living Polymer Networks Based on a RAFT Cross-Linker: Toward 3D and 4D Printing Applications. *ACS Appl. Polym. Mater.* **2021**, *3* (6), 2921–2930. https://doi.org/10.1021/acsapm.1c00048.

(14) Göpferich, A. Mechanisms of Polymer Degradation and Erosion. *Biomater. Silver Jubil. Compend.* **1996**, *17* (2), 117–128. https://doi.org/10.1016/B978-008045154-1.50016-2.

(15) Burkersroda, F. Von; Schedl, L.; Göpferich, A. Why Degradable Polymers Undergo Surface

Erosion or Bulk Erosion. *Biomaterials* **2002**, *23* (21), 4221–4231. https://doi.org/10.1016/S0142-9612(02)00170-9.

(16) Worrell, B. T.; Mavila, S.; Wang, C.; Kontour, T. M.; Lim, C. H.; McBride, M. K.; Musgrave, C. B.; Shoemaker, R.; Bowman, C. N. A User's Guide to the Thiol-Thioester Exchange in Organic Media: Scope, Limitations, and Applications in Material Science. *Polym. Chem.* **2018**, *9* (36), 4523–4534. https://doi.org/10.1039/c8py01031e.

(17) Ishibashi, J. S. A.; Kalow, J. A. Vitrimeric Silicone Elastomers Enabled by Dynamic Meldrum's Acid-Derived Cross-Links. *ACS Macro Lett.* **2018**, *7* (4), 482–486. https://doi.org/10.1021/acsmacrolett.8b00166.

(18) El-Zaatari, B. M.; Ishibashi, J. S. A.; Kalow, J. A. Cross-Linker Control of Vitrimer Flow. *Polym. Chem.* **2020**, *11* (33), 5339–5345. https://doi.org/10.1039/d0py00233j.

(19) Fairbanks, B. D.; Scott, T. F.; Kloxin, C. J.; Anseth, K. S.; Bowman, C. N. Thiol-Yne Photopolymerizations: Novel Mechanism, Kinetics, and Step-Growth Formation of Highly Cross-Linked Networks. *Macromolecules* **2009**, *42* (1), 211–217. https://doi.org/10.1021/ma801903w.

(20) Van Herck, N.; Maes, D.; Unal, K.; Guerre, M.; Winne, J. M.; Du Prez, F. E. Covalent Adaptable Networks with Tunable Exchange Rates Based on Reversible Thiol–Yne Cross-Linking. *Angew. Chemie - Int. Ed.* **2020**, *59* (9), 3609–3617. https://doi.org/10.1002/anie.201912902.

(21) Ghobril, C.; Charoen, K.; Rodriguez, E. K.; Nazarian, A.; Grinstaff, M. W. A Dendritic Thioester Hydrogel Based on Thiol-Thioester Exchange as a Dissolvable Sealant System for Wound Closure. *Angew. Chemie - Int. Ed.* **2013**, *52* (52), 14070–14074. https://doi.org/10.1002/anie.201308007.

(22) Pietrocola, F.; Galluzzi, L.; Bravo-San Pedro, J. M.; Madeo, F.; Kroemer, G. Acetyl Coenzyme A: A Central Metabolite and Second Messenger. *Cell Metab.* **2015**, *21* (6), 805–821. https://doi.org/10.1016/j.cmet.2015.05.014.

(23) Carberry, B. J.; Hergert, J. E.; Yavitt, F. M.; Hernandez, J. J.; Speckl, K. F.; Bowman, C. N.; McLeod, R. R.; Anseth, K. S. 3D Printing of Sacrificial Thioester Elastomers Using Digital Light Processing for Templating 3D Organoid Structures in Soft Biomatrices. *Biofabrication* **2021**, *13* (4). https://doi.org/10.1088/1758-5090/ac1c98.

(24) Podgórski, M.; Huang, S.; Bowman, C. N. Additive Manufacture of Dynamic Thiol-Ene Networks Incorporating Anhydride-Derived Reversible Thioester Links. *ACS Appl. Mater. Interfaces* **2021**, *13* (11), 12789–12796. https://doi.org/10.1021/acsami.0c18979.

(25) Yu, K.; Yang, H.; Dao, B. H.; Shi, Q.; Yakacki, C. M. Dissolution of Covalent Adaptable Network Polymers in Organic Solvent. *J. Mech. Phys. Solids* **2017**, *109*, 78–94. https://doi.org/10.1016/j.jmps.2017.08.006.

(26) Kuang, X.; Shi, Q.; Zhou, Y.; Zhao, Z.; Wang, T.; Qi, H. J. Dissolution of Epoxy Thermosets: Via Mild Alcoholysis: The Mechanism and Kinetics Study. *RSC Adv.* **2018**, *8* (3), 1493–1502. https://doi.org/10.1039/c7ra12787a.

(27) Hamel, C. M.; Kuang, X.; Chen, K.; Qi, H. J. Reaction-Diffusion Model for Thermosetting Polymer Dissolution through Exchange Reactions Assisted by Small-Molecule Solvents. *Macromolecules* **2019**, *52* (10), 3636–3645. https://doi.org/10.1021/acs.macromol.9b00540.

(28) Marco-Dufort, B.; Willi, J.; Vielba-Gomez, F.; Gatti, F.; Tibbitt, M. W. Environment Controls Biomolecule Release from Dynamic Covalent Hydrogels. *Biomacromolecules* **2021**, *22* (1), 146–157. https://doi.org/10.1021/acs.biomac.0c00895.

(29) Metters, A. T.; Bowman, C. N.; Anseth, K. S. A Statistical Kinetic Model for the Bulk Degradation of PLA-b-PEG-b-PLA Hydrogel Networks. *J. Phys. Chem. B* **2000**, *104* (30), 7043–7049. https://doi.org/10.1021/jp000523t.
(30) Martens, P.; Metters, A. T.; Anseth, K. S.; Bowman, C. N. A Generalized Bulk-Degradation Model for Hydrogel Networks Formed from Multivinyl Cross-Linking Molecules. *J. Phys. Chem. B* **2001**, *105* (22), 5131–5138. https://doi.org/10.1021/jp004102n.
(31) Metters, A.; Hubbell, J. Network Formation and Degradation Behavior of Hydrogels Formed by Michael-Type Addition Reactions. *Biomacromolecules* **2005**, *6* (1), 290–301. https://doi.org/10.1021/bm049607o.
(32) Rydholm, A. E.; Reddy, S. K.; Anseth, K. S.; Bowman, C. N. Development and Characterization of Degradable Thiol-Allyl Ether Photopolymers. *Polymer (Guildf).* **2007**, *48* (15), 4589–4600. https://doi.org/10.1016/j.polymer.2007.05.063.
(33) Shih, H.; Lin, C. C. Cross-Linking and Degradation of Step-Growth Hydrogels Formed by Thiol-Ene Photoclick Chemistry. *Biomacromolecules* **2012**, *13* (7), 2003–2012. https://doi.org/10.1021/bm300752j.
(34) Worrell, B. T.; McBride, M. K.; Lyon, G. B.; Cox, L. M.; Wang, C.; Mavila, S.; Lim, C. H.; Coley, H. M.; Musgrave, C. B.; Ding, Y.; Bowman, C. N. Bistable and Photoswitchable States of Matter. *Nat. Commun.* **2018**, *9*, 1–7. https://doi.org/10.1038/s41467-018-05300-7.
(35) Long, T. R.; Elder, R. M.; Bain, E. D.; Masser, K. A.; Sirk, T. W.; Yu, J. H.; Knorr, D. B.; Lenhart, J. L. Influence of Molecular Weight between Crosslinks on the Mechanical Properties of Polymers Formed: Via Ring-Opening Metathesis. *Soft Matter* **2018**, *14* (17), 3344–3360. https://doi.org/10.1039/c7sm02407j.
(36) Macosko, C. W.; Miller, D. R. A New Derivation of Average Molecular Weights of Nonlinear Polymers. *Macromolecules* **1976**, *9* (2), 199–206. https://doi.org/10.1021/ma60050a003.
(37) Hiemenz, P. C.; Lodge, T. P. *Polymer Chemistry Second Edition*; CRC Press Taylor & Francis Group, 2007. https://doi.org/10.1201/9781420018271-4.
(38) Flory, P. J. Molecular Size Distribution in Three Dimensional Polymers. I. Gelation1. *J. Am. Chem. Soc.* **1941**, *63* (11), 3083–3090. https://doi.org/10.1021/ja01131a008.
(39) Chen, J. S.; Ober, C. K.; Poliks, M. D.; Zhang, Y.; Wiesner, U.; Cohen, C. Controlled Degradation of Epoxy Networks: Analysis of Crosslink Density and Glass Transition Temperature Changes in Thermally Reworkable Thermosets. *Polymer (Guildf).* **2004**, *45* (6), 1939–1950. https://doi.org/10.1016/j.polymer.2004.01.011.
(40) Cargoët, M.; Diemer, V.; Snella, B.; Desmet, R.; Blanpain, A.; Drobecq, H.; Agouridas, V.; Melnyk, O. Catalysis of Thiol-Thioester Exchange by Water-Soluble Alkyldiselenols Applied to the Synthesis of Peptide Thioesters and SEA-Mediated Ligation. *J. Org. Chem.* **2018**, *83* (20), 12584–12594. https://doi.org/10.1021/acs.joc.8b01903.
(41) Bracher, P. J.; Snyder, P. W.; Bohall, B. R.; Whitesides, G. M. The Relative Rates of Thiol-Thioester Exchange and Hydrolysis for Alkyl and Aryl Thioalkanoates in Water. *Orig. Life Evol. Biosph.* **2011**, *41* (5), 399–412. https://doi.org/10.1007/s11084-011-9243-4.
(42) Um, I. H.; Lee, J. Y.; Bae, S. Y.; Buncel, E. Effect of Modification of the Electrophilic Center on the α Effect. *Can. J. Chem.* **2005**, *83* (9), 1365–1371. https://doi.org/10.1139/v05-157.
(43) Hopfenberg, H. B. Controlled Release from Erodible Slabs, Cylinders, and Spheres. In *Am Chem Soc Div Org Coat Plast Chem Prepr*; 1976; Vol. 36, pp 26–32. https://doi.org/10.1021/bk-1976-0033.ch003.

(44) Yu, K.; Shi, Q.; Dunn, M. L.; Wang, T.; Qi, H. J. Carbon Fiber Reinforced Thermoset Composite with Near 100% Recyclability. *Adv. Funct. Mater.* **2016**, *26* (33), 6098–6106. https://doi.org/10.1002/adfm.201602056.
(45) Taynton, P.; Ni, H.; Zhu, C.; Yu, K.; Loob, S.; Jin, Y.; Qi, H. J.; Zhang, W. Repairable Woven Carbon Fiber Composites with Full Recyclability Enabled by Malleable Polyimine Networks. *Adv. Mater.* **2016**, *28* (15), 2904–2909. https://doi.org/10.1002/adma.201505245.

3.8 Supporting Information

3.8.1 Supporting Tables and Figures

Table S3.1. 3-D printing parameters used to print thioester (TEDE-PETMP), control (DAA-PETMP), and thioester composite (TEDE-PETMP-20wt%PS) rings on a Prusa SL1 3-D printer.

Material	Initial layer time (s)	Other layer time (s)	Layer Height (μm)	E_c ($\frac{mJ}{cm^2}$)	D_P (μm)
Thioester	35	10	100	1.7	335
Control	35	13	100	1.5	453
Composite	35	12	100	1.6	478

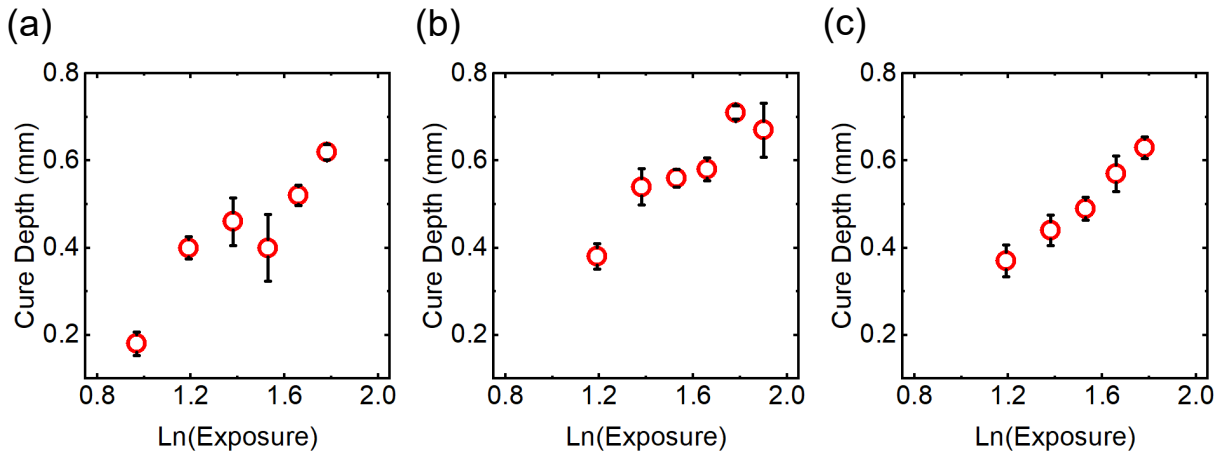

Figure S3.1. E_cD_p curves used to 3-D print (a) thioester (TEDE-PETMP), (b) thioester composite (TEDE-PETMP-20wt%PS), and (c) control (DAA-PETMP) rings.

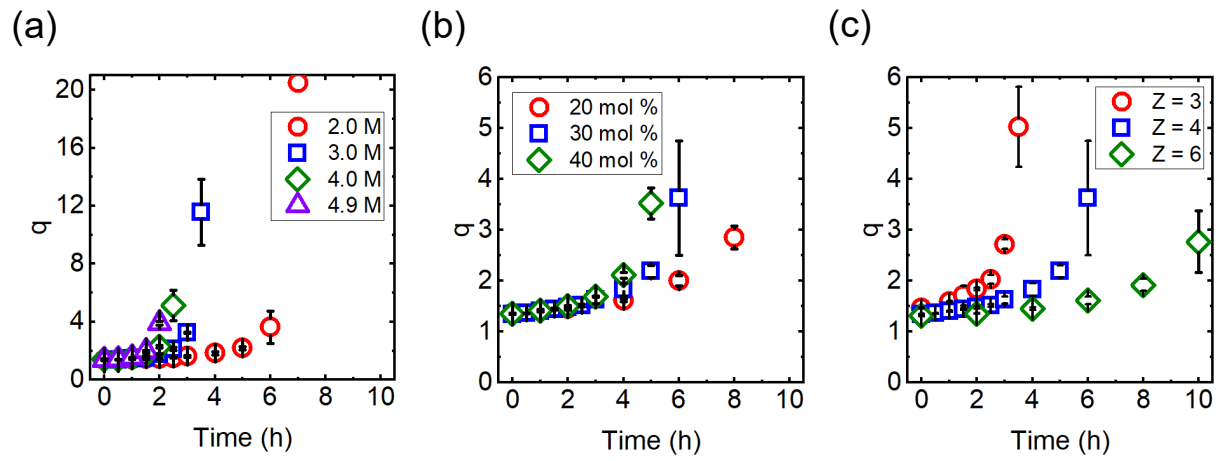

Figure S3.2. Mass swelling ratio, $\boldsymbol{q}$, as a function of (a) concentration of free thiol BMP, (b) TEA mol ratio, and (c) monomer functionality *Z*. Samples were repeated in triplicate.

Mass swelling ratio, q, was calculated by

$$q = \frac{m_{deg}}{m_{final}} \qquad \text{(S2)}$$

where m_{deg} stands for the mass of thin films after the films were removed from degradation solution and patted dry with a Kimwipe, and m_{final} is the mass of thin films after degradation and drying in a vacuum oven.[1]

Figure S3.3. Five thin films were degraded in a Petri dish at once, with each film sitting atop a steel mesh at a marked location. The Petri dish was covered with parafilm to prevent solvent evaporation.

Degradation proceeded in covered 100 x 50 mm Pyrex Petri dishes (Figure S3). A stainless-steel mesh was placed on the bottom of the Petri dishes, allowing for a stir bar to spin at 400 RPM to let degrading solution flow above and below thin films. Acetone was used as a co-solvent as polar solvents stabilize thiol-thioester exchange.[2,3] The concentration of acetone-BMP solutions for soaking films prior to degradation was the same as degradation conditions studied but omitted TEA (e.g. to test 4.0M BMP with 30 mol% TEA the appropriate volumes of acetone and BMP were added to the dish, while omitting TEA).

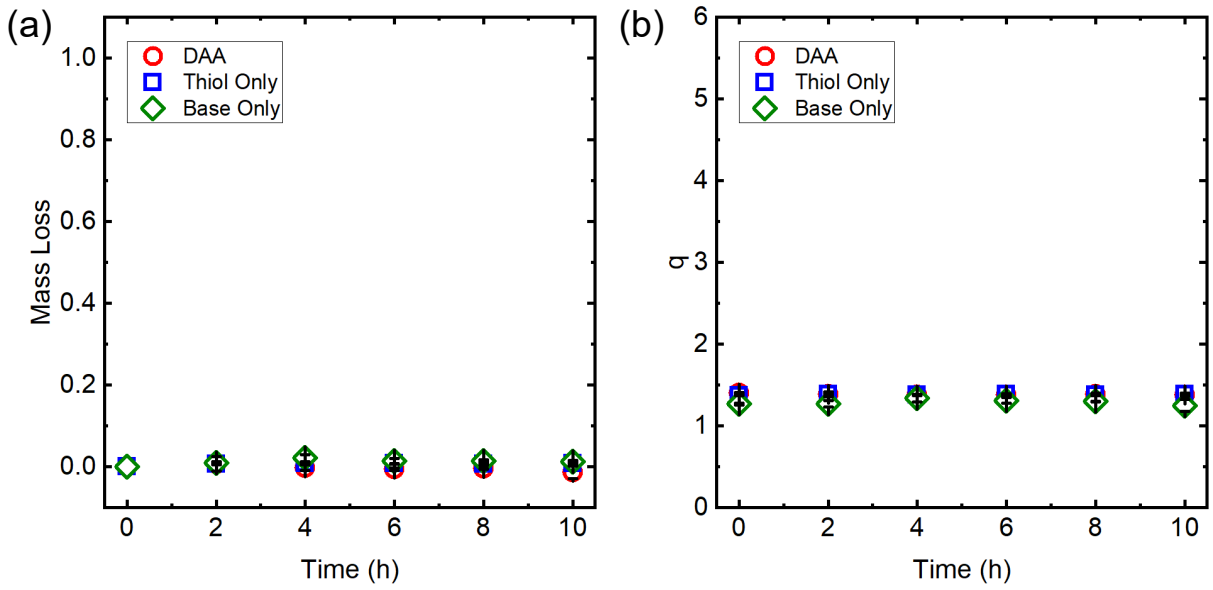

Figure S3.4. Control experiments for thiol-thioester exchange-facilitated degradation show that all three components (thioester groups, free thiol, and base catalyst) were required for a network to undergo significant degradation. "DAA" was a DAA-PETMP network degraded in a solution of 4.9M BMP and 30 mol % TEA, "Thiol only" a TEDE-PETMP network degraded in 4.9M BMP without base, and "Base only" a TEDE-PETMP network degraded in 30 mol % TEA (1.5M TEA) without free thiol. (a) Mass loss over time for different control scenarios. (b) Mass swelling ratio over time for different control scenarios.

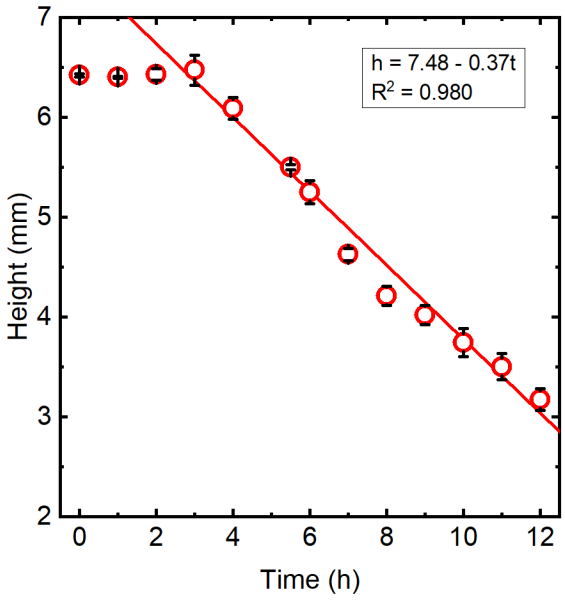

Figure S3.5. Surface degradation of 3-D printed slabs composed of TEDE-PETMP. The slabs exhibited a linear height decrease of 0.37 ± 0.02 mm / hour, including standard error, when placed in a 2.0M BMP, 30 mol % TEA degrading solution.

A surface degradation model for thiol-thioester exchange facilitated degradation was developed by utilizing 1-D slabs. The 1-D slabs experienced mass loss through changes in height, making fractional mass loss:

$$ML_{1-D} = \frac{m_0 - m_t}{m_0} = \frac{h_0 - h_t}{h_0}$$

where m_0 is initial mass, m_t is mass at time t, h_0 is initial slab height, and h_t is slab height at time t.[10] From Hopfenberg,[11] height of a slab as a function of time can be said to be controlled by a zero-order process and thus changes proportionally with time:

$$h_t = h_0 - Ct$$

where C is an empirically-determined lump sum constant with units of distance / time and depends heavily on degradation conditions. Combining the two equations above, recognizing that when slabs achieved complete degradation ML_{1-D} = 1, and rearranging, the time for a 1-D slab to completely degrade via surface degradation was:

$$t_{degrade} = \frac{h_0}{C}$$

To determine the lump sum constant C, which was specific to degrading thioester networks via thiol-thioester exchange, three SLA 3-D printed 5 x 50 x 50 mm slabs were degraded in a solution of 2.0M BMP, 30 mol % TEA. The slabs were first swelled in an acetone-BMP bath overnight to reach equilibrium swelling, resulting in a starting height of 6.40 mm. Degradation began by adding TEA. Measuring the height of slabs every hour, and fitting the data to the equation for h_t yielded a value of 0.37 ± 0.02 mm / hour for C (Figure S5).

3.8.2 Derivations

3.8.2.1 Concentration of Thiolate

The equilibrium constant for acid-base reactions was calculated as 10 raised to the difference between the pKa's of the two reactants. Combining that relationship with the definition that an equilibrium constant equals the concentration of products over the concentration of reactants for an ideal solution, the pKa's of the acid-base reaction were related to equilibrium concentrations of products and reactants via:

$$10^{\Delta pKa} = K_{eq} = \frac{[S^-][BH^+]}{[SH][B]} = \frac{[S^-]^2}{([SH]_o - [S^-])([B]_o - [S^-])} \qquad \text{(S3)}$$

3.8.2.2 Molecular Weight Between Crosslinks

Metters and co-workers developed a bulk degradation model that predicts molecular weight between crosslinks, M_c, as

$$M_c = \frac{Z * M_{c,inilal}}{\sum_{i=3}^{Z} i * F_{i,Z}} \quad \text{(S4)}$$

where Z stands for monomer functionality, i the number of arms per crosslink considered to be attached to the network, and $F_{i,Z}$ the fraction of elastically active crosslinks with i number of arms still attached to the network.[4] The sum in equation S4 starts with $i = 3$ because each crosslink needs at least 3 arms still attached to the network to be elastically active. $F_{i,Z}$ is calculated by

$$F_{i,Z} = \frac{Z!}{(Z-i)!i!} P^{(Z-i)}(1-P)^i \quad \text{(S5)}$$

and shows that $F_{i,Z}$ depends on P, the probability that a random thioester crosslink has cleaved. Combining equations S4, S5, and 11 allowed M_c to be predicted as a function of time.

3.8.2.3 Diffusion and Reaction Times

Characteristic diffusion and reaction times were compared to determine which occurred significantly faster.[5] Characteristic reaction time was calculated by

$$t_r = \frac{1}{k[S^-]} \quad \text{(S6)}$$

where k is the rate constant of thiol-thioester exchange and $[S^-]$ is the concentration of unlinked thiolate. Literature values for k range from 10^{-5} to 10^3 $M^{-1}min^{-1}$,[6–8] and model fit to experimental results in this work gave a value of ≈ 0.004 $M^{-1}min^{-1}$ for k, fitting within past studies. Using a value of 0.004 $M^{-1}min^{-1}$ for k and 0.60 M for $[S^-]$ resulted in t_r of ≈ 420 min. Characteristic diffusion time was calculated by

$$t_d = \frac{L^2}{D_{eff}} \quad \text{(S7)}$$

where L is half the length of degrading films and D_{eff} is the effective diffusivity of free BMP thiolates diffusing into said films. D_{eff} for BMP thiolate (M_w = 161.3 g/mol) was approximated

as 0.0005 mm^2/min because its molecular diffusivity is similar to a fluorophore (M_w = 297 g/mol) diffusing through an identical crosslinked and swollen network.[9] Using a value of 0.05 mm for *L* and 0.0005 mm^2/min for D_{eff} resulted in t_d of ≈ 5 min. Comparing t_r and t_d showed diffusion occurred ≈100x faster than reaction, justifying the claim that diffusion was significantly faster in the films studied and further supporting the claim that the networks investigated underwent bulk degradation.

3.8.2.4 Derivation of q

To find *q*, the fraction of thioesters cleaved but still attached to the network, all cases where an individual thioester bond can be cleaved but still attached to the infinite network were considered. In particular, the half of the thioester bond where thiol has added was monitored. For *Z = 4*, there are three distinct cases where thioesters are cleaved but still attached to the network:

Case 1: All adjacent arms are attached to the network

In this case, there is a probability *P/2* that the thioester in question (left) has cleaved and is oriented so a free thiol adds to this crosslink. Then, there is a probability *(1-y)* that each of the adjacent arms are attached. This provides a total fraction of $(P/2)(1-y)^3$.

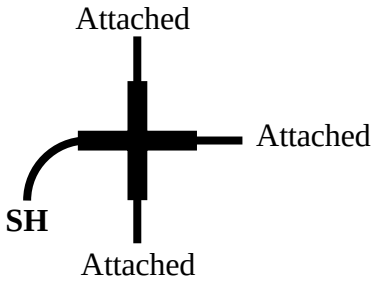

Case 2: Two adjacent arms are attached to the network

In this case, there is a probability *P/2* that the thioester in question (left) has cleaved and is oriented so a free thiol adds to this crosslink. Then, there is a probability *(1-y)* that each of the two arms are attached to the network. There is a probability *y* that the remaining arm is detached. Because there are three arrangements for this scenario, the probability is multiplied by 3. This provides a total fraction of $3(P/2)y(1-y)^2$.

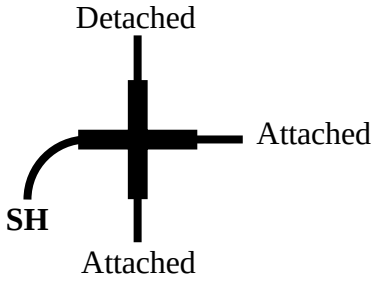

Case 3: One adjacent arm is attached to the network

In this case, there is a probability *P* that the thioester in question (left) has cleaved and is oriented so a free thiol adds to this crosslink. Then, there is a probability *y* that each of the two arms are detached from the network. There is a probability *(1-y)* that the remaining arm is attached. Because there are three arrangements for this scenario, the probability is multiplied by 3. This provides a total fraction of $3(P/2)y^2(1-y)$.

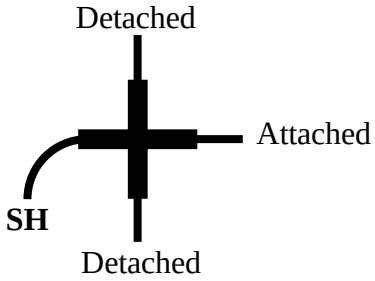

Therefore, for $Z = 4$, $q = (P/2)(1-y)^3 + 3(P/2)y(1-y)^2 + 3(P/2)y^2(1-y)$. This is generalizable to any *Z*:

$$q = \sum_{k=0}^{Z-2} \left(\frac{\mathrm{P}}{2}\right) \binom{Z-1}{k} y^k (1-y)^{Z-1-k}$$

where $\binom{Z-1}{k}$ is the combinatorial factor for choosing *k* elements from *Z*-1 possibilities. The probability (*P/2*) is independent of the variable of summation and can be factored out of the sum. Adding the $k = Z\text{-}1$ case to this sum and subtracting it outside the sum to maintain equality allows for a different form of the equation:

$$q = \left(\frac{\mathrm{P}}{2}\right)\sum_{k=0}^{Z-1}\left\{\binom{Z-1}{k} y^k(1-y)^{Z-1-k}\right\} - \left(\frac{\mathrm{P}}{2}\right) y^{Z-1}$$

The summation term can be recognized as the binomial expansion of $((1-y) + y)^{Z-1}$. This simply reduces to 1, so q can be simplified and rewritten as:

$$q = \left(\frac{\mathrm{P}}{2}\right) - \left(\frac{\mathrm{P}}{2}\right) y^{Z-1} = \frac{1}{2}P(1-y^{Z-1})$$

3.8.2.5 Fractional Mass Gain

With q, the fractional mass gain in the network was derived. The moles of thioesters contributing to mass gain is the fraction of thioesters cleaved but still attached to the network (q) multiplied by the total number of moles of thioesters ($n_{TE,0}$). Each of these will have reacted with free thiol (*SH*) to increase the mass of the network by the mass of one thiol molecule. Therefore, total mass gain is given by:

$$Mass\ Gain\ (g) = q \cdot n_{TE,0} \cdot \frac{1\ mol\ SH}{1\ mol\ TE} \cdot \frac{MW\ SH(g)}{1\ mol\ SH} = qn_{TE,0}MW_{SH}$$

where MW_{SH} is the molecular weight of the free thiol degrading the network. Because thioesters come entirely from the diene crosslinker, the total number of thioester groups present initially is equal to the number of diene molecules (n_{diene}) used in the formulation of the network:

$$Mass\ Gain\ (g) = qn_{diene}MW_{SH}$$

For fractional mass gain, this expression must be normalized to the initial mass, m_0. Given the stoichiometry of the network formulation, initial mass can be related to functionality of the multifunctional thiol, functionality of the diene, and stoichiometry:

$$m_0 = m_M + m_{diene} = nMW_M + n_{diene}MW_{diene} = \frac{2}{Z}n_{diene}MW_M + n_{diene}MW_{diene}$$

The equation for fractional mass gain is acquired from substituting for q in the mass gain expression, dividing the expression by initial mass m_0, and slightly rearranging:

$$MG = \frac{ZP(1 - y^{Z-1})MW_{SH}}{2(2\ MW_M + Z \cdot MW_{diene})}$$

3.8.2.6 Comparison of P_c With Flory Prediction

Flory Prediction

According to Flory,[12] for a polymer composed of monomers with functionality *f*, the critical conversion at which gelation occurs, P_{gel}, is described by:

$$P_{gel} = \frac{1}{f - 1} = 1 - P_{c,rev\ gel}$$

where $P_{c,\ rev\ gel}$ is the critical conversion for reverse gelation. Recognizing that $f = Z$ in this study, the equation can be solved for P_c:

$$P_c = \frac{f - 2}{f - 1} = \frac{Z - 2}{Z - 1}$$

Model Prediction

From the derived model, equation 4 details *y* as:

$$\sum_{k=1}^{k=Z-2} y^k = \frac{P}{1 - P}$$

Reverse gelation occurs when every arm is detached from the infinite network, or when $y = 1$ and $P = P_c$. Putting $y = 1$ in the left-hand side and summing from 1 to Z-2 provides a simple closed form:

$$Z - 2 = \frac{P_c}{1 - P_c}$$

Solving this equation for P_c gives the same prediction for reverse gelation as Flory theory.

3.8.3 References

(1) Shih, H.; Lin, C. C. Cross-Linking and Degradation of Step-Growth Hydrogels Formed by Thiol-Ene Photoclick Chemistry. *Biomacromolecules* **2012**, *13* (7), 2003–2012. https://doi.org/10.1021/bm300752j.

(2) Worrell, B. T.; Mavila, S.; Wang, C.; Kontour, T. M.; Lim, C. H.; McBride, M. K.; Musgrave, C. B.; Shoemaker, R.; Bowman, C. N. A User's Guide to the Thiol-Thioester Exchange in Organic Media: Scope, Limitations, and Applications in Material Science. *Polym. Chem.* **2018**, *9* (36), 4523–4534. https://doi.org/10.1039/c8py01031e.

(3) Wang, C.; Goldman, T. M.; Worrell, B. T.; McBride, M. K.; Alim, M. D.; Bowman, C. N. Recyclable and Repolymerizable Thiol-X Photopolymers. *Mater. Horizons* **2018**, *5* (6), 1042–1046. https://doi.org/10.1039/c8mh00724a.

(4) Metters, A.; Hubbell, J. Network Formation and Degradation Behavior of Hydrogels Formed by Michael-Type Addition Reactions. *Biomacromolecules* **2005**, *6* (1), 290–301. https://doi.org/10.1021/bm049607o.

(5) Metters, A. T.; Anseth, K. S.; Bowman, C. N. A Statistical Kinetic Model for the Bulk Degradation of PLA-b-PEG-b-PLA Hydrogel Networks: Incorporating Network Non-Idealities. *J. Phys. Chem. B* **2001**, *105* (34), 8069–8076. https://doi.org/10.1021/jp004083h.

(6) Bracher, P. J.; Snyder, P. W.; Bohall, B. R.; Whitesides, G. M. The Relative Rates of Thiol-Thioester Exchange and Hydrolysis for Alkyl and Aryl Thioalkanoates in Water. *Orig. Life Evol. Biosph.* **2011**, *41* (5), 399–412. https://doi.org/10.1007/s11084-011-9243-4.

(7) Um, I. H.; Lee, J. Y.; Bae, S. Y.; Buncel, E. Effect of Modification of the Electrophilic Center on the α Effect. *Can. J. Chem.* **2005**, *83* (9), 1365–1371. https://doi.org/10.1139/v05-157.

(8) Cargoët, M.; Diemer, V.; Snella, B.; Desmet, R.; Blanpain, A.; Drobecq, H.; Agouridas, V.; Melnyk, O. Catalysis of Thiol-Thioester Exchange by Water-Soluble Alkyldiselenols Applied to the Synthesis of Peptide Thioesters and SEA-Mediated Ligation. *J. Org. Chem.* **2018**, *83* (20), 12584–12594. https://doi.org/10.1021/acs.joc.8b01903.

(9) Meng, Y.; Fenoli, C. R.; Aguirre-Soto, A.; Bowman, C. N.; Anthamatten, M. Photoinduced Diffusion Through Polymer Networks. *Adv. Mater.* **2014**, *26* (37), 6497–6502. https://doi.org/10.1002/adma.201402097.

(10) Khawam, A.; Flanagan, D. R. Solid-State Kinetic Models: Basics and Mathematical Fundamentals. *J. Phys. Chem. B* **2006**, *110* (35), 17315–17328. https://doi.org/10.1021/jp062746a.

(11) Hopfenberg, H. B. Controlled Release from Erodible Slabs, Cylinders, and Spheres. In *Am Chem Soc Div Org Coat Plast Chem Prepr*; 1976; Vol. 36, pp 26–32. https://doi.org/10.1021/bk-1976-0033.ch003.

(12) Flory, P. J. Molecular Size Distribution in Three Dimensional Polymers. I. Gelation1. *J. Am. Chem. Soc.* **1941**, *63* (11), 3083–3090. https://doi.org/10.1021/ja01131a008.

Chapter 4: Modeling Degradation of Thioester Networks Controlled by Oligomer Structure and Thiol-Thioester Exchange

This chapter to be submitted as a manuscript to Macromolecules with the following coauthors:
Juan J. Hernandez, Sean P. Keyser, Adam L. Dobson, Alexa S. Kuenstler, Christopher N. Bowman

4.1 Abstract

The oligomeric structure of thioester covalent adaptable networks (CANs) is used to tune the bulk degradation of thioester networks via the thiol-thioester exchange (TTE) reaction. A statistical kinetic model for the degradation was developed that considered the exchange reaction rate, the number of thioester links within oligomers, and the dispersity of these oligomers. Model predictions showed changing the number of thioester links within oligomers impacted degradation by as much as tenfold while narrowing oligomer dispersity impacted degradation by up to twofold. To evaluate model predictions with experimental degradation studies, thioester oligomers were synthesized, photocured into films, and degraded via submerging them in a solution of 1 M butyl-3-mercaptopropionate, 0.3 M triethylamine, and acetone. Model predictions matched experimental results, showing increasing thioester links in oligomers from 1 to 4 decreased time for complete mass loss from 25 to 4 h while only using a single fitting parameter, the reaction rate constant *k*, which ranged from 0.0024 to 0.0040 $M^{-1}min^{-1}$. Mixing oligomers containing 1 or 4 thioester links created blended disperse CANs, and these blended networks indicated that changing the mole ratio controlled how rapidly films degraded in a 4 to 25 h time span. Lastly, mass release studies using the model dye Nile red confirmed that thioester oligomers in CANs enable quantifiable mass release by using the Beer-Lambert law. This research demonstrates that multifunctional oligomer structure within CANs represents a viable way to control the degradation profiles these materials.

4.2 Introduction

There is substantial research exploring the breakdown of thermoset polymers to create smart materials, leading to advancements in triggered drug release,[1,2] material actuation,[3,4] and dissolvable wound sealants.[5] Of the various chemically triggered degradation methods, including hydrolysis[6–8] and pH changes,[1,9] reversible exchange reactions[10,11] have shown ease of reprocessibility in their resultant materials, separating this degradation method from others by enabling the degradation and repolymerization of polymers under mild conditions.[12,13] Polymer networks enabling these reversible exchange reactions are referred to as covalent adaptable networks (CANs), and the dynamic bonds that are present alter the network topology which facilitates reprocessing of polymer networks via traditional means such as compression molding[14,15] and twin-screw extrusion.[16] While various chemistries have been developed to experimentally degrade CANs,[10,17–20] the field would continue to benefit from refined quantitative models that predict the degradation processes through which CANs lose mass.

Degradation is the permanent loss of mass from a polymer and occurs when all covalent bonds to a segment are broken and these unattached segments of the polymer diffuse out.[21,22] For polymer networks, a scission reaction is required to break the covalent bonds connecting these polymer segments, but within CANs this scission reaction is replaced by a reversible exchange reaction. Reversible exchange reactions lead to degradation by exchanging an elastically connected group with a terminal group, reducing the crosslink density of the network. Mass loss then occurs when all arms of a crosslink segment are detached, as shown in **Scheme 4.1**.

A number of models describe the exchange-facilitated degradation of CANs by taking diffusion and reaction timescales into account, and these models have been developed for CANs chemistries including transesterification,[23,24] boronic-ester exchange,[25] and thiol-thioester exchange

(TTE).[26,27] However, few models have been developed that specifically focus on how the network structure of CANs may be used to control degradation. Controlling network structure as opposed to reaction chemistry would allow CANs to degrade at vastly different timescales when exposed to only a single set of exchange reaction conditions. It would also provide a means for creating networks from a single chemistry that could be tuned to exhibit complex degradation processes such as staged degradation.

As one specific example of controlling the network structure, tuning oligomer structure within CANs offers a promising way to control the degradation process by means of network structure. Oligomers consist of covalently-bonded monomers and may be characterized by their length or dispersity.[28,29] In traditional polymer networks, oligomer length and dispersity have been shown to impact degradation profiles in poly-lactic acids,[7,30] acrylate esters,[31,32] and self-immolating polymers,[33] which has justified the creation of theoretical models that track both oligomer length and dispersity throughout the degradation process.[34,35] Within CANs, oligomers have been used to contain dynamic exchange groups, enabling control over the number of active exchange sites and the effects of exchange by simply changing oligomer length.[36] Manipulating these oligomeric CANs has contributed to research in material actuation,[37] shape-changing microparticles,[38] and reconfigurable 3D printing.[39] Of the various CAN chemistries available to start modeling how oligomer structure impacts CAN degradation, the TTE reaction offers a promising route due to past degradation studies and ease of synthesis in a variety of oligomer structures.

The TTE reaction exchanges the groups on the thiol and thioester moieties, as shown in **Scheme 4.2**. This reaction may be base or nucleophile catalyzed and has been studied extensively due to its rapid kinetics,[15] selective reaction,[40] and ability to be triggered under mild conditions.[41] Past work has shown that the TTE exchange may be used to successfully degrade thioester-containing

networks,[26,27,42] and repolymerize these networks when the depolymerized solution is mixed with additional monomer.[12] Within the context of oligomers, TTE exchange has been used to create thioester-containing oligomers,[43] and these oligomers have applications in creating DNA polymer mimics,[44] self-immolating oligonucleotides[45] and self-immolating hydrogels.[46] By building off past work that developed models to describe the bulk degradation of thioester networks via the TTE reaction,[26,27] this work adapts these models to focus on how the oligomer structure of thioester CANs controls the degradation process.

The oligomer structure of thioester CANs was used here to tune the bulk degradation of these networks via the TTE reaction. A statistical kinetic model was developed that took into account the kinetics of the TTE reaction, the number of thioester links within oligomers, and the dispersity of these oligomers. Thioester-containing oligomers were then synthesized and photocured into networks to compare the model predictions with experimental mass loss studies. The mass loss profiles of blended CANs, created by mixing oligomers containing either 1 or 4 thioester links, were also compared to model predictions. Lastly, mass release studies using the model dye Nile red evaluated the use of oligomer structure as a way to achieved controlled mass release. This research demonstrates that oligomer structure within CANs is a viable way to control the degradation profiles of CANs, and while this work focused on thioester chemistry, the developed oligomer models are chemistry agnostic and may be used for a number of different reactions, contributing to the growing field of degradable networks.

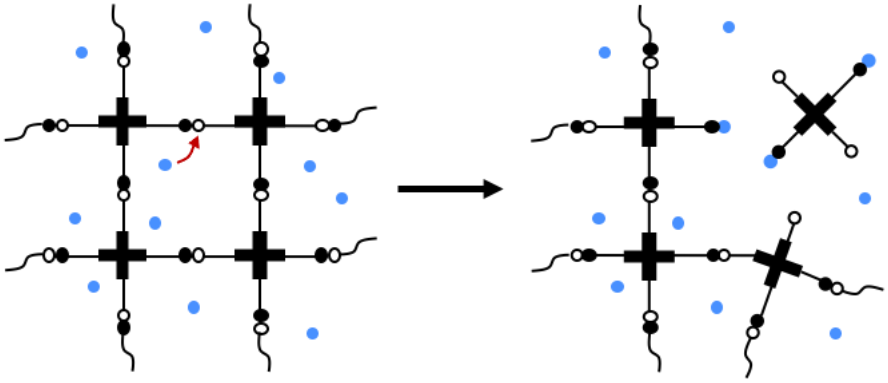

Scheme 4.1. Within a crosslinked network, exchange reactions between a tethered group (empty circle) with a terminal group (filled circle) result in a drop of crosslinking density and degrade the network (*left*). When all connections of a crosslink segment are broken, these segments are able to diffuse out which leads to mass loss (*right*).

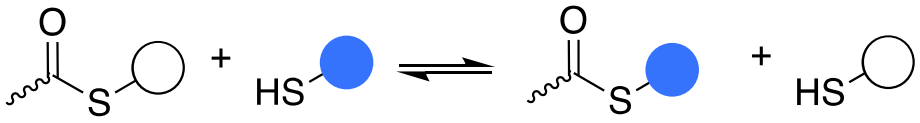

Scheme 4.2. Thiol-thioester exchange dynamically interconverts groups attached to a thioester with a group attached to a free thiol. Exchange occurs rapidly at room temperature in the presence of a base or nucleophile catalyst.

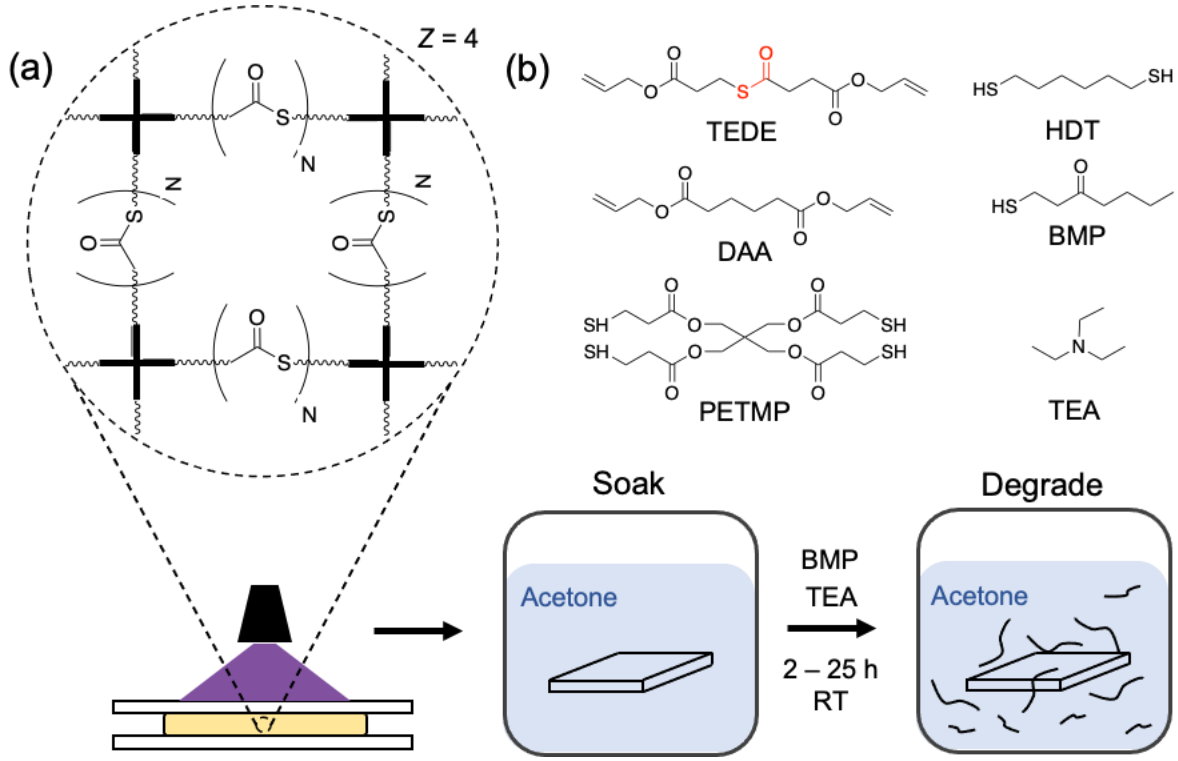

Figure 4.1. Thiol-thioester exchange leads to depolymerization of thioester containing networks. (a) Networks containing *N* thioester links were photocured into 100 μm thick films, soaked in acetone, and exposed to thiol (BMP) and base (TEA) to trigger degradation via exchange. (b) Reagents used to create and degrade thioester networks.

4.3 Materials and Methods

4.3.1 Materials

TEDE was synthesized by a previously reported method.[15] All other materials were purchased commercially. 2,2'-azobis(2-methylpropionitrile) (AIBN), butyl 3-mercaptopropionate (BMP), diallyl adipate (DAA), 1,6-hexanedithiol (HDT), pentaerythritol tetrakis(3-mercaptopropionate) (PETMP), and triethylamine (TEA) were purchased from Sigma Aldrich. Dichloroethane (DCE) was purchased from Fischer Scientific, and Irgacure 819 (I819) from IGM Resins.

4.3.2 Thioester Oligomer Synthesis and Characterization

4.3.2.1 Synthesis

TEDE and HDT were mixed in ratios of 33 - 100 mol % excess ene (relative to the thiol), and then combined with 5 mol % AIBN. The solution was mixed with 10x excess by volume DCE to allow for higher temperature reactions, spun at 250 RPM, and reacted for 24 h at 80 °C.[47] The crude reaction mixture was dried using roto-evaporation and high-vacuum at RT, and the purity verified using NMR. The number-average degree of polymerization for oligomers was predicted using the Carothers equation,

$$X_N = \frac{1+r}{1-r} \quad (1)$$

where X_N is the number-average degree of polymerization and r is the ratio of thiol : ene groups with $r \leq 1$. The number of thioester links within the oligomers was calculated for odd-numbered degree of polymerizations,

$$N = \frac{X_{N,odd}}{2} + 0.5 \quad (2)$$

where N is the number of thioester links and $X_{n,odd}$ is the odd-numbered degree of polymerization. Oligomers containing 1, 2, 3, or 4 thioester links (N) were synthesized, which had degrees of polymerization (X_N) of 1, 3, 5, or 7, respectively.

4.3.2.2 GPC

The molecular weight distribution of each oligomer was analyzed via GPC size exclusion chromatography. Samples were prepared by first dissolving oligomers in chloroform at 10 mM and then filtering them through a 0.2 μm PTFE filter. The molecular weight distributions of the

samples were then analyzed on an Ecosec HLC-8320 GPC instrument from TOSOH with chloroform solvent, using a polystyrene standard.

4.3.2.3 MALDI-TOF

The molecular weight of each oligomer was also confirmed via MALDI-TOF mass spectrometry. Samples were prepared by first dissolving oligomers in chloroform at 10 mM, and then spotting them sequentially with dithranol and sodium trifluoroacetate at concentrations of 5 mg/mL and 10 mg/mL, respectively. The samples were then run on a Shimadzu 7090 MALDI-TOF instrument utilizing positive ion and linear high mass modes. Mass analysis subtracted 23 Daltons to account for sodium counter ions.

4.3.3 Mass Loss

TEDE oligomers containing an average of 1 – 4 thioester links were mixed with PETMP and I819 in a 1 thiol : 1 ene : 0.025 I819 molar ratio, with neat TEDE monomer representing a $N = 1$ oligomer due to its preexisting internal thioester link. The solution was placed between glass slides separated by 100 μm spacers and exposed to 400 – 500 nm light at 2.5 mW/cm^2 for 5 min on each side. The resulting cured films were cut into 2 cm x 3 cm x 100 μm films. The initial weight (m_o) of the films was measured, the films were swollen in acetone for 1 h to remove sol-fraction, and finally films were placed in a degrading solution containing 1.0 M BMP, 0.3 M TEA, and acetone. Films were removed from the degrading solution at specific times, vacuum dried at 50 °C for 24 h, then weighed again, m_{final}. Film mass loss, ML_{exp}, was calculated via

$$ML_{exp} = \frac{m_o - m_{final}}{m_o} \quad (3)$$

4.3.4 Blended Networks

Blended thioester networks were created by mixing N = 1 with N = 4 oligomers in varying molar ratios. The average number of thioester links within the oligomer blends, $\overline{\mathrm{N}}$, was calculated as,

$$\overline{\mathrm{N}} = 4 - 3\mathrm{f} \quad (4)$$

where f is the ratio of N = 1 : N = 4 oligomer and $f \leq 1$.

4.3.5 Nile Red Mass Release

4.3.5.1 Degradation Visuals

Films composed of oligomers containing varying thioester linkages (N = 1, 2, and 4) were photocured following the method described in Section 4.3.3, with an additional 0.5 wt % of Nile red. After irradiation, the films were cut, weighed, and swelled in acetone for 16 h to remove the sol-fraction and any unencapsulated dye. These films were then placed into specially prepared scintillation vials (contained a stir bar and a protective wire mesh bottom), submerged in 20 mL of degradation solution, and the vials were sealed using Teflon and parafilm. These vials were placed in a lightbox and photographed every 4 h.

4.3.5.2 UV-Vis

Network films composed of oligomers containing 2 thioesters groups (N = 2) were prepared and degraded in the same way as in Section 4.3.5.1. 1 mL aliquots were taken every 2 h and were run on an Evolution 300 UV-Vis instrument from Thermo Scientific, recording absorbance from 350 – 700 nm. The Beer-Lambert law, $A = \varepsilon lc$, was applied to the Nile red absorbance peak at

552 nm to determine concentration, where A represents absorbance, ε molar extinction coefficient, l path length (cm^{-1}), and c concentration (M). A value of 33,000 $\pm$ 4,000 $cm^{-1}M^{-1}$ was calculated for ε based on calibration experiments which measured the absorbance of three 10 μM solutions of Nile red in a 1 cm cuvette, matching previous literature values.[48] The 10 μM solutions of Nile red were composed of 1.0 M BMP, 0.3 M TEA, and acetone.

4.3.6 Model Development

Modeling degradation of a thioester network composed of crosslinks with varying dispersity required analysis of both the polymer network structure and the kinetics of the thiol-thioester exchange (TTE). Building from past models derived by Metters *et al.*,[31] Rydholm *et al.*,[49] and Hernandez *et al.*,[26] this work developed a new statistical model that took into account the number of thioester links within crosslink arms composed of oligomers, the distribution of these oligomers, and the reaction rate of TTE. Several simplifying assumptions were made to develop this model: (i) the polymers under consideration formed ideal distributions; (ii) the kinetic coefficient for the TTE remained constant throughout degradation and for every thioester in the network; (iii) completely cleaved segments diffused nearly immediately out of the degrading network; and (iv) no further TTE reactions occurred in cleaved segments. These assumptions will not hold for all networks, such as in thick samples, systems with significant oligomer cyclization,[50] with pendant chain and cycle formation during polymerization,[49] and with non-isothermal exchange reactions that impact the reaction rate constant.[23]

4.3.6.1 Structure Component of Model

The structural component of this model first considered the network to be homogenous and monodisperse, where each crosslink was attached to a *Z* number of arms and each arm was an oligomer that contained an *N* number of thioester links, **Figure 4.1a**. As this network degrades via TTE, only one of the available thioester groups on an arm must exchange for that entire arm to be releasable. This realization results in an equation describing the fraction of broken arms as determined by the extent of TTE:

$$A = 1 - (1 - P)^N \quad (5)$$

where *A* is the fraction of broken arms, *P* is fractional TTE conversion, and *N* is the number of thioester links per oligomer or crosslink arm.

Mass loss for a network of this type occurs when all arms of a crosslink's segment are completely broken, allowing the segment to detach and diffuse out of the system, **Scheme 4.1** (*right*). The probability that an arm of a crosslink segment is broken may be described by *y*, with *1-y* describing the probability an arm not being broken. Arms may break in two ways: (i) the arm is directly broken (probability *A*), or (ii) the arm is still intact (probability 1-*A*) but all other arms on its adjacent crosslink segment are broken (probability y^{Z-1}). This results in the relationship,

$$y = A + (1 - A)y^{Z-1} \quad (6)$$

Mass loss is then defined as occurring when all arms of a crosslink segment are broken, as these fragments can then be released. This behavior is mathematically described by,

$$ML = y^Z \quad (7)$$

where *ML* is the fractional mass loss that results from these released segments. Combining equations 5, 6, and 7 combines the effects of fractional TTE conversion with the fraction of arms that are broken and the fractional mass loss as a result of these broken arms, resulting in one

simplified equation that gives mass loss as a function of the extent of TTE for a homogenous, monodisperse network. When this network has Z = 4 arms per crosslink segment, mass loss is described precisely in terms of A or in terms of P and N by,

$$ML_{mono} = \left(-\frac{1}{2} + \sqrt{\frac{\mathrm{A}}{1-\mathrm{A}} + \frac{1}{4}}\right)^4 = \left(-\frac{1}{2} + \sqrt{(1-P)^{-N} - \frac{3}{4}}\right)^4 \quad (8)$$

The above equation describes mass loss until a $P_{critical}$ value is reached, at which point ML_{mono} = 1 because the network undergoes reverse-gelation and all residual mass is assumed to immediately dissolve into solution. Past work for the degradation of a non-oligomeric thioester networks defines $P_{critical}$ *as* $P_{critical} = \frac{Z-2}{Z-1}$.[26] As degradation within non-oligomeric thioester networks requires only one thioester to disconnect for a crosslink to be broken, the fraction of broken crosslinks in non-oligomeric networks (*P)* equals the fraction of broken arms in oligomeric networks (*A*). As such, a critical fraction of broken arms may be defined beyond which *ML* = 1,

$$A_{critical} = \frac{Z-2}{Z-1} \quad (9)$$

Combining equation 9 with equation 5 for a Z = 4 network solves for $P_{critical}$ in these monodisperse networks under consideration,

$$\mathrm{P_{critical}} = 1 - \mathrm{e}^{-\frac{\ln 3}{\mathrm{N}}} \qquad (10)$$

4.3.6.2 Accounting for Dispersity

As opposed to a monodisperse network where each arm contains the same number of *N* thioester links, dispersity in the model considers a network composed of arms with a distribution of *N* thioester links. To account for dispersity in these oligomeric arms, a number-average probability distribution for oligomer size was determined. A modified Flory-Schulz distribution was formulated that allows for off-stoichiometric quantities of reactive groups, and detailed

derivation of this distribution and all subsequent equations is found in Section 4.8.1 of the Supporting Information. The result is a statistical distribution profile that divides oligomers into odd and even degrees of polymerization:

$$x(i_{odd}) = \left[\frac{1-rp}{1+r-2rp}\right](1-rp)(rp^2)^k + \left[\frac{r(1-p)}{1+r-2rp}\right](1-p)(rp^2)^k;\ i = 2k+1 \quad (11)$$

$$x(i_{even}) = \left[\frac{1-rp}{1+r-2rp}\right]rp(1-p)(rp^2)^k + \left[\frac{r(1-p)}{1+r-2rp}\right]p(1-rp)(rp^2)^k;\ i = 2k+2 \quad (12)$$

where $x(i)$ is the number-average probability, or mole fraction, of oligomers of length i; r is the stoichiometric ratio of reactants as defined by Carothers; p is the degree of conversion of the limiting reactive group; and k is an integer dummy variable that ranges from zero to infinity. In the case of equimolar reactants (r = 1), these equations reduce to the familiar Flory-Schulz distribution $x(i) = (1-p)p^{i-1}$.[51] The number-average degree of polymerization of the distribution, $\bar{X}_N$, is found by the sum of all $ix(i)$, which reproduces the Carothers equation $\bar{X}_N = \frac{1+r}{1+r-2rp}$ for one reactant in excess. Both the Flory-Schulz distribution and the modified distribution for thioester links are plotted in **Figure S4.1**.

With this distribution, mean-field approximations of model parameters are used to adjust the monodisperse model to a polydisperse one. For the probability that an arm is broken (y), a number-average of y values for all oligomer sizes is obtained:

$$\bar{y} = \bar{A} + (1-\bar{A})\bar{y}^{Z-1} \quad (13)$$

where $\bar{y}$ is the number-average probability the arm of a crosslink segment is broken, $\bar{A}$ is the number-average fraction of arms broken, and Z is the number of arms per crosslink segment. The form of this equation is mathematically identical to that of equation 6 for the monodisperse model, requiring only identification of $\bar{A}$. If complete conversion of the limiting reactant during oligomer synthesis is assumed, $\bar{A}$ is given by

$$\bar{A} = \sum_i x(i)A(i) = \sum_{k=0,1,2,\ldots}[(1-r)r^k][1-(1-P)^{k+1}] = \frac{P}{1-r(1-P)} \quad (14)$$

Mass loss is then given by $ML = \bar{y}^Z$ which simplifies to the following when $Z = 4$,

$$ML_{poly} = \left(-\frac{1}{2} + \sqrt{\frac{\bar{A}}{1-\bar{A}} + \frac{1}{4}}\right)^4 \quad (15)$$

4.3.6.3 Kinetic Component of Model

The kinetics of the TTE reaction contribute to the degradation process of thioester networks. The exchange reaction proceeds by exchanging the groups attached to the thiol and the thioester. However, this reaction requires the thiol to become a thiolate and so the exchange kinetics depend on the concentration of thiolate and not that of thiol.[41] Past work has shown that if thiolate concentration in the degrading solution greatly exceeds thioester concentration in the material to be degraded, the second order TTE may be treated as a pseudo-first order reaction where thiol concentration is fixed and only thioester concentration changes.[26,27] All degradation studies in this work degraded thioester networks in a solution containing at least 25 times excess thiol, enabling the treatment of TTE as a pseudo-first order reaction, described by

$$[TE] = [TE]_o e^{-k[S^-]t} \quad (16)$$

where *[TE]* is the current concentration of connected thioesters within the network, $[TE]_o$ is the initial concentration of connected thioesters within the network, *k* is the reaction rate constant for the TTE reaction, $[S^-]$ is the concentration of thiolate, and *t* is the time.

The kinetic component of this model may be combined with the structural model components described earlier by relating *P* to *[TE]*,

$$P = \frac{[TE]_o - [TE]}{[TE]_o} = 1 - e^{-k[S^-]t} \quad (17)$$

Combining equation 17 with equation 8 gives model predictions for how a monodisperse Z = 4 network undergoes mass loss, while combining equation 17 with 15 gives mass loss predictions for a polydisperse Z = 4 network.

4.4 Results and Discussion

4.4.1 Model Results

This work sought to investigate how oligomer structure within CANs may be used to control degradation when exposing these networks to only a single set of exchange reaction conditions. To that end, this work focused on the TTE reaction and thioester CANs as a representative system but the structural models described herein are chemistry agnostic and apply to various degradation reactions. To study the specific impact of oligomer structure on thioester CANs, a statistical kinetic model was developed that considered the kinetics of the TTE reaction, the number of thioester links within oligomers, and the dispersity of these oligomers.

The developed model predicts that as the number of thioester links within the oligomer (N) increases, mass loss occurs more rapidly. **Figure 4.2** plots the predicted mass loss for a tetramer-based network as a function of time (t), of fraction of arms broken (A), and of fractional TTE conversion (P). **Figure 4.2a** shows a graphical representation of all the variables under consideration in this work, including an example of how the fractional TTE conversion and the fraction of arms broken are calculated when considering only the two arms drawn. Only one of the thioester links on an arm must be broken via the exchange reaction for an entire arm to become disconnected. **Figure 4.2b** shows how predicted mass loss changed as a function of time as the oligomer length, N, increased from 1 – 50. Mass loss in **Figure 4.2b** was predicted by combining equations 8 and 17, and setting k to a value of 0.0040 $M^{-1}min^{-1}$ as established by previous work.[26]

Greater values of *N* resulted in faster mass loss, with time for complete dissolution showing a more than tenfold decrease, dropping from 15.5 to 0.5 h as *N* increased from 1 – 50.

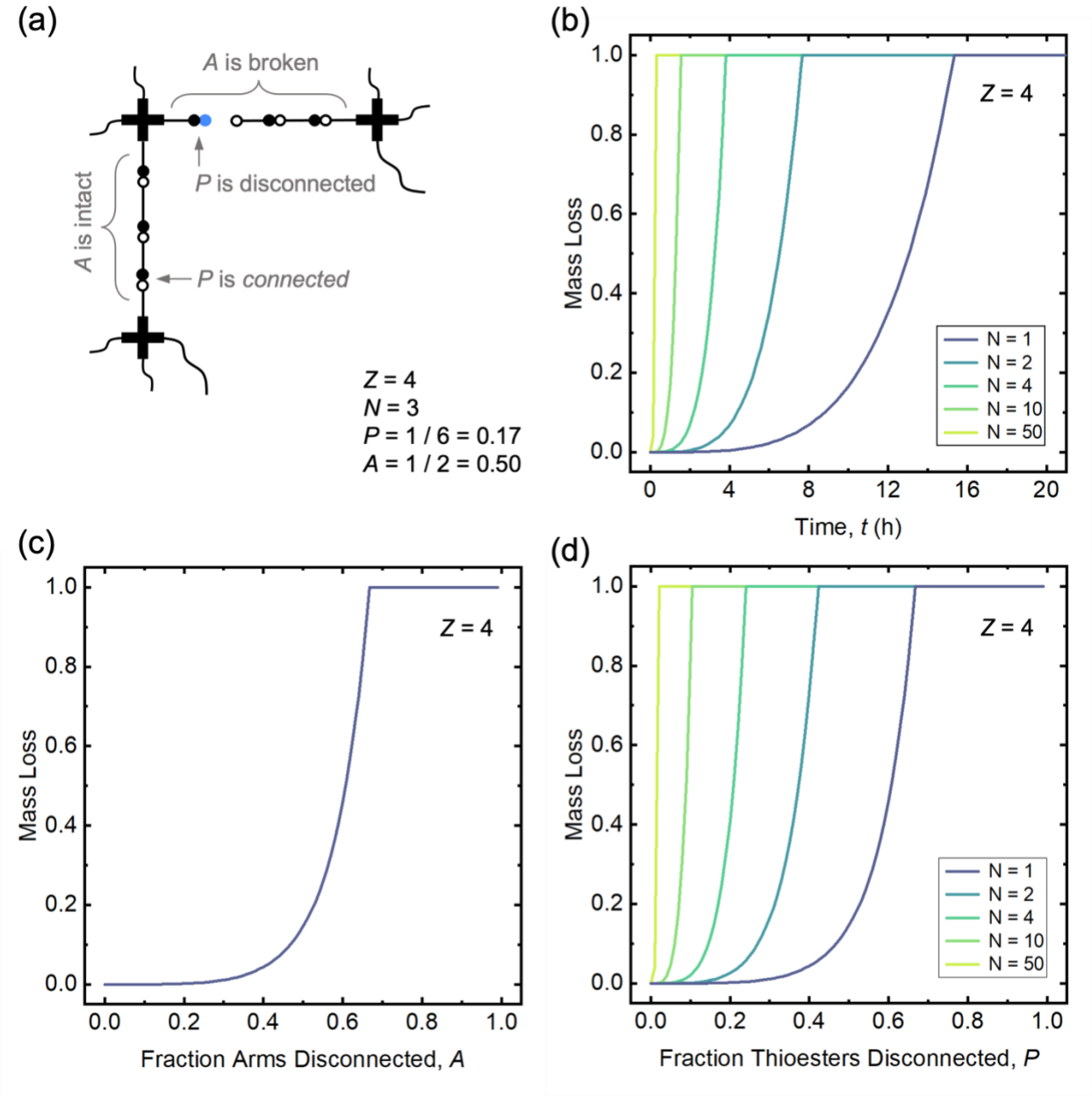

Figure 4.2. Model predictions show arms with more thioester links, *i.e.* longer oligomers, lose mass faster. (a) Diagram showing all the components of the oligomer CAN structure under consideration. (b) Predicted mass loss as a function of time, with thioester links within oligomers (*N*) increasing from 1 – 50. (c) Predicted mass loss as a function of fraction of arms broken (*A*), which is the same for all *N* values in a *Z* = 4 network. (d) Predicted mass loss as a function of fractional TTE conversion (*P*), with thioester links within oligomers increasing from 1 – 50.

Figures 4.2c and **4.2d** show how predicted mass loss changed with structurally relevant, but difficult to measure variables including the fraction of arms broken (A) and fractional TTE conversion (P). **Figure 4.2c** used equation 8 to plot mass loss, and this single curve represents all N values in a $Z = 4$ network. A single curve describes all N values because in these CANs mass is lost when all arms of a crosslink segment are broken and this segment diffuses out. However, the number of thioester links within each broken arm does not matter, only the number of arms per crosslink segment (Z) matter. For the $Z = 4$ network predictions considered here, when A equals 0.67, the mass loss reached a value of 1, indicating complete dissolution and indicating that 0.67 is the value of $A_{critical}$, which matches the prediction from equation 9. **Figure 4.2d** used equation 8 to plot predicted mass loss as well, but instead looked into the relevant contributions from fractional TTE conversion (P) and number of thioester links within oligomers (N). As P increased, more mass is lost, while as N increased, mass loss is achieved at lower and lower extents of TTE. When $N = 1$ the variables A and P are identical and their curves overlap, but as N approached values of 10 or greater only 10 % of thioesters need to disconnect ($P = 0.1$) for complete dissolution. When N reached 50, only 2 % of thioesters ($P = 0.02$) must disconnect for complete dissolution, which explains why the $N = 50$ mass loss in **Figure 4.2b** fully degrades in only 0.5 h.

While **Figure 4.2** evaluates degradation of a monodisperse network, past theory[29,52] and experimental studies[50] have shown that synthesized oligomers are often a polydisperse distribution of chain lengths. As oligomer distribution has been to shown to impact mass loss in traditional polymer networks,[30–32] this work investigated how dispersity in a thioester oligomer would influence degradation. To this end, a structural model was developed to track how the mass loss, the fraction of arms broken (A), and the fractional TTE conversion (P) changed as oligomer

distribution shifted from monodisperse to polydisperse with the results from that approach presented in **Figure 4.3**.

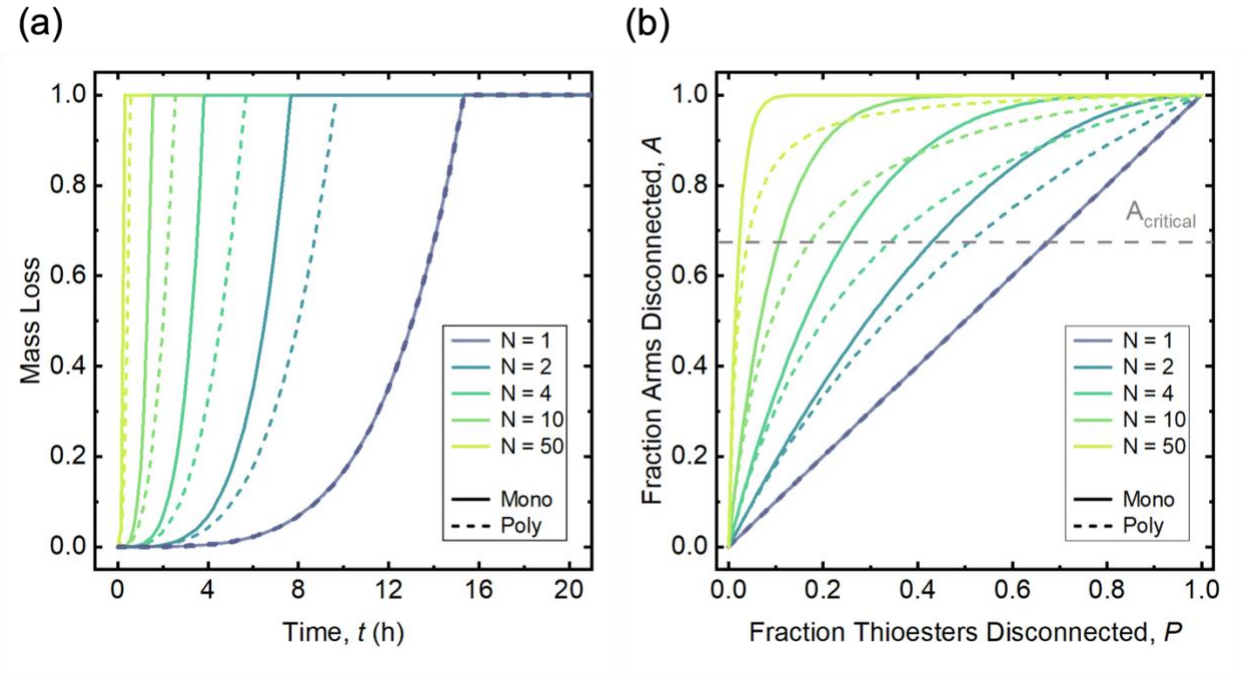

Figure 4.3. Thioester networks composed of monodisperse oligomers are predicted to degrade more rapidly than networks containing polydisperse oligomers for equivalent average oligomer lengths. (a) Predicted mass loss as a function of time for thioester networks composed of either mono (solid) or poly (dashed) disperse oligomers, with thioester links within oligomers (*N*) increasing from 1 – 50. (b) Fraction of arms broken (*A*) as a function of fractional TTE (*P*) for mono (solid) or poly (dashed) disperse oligomers, with *N* increasing from 1 – 50.

Model predictions show that thioester networks composed of monodisperse oligomers lose mass more rapidly than those composed of polydisperse oligomers. **Figure 4.3a** plots predicted mass loss as a function of time as *N* increase from 1 – 50 for both mono and poly disperse oligomers by using equations 8, 15, 17, and a value of 0.0040 $M^{-1}min^{-1}$ for *k*. For both networks, as *N* increased less time is required to achieve mass loss. When $N = 1$ the mono and poly disperse systems degrade identically, but for larger *N* values polydisperse oligomers degrade more slowly, requiring approximately 25% more time when $N = 2$ and increasing to nearly double the time when $N = 50$. The polydisperse oligomers likely require more time for mass loss because their distribution

contains oligomer lengths shorter than their number-average degree of polymerization, $\bar{X}_N$, which take longer to degrade. As *N* increases from 1 to 50, the range of available shorter oligomer lengths grows which explains why larger *N* oligomers experience a greater impact from dispersity changes. The complete distribution for polydisperse oligomers is shown in the Supplementary Information, **Figures S4.1** and **S4.2**. Nevertheless, the impact of polydispersity on mass loss time can still be outweighed by the effects of changing *N*.

Figure 4.3b shows that thioester networks composed of monodisperse oligomers require lower values of TTE conversion (*P*) to reach complete dissolution. **Figure 4.3b** plots the fraction of arms broken (*A*) as a function of fractional TTE (*P*) as *N* increased from 1 – 50 by using equations 5 and 14. As *N* increased, both the mono and poly disperse oligomers required lower values of *P* to reach $A_{critical}$, the grey dashed line located at $A = 0.67$ which indicates complete mass loss. While both dispersities produced curves that look similar, the curves for monodisperse oligomers (solid lines) have a steeper slope at low *P* values, a flatter slope at high *P* values, and reach $A_{critical}$ faster than the curves for polydisperse oligomers.

TTE continues within thioester networks even after complete dissolution, and **Figure 4.3b** shows that exchange that proceeds in the region of $A > A_{critical}$ must occur within already the already dissolved network. In situations where $A = 1$ but $P < 1$, the thioester network has entirely degraded into single crosslink segments with each segment composed of arms containing unreacted thioester links, **Figure S4.3**. The $N = 50$ curve for monodisperse oligomers provides a clear example: here all arms of the network are broken when the fraction of TTE conversion exceeds 0.15, indicating the unreacted thioester links must be contained in single crosslink segments containing very long arms. The above suggests that thioester networks composed of monodisperse oligomers degrade

into single crosslink segments containing very long arms while those composed of polydisperse oligomers degrade into crosslink segments still connected to each other.

4.4.2 Network Mass Loss

Having explored a theoretical model that describes how oligomer structure may be used to control the degradation of thioester CANs, this worked moved to test model predictions and track mass loss of photocured thioester networks. Physical networks were created by first synthesizing oligomers containing thioester links, mixing these oligomers with PETMP, and photocuring the mixtures. These networks were then submerged in a solution of 1 M butyl-3-mercaptopropionate, 0.3 M triethylamine, and acetone to trigger the TTE and begin the mass loss process. The process to synthesize the oligomers which contained thioester links utilized a thermally-initiated thiol-ene polymerization reaction, **Figure 4.4**.

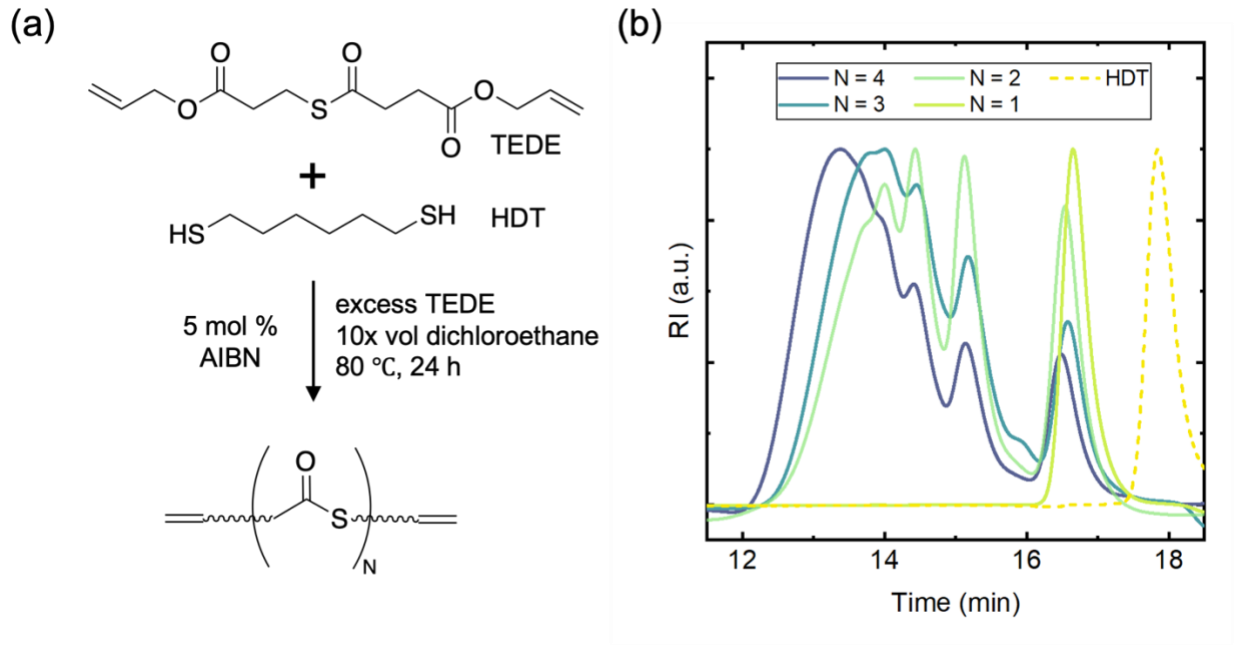

Figure 4.4. Oligomers containing *N* number of thioester links were synthesized via a thermally initiated thiol-ene polymerization reaction. (a) Scheme of oligomerization reaction, with TEDE in excess. (b) GPC curves for synthesized thioester oligomers and their constituents, showing mass fractions versus time as measured by refractive index (RI).

The thermally-initiated thiol-ene polymerization reaction was used to create thioester oligomers containing 1 – 4 thioester links. **Figure 4.4a** shows the scheme used to synthesize the thioester oligomers, where TEDE was in excess and the number-average degree of polymerization, $\bar{X}_N$, was calculated via equation 1. Since only the TEDE monomer contained thioester links, the degree of polymerization (X_N) for an oligomer did not match the number of thioester links within that oligomer (*N*), and the two are instead related via equation 2. For clarity, in this work oligomers containing 1, 2, 3, or 4 thioester links are studied, and these oligomers have degrees of polymerization of 1, 3, 5, or 7, respectively. **Figure 4.4b** shows GPC traces of the synthesized oligomers, with refractive index plotted as a function of elution time. As the ratio of thiol : ene groups (*r*) decreased, the synthesized oligomers achieved larger molecular weights and larger dispersity values which increased from 1.01 to 1.33, **Figure S4.4**. GPC mass fractions showed distinct peaks for each degree of polymerization, with the GPC peaks at 16.5, 16, 15, 14.5, 14,

13.8, and 13.2 minutes representing X_N of 1 – 7, respectively. Only a small mass fraction of dimer, and no unreacted HDT, was observed in the oligomer distributions.

MALDI and NMR spectroscopy were used in conjunction to characterize further the synthesized oligomers. Similar to the GPC data, MALDI showed the oligomers were polydisperse containing degrees of polymerization ranging from 1 – 9, **Figure S4.5**. NMR showed the experimental number-average degree of polymerization for oligomers, calculated by comparing the ratio of unreacted TEDE allyl peaks (5.25 ppm) to reacted TEDE thioester peaks (3.12 ppm), matched the theoretical predictions from equation 1, **Figure S4.6**. Furthermore, NMR confirmed the consumption of all HDT monomer. The combination of GPC, MALDI, and NMR justify the treatment of synthesized oligomers as polydisperse distributions with a number-average degree of polymerization (X_N) calculated by equation 1.

After establishing a reliable method to synthesize the thioester oligomers, and confirming the oligomer structure met model requirements, this work proceeded to mix these oligomers with PETMP and I819 and photocure the solution into 100 μm free-standing films. These films were submerged in a solution of 1 M BMP, 0.3 M TEA, and acetone to trigger the TTE reaction. Mass loss was then tracked over time to characterize the degradation process, **Figure 4.5**.

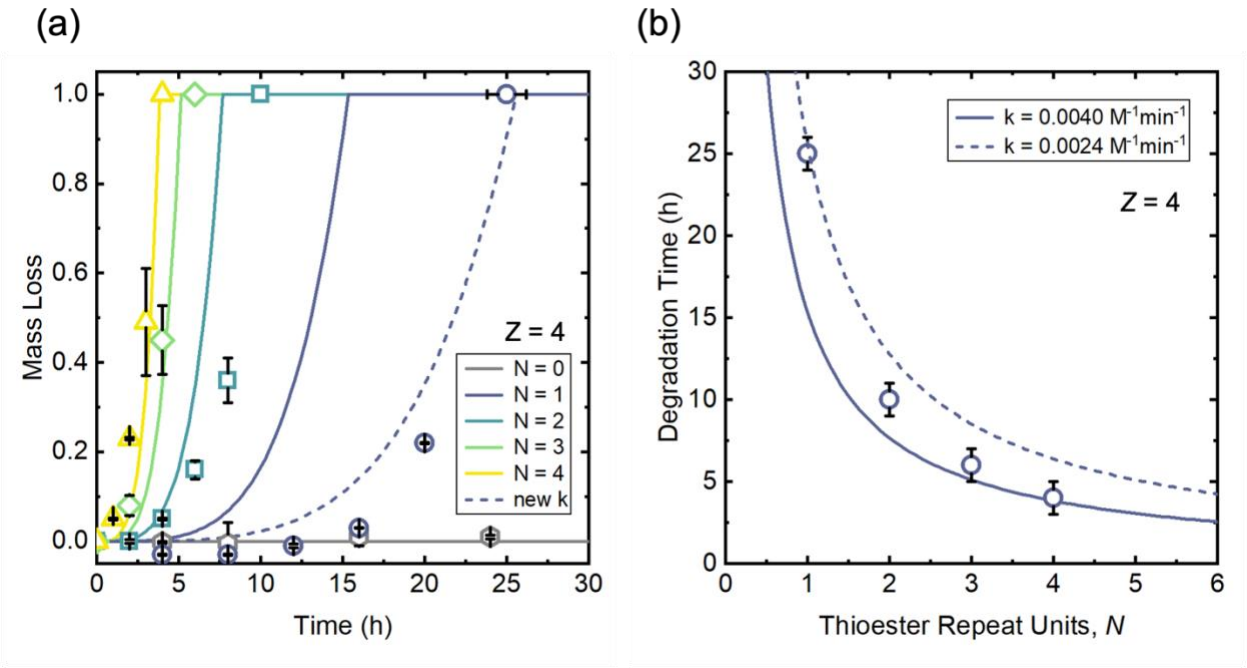

Figure 4.5. Experimental mass loss studies showed the model accurately predicted mass loss for large oligomers ($N \geq 3$), but underpredicted mass loss for small ($N < 3$) oligomers. (a) Mass loss for thioester networks as a function of time, with thioester links within oligomers (N) increasing from 0 – 4. (b) Time required for complete network dissolution to occur as a function of thioester links within oligomers (N), showing model predictions for two values of k. In both plots $Z = 4$, solid lines are model predictions using $k = 0.004$ $M^{-1}min^{-1}$, dashed lines are model predictions using $k = 0.0024$ $M^{-1}min^{-1}$, markers are experimental data, and error bars are standard deviation.

Model predictions were found to match experimental results, showing that a larger number of thioester links within the oligomers (N) resulted in faster mass loss. **Figure 4.5a** shows how experimental mass loss (markers) and predicted mass loss (lines) changed as a function of time as N increased from 0 – 4. The model predictions were calculated using equations 8 and 17, with values of 0.0040 $M^{-1}min^{-1}$ for k and 0.30 M for $[S^-]$ as set by a previous studies on thioester network degradation.[26] Model predictions for mass loss matched experimental data for large oligomers ($N \geq 3$) but underpredicted the time required for shorter oligomers ($N < 3$), with experimental results for the $N = 1$ films requiring 56 % longer to degrade completely than predicted (16 h versus 25 h). While seemingly large, this deviation was readily overcome by decreasing the one fitting parameter for this model, *i.e.* the reaction rate constant k, by a small amount. Reducing k by only

40 % from 0.0040 to 0.0024 $M^{-1}min^{-1}$ showed good agreement between the new model prediction (**Figure 4.5a** dashed line) and experimental data. A number of differences may explain why smaller oligomer lengths require smaller *k* values to better predict mass loss, including: polarity in the thioester network changes as oligomer length changes, crosslink density changes as oligomer length changes, and longer oligomers may contain unreacted thioester links which further disconnect with time and diffuse out more readily.[24]

Figure 4.5a also shows that mass gain was observed for the thioester network composed of the smallest oligomer, $N = 1$. Mass loss for $N = 1$ reached – 0.03 at the 12 h time point, indicating a 3 % mass gain and no other oligomer lengths exhibited this effect. Mass gain was likely not observed in longer oligomers because the mass of BMP adding into the oligomers was too small compared to the total oligomer molecular weight. Therefore, mass loss from detached crosslink segments diffusing out of the network was significantly larger than the mass gain from BMP connecting into oligomer arms when $N > 1$.

Figure 4.5b shows that the time required for complete dissolution of thioester networks decreased as the number of thioester links within the oligomers (*N*) increased. **Figure 4.5b** plots the total degradation time (when mass loss = 1) as a function of *N*, comparing experimental data (markers) to model predictions (lines). Model predictions were derived using equations 10 and 17, and these predictions were repeated for both values of the *k* parameter derived in **Figure 4.5a**, 0.0040 (solid line) versus 0.0024 $M^{-1}min^{-1}$ (dashed line). As *N* increased, the total degradation time required for mass loss decreased, with the slope dropping rapidly from – 15 h/link at $N = 1$ to – 1 h/link at $N = 4$. This decreasing slope explains why larger values of *N* see little change in their total degradation time while smaller values of *N* see large changes. This behavior is evident

when observing the mass loss predictions in **Figure 4.2b**: *N* increasing from 10 – 50 decreased mass loss time by 1.25 h while *N* increasing from 1 – 2 decreased mass loss time by 8 h.

Rapid diffusion of detached crosslink segments out of the network was a key model assumption in creating **Figure 4.5**. In reality, diffusion of detached segments was likely non-instantaneous and resulted in mass being kinetically trapped within the network as observed in other degrading polymer systems.[34] To test diffusion limitations, thioester films were submerged in degrading solution for a specified time, removed and submerged in acetone for 24 h, dried, and weighed. This additional post-degradation soak in acetone enabled kinetically trapped segments to diffuse out. The results are plotted in **Figure S4.7** and show that while these thioester CANs did contain detached segments kinetically trapped inside the films, their contribution to mass loss was small. The largest mass loss changes were observed right before films reached reverse gelation, but even these changes only decreased mass loss time by a maximum of 2 h which did not change the overall mass loss curve profile or the timescale.

The experimental results examined describe how synthesized oligomers may be used to tune degradation of thioester CANs. However, there exists potential to tune the degradation process even further by mixing these oligomers to create blended CANs, and in this way achieve more comprehensive control over the degradation timescale by simply changing the mixing ratio. To explore these blended CANs, this work mixed $N = 1$ with $N = 4$ oligomers in varying ratios, photocured the mixtures into blended networks, and tracked the mass loss of those networks.

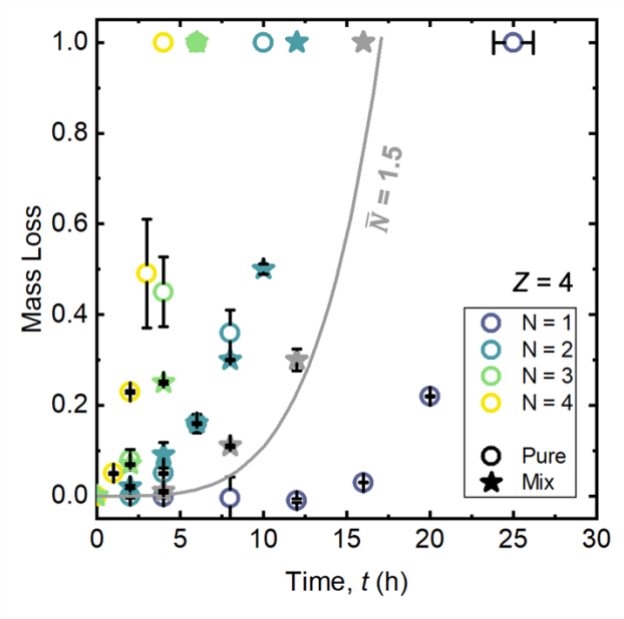

Figure 4.6. Mixing $N = 1$ with $N = 4$ oligomers in varying ratios created blended networks, where the degradation process could be tuned by simply changing the ratio of these oligomers. Mass loss as a function of degradation time, showing homogenous networks (circles) and blended networks (stars). The solid line indicates model prediction for the $N = 1.5$ network.

Combining the $N = 1$ and $N = 4$ oligomers in various ratios shows blended CANs span the entire 4 to 25 h degradation timescale and may be tuned to match the degradation profiles of homogenous CANs. **Figure 4.6** plots mass loss as a function of degradation time for homogenous networks as N increased from 1 – 4 (circles) and for blended networks as the ratio of $N = 1 : N = 4$ oligomers (f) decreased (stars). The blended networks consisted of fractions $f = 0.83$, 0.67, and 0.33 which described oligomers where $\bar{N} = 1.5$, 2, and 3, respectively. The $\bar{N} = 2$ and $N = 2$ networks had identical degradation profiles, achieving complete dissolution within 4 h. The $\bar{N} = 3$ and $N = 3$ networks were almost identical, where the blended network required an additional 2 h to achieve complete dissolution. This longer mass loss time may be due to the smaller mesh size produced by $N = 1$ oligomers in the blended CANs, which inhibits diffusion of detached segments. However, these deviations remain small and the degradation profiles for networks describes by $\bar{N}$ or N are nearly functionally equivalent.

To demonstrate that mixing oligomers into blended CANs resulted in greater control over degradation profiles, a $\bar{N}$ = 1.5 thioester network was created to achieve mass loss times not attainable in the homogenous networks. **Figure 4.6** shows complete dissolution of the $\bar{N}$ = 1.5 network occurred in 16 h, a time in between the N = 1 and N = 2 networks. The model prediction for N = 1.5 (solid line) closely followed experimental mass loss data, showing that a value of k = 0.0024 $M^{-1}min^{-1}$ more accurately predicts mass loss for blended networks composed of a large molar ratio of N = 1 oligomer. This experiment shows that the developed model accurately predicts mass loss for oligomers spanning a variety of molecular weights, and other researchers may choose to expand this model to predict the degradation of blended CANs composed of arbitrary polymer distributions.

4.4.3 Controlled Mass Release

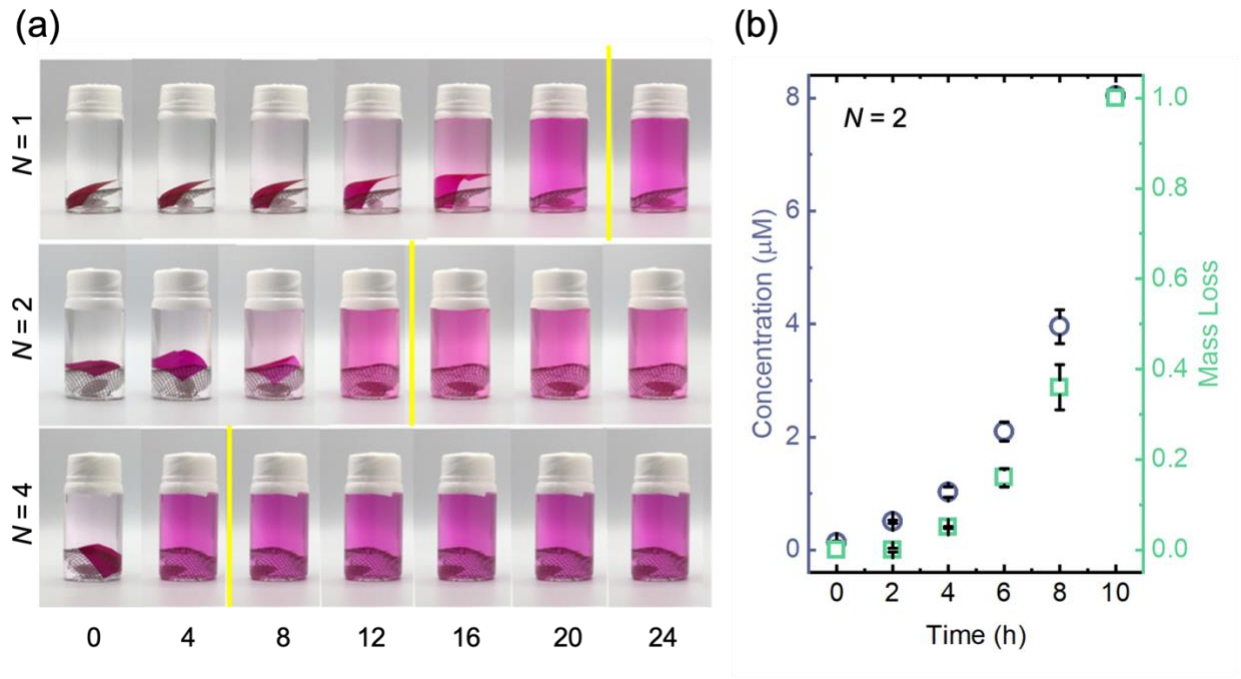

Figure 4.7. Controlled release of Nile red from degrading thioester networks showed oligomer structure was useful to tune the mass release profile. (a) Photographs of thioester networks that

contained Nile red submerged in degrading solution, evolving over time with N varying from 1 – 4. (b) Concentration of Nile red over time for N = 2 samples, calculated using UV-Vis and the Beer-Lambert Law and compared to mass loss. Error bars indicate standard deviation for three samples.

In order to visualize the dependence of mass release on the number of thioester linkages in each crosslink, several films of varying oligomer lengths were photocured with the benzophenoxazone dye Nile red encapsulated into their networks. The films were then degraded, utilizing the evolution of color in the surrounding media to represent the release of each film's encapsulated payload. Encapsulation was chosen over covalent attachment into the network to evaluate these materials as capable of releasing payloads without inherent reactive groups.

Figure 4.7a shows the progression of dye release in each sample over time with the yellow line indicating the time of the film's observed degradation. As in the previous degradation studies, films crosslinked by oligomers with more thioester linkages degraded faster than those with fewer thioester linkages and resulted in a more rapid release of color throughout the degradation media. The degradation times of each film roughly corresponded to the values predicted by the model with $N = 4$, $N = 2$, and $N = 1$ films degrading at approximately 3, 10, and 20 h, respectively. Small deviations of these degradation times from their corresponding mass loss profiles are attributed to carrying out the mass release studies in vials with a more narrow aspect ratio. These narrow vials likely resulted in a faster mixing rate, which generally accelerated the degradation process and resulted in lower degradation times in all but the $N = 2$ trial. These results firmly demonstrate the potential of these materials to be tuned to achieve different degradation times and highlight their possible utility in future controlled mass release applications.

UV-Vis spectra were collected from aliquots of the degradation media in order to quantify the release of dye in each sample. **Figure S4.8** shows a representative plot of Nile red absorbance over time for the N = 2 sample while **Figure 4.7b** shows the concentration of Nile red over time for

these samples found using the Beer-Lambert law. As expected, the N = 2 samples exhibited an increase in absorbance over time at ~550 nm, corresponding to the characteristic absorbance of Nile red.[53,54] Fortuitously, this peak formation exhibited minimal impact from base interactions as may occur with solvatochromic dyes.[55] The subsequently calculated concentration of Nile red exhibited a trend that agreed with the mass loss profiles for N = 2 networks, **Figure 4.7b**. All samples reached the same concentration (8 μM) over the course of 10 h, although dye release occurred faster than mass loss for shorter degradation times.

4.5 Conclusions

By controlling oligomer structure, this work was able to tune the degradation profile of thioester CANs as mediated by the TTE reaction. A statistical kinetic model was derived that considered the number of thioester links within oligomers (N), the dispersity of these oligomers (mono versus poly disperse), and the kinetics of the TTE reaction. Model predictions indicated that the oligomer length had a much larger impact on degradation than dispersity, changing the time required for complete dissolution by tenfold versus twofold. Thioesters oligomers were synthesized to test the predicted effects of changing N, and model predictions matched experimental data showing that increasing N resulted in faster degradation, reducing mass loss time from 25 to 4 h, and showing that a single fitting parameter k could accurately capture experimental data using a range of only 0.0024 to 0.0040 $M^{-1}min^{-1}$. Blended CANs, created by mixing N = 1 with N = 4 oligomers in different ratios, showed mixing oligomers achieved mass loss times not obtainable by homogenous networks, such as the $\overline{N}$ = 1.5 network degrading in 16 h. Lastly, mass release studies using Nile red showed thioester CANs may be used for quantitative payload applications as calculated by the Beer-Lambert law.

Work of this nature provided new models to describe how the structure of CANs may be used to tune degradation mediated by an exchange reaction. While this research focused on thioester networks and the TTE reaction, the structural components of the developed model are chemistry agnostic and may be readily applied to a number of different degradation schemes. Furthermore, the developed model may be used to extract the reaction rate constant *k* from mass loss data, serving as a tool to study degradation pathways where the precise reaction kinetics are unknown. Altogether, this work shows the versatility of CANs network structure as a means to design controllable degrading thermosets for smart material applications.

4.6 Acknowledgments

This work was made possible by funding from the Graduate Assistance in Areas of National Need (GAANN) and a National Science Foundation's Grant DMR 1809841. A.S.K. acknowledges support from an Arnold O. Beckman Post-doctoral Fellowship.

4.7 References

(1) Liu, Y.; Wang, W.; Yang, J.; Zhou, C.; Sun, J. PH-Sensitive Polymeric Micelles Triggered Drug Release for Extracellular and Intracellular Drug Targeting Delivery. *Asian J. Pharm. Sci.* **2013**, *8* (3), 159–167. https://doi.org/10.1016/j.ajps.2013.07.021.

(2) Klose, D.; Siepmann, F.; Elkharraz, K.; Siepmann, J. PLGA-Based Drug Delivery Systems: Importance of the Type of Drug and Device Geometry. *Int. J. Pharm.* **2008**, *354* (1–2), 95–103. https://doi.org/10.1016/j.ijpharm.2007.10.030.

(3) Javed, M.; Tasmim, S.; Abdelrahman, M. K.; Ambulo, C. P.; Ware, T. H. Degradation-Induced Actuation in Oxidation-Responsive Liquid Crystal Elastomers. *Crystals* **2020**, *10* (5). https://doi.org/10.3390/cryst10050420.

(4) Hu, L.; Zhang, Q.; Li, X.; Serpe, M. J. Stimuli-Responsive Polymers for Sensing and Actuation. *Mater. Horizons* **2019**, *6* (9), 1774–1793. https://doi.org/10.1039/c9mh00490d.

(5) Ghobril, C.; Charoen, K.; Rodriguez, E. K.; Nazarian, A.; Grinstaff, M. W. A Dendritic Thioester Hydrogel Based on Thiol-Thioester Exchange as a Dissolvable Sealant System for Wound Closure. *Angew. Chemie - Int. Ed.* **2013**, *52* (52), 14070–14074. https://doi.org/10.1002/anie.201308007.

(6) Mabey, W.; Mill, T. Critical Review of Hydrolysis of Organic Compounds in Water under Environmental Conditions. *J. Phys. Chem. Ref. Data* **1978**, *7* (2), 383–415. https://doi.org/10.1063/1.555572.

(7) Farah, S.; Anderson, D. G.; Langer, R. Physical and Mechanical Properties of PLA, and Their Functions in Widespread Applications — A Comprehensive Review. *Adv. Drug Deliv. Rev.* **2016**, *107*, 367–392. https://doi.org/10.1016/j.addr.2016.06.012.

(8) Li, Q.; Ma, S.; Wang, S.; Yuan, W.; Xu, X.; Wang, B.; Huang, K.; Zhu, J. Facile Catalyst-Free Synthesis, Exchanging, and Hydrolysis of an Acetal Motif for Dynamic Covalent Networks. *J. Mater. Chem. A* **2019**, *7* (30), 18039–18049. https://doi.org/10.1039/c9ta04073k.

(9) Xu, Z.; Liang, Y.; Ma, X.; Chen, S.; Yu, C.; Wang, Y.; Zhang, D.; Miao, M. Recyclable Thermoset Hyperbranched Polymers Containing Reversible Hexahydro-s-Triazine. *Nat. Sustain.* **2020**, *3* (1), 29–34. https://doi.org/10.1038/s41893-019-0444-6.

(10) Podgórski, M.; Fairbanks, B. D.; Kirkpatrick, B. E.; McBride, M.; Martinez, A.; Dobson, A.; Bongiardina, N. J.; Bowman, C. N. Toward Stimuli-Responsive Dynamic Thermosets through Continuous Development and Improvements in Covalent Adaptable Networks (CANs). *Adv. Mater.* **2020**, *32* (20), 1–26. https://doi.org/10.1002/adma.201906876.

(11) Guerre, M.; Taplan, C.; Winne, J. M.; Du Prez, F. E. Vitrimers: Directing Chemical Reactivity to Control Material Properties. *Chem. Sci.* **2020**, *11* (19), 4855–4870. https://doi.org/10.1039/d0sc01069c.

(12) Wang, C.; Goldman, T. M.; Worrell, B. T.; McBride, M. K.; Alim, M. D.; Bowman, C. N. Recyclable and Repolymerizable Thiol-X Photopolymers. *Mater. Horizons* **2018**, *5* (6), 1042–1046. https://doi.org/10.1039/c8mh00724a.

(13) García, J. M.; Jones, G. O.; Virwani, K.; Mccloskey, B. D.; Boday, D. J.; Huurne, G. M.; Horn, H. W.; Coady, D. J.; Bintaleb, A. M.; Alabdulrahman, A. M. S.; Alsewailem, F.; Almegren, H. A. A.; Hedrick, J. L. Recyclable, Strong Thermosets and Organogels via Paraformaldehyde Condensation with Diamines. *Science (80-.).* **2014**, *13073* (May), 732–735. https://doi.org/10.1126/science.1251484.

(14) Taplan, C.; Guerre, M.; Du Prez, F. E. Covalent Adaptable Networks Using β-Amino Esters

as Thermally Reversible Building Blocks. *J. Am. Chem. Soc.* **2021**, *143* (24), 9140–9150. https://doi.org/10.1021/jacs.1c03316.
(15) Worrell, B. T.; McBride, M. K.; Lyon, G. B.; Cox, L. M.; Wang, C.; Mavila, S.; Lim, C. H.; Coley, H. M.; Musgrave, C. B.; Ding, Y.; Bowman, C. N. Bistable and Photoswitchable States of Matter. *Nat. Commun.* **2018**, *9*, 1–7. https://doi.org/10.1038/s41467-018-05300-7.
(16) Taplan, C.; Guerre, M.; Winne, J. M.; Du Prez, F. E. Fast Processing of Highly Crosslinked, Low-Viscosity Vitrimers. *Mater. Horizons* **2020**, *7* (1), 104–110. https://doi.org/10.1039/c9mh01062a.
(17) Capelot, M.; Unterlass, M. M.; Tournilhac, F.; Leibler, L. Catalytic Control of the Vitrimer Glass Transition. *ACS Macro Lett.* **2012**, *1* (7), 789–792. https://doi.org/10.1021/mz300239f.
(18) Chao, A.; Zhang, D. Investigation of Secondary Amine-Derived Aminal Bond Exchange toward the Development of Covalent Adaptable Networks. *Macromolecules* **2019**, *52* (2), 495–503. https://doi.org/10.1021/acs.macromol.8b02654.
(19) Denissen, W.; Rivero, G.; Nicolaÿ, R.; Leibler, L.; Winne, J. M.; Du Prez, F. E. Vinylogous Urethane Vitrimers. *Adv. Funct. Mater.* **2015**, *25* (16), 2451–2457. https://doi.org/10.1002/adfm.201404553.
(20) Melchor Bañales, A. J.; Larsen, M. B. Thermal Guanidine Metathesis for Covalent Adaptable Networks. *ACS Macro Lett.* **2020**, *9* (7), 937–943. https://doi.org/10.1021/acsmacrolett.0c00352.
(21) Göpferich, A. Mechanisms of Polymer Degradation and Erosion. *Biomater. Silver Jubil. Compend.* **1996**, *17* (2), 117–128. https://doi.org/10.1016/B978-008045154-1.50016-2.
(22) Göpferich, A. Polymer Bulk Erosion. *Macromolecules* **1997**, *30* (9), 2598–2604. https://doi.org/10.1021/ma961627y.
(23) Kuang, X.; Shi, Q.; Zhou, Y.; Zhao, Z.; Wang, T.; Qi, H. J. Dissolution of Epoxy Thermosets: Via Mild Alcoholysis: The Mechanism and Kinetics Study. *RSC Adv.* **2018**, *8* (3), 1493–1502. https://doi.org/10.1039/c7ra12787a.
(24) Yu, K.; Yang, H.; Dao, B. H.; Shi, Q.; Yakacki, C. M. Dissolution of Covalent Adaptable Network Polymers in Organic Solvent. *J. Mech. Phys. Solids* **2017**, *109*, 78–94. https://doi.org/10.1016/j.jmps.2017.08.006.
(25) Marco-Dufort, B.; Willi, J.; Vielba-Gomez, F.; Gatti, F.; Tibbitt, M. W. Environment Controls Biomolecule Release from Dynamic Covalent Hydrogels. *Biomacromolecules* **2021**, *22* (1), 146–157. https://doi.org/10.1021/acs.biomac.0c00895.
(26) Hernandez, J. J.; Dobson, A. L.; Carberry, B. J.; Kuenstler, A. S.; Shah, P. K.; Anseth, K. S.; White, T. J.; Bowman, C. N. Controlled Degradation of Cast and 3-D Printed Photocurable Thioester Networks via Thiol–Thioester Exchange. *Macromolecules* **2022**, *55*, 1376–1385. https://doi.org/10.1021/acs.macromol.1c02459.
(27) Carberry, B. J.; Hernandez, J. J.; Dobson, A.; Bowman, C. N.; Anseth, K. S. Kinetic Analysis of Degradation in Thioester Cross-Linked Hydrogels as a Function of Thiol Concentration, p Ka, and Presentation. *Macromolecules* **2022**, *55* (6), 2123–2129. https://doi.org/10.1021/acs.macromol.1c02396.
(28) De Neve, J.; Haven, J. J.; Harrisson, S.; Junkers, T. Deconstructing Oligomer Distributions: Discrete Species and Artificial Distributions. *Angew. Chemie - Int. Ed.* **2019**, *58* (39), 13869–13873. https://doi.org/10.1002/anie.201906842.
(29) Hiemenz, P. C.; Lodge, T. P. *Polymer Chemistry Second Edition*; CRC Press Taylor & Francis Group, 2007. https://doi.org/10.1201/9781420018271-4.

(30) Vu, D. T.; Kolah, A. K.; Asthana, N. S.; Peereboom, L.; Lira, C. T.; Miller, D. J. Oligomer Distribution in Concentrated Lactic Acid Solutions. *Fluid Phase Equilib.* **2005**, *236* (1–2), 125–135. https://doi.org/10.1016/j.fluid.2005.06.021.
(31) Metters, A. T.; Bowman, C. N.; Anseth, K. S. A Statistical Kinetic Model for the Bulk Degradation of PLA-b-PEG-b-PLA Hydrogel Networks. *J. Phys. Chem. B* **2000**, *104* (30), 7043–7049. https://doi.org/10.1021/jp000523t.
(32) Rydholm, A. E.; Reddy, S. K.; Anseth, K. S.; Bowman, C. N. Controlling Network Structure in Degradable Thiol-Acrylate Biomaterials to Tune Mass Loss Behavior. *Biomacromolecules* **2006**, *7* (10), 2827–2836. https://doi.org/10.1021/bm0603793.
(33) McBride, R. A.; Gillies, E. R. Kinetics of Self-Immolative Degradation in a Linear Polymeric System: Demonstrating the Effect of Chain Length. *Macromolecules* **2013**, *46* (13), 5157–5166. https://doi.org/10.1021/ma4009753.
(34) Han, X.; Pan, J. Polymer Chain Scission, Oligomer Production and Diffusion: A Two-Scale Model for Degradation of Bioresorbable Polyesters. *Acta Biomater.* **2011**, *7* (2), 538–547. https://doi.org/10.1016/j.actbio.2010.09.005.
(35) Lazzari, S.; Codari, F.; Storti, G.; Morbidelli, M.; Moscatelli, D. Modeling the PH-Dependent PLA Oligomer Degradation Kinetics. *Polym. Degrad. Stab.* **2014**, *110*, 80–90. https://doi.org/10.1016/j.polymdegradstab.2014.08.012.
(36) Moorhoff, C. M.; Cook, W. D.; Braybrook, C. Novel Synthesis of Symmetrical 3,3′-Allyl Dithioethers as Photoplastic Monomer Precursors by Equal Molar Rate Addition of Reactants and Solvent Controlled Oligomerization. *Monatshefte fur Chemie* **2013**, *144* (6), 891–902. https://doi.org/10.1007/s00706-013-0942-6.
(37) Davidson, E. C.; Kotikian, A.; Li, S.; Aizenberg, J.; Lewis, J. A. 3D Printable and Reconfigurable Liquid Crystal Elastomers with Light-Induced Shape Memory via Dynamic Bond Exchange. *Adv. Mater.* **2020**, *32* (1), 1–6. https://doi.org/10.1002/adma.201905682.
(38) Martinez, A. M.; Cox, L. M.; Killgore, J. P.; Bongiardina, N. J.; Riley, R. D.; Bowman, C. N. Permanent and Reversibly Programmable Shapes in Liquid Crystal Elastomer Microparticles Capable of Shape Switching. *Soft Matter* **2021**, *17* (3), 467–474. https://doi.org/10.1039/d0sm01836h.
(39) Cui, C.; An, L.; Zhang, Z.; Ji, M.; Chen, K.; Yang, Y.; Su, Q.; Wang, F.; Cheng, Y.; Zhang, Y. Reconfigurable 4D Printing of Reprocessable and Mechanically Strong Polythiourethane Covalent Adaptable Networks. *Adv. Funct. Mater.* **2022**, *32* (29), 1–9. https://doi.org/10.1002/adfm.202203720.
(40) Bracher, P. J.; Snyder, P. W.; Bohall, B. R.; Whitesides, G. M. The Relative Rates of Thiol-Thioester Exchange and Hydrolysis for Alkyl and Aryl Thioalkanoates in Water. *Orig. Life Evol. Biosph.* **2011**, *41* (5), 399–412. https://doi.org/10.1007/s11084-011-9243-4.
(41) Worrell, B. T.; Mavila, S.; Wang, C.; Kontour, T. M.; Lim, C. H.; McBride, M. K.; Musgrave, C. B.; Shoemaker, R.; Bowman, C. N. A User's Guide to the Thiol-Thioester Exchange in Organic Media: Scope, Limitations, and Applications in Material Science. *Polym. Chem.* **2018**, *9* (36), 4523–4534. https://doi.org/10.1039/c8py01031e.
(42) Carberry, B. J.; Hergert, J. E.; Yavitt, F. M.; Hernandez, J. J.; Speckl, K. F.; Bowman, C. N.; McLeod, R. R.; Anseth, K. S. 3D Printing of Sacrificial Thioester Elastomers Using Digital Light Processing for Templating 3D Organoid Structures in Soft Biomatrices. *Biofabrication* **2021**, *13* (4). https://doi.org/10.1088/1758-5090/ac1c98.
(43) Wang, C.; Mavila, S.; Worrell, B. T.; Xi, W.; Goldman, T. M.; Bowman, C. N. Productive Exchange of Thiols and Thioesters to Form Dynamic Polythioester-Based Polymers. *ACS*

Macro Lett. **2018**, *7* (11), 1312–1316. https://doi.org/10.1021/acsmacrolett.8b00611.
(44) Mavila, S.; Worrell, B. T.; Culver, H. R.; Goldman, T. M.; Wang, C.; Lim, C. H.; Domaille, D. W.; Pattanayak, S.; McBride, M. K.; Musgrave, C. B.; Bowman, C. N. Dynamic and Responsive DNA-like Polymers. *J. Am. Chem. Soc.* **2018**, *140* (42), 13594–13598. https://doi.org/10.1021/jacs.8b09105.
(45) Mavila, S.; Culver, H. R.; Anderson, A. J.; Prieto, T. R.; Bowman, C. N. Athermal, Chemically Triggered Release of RNA from Thioester Nucleic Acids. *Angew. Chemie - Int. Ed.* **2022**, *61* (1), 1–5. https://doi.org/10.1002/anie.202110741.
(46) Soars, S. M.; Kirkpatrick, B. E.; Fairbanks, B. D.; Kamps, J. T.; Anseth, K. S.; Bowman, C. N. Synthesis, Selective Decoration and Photocrosslinking of Self-Immolative Poly(Thioester)-PEG Hydrogels. *Polym. Int.* **2022**, *71* (7), 906–911. https://doi.org/10.1002/pi.6388.
(47) Uygun, M.; Tasdelen, M. A.; Yagci, Y. Influence of Type of Initiation on Thiol-Ene "Click" Chemistry. *Macromol. Chem. Phys.* **2010**, *211* (1), 103–110. https://doi.org/10.1002/macp.200900442.
(48) Martinez, V.; Henary, M. Nile Red and Nile Blue: Applications and Syntheses of Structural Analogues. *Chem. - A Eur. J.* **2016**, *22* (39), 13764–13782. https://doi.org/10.1002/chem.201601570.
(49) Rydholm, A. E.; Reddy, S. K.; Anseth, K. S.; Bowman, C. N. Development and Characterization of Degradable Thiol-Allyl Ether Photopolymers. *Polymer (Guildf).* **2007**, *48* (15), 4589–4600. https://doi.org/10.1016/j.polymer.2007.05.063.
(50) Yang, J.; Chen, L.; Zhu, M.; Ishaq, M. W.; Chen, S.; Li, L. Investigation of the Multimer Cyclization Effect during Click Step- Growth Polymerization of AB-Type Macromonomers. *Macromolecules* **2022**. https://doi.org/10.1021/acs.macromol.2c01087.
(51) Flory, P. J. Molecular Size Distribution in Three Dimensional Polymers. I. Gelation1. *J. Am. Chem. Soc.* **1941**, *63* (11), 3083–3090. https://doi.org/10.1021/ja01131a008.
(52) Stille, J. K. Step-Growth Polymerization. *J. Chem. Educ.* **1981**, *58* (11), 862–866.
(53) Kalathimekkad, S.; Missinne, J.; Schaubroeck, D.; Mandamparambil, R.; Van Steenberge, G. Alcohol Vapor Sensor Based on Fluorescent Dye-Doped Optical Waveguides. *IEEE Sens. J.* **2015**, *15* (1), 76–81. https://doi.org/10.1109/JSEN.2014.2338916.
(54) Deye, J. F.; Berger, T. A.; Anderson, A. G. Nile Red as a Solvatochromic Dye for Measuring Solvent Strength in Normal Liquids and Mixtures of Normal Liquids with Supercritical and Near Critical Fluids. *Anal. Chem.* **1990**, *62* (14), 1552. https://doi.org/10.1021/ac00213a044.
(55) Reichardt, C. Solvatochromic Dyes as Solvent Polarity Indicators. *Chem. Rev.* **1994**, *94* (8), 2319–2358. https://doi.org/10.1021/cr00032a005.

4.8 Supporting Information

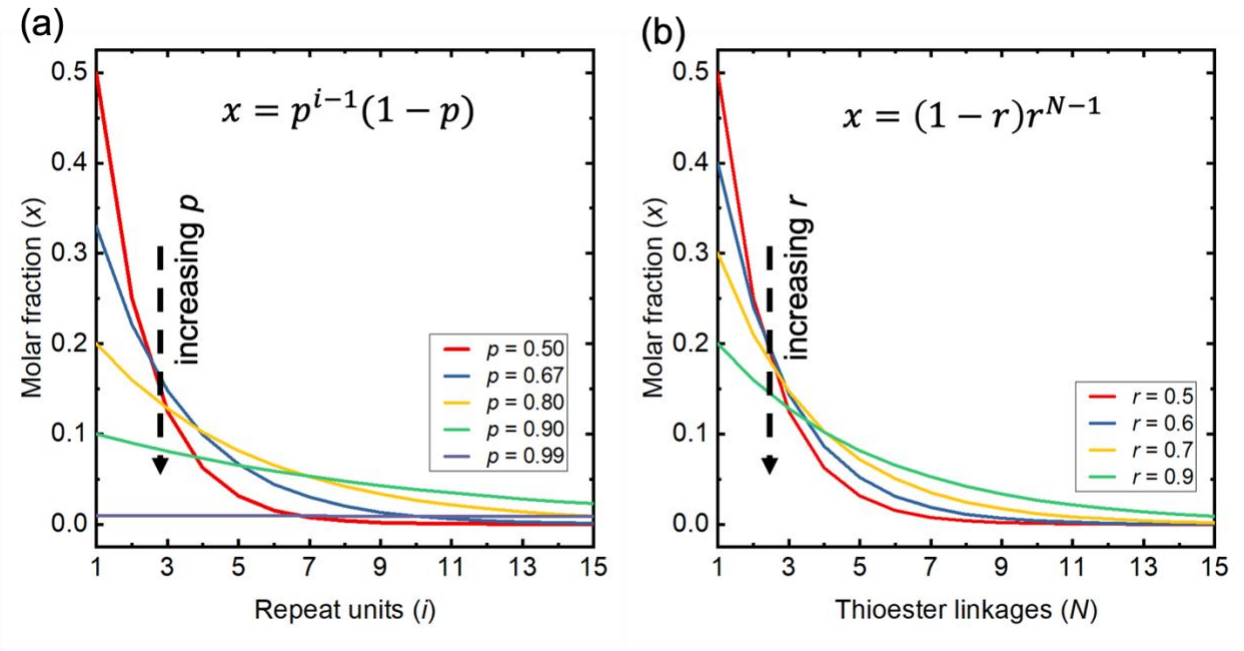

Figure S4.1. (a) Flory-Schulz distribution for oligomers as a function of repeat units (*i*), using the listed equation where *x* is the molar fraction, *p* the conversion, and *i* the oligomer length. (b) Derived polydisperse distribution for odd-numbered oligomers, plotting molar fraction versus thioester linkages per oligomer. Distribution uses the listed equation where *r* is the ratio of HDT : TEDE and *N* the number of thioester linkages per oligomer.

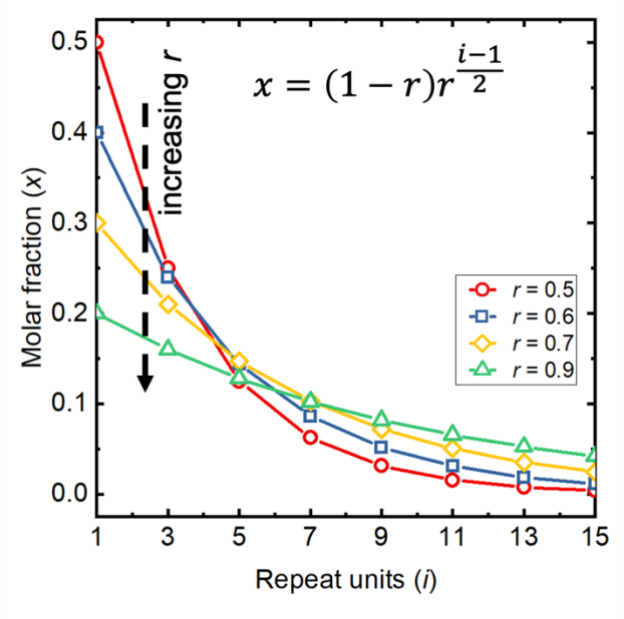

Figure S4.2. Derived polydisperse distribution for odd-numbered oligomers, plotting molar fraction versus number of repeat units (*i*). Only odd-numbered repeat units are considered, and repeat units (*i*) translates to thioester linkages (*N*) via $\boldsymbol{N = \frac{i+1}{2}}$.

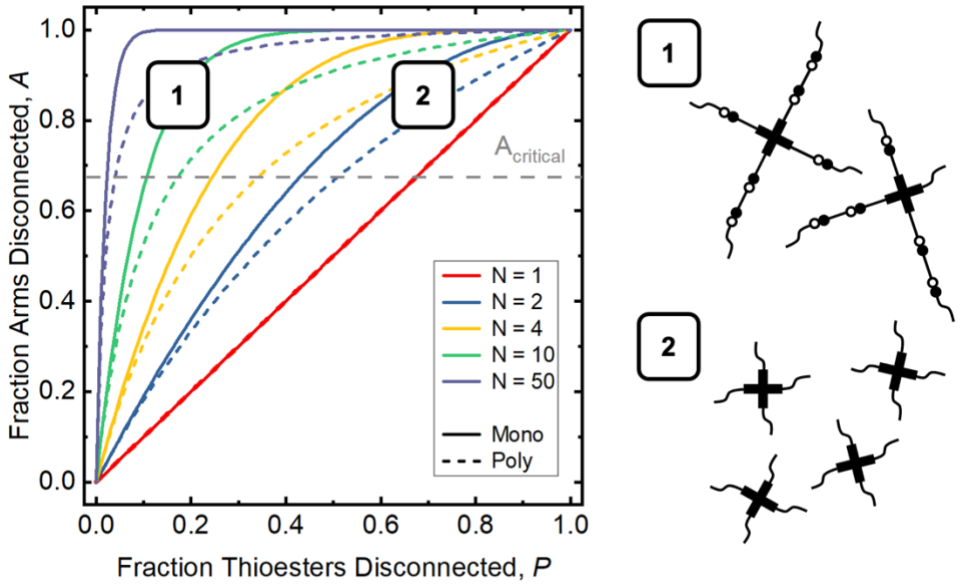

Figure S4.3. Two regions (1, 2) are visible when comparing the fraction of arms broken versus the fraction of thioesters disconnected. Changing *N* or dispersity (mono versus poly) controls which region degradation occurs in.

(a)

$\overline{X_n}$	r	N	$Đ_X$
1	0	1	1.01
3	0.50	2	1.31
5	0.67	3	1.28
7	0.75	4	1.33

(b)

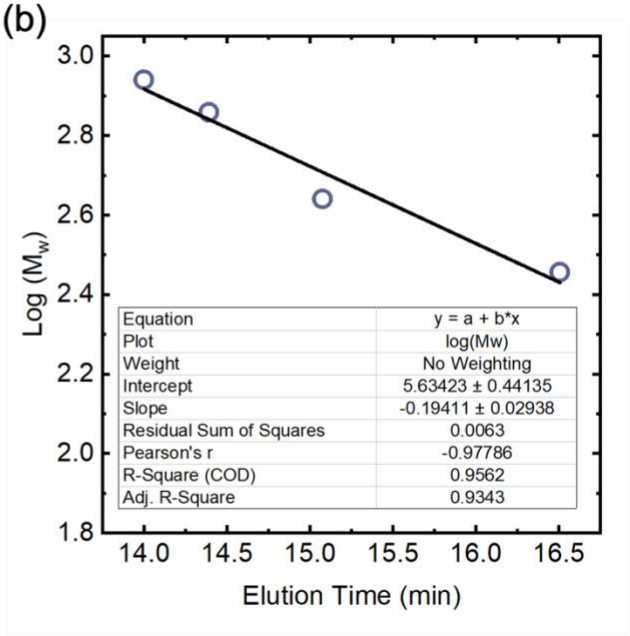

Figure S4.4. (a) Characteristic values for thioester oligomers created by reacting TEDE with HDT in varying stoichiometric ratios. $\overline{X_n}$ was calculated using equation 1, r is the molar ratio of [TEDE] : [HDT], N the number of thioester linkages per oligomer, and $Đ_X$ the oligomer dispersity as calculated by GPC. (b) Calibration curve used to determine oligomer M_w and dispersity. The curve was created using elution times for known low M_w oligomers and followed a previously established literature method.[1]

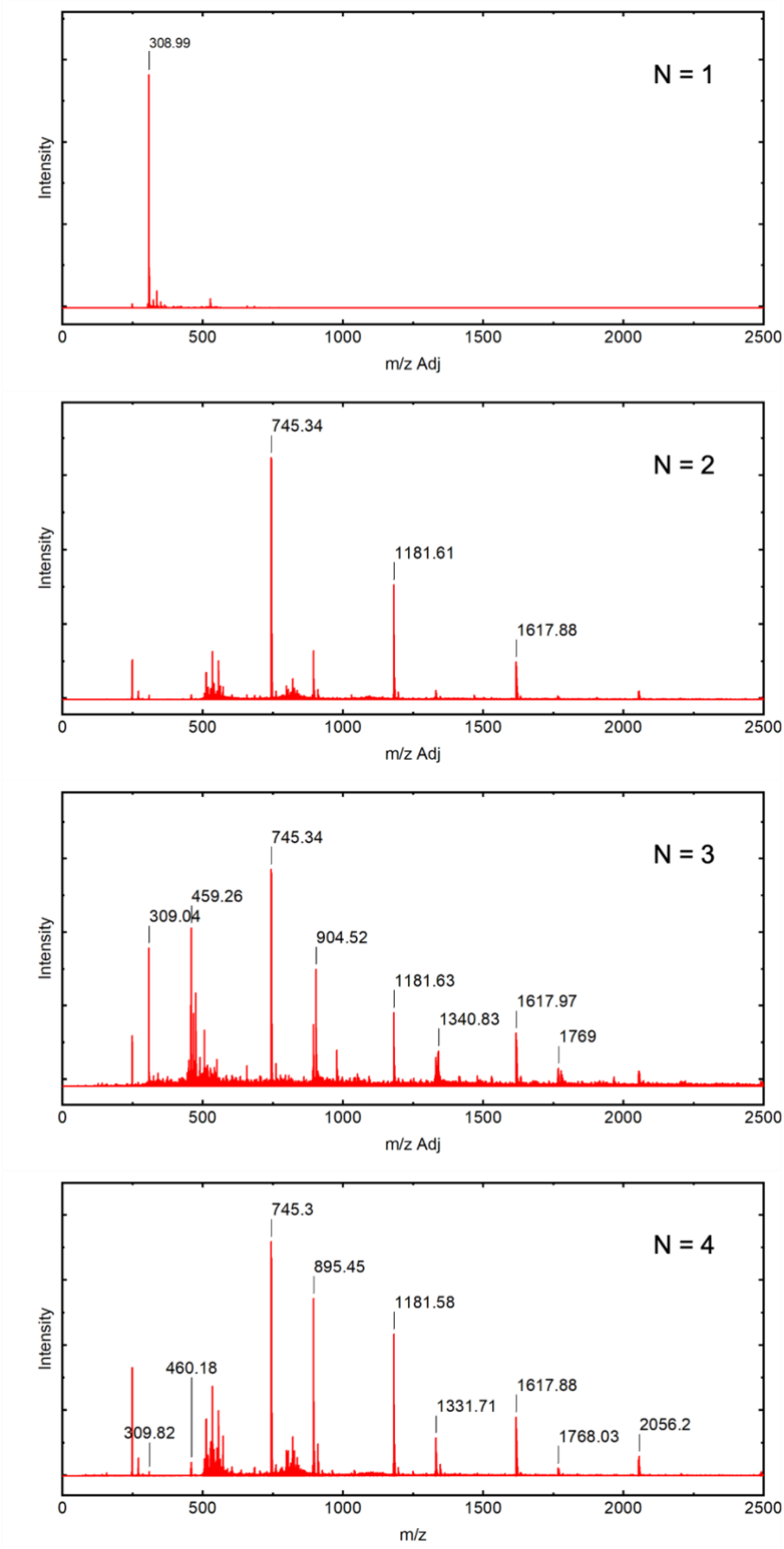

Figure S4.5. MALDI-TOF spectra for the *N* = 1, 2, 3, and 4 oligomer distributions.

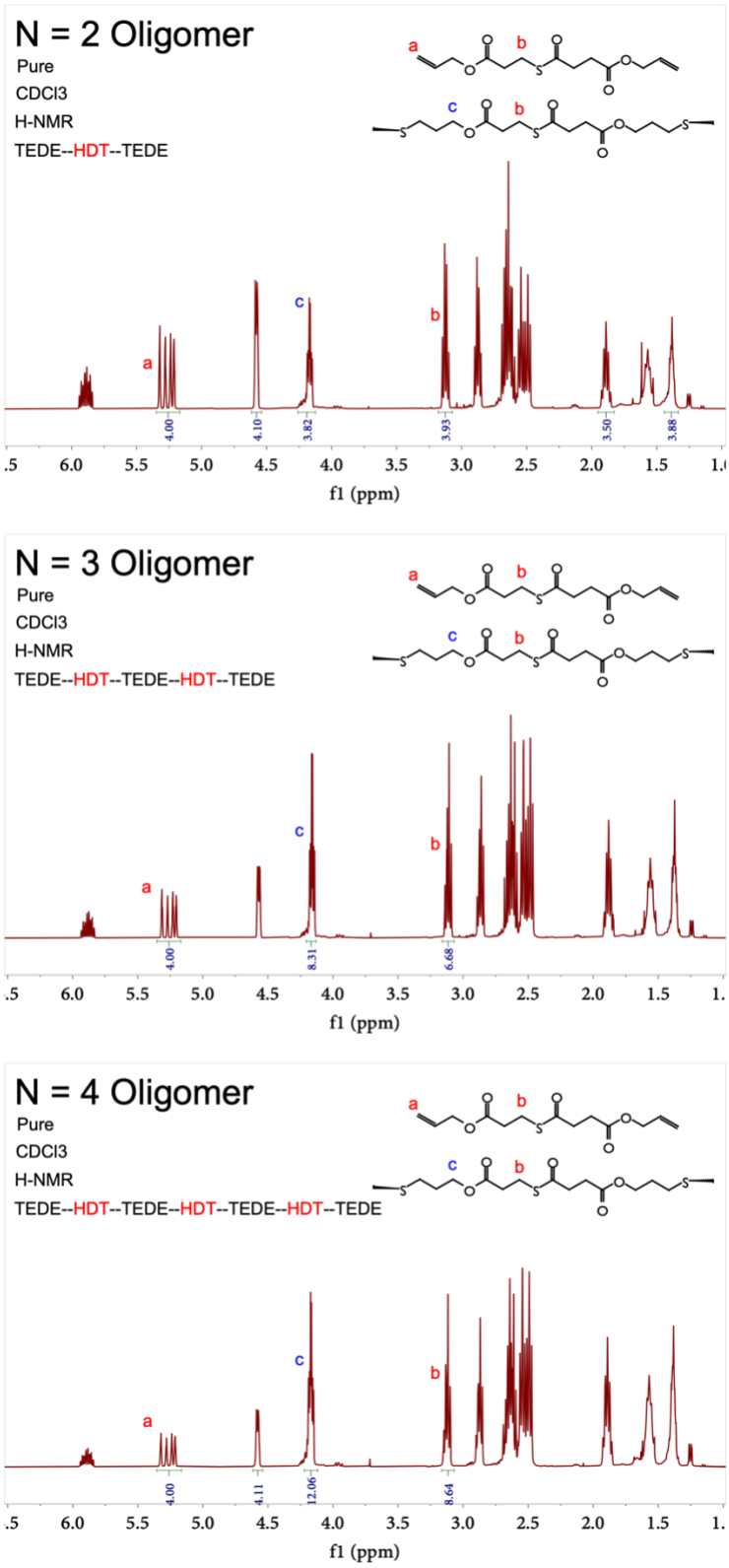

Figure S4.6. NMR spectra and end-group analysis for *N* = 2, 3, and 4 oligomers. For end-group analysis, the theoretical and actual values of integral C are compared.

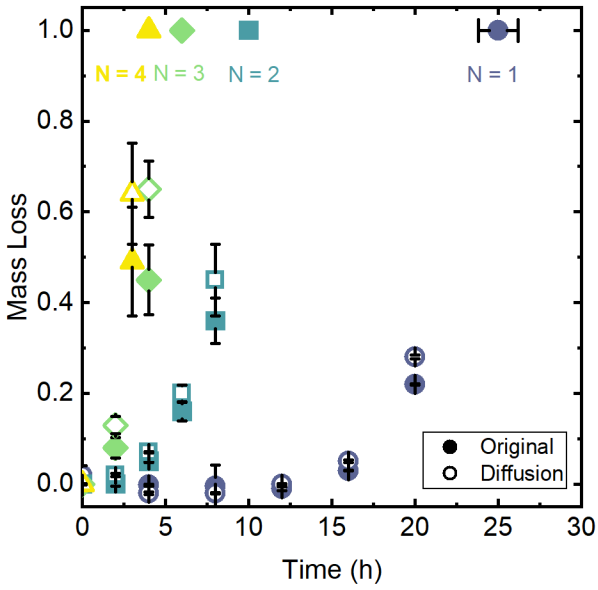

Figure S4.7. Extra diffusion effects on mass loss profiles. Samples with more diffusion time were soaked in acetone for an additional 24h.

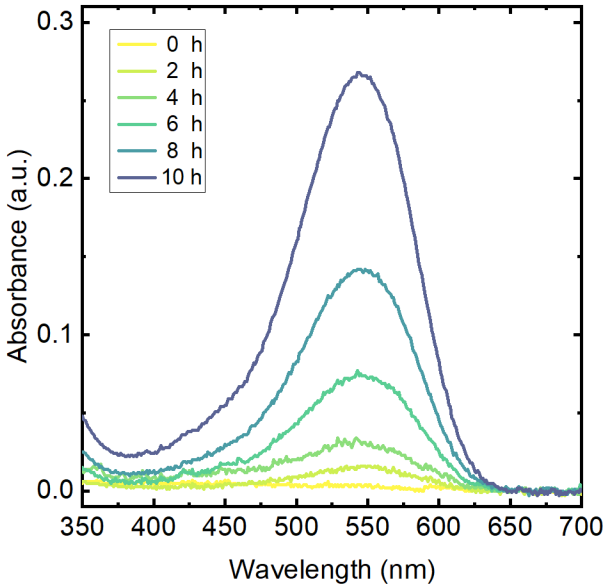

Figure S4.8. Representative UV-Vis absorbance spectra of the degradation solution over time for a $N = 2$ sample. Absorbance for Nile red was taken at 552 nm, as guided by past literature.[2]

4.8.1 Model Derivations

4.8.1.1 Oligomer Degree of Polymerization Distribution for Off-Stoichiometric Monomers

For the step-growth reaction of two difunctional monomers AA and BB with one reagent in excess, a statistical approach is used to determine the oligomer number-average size distribution. After polymerization, a randomly selected oligomer can fall into one of four categories: 1. An i-mer beginning with unreacted A, where i is an odd integer, 2. An i-mer beginning with unreacted B, where i is an odd integer, 3. An i-mer beginning with unreacted A, where i is an even integer, or 4. An i-mer beginning with unreacted B, where i is an even integer.

$$A-(AB-BA)_k-A; \qquad i=2k+1;\ \ k=0,1,2,\ldots$$

$$B-(BA-AB)_k-B; \qquad i=2k+1;\ \ k=0,1,2,\ldots$$

$$A-(AB-BA)_k-AB-B; \qquad i=2k+2;\ \ k=0,1,2,\ldots$$

$$B-(BA-AB)_k-BA-A; \qquad i=2k+2;\ \ k=0,1,2,\ldots$$

Starting with A or B

The probability of starting with an unreacted A is the mole fraction of all unreacted A with respected to all unreacted functional groups (y_A), or

$$y_A=\frac{N_A}{N_A+N_B}$$

The numbers of unreacted A (N_A) and unreacted B (N_B) are related to their individual degrees of conversion and initial values, or

$$y_A=\frac{N_A}{N_A+N_B}=\frac{N_{A0}(1-p_A)}{N_{A0}(1-p_A)+N_{B0}(1-p_B)}=\frac{1-p_A}{1-p_A+\frac{N_{B0}}{N_{A0}}(1-p_B)}$$

If A is the functional group in excess, $\frac{N_{B0}}{N_{A0}} = r$ and $p_A = rp_B$. Combining these and dropping the subscript B in p_B for clarity provide an expression for the mole fraction of unreacted A with respect to all unreacted functional groups:

$$y_A = \frac{1 - rp}{1 + r - 2rp}$$

Therefore, the probability of starting with Case 1 or Case 3 is y_A while the probability of starting with Case 2 or Case 4 is $1 - y_A$.

Growing Oligomers by Two Units

For all cases, for every increment in size by two monomer units (or, equivalently, every increment in dummy variable k), the bracketed portion of the oligomer requires one reaction of A and one reaction of B. These occur with probability $p_A = rp_B$ and p_B, respectively. Therefore, the probability of an oligomer growing by two monomer units is $(rp^2)^k$.

Ending with an Odd or Even Degree of Polymerization

Lastly, the end group on each oligomer must be established. For Case 1, an A group must remain unreacted, which occurs with probability $1 - p_A = 1 - rp$. For Case 2, a B group must remain unreacted, which occurs with probability $1 - p_B = 1 - p$. In Case 3, one A group must react followed by one B group not reacting. This occurs with probability $p_A(1 - p_B) = rp(1 - p)$. Similarly for Case 4, one B group reacts followed by one A group remaining unreacted, with probability $p(1 - rp)$.

4.8.1.2 Number-Average Degree of Polymerization Distribution and Reduction to Flory-Schulz

Combining all these together provides the number-average size distribution of oligomers in an off-stoichiometric step-growth reaction:

$$y_A \quad (rp^2)^k \quad (1-rp) \qquad i = 2k+1;\ \ k = 0, 1, 2, \ldots$$

$$(1-y_A)(rp^2)^k \quad (1-p) \qquad i = 2k+1;\ \ k = 0, 1, 2, \ldots$$

$$y_A \quad (rp^2)^k \quad rp(1-p) \qquad i = 2k+2;\ \ k = 0, 1, 2, \ldots$$

$$(1-y_A)(rp^2)^k \quad p(1-rp) \qquad i = 2k+2;\ \ k = 0, 1, 2, \ldots$$

Flory-Schulz Distribution

In the case of equimolar concentrations of reactive functional groups or the case of homopolymerization (r=1), the distribution simplifies to the familiar Flory-Schulz distribution. For odd i (Case 1 and Case 2), $k = \frac{i-1}{2}$ and for even i (Case 3 and Case 4), $k = \frac{i-2}{2}$. Therefore, in the equimolar case for odd i,

$$x(i_{odd}) = y_A(p^2)^k(1-p) + (1-y_A)(p^2)^k(1-p)$$

$$= y_A(p)^{2k}(1-p) + (1-y_A)(p)^{2k}(1-p)$$

$$= y_A(p)^{\frac{2(i-1)}{2}}(1-p) + (1-y_A)(p)^{\frac{2(i-1)}{2}}(1-p)$$

$$x(i_{odd}) = (p)^{i-1}(1-p)$$

Similarly, for the equimolar case for even i:

$$x(i_{even}) = y_A(p^2)^k p(1-p) + (1-y_A)(p^2)^k p(1-p)$$

$$= y_A(p)^{2k} p(1-p) + (1-y_A)(p)^{2k} p(1-p)$$

$$= y_A(p)^{\frac{2(i-2)}{2}} p(1-p) + (1-y_A)(p)^{\frac{2(i-2)}{2}} p(1-p)$$

$$y_A(p)^{i-2+1}(1-p) + (1-y_A)(p)^{i-2+1}(1-p)$$

$$x(i_{even}) = (p)^{i-1}(1-p)$$

4.8.1.3 Determination of $\bar{y}$

The probability of an arm of a crosslinking monomer becoming disconnected from the network depends on the oligomer length of that arm. To simplify the mass loss calculation, a weighted average is used to determine a number-average effective y, or $\bar{y}$, via

$$\bar{y} = \sum_{N=1,2,\ldots} x(N)y(N) = \sum_{k=0,1,2,\ldots} x(k)y(k)$$

where N is the number of thioesters in an arm, x(N) is the number-average distribution of arms with N thioesters, and y(N) is the probability of an arm with N thioesters becoming disconnected from the network. Although a general formula for $\bar{y}$ for any oligomer size can be determined, if an ideal network is assumed, only odd-sized oligomers beginning with excess unreacted ene (Case 1, with ene identified as A and thiol identified as B) are possible. In this scenario, N = k+1, where k is the same dummy variable used in the Case 1 distribution, and $p = 1$. For a given number of thioesters in an arm, the following expression for $y(j)$ holds for Z = 4:

$$y(j) = A(j) + \big(1 - A(j)\big) \sum_{l=0,1,2,\ldots} \sum_{m=0,1,2,\ldots} \sum_{n=0,1,2,\ldots} [x(l)y(l)][x(m)y(m)][x(n)y(n)]$$

Here, A represents the probability that at least one thioester has cleaved on the oligomer arm containing j thioesters. When no thioesters have cleaved on the oligomer arm, the arm can still be disconnected if all arms of the adjacent crosslinking monomer are disconnected. The triple summation is necessary because each of these arms on the adjacent monomer can be of different length, each with its own probability distribution. By factoring out each term that is constant in the summation, a more manageable form of this expression is obtained:

$$y(j) = A(j) + \big(1 - A(j)\big) \sum_{l=0,1,2,\ldots} x(l)y(l) \sum_{m=0,1,2,\ldots} x(m)y(m) \sum_{n=0,1,2,\ldots} x(n)y(n)$$

$$y(j) = A(j) + \big(1 - A(j)\big)\bar{y}^3$$

Multiplying this by x(j) and summing over all possible j gives $\bar{y}$:

$$\sum_{j=0,1,2,\ldots} x(j)y(j) = \sum_{j=0,1,2,\ldots} x(j)A(j) + x(j)\big(1 - A(j)\big)\bar{y}^3$$

$$\bar{y} = \bar{A} + (1 - \bar{A})\bar{y}^{Z-1}$$

where the relation $\bar{A} = \sum x(j)A(j)$ was used and the equation is generalized for crosslinking monomer functionality of Z.

4.8.1.4 Determination of $\bar{A}$

To use this equation for $\bar{y}$, the same weighted average method for determining $\bar{A}$ is used. As before, a fully generalizable form is available but significant simplifications to the process occur when assuming an ideal network. In an ideal network, x(k) and A(k) have the following forms:

$$x(k) = (1 - r)r^k$$

$$A(k) = 1 - (1 - P)^{k+1}$$

where the relationship N = k+1 was used. From here, $\bar{A}$ is determined:

$$\bar{A} = \sum_{k=0,1,2,\ldots} x(k)A(k) = \sum_{k=0,1,2,\ldots} [(1 - r)r^k][1 - (1 - P)(1 - P)^k]$$

$$= (1 - r)\sum_k \{r^k\} - (1 - r)(1 - P)\sum_k \Big\{\big(r(1 - P)\big)^k\Big\}$$

$$= \frac{(1 - r)}{1 - r} - \frac{(1 - r)(1 - P)}{1 - r(1 - P)}$$

$$\bar{A} = \frac{P}{1 - r(1 - P)}$$

4.8.2 References

(1) Han, X.; Fairbanks, B. D.; Sinha, J.; Bowman, C. N. Sequence-Controlled Synthesis of Advanced Clickable Synthetic Oligonucleotides. *Macromol. Rapid Commun.* **2020**, *41* (16), 1–9. https://doi.org/10.1002/marc.202000327.

(2) Martinez, V.; Henary, M. Nile Red and Nile Blue: Applications and Syntheses of Structural Analogues. *Chem. - A Eur. J.* **2016**, *22* (39), 13764–13782. https://doi.org/10.1002/chem.201601570.

Chapter 5: Low-Temperature Reprocessing of Covalent Adaptable Networks via Thiol-Thioaminal Exchange

This chapter to be submitted as a manuscript to Macromolecules with the following coauthors: Juan J. Hernandez, Claire E. Niemet, Cassandra M. Sanchez, Shafer Soars, Sudheendran Mavila, Timothy J. White, Christopher N. Bowman

5.1 Abstract

This work explored the thiol-thioaminal exchange reaction within covalent adaptable networks (CANs) to establish reversible exchange CANs with near-ambient temperature reprocessability. A small molecule system was developed that extracted kinetic parameters (k_f, k_r, K_{eq}, $t_{1/2,eq}$) from the thiol-thioaminal exchange reaction between a thioaminal (DMTA) and three thiols (BMP, BTG, TP) by means of an established model. Changing thiol most impacted the reverse reaction rate constant (k_r), increasing over 100 times from 0.2 to 20 $mM^{-1}min^{-1}$. Thioaminal-containing networks were photocured and stress relaxed via the thiol-thioaminal exchange reaction, displaying an activation energy ($E_{a,SR}$) of 87 $\pm$ 8 kJ/mol. Excess thiol and elevated temperatures both lead to faster stress relaxation, with a stress relaxation time of as little as 10 s at 95 °C. Frequency sweeps of thioaminal networks resulted in a similar activation energy ($E_{a,FS}$) of 107 $\pm$ 8 kJ/mol and confirmed thiol-thioaminal exchange leads to reversible exchange type CANs. Thioaminal films were submerged in four thiols (BMP, BTG, TP, HT) to track network degradation via thiol-thioaminal exchange, and showed that choice of thiol gave ~100 times control over degradation time (380 min versus 4 min). The thiol-thioaminal exchange reaction represents a new CAN chemistry with potential in applications in need of rapid exchange reactions under near-ambient conditions.

5.2 Introduction

Recent interest in developing reprocessable crosslinked polymers has led to innovations in sustainable materials,[1,2] on-demand constructing-then-destructing photomasks,[3] and triggered drug release capsules.[4,5] Of the numerous ways to add post-functionalization to crosslinked polymers, such as addition of photoreactive groups[5–8] or cleavable chemical groups,[9–11] adding dynamic covalent bonds to polymers results in the creation of covalent adaptable networks (CANs).[12,13] When triggered, these dynamic covalent bonds rearrange network topology, giving CANs the benefits of crosslinked polymers while still allowing for material reprocessing via this rearrangement.[14]

CANs may be sub-divided into two categories based on the nature of the dynamic covalent chemistry: reversible addition and reversible exchange reaction-based networks. Reversible addition CANs rearrange chemical groups by disconnecting covalent bonds through a dissociated transition state, leading to a critical reverse-gelation point beyond which the polymer is no longer a network.[12,15] Conversely, reversible exchange CANs rearrange chemical groups by connecting covalent bonds through an associated transition state, resulting in a lack of reverse-gelation temperature, as the average crosslink density does not change with the applied stimulus. This constant crosslink density grants reversible exchange CANs increased dimensional stability and solvent resistance which justifies continued exploration.[12,16] While reversible exchange CANs may be triggered by various means, including light[17,18] and mechanical strain,[19,20] temperature serves as a favorable trigger due to its larger penetration depth,[21] facile coupling with other triggers,[22,23] and established infrastructure arising from thermal reprocessing of thermoplastics.[24–26] Recently, there has been a push to design reversible exchange CANs that rearrange rapidly enough that these networks may also be reprocessed by the traditional means developed for thermoplastics.

Several dynamic chemistries have enabled thermally-triggered reversible exchange CANs that may be reprocessed by traditional means. Transesterification has enabled reprocessing by reactive extrusion,[25,27] vinylogous urethanes by twin-screw extrusion,[24] and numerous other chemistries by compression molding.[28–32] However, all of these dynamic chemistries require temperatures above 100 °C for rapid rearrangement and most require exogenous catalyst, limiting the reworking of these networks at near-ambient conditions. Past work on reversible addition CANs[33–35] and supramolecular polymers[36] has shown that rearrangement at near-ambient conditions opens doors for room-temperature self-healing, material blending, and post-functionalization while also having a significant potential negative of ambient temperature creep behavior. Since creep behavior within polymers may be hindered by mixing reversible crosslinks with irreversible crosslinks[37,38] or sidestepped by confining dynamic networks to non-load-bearing applications,[39] there is still promise in designing a reversible exchange CANs capable of rapid rearrangement at sub 100 °C temperatures. Due to its rapid and self-catalyzed exchange, the thiol-thioaminal exchange reaction may permit these desired CANs.

The thiol-thioaminal exchange reaction exchanges the groups attached to a thiol and a thioaminal, as seen in **Scheme 5.1**. The exchange reaction is mediated by a thiolate anion, formed by deprotonation of the thiol by the thioaminal nitrogen, and the reaction exchanges its functional groups via a connected transition state.[40] Past work on thiol-thioaminal exchange has explored its use in biologically-active amino acids,[41] dynamic linear polymers,[40] and photolithography[42] but to these authors' knowledge no work has explored how thiol-thioaminal exchange may create CANs. Since thiol-thioaminal exchange occurs rapidly at near-ambient conditions and without catalyst, incorporating thioaminal groups into polymers seems to be a logical step.

This work investigates the thiol-thioaminal exchange reaction as a means to create reversible exchange CANs that are rapidly reprocessable under near-ambient conditions. A small molecule system was developed that extracted kinetic parameters (k_f, k_r, K_{eq}, $t_{1/2,eq}$) from the thiol-thioaminal exchange reaction between a thioaminal (DMTA) and one of three thiols (BMP, BTG, TP). After understanding the reaction through experiments on the small molecule system, thioaminal networks were formed via the thiol-ene photopolymerization reaction. These networks were stress relaxed via constant force shear rheology and the relaxation rates were analyzed via frequency sweep experiments at various temperatures (60 – 95 °C). Lastly, thioaminal networks were submerged in four thiol monomers (BMP, BTG, TP, HT) to investigate degradation via the thiol-thioaminal exchange reaction. While this work focused on polymers, the reaction kinetics and trends of thiol-thioaminal exchange addressed within may readily by adapted to other systems where rapid exchange is desired, contributing to the field of dynamic exchange reactions generally.

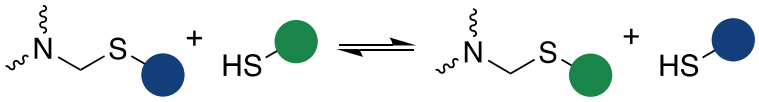

Scheme 5.1. Thiol-thioaminal exchange replaces the groups attached to the thiol and the thioaminal. This exchange occurs readily under ambient conditions without additional triggers or catalyst.

5.3 Materials and Experimental Methods

5.3.1 Materials

Thioaminal molecules dimethylthioaminal (DMTA) and allylthioaminal (ATA) were synthesized according to procedures described in the Supporting Information, **Scheme S5.1** and **Scheme S5.2**. All other materials were purchased commercially and used without further

purification. 1-Hexanethiol (HT), 1,6-hexanedithiol (HDT), butyl 3-mercaptopropionate (BMP), butyl glycolate (BTG), and thiophenol (TP) were purchased from Sigma Aldrich and Irgacure 819 (I819) from IGM Resins.

5.3.2 Small Molecule Exchange

Thiol-thioaminal exchange proceeded by mixing DMTA with one of three thiols (BMP, BTG, or TP) in a 1 : 1 molar ratio under neat conditions, ensuring the total solution was ~2 mL. The solution was stirred at 100 RPM in a 100 mL round bottom flask. At specific times, 10 μL of solution were removed from the flask and mixed with 500 μL of a 20 mM solution of dimethylsulfone in $CDCl_3$. NMR spectra of these samples were taken on a 400 MHz Avance III instrument from Bruker. Concentrations of DMTA, TA2 (the newly formed thioaminal), thiol, and HT (the newly formed thiol) were tracked by comparing integral values to the dimethylsulfone standard (2.98 ppm). The equilibrium constant (K_{eq}) was calculated via

$$K_{eq} = \frac{[TA2][HT]}{[DMTA][HSR]} \quad (1)$$

where [HSR] is the concentration of the thiol investigated for exchange (BMP, BTG, or TP). Reaction rate constants (k_f, k_r) and ½ of the equilibration time ($t_{1/2,eq}$) were calculated using a previously developed model for reversible second order reactions,[43] with the full solution in **Scheme S5.3**.

5.3.3 Fourier Transform Infrared Spectroscopy

Real-time FTIR was measured on a Nicolet 6700 FTIR instrument from Thermo Scientific. Samples were placed between KOH salt plates and exposed to 400 – 500 nm light at 30 mW/cm^2

for 5 min while spectra were measured from 4000 cm^{-1} to 650 cm^{-1} under ambient conditions. Conversion tracked area under the curve for the thiol (2560 cm^{-1}) and the ene (3070 cm^{-1}) peaks.

5.3.4 Photopolymerization

Thioaminal networks were cured by first combining HDT with I819 in a 0.7 thiol : 0.005 I819 molar ratio, heating the mixture at 90 °C for 15 min, and letting it cool to room temperature. ATA was then added to the mixture to create a solution of 0.7 thiol : 1 ene : 0.005 I819 and the solution was placed between glass slides coated in RainX, separated by 100 μm spacers, and clamped together using binder clips. The films were then cured under a 400 – 500 nm light source at 30 mW/cm^2 for 34 s on each side, removed from the glass slides, and subsequently used for stress relaxation and frequency sweep experiments.

5.3.5 Stress Relaxation

Stress relaxation was measured using an Ares-G2 Rheometer from TI Instruments. 100 μm films were loaded between an 8 mm quartz parallel plate and a Peltier plate with 2 N of pre-load axial force and 10 % shear stress. This experiment was performed at 30, 60, 80, and 95°C. The storage (*G'*) and loss moduli (*G''*) were tracked over time, and the time for stress relaxation (τ) was defined as the time required for normalized *G'* to reach 1/e (≈37%). Activation energy for stress relaxation was calculated via

$$\tau = \tau_0 \exp\left(\frac{E_{a,SR}}{RT}\right) \quad (2)$$

where τ_0 represents the initial stress relaxation time, $E_{a,SR}$ the activation energy for thiol-thioaminal exchange via stress relaxation, *R* the universal gas constant, and *T* the temperature in Kelvin. $E_{a,SR}$ was found using a best fit Arrhenius plot comparing $\ln(\tau)$ to *1/T* since the slope = $E_{a,SR}$ / *R*.

5.3.6 Frequency Sweep

Frequency sweeps were measured using an Ares-G2 Rheometer from TA Instruments. Similar to the stress relaxation procedure, 100 μm films were loaded between an 8 mm quartz plate and a Peltier plate, used 2 N of pre-load axial force, 10 % shear stress, and the test was performed at 60, 80, and 95°C. The storage (*G'*) and loss moduli (*G''*) were tracked as frequency increased from 10^{-3} – 10^{2} rad/s. Activation energy for frequency sweep relaxation ($E_{a,FS}$) was calculated via equation 2, but this time stress relaxation time (τ_{FS}) was determined via

$$\tau_{FS} = \frac{1}{\omega_C} \quad (3)$$

where ω_C represents the angular velocity in rad/s at which the storage and loss moduli crossover.

5.3.7 Film Degradation

A [0.7 thiol : 1 ene : 0.005 I819] solution composed of HDT, ATA, and I819 was mixed and placed between glass slides following the procedure described in Section 5.3.4. The solution was then cured under a 405 nm LED light bar for 2 min at 2.5 mW/cm^2, removed from the glass slides, and cut into ~2.5 x 2.5 cm squares which weighed ~50 mg. Each square was placed into a vial containing 2.5 mL of a designated thiol (> 200 times excess thiol), and visually inspected to note the degradation time for films, *i.e.* the total time it took for the films to fully dissolve. This procedure was repeated in triplicate for four thiols: BMP, BTG, TP, and HT.

5.4 Results and Discussion

5.4.1 Small Molecule Study

This work sought to investigate the thiol-thioaminal exchange reaction as a means to create reversible exchange CANs that rearrange under near-ambient conditions. To that end, a model thioaminal molecule was synthesized to study the kinetics of the thiol-thioaminal exchange reaction, specifically looking to understand how the choice of thiol may impact reaction rate constants (k_f, k_r), equilibrium constant (K_{eq}), and may generally be used to control the reaction.

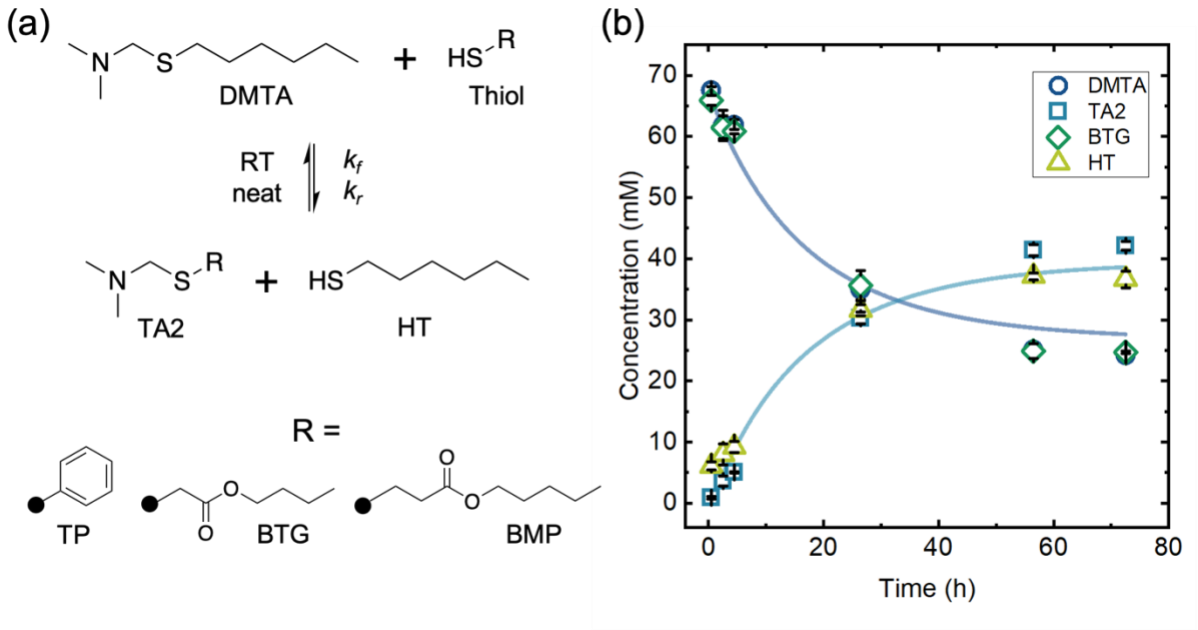

Figure 5.1. A small molecule study of thiol-thioaminal exchange shows that the choice of thiol greatly impacts reaction rate and equilibrium parameters. (a) Thioaminal DMTA was mixed with one of three thiols in a 1 thioaminal : 1 thiol molar ratio under neat, ambient conditions. (b) Concentrations of reactants and products as a function of time, showing the BTG-DMTA exchange reaction as a representative sample. Concentration values (markers) were calculated via NMR using a dimethylsulfone internal standard in $CDCl_3$ and compared to model predictions (lines).

The choice of thiol used for thiol-thioaminal exchange was found to be an effective means to control the reaction kinetics and equilibrium extent of reaction. **Figure 5.1** shows the small molecule system used to probe the thiol-thioaminal exchange reaction and a table of kinetic

parameters abstracted from the data. **Figure 5.1a** describes the procedure used to conduct the exchange reaction: DMTA and one of three thiols were mixed in a 1 thioaminal : 1 thiol ratio and stirred at 100 RPM under ambient conditions. At specific times, aliquots of the reaction solution were removed and these aliquots were used to plot concentrations of all the reactants and products over time, **Figure 5.1b**. At 0 h, ~100 % of all observed species were reactants, showing concentrations of 66 $\pm$ 1 and 68 $\pm$ 1 mM for BTG and DMTA, respectively. Over 60 h, these concentrations both dropped to 25 $\pm$ 1 mM while the concentrations of HT and TA2 increased at an equal rate, rising from 6 $\pm$ 1 and 1 $\pm$ 1 up to 37 $\pm$ 1 and 41 $\pm$ 1 mM, respectively. After 60 h, all concentration values had plateaued. The formation of HT, formation of TA2, and the equal rate of change for all components confirmed that these thioaminal small molecules were undergoing a reversible second order thiol-thioaminal exchange reaction. Fitting this experimental data for reversible second order reactions,[43] theoretical predictions for the [DMTA] and [TA2] over time were created and plotted as solid lines in **Figure 5.1b**. Experimental data fit model predictions well, requiring input of initial concentrations ($[BTG]_o$, $[DMTA]_o$) and K_{eq} and using a single fitting parameter (k_f) to extract reaction rate constants (k_f, k_r) and ½ of the equilibration time ($t_{1/2,eq}$). The detailed solution for fitting reversible second order reactions is described in **Scheme S5.3**.

Table 5.1. Resulting reaction rate constants (k_f, k_r), equilibrium constants (K_{eq}), and ½-lives of the equilibration time ($t_{1/2,eq}$) of the thiol-thioaminal exchange reaction between DMTA and three thiols (BTG, TP, BMP).

	BTG	TP	BMP
K_{eq}	2.5 ± 0.1	1.7 ± 0.1	1.0 ± 0.1
k_f ($mM^{-1}s^{-1}$)	0.4 ± 0.1	0.8 ± 0.1	20 ± 3
k_r ($mM^{-1}s^{-1}$)	0.2 ± 0.1	0.5 ± 0.1	20 ± 3
$t_{1/2,eqm}$ (h)	12 ± 1	8 ± 1	3 ± 1

Table 5.1 shows the reaction rate constants (k_f, k_r), equilibrium constants (K_{eq}), and ½ of the equilibration times ($t_{1/2,eq}$) for all the thiols studied as calculated by model predictions. All of these kinetic parameters changed with the choice of thiol, with the equilibrium constants decreasing from 2.5 to 1.0 as the thiol changed from BTG to TP and BMP. The equilibration times decreased from BTG ($t_{1/2,eq}$ of 12 ± 1) to BMP ($t_{1/2,eq}$ of 3 ± 1) and accordingly the reaction rate constants increased, with the reverse reaction rate constants increasing by 100 times from 0.2 to 20 $mM^{-1}s^{-1}$. BMP exhibited reaction rate constants much larger than the other thiols, 20 ± 3 $mM^{-1}s^{-1}$ for both the forward and reverse reaction rate constants, and these values were over 20 times larger than those for the next closest thiol. These trends in reaction rate constants, equilibrium constant, and equilibration time are likely due to a balance between the relative amount of thiolate formed and the stability of these thiolates. Electron-rich substituents, such as longer alkyl chains, are known to destabilize thiolate anions and increase their pKa,[44,45] leading to both a lower concentration of these thiolates and decreased stability. This hypothesis likely explains why BMP has both the lowest equilibrium constant and the fastest equilibration time of the three thiols investigated. It is, therefore, expected that BTG, which has a lower pKa (8.8 versus 10.4),[45] results

in a higher equilibrium constant but takes longer to equilibrate due to its increased thiolate stability. TP likely exhibits behavior between BMP and BTG because resonance on its ring stabilizes the thiolate, leading to a longer equilibration time, but this resonance also lowers the nucleophilicity of the thiolate, leading to an intermediate value of K_{eq}.[46] Nevertheless the trends for TP are still somewhat decoupled, with K_{eq} between BMP and BTG but k_f and k_r much closer to BTG, which shows that it is possible to tune both the speed and the extent of thiol-thioaminal exchange separately by choosing an appropriate thiol.

5.4.2 Characterizing Networks

Having shown that thiol-thioaminal exchange occurs readily under ambient conditions and may be tuned with the choice of thiol, this work moved on to study how thiol-thioaminal exchange proceeds within polymer networks. To this end, a polymerizable thioaminal monomer (ATA) was synthesized and mixed with HDT and I819 in a [0.7 thiol : 1 ene : 0.005 I819] molar ratio. Curing this solution via the thiol-ene photopolymerization reaction created thioaminal networks that could potentially undergo thiol-thioaminal exchange as seen in **Figure 5.2**.

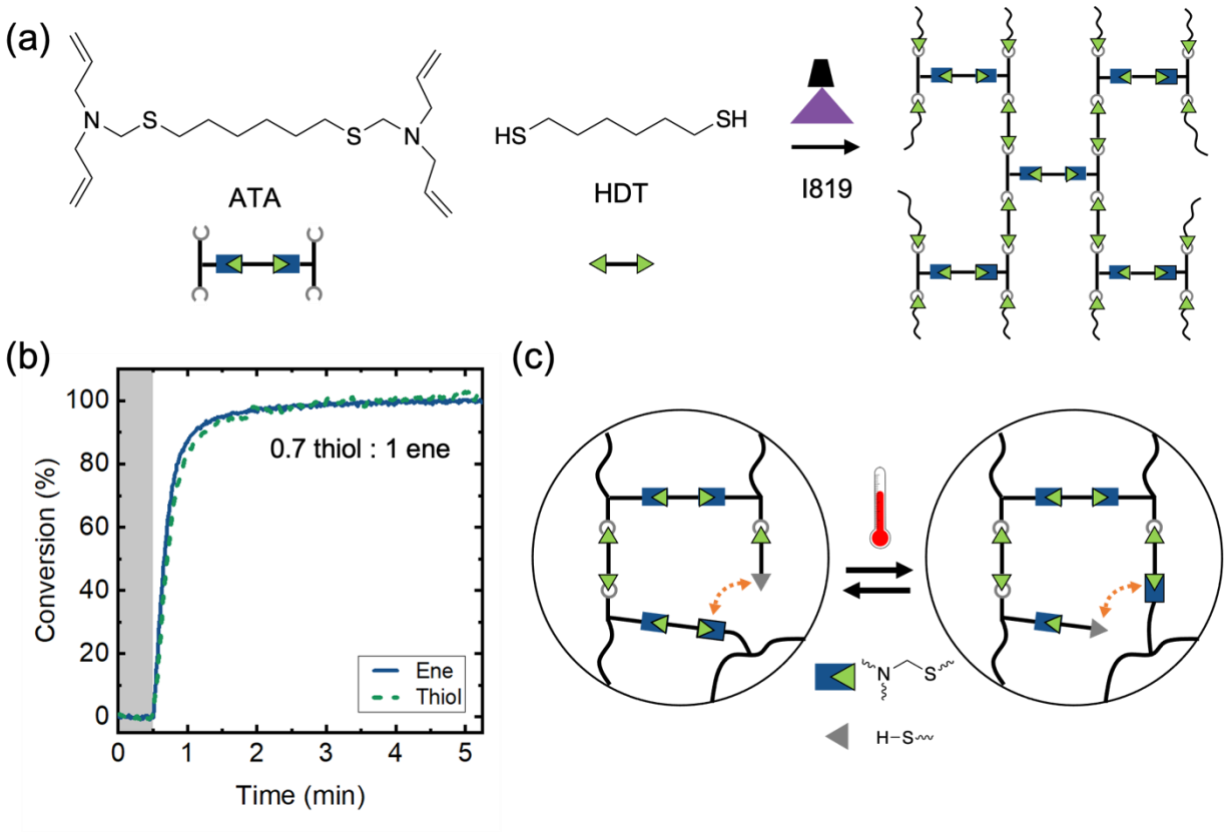

Figure 5.2. Thioaminal networks were photopolymerized to investigate rearrangement via the thiol-thioaminal exchange reaction. (a) Monomers ATA and HDT were mixed in 0.64 :1, 0.7 : 1, or 0.77: 1 thiol : ene ratios and cured via thiol-ene photopolymerization. The resulting networks had crosslinks containing two thioaminal groups and backbones containing no thioaminal groups. (b) Conversion of thiol and ene functional groups during photopolymerization as measured via real-time FTIR, showing that a 0.7 thiol : 1 ene ratio resulted in near quantitative conversion. (c) Visual representation of how thermally triggered thiol-thioaminal exchange rearranges network topology.

Figure 5.2 shows that monomer ATA enables the facile formation of thioaminal containing networks via the thiol-ene photopolymerization reaction. Meanwhile, **Figure 5.2a** shows that mixing ATA with HDT and I819 produced networks containing two thioaminal groups within crosslinks and no thioaminal groups within the polymer backbone. This photocure was repeated for 0.64 : 1, 0.7 : 1, and 0.77 : 1 thiol : ene molar ratios which were used to create 10 % excess ene, 0 % excess thiol, and 10 % excess thiol networks respectively. The 0.7 thiol : 1 ene ratio was set as the 0 % excess thiol network due to allyl homopolymerization of ATA, as shown in **Figure**

S5.3. **Figure 5.2b** shows how conversion for the thiol and ene groups over time for the 0.7 thiol : 1 ene material. At 0.5 min, the mixture was exposed to a 400 – 500 nm light source at 30 mW/cm^2, and within 30 s (total time of one minute) both thiol and ene groups had reached ~90 % conversion. **Figure 5.2c** shows a diagram of how these photocured thioaminal networks may undergo topology rearrangement via thiol-thioaminal exchange. In the exchange, pendant thiols on the polymer backbone interact with thioaminal groups contained within the crosslinks, rearranging the chain connections and enabling stress relaxation. This diagram also shows that thiols are required for the exchange to proceed.

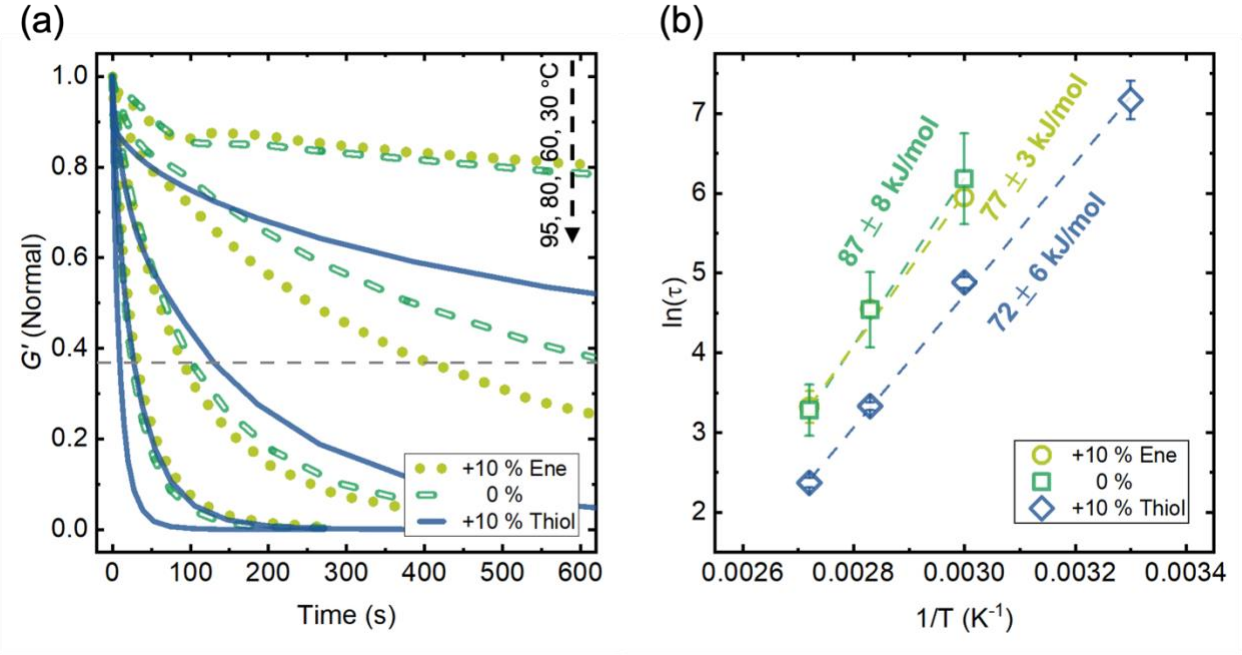

Figure 5.3. Thioaminal networks stress relaxed rapidly, with a network containing 10 % excess thiol relaxing in 10 s at 95 °C. (a) Normalized shear storage modulus (G') as a function of time during stress relaxation as temperature increased from 30 – 95 °C. Stress relaxation was repeated for networks containing 10 % excess ene, no excess, or 10 % excess thiol with stress relaxation time ($\boldsymbol{\tau}$) determined as 1/e (~37 %, grey dashed line). (b) Arrhenius plot of thioaminal networks containing 10 % excess ene, no excess, or 10 % excess thiol, calculating $E_{a,SR}$ via equation 2. Error bars indicate standard deviation for three samples.

Since stress relaxation is a distinct trait of CANs and has been used to characterize a number of CAN chemistries,[12,13,47] the stress relaxation of thioaminal networks was explored. **Figure 5.3a** shows the change in normalized shear storage modulus (G') as a function of time as temperature was increased from 30 - 95 °C. All networks stress relaxed, with excess thiol resulting in faster relaxation such that the 10 % excess thiol network relaxed the fastest (10 s at 95 °C) and the 10 % excess ene relaxed the slowest (34 s at 95 °C). This result shows that excess thiol, or lack thereof, may be used to tune the stress relaxation of thioaminal networks. Furthermore, this result is consistent with our proposed theory that thioaminal networks stress relax via the thiol-thioaminal exchange reaction, as this reaction requires thiol for exchange. At 30 °C a stress relaxation time was observed for the 10 % excess thiol networks but not for the other networks. These other networks likely do exchange, but require hours to do so which matches the hours-long timescale required for small molecule thiol-thioaminal exchange at room temperature, as detailed in **Figure 5.1**. Interestingly, both the no excess (0 %) and the 10 % excess ene networks stress relaxed, and did so on a similar timescale, despite a lack of exogenous pendant thiols. This behavior is unexpected as the proposed mechanism of stress relaxation requires thiolates formed by pendant thiols. A probable explanation is that there is an equilibrium of thiolates that spontaneously form within thioaminal networks via thioaminal bond dissociation.

Figure 5.3b shows an Arrhenius plot for the three thioaminal networks under consideration, with the stress relaxation time plotted as a function of inverse temperature and $E_{a,SR}$ calculated using equation 2. Stress relaxation time was defined as the time required for the normalized shear modulus in **Figure 5.3a** to reach a value of $1/e$ (~37 %, grey dashed line). Stress relaxation within 10 s ($\ln(\tau)$ of 2.3) at 95 °C was observed, which is rare among the thermally-driven CANs presented in the literature. To date, vinylogous-urethane CANs have exhibited faster speeds (0.3

s), but this chemistry required both higher temperatures (160 °C) and exogenous catalyst (acid *p*TsOH)[24] as compared to the thioaminal networks. The data also shows that the 10 % excess thiol, no excess (0 %), and 10 % excess ene networks exhibited $E_{a,SR}$ of 77 ± 3, 87 ± 8, and 72 ± 6 kJ/mol respectively. This narrow range of $E_{a,SR}$ suggests two things: 1) all networks stress relaxed via the same mechanism, supporting the claim that spontaneous thiolate formation occurred within the no excess and 10 % excess ene networks, and 2) changing the amount of excess thiol in thioaminal networks affords tunable relaxation times without dramatically impacting $E_{a,SR}$. Furthermore, the $E_{a,SR}$ of thioaminal networks is similar to that of chemically adjacent CANs, with aminal exchange CANs exhibiting ~50 – 80 kJ/mol[48] and imine exchange CANs exhibiting ~48 – 70 kJ/mol.[49,50] Having shown that thiol-thioaminal exchange creates CANs with rapid and tunable stress relaxation, the mechanism through which this exchange occurs is next discussed.

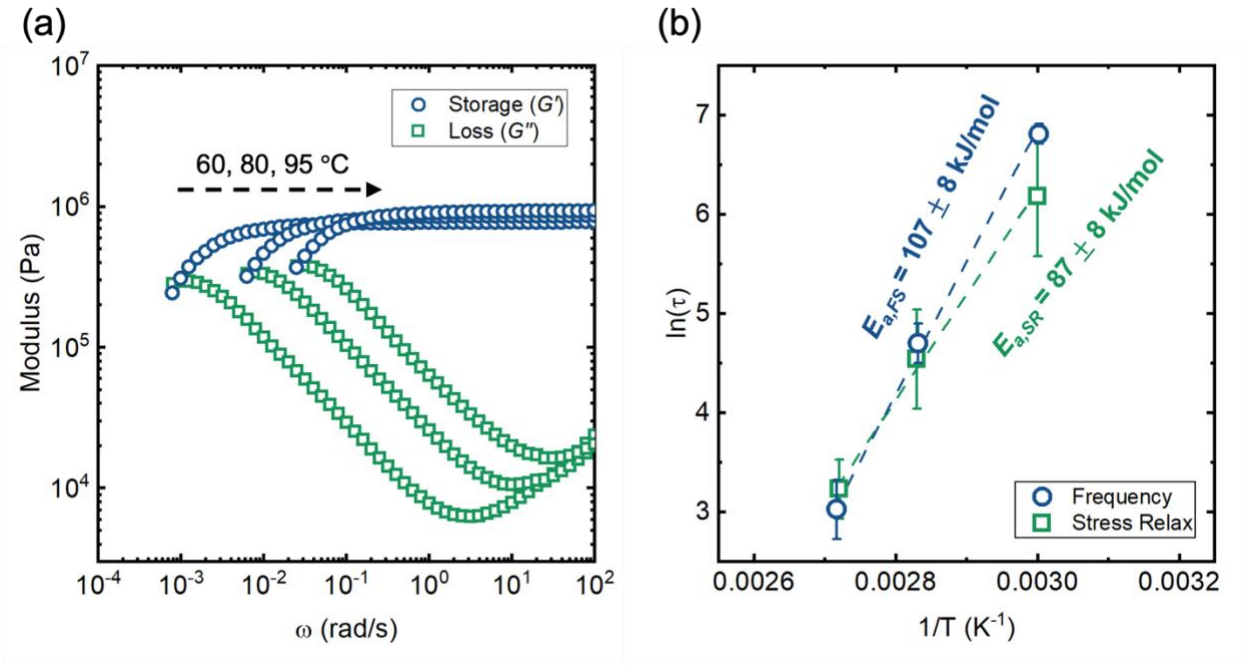

Figure 5.4. Frequency sweeps showed thiol-thioaminal exchange proceeded through a reversible exchange type mechanism. (a) Shear storage (*G'*) and loss (*G''*) moduli plotted as a function of frequency for temperatures increasing from 60 – 95 °C. (b) Arrhenius plot showing relaxation time ($\boldsymbol{\tau}$) as a function of inverse temperature for both the stress relaxation and frequency sweep data.

All data was collected for the no excess (0 %) network, and error bars indicate standard deviation for three samples.

To understand whether the thioaminal reaction was proceeding by a reversible addition or exchange reaction, exploration of the reaction mechanism and its impact on stress relaxation behavior was undertaken. **Figure 5.4a** plots how the shear storage (G') and loss (G'') moduli of the no excess network changed as shear oscillation frequency increased from 10^{-3} to 10^{2} rad/s and as temperature increased from 60 – 95 °C. At lower frequencies, G'' exceeded G' for all temperatures, but as the frequency increased, crossover points were observed after which all networks settled at a rubbery plateau storage modulus (G') around 0.9 MPa. Interestingly, increasing the temperature increased the crossover point frequency (10^{-3} to 5 x 10^{-2} rad/s) but did not impact the crossover point storage modulus (~0.3 MPa) or the final rubbery plateau storage modulus (~0.9 MPa). These temperature trends indicate the average crosslinking density of these thioaminal networks was largely temperature independent, and therefore, the thiol-thioaminal exchange occurs primarily through a reversible exchange type mechanism under these conditions.[14,24]

Figure 5.4b contains an Arrhenius plot showing how relaxation time (τ) changed as a function of inverse temperature for both the frequency sweep experiment and the previous stress relaxation experiment. $E_{a,FS}$ was calculated from frequency sweep data by converting the crossover points into a relaxation time and using equation 3. Both experiments exhibited similar relaxation times and E_a, 107 $\pm$ 8 versus 87 $\pm$ 8 kJ/mol for $E_{a,FS}$ and $E_{a,SR}$, respectively, confirming both the reliability of the performed stress relaxation experiments and the mechanism that leads to rapid stress relaxation within thioaminal networks.

5.4.3 Degradation

A unique property of CANs is their ability to readily degrade by simply exposing the material to an excess of monomer and triggering its exchange reaction. This exchange reaction replaces elastically active arms with the excess terminal monomer, decreasing crosslink density and resulting in complete polymer dissolution.[12,51] To investigate how thioaminal networks may exhibit this CANs trait, this work explored the degradation of thioaminal networks via the thiol-thioaminal exchange reaction. To test the degradation of thioaminal networks, films were photocured and submerged into vials containing 2.5 mL of thiol monomer, equaling over a 200 times molar excess of thiol which ensured sufficient thiol was present to degrade the network. Degradation by four thiols (BMP, BTG, TP, and HT) was tracked and the time for films to fully degrade was noted.

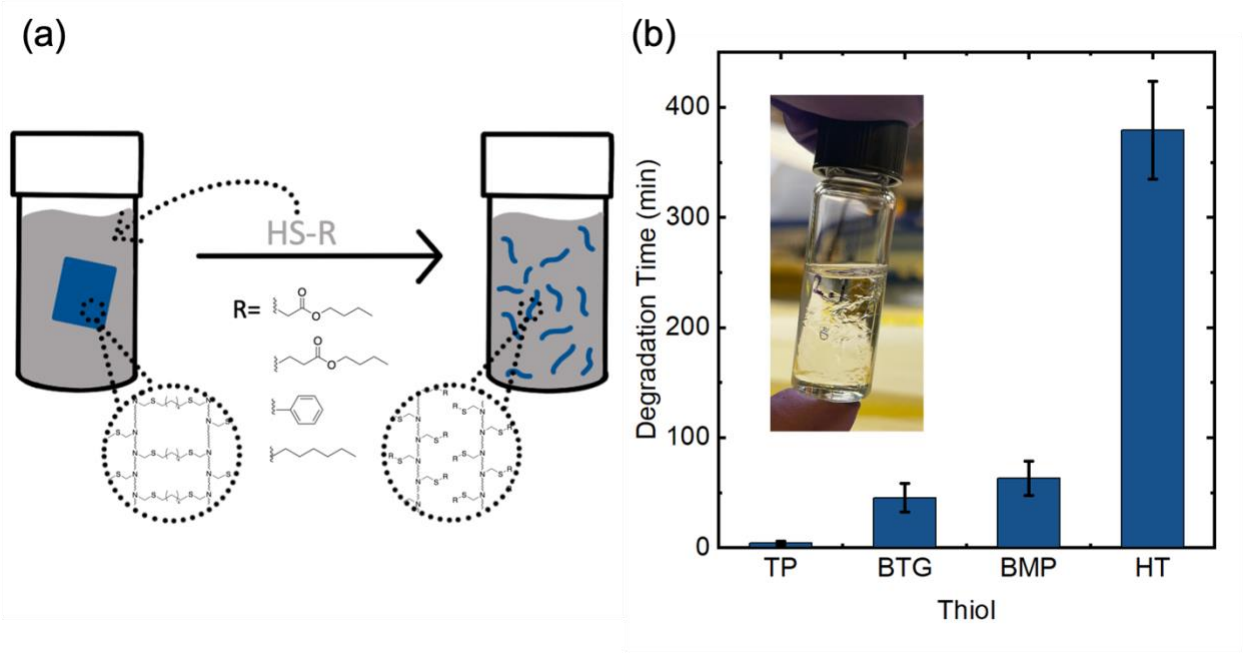

Figure 5.5. Exposing thioaminal networks to excess thiol triggered rapid degradation via the thiol-thioaminal exchange reaction. (a) Procedure used to degrade thioaminal networks by submerging films in one of four thiols under ambient conditions. (b) Time for complete dissolution of films

via each thiol, with a photographic inset of a representative vial. Errors bars indicate standard deviation for three samples.

Figure 5.5 shows the average time for degradation of films by each thiol. As the pKa values of the thiols increased (6.5, 8.8, 10.4, and 11 for TP, BTG, BMP, and HT, respectively)[45,52,53] so too did the average time required for degradation. It is shown that TP resulted in the fastest degradation, 4 ± 2 min, and this likely occurred because TP was the most acidic thiol, readily forming thiolates that underwent thiol-thioaminal exchange. Interestingly, degradation by TP was so fast the films decreased in size throughout the process, indicating a surface degradation mechanism.[54] On the other hand, HT resulted in the slowest degradation, 380 ± 40 min, also likely driven by its pKa. These HT films swelled in size throughout the process, instead likely indicating a bulk degradation mechanism.[54,55] The trend between lower pKa and faster degradation is plotted in **Figure S5.4**, and this trend differs from how the kinetic parameters for small molecule thiol-thioaminal exchange relate to pKa, **Table 5.1**. Some possible explanations for this deviation between the two experiments include differences in local concentrations, local polarities, and stoichiometric ratios of reactants. Nevertheless, these degradation experiments show that not only do thioaminal networks degrade through the thiol-thioaminal exchange reaction, but that both the degradation timescale (~100 times range) and mechanism (surface to bulk) are readily tailored by the choice of thiol. Researchers interested in further exploring thioaminal CAN degradation may consider using these networks for selective degradation of 3-D printed scaffolds[56] or hydrogels[57,58] in thiol-containing media.

5.5 Conclusions

This work investigated the thiol-thioaminal exchange as a means to create reversible exchange CANs that rapidly rearrange under near-ambient conditions. Small molecule studies using DMTA

showed the choice of thiol could separately control the speed of the thiol-thioaminal exchange and the extent of reaction. BMP exhibited the fastest exchange time ($t_{1/2,eq}$ of 3 $\pm$ 1 h) while BTG exhibited the greatest extent of reaction (K_{eq} of 2.5 $\pm$ 0.1). Kinetic parameters extracted from the model predictions showed exchange with BTG resulted in the largest forward and reverse reaction rate parameters, with values of 20 $\pm$ 3 $mM^{-1}s^{-1}$ for both. Stress relaxation of thioaminal networks showed that excess thiol and elevated temperatures resulted in faster stress relaxation, with the 10 % excess thiol network relaxing in 10 s at 95 °C. Relaxation experiments also showed spontaneous formation of thiolate at elevated temperatures, enabling stress relaxation in all the studied networks and with all networks showing an $E_{a,SR}$ around 87 $\pm$ 8 kJ/mol. Frequency sweeps of these thioaminal networks gave $E_{a,FS}$ of 107 $\pm$ 8 kJ/mol and showed network rearrangement of thioaminal CANs occurred through a reversible exchange process. Lastly, thioaminal CANs were photocured into films and submerged in thiol to degrade via the thiol-thioaminal exchange reaction. This process showed decreasing pKa resulted in faster degradation, with thiophenol degrading networks in 4 $\pm$ 2 min and also showed the choice of thiol tuned whether dissolution occurred via surface or bulk degradation. Investigating thiol-thioaminal exchange within polymer networks has expanded the library of thermally-activated reversible exchange CANs, and aside from directly contributing to self-healing applications at room-temperature, the reaction kinetics explored within this work may be adapted towards general research on thiol-thioaminal exchange in other systems.

5.6 Acknowledgements

This work was made possible by funding from the Graduate Assistance in Areas of National Need (GAANN) and a National Science Foundation's Grant DMR 1809841.

5.7 References

(1) Raquez, J. M.; Deléglise, M.; Lacrampe, M. F.; Krawczak, P. Thermosetting (Bio)Materials Derived from Renewable Resources: A Critical Review. *Prog. Polym. Sci.* **2010**, *35* (4), 487–509. https://doi.org/10.1016/j.progpolymsci.2010.01.001.

(2) Zhang, B.; Kowsari, K.; Serjouei, A.; Dunn, M. L.; Ge, Q. Reprocessable Thermosets for Sustainable Three-Dimensional Printing. *Nat. Commun.* **2018**, *9* (1). https://doi.org/10.1038/s41467-018-04292-8.

(3) Walker, W. D.; Sandoz, M. J.; Roland, S.; Buster, T. M.; Newman, J. K.; Patton, D. L. Command-Destruct Thermosets: Via Photoinduced Thiol-Catalyzed β-Scission of Acyclic Benzylidene Acetals. *Polym. Chem.* **2020**, *11* (43), 6873–6878. https://doi.org/10.1039/d0py01006e.

(4) Wang, H. C.; Zhang, Y.; Possanza, C. M.; Zimmerman, S. C.; Cheng, J.; Moore, J. S.; Harris, K.; Katz, J. S. Trigger Chemistries for Better Industrial Formulations. *ACS Appl. Mater. Interfaces* **2015**, *7* (12), 6369–6382. https://doi.org/10.1021/acsami.5b00485.

(5) Romano, A.; Roppolo, I.; Rossegger, E.; Schlögl, S.; Sangermano, M. Recent Trends in Applying Ortho-Nitrobenzyl Esters for the Design of Photo-Responsive Polymer Networks. *Materials (Basel).* **2020**, *13* (12), 1–26. https://doi.org/10.3390/ma13122777.

(6) Pasparakis, G.; Manouras, T.; Selimis, A.; Vamvakaki, M.; Argitis, P. Laser-Induced Cell Detachment and Patterning with Photodegradable Polymer Substrates. *Angew. Chemie* **2011**, *123* (18), 4228–4231. https://doi.org/10.1002/ange.201007310.

(7) Russew, M. M.; Hecht, S. Photoswitches: From Molecules to Materials. *Adv. Mater.* **2010**, *22* (31), 3348–3360. https://doi.org/10.1002/adma.200904102.

(8) Klajn, R. Spiropyran-Based Dynamic Materials. *Chem. Soc. Rev.* **2014**, *43* (1), 148–184. https://doi.org/10.1039/c3cs60181a.

(9) Ma, S.; Webster, D. C. Degradable Thermosets Based on Labile Bonds or Linkages: A Review. *Prog. Polym. Sci.* **2018**, *76*, 65–110. https://doi.org/10.1016/j.progpolymsci.2017.07.008.

(10) Mabey, W.; Mill, T. Critical Review of Hydrolysis of Organic Compounds in Water under Environmental Conditions. *J. Phys. Chem. Ref. Data* **1978**, *7* (2), 383–415. https://doi.org/10.1063/1.555572.

(11) García, J. M.; Jones, G. O.; Virwani, K.; Mccloskey, B. D.; Boday, D. J.; Huurne, G. M.; Horn, H. W.; Coady, D. J.; Bintaleb, A. M.; Alabdulrahman, A. M. S.; Alsewailem, F.; Almegren, H. A. A.; Hedrick, J. L. Recyclable, Strong Thermosets and Organogels via Paraformaldehyde Condensation with Diamines. *Science (80-.).* **2014**, *13073* (May), 732–735. https://doi.org/10.1126/science.1251484.

(12) Podgórski, M.; Fairbanks, B. D.; Kirkpatrick, B. E.; McBride, M.; Martinez, A.; Dobson, A.; Bongiardina, N. J.; Bowman, C. N. Toward Stimuli-Responsive Dynamic Thermosets through Continuous Development and Improvements in Covalent Adaptable Networks (CANs). *Adv. Mater.* **2020**, *32* (20), 1–26. https://doi.org/10.1002/adma.201906876.

(13) Guerre, M.; Taplan, C.; Winne, J. M.; Du Prez, F. E. Vitrimers: Directing Chemical Reactivity to Control Material Properties. *Chem. Sci.* **2020**, *11* (19), 4855–4870. https://doi.org/10.1039/d0sc01069c.

(14) Kloxin, C. J.; Bowman, C. N. Covalent Adaptable Networks: Smart, Reconfigurable and Responsive Network Systems. *Chem. Soc. Rev.* **2013**, *42* (17), 7161–7173. https://doi.org/10.1039/c3cs60046g.

(15) Scheutz, G. M.; Lessard, J. J.; Sims, M. B.; Sumerlin, B. S. Adaptable Crosslinks in Polymeric Materials: Resolving the Intersection of Thermoplastics and Thermosets. *J. Am. Chem. Soc.* **2019**, *141* (41), 16181–16196. https://doi.org/10.1021/jacs.9b07922.
(16) Denissen, W.; Winne, J. M.; Du Prez, F. E. Vitrimers: Permanent Organic Networks with Glass-like Fluidity. *Chem. Sci.* **2016**, *7* (1), 30–38. https://doi.org/10.1039/c5sc02223a.
(17) Scott, T. F.; Schneider, A. D.; Cook, W. D.; Bowman, C. N. Chemistry: Photoinduced Plasticity in Cross-Linked Polymers. *Science (80-.).* **2005**, *308* (5728), 1615–1617. https://doi.org/10.1126/science.1110505.
(18) Worrell, B. T.; McBride, M. K.; Lyon, G. B.; Cox, L. M.; Wang, C.; Mavila, S.; Lim, C. H.; Coley, H. M.; Musgrave, C. B.; Ding, Y.; Bowman, C. N. Bistable and Photoswitchable States of Matter. *Nat. Commun.* **2018**, *9*, 1–7. https://doi.org/10.1038/s41467-018-05300-7.
(19) Fortman, D. J.; Brutman, J. P.; Cramer, C. J.; Hillmyer, M. A.; Dichtel, W. R. Mechanically Activated, Catalyst-Free Polyhydroxyurethane Vitrimers. *J. Am. Chem. Soc.* **2015**, *137* (44), 14019–14022. https://doi.org/10.1021/jacs.5b08084.
(20) De Alwis Watuthanthrige, N.; Ahammed, B.; Dolan, M. T.; Fang, Q.; Wu, J.; Sparks, J. L.; Zanjani, M. B.; Konkolewicz, D.; Ye, Z. Accelerating Dynamic Exchange and Self-Healing Using Mechanical Forces in Crosslinked Polymers. *Mater. Horizons* **2020**, *7* (6), 1581–1587. https://doi.org/10.1039/c9mh01938c.
(21) Arie, M. A.; Shooshtari, A. H.; Tiwari, R.; Dessiatoun, S. V.; Ohadi, M. M.; Pearce, J. M. Experimental Characterization of Heat Transfer in an Additively Manufactured Polymer Heat Exchanger. *Appl. Therm. Eng.* **2017**, *113*, 575–584. https://doi.org/10.1016/j.applthermaleng.2016.11.030.
(22) Jaque, D.; Martínez Maestro, L.; Del Rosal, B.; Haro-Gonzalez, P.; Benayas, A.; Plaza, J. L.; Martín Rodríguez, E.; García Solé, J. Nanoparticles for Photothermal Therapies. *Nanoscale* **2014**, *6* (16), 9494–9530. https://doi.org/10.1039/c4nr00708e.
(23) Gharde, S.; Kandasubramanian, B. Mechanothermal and Chemical Recycling Methodologies for the Fibre Reinforced Plastic (FRP). *Environ. Technol. Innov.* **2019**, *14*, 100311. https://doi.org/10.1016/j.eti.2019.01.005.
(24) Taplan, C.; Guerre, M.; Winne, J. M.; Du Prez, F. E. Fast Processing of Highly Crosslinked, Low-Viscosity Vitrimers. *Mater. Horizons* **2020**, *7* (1), 104–110. https://doi.org/10.1039/c9mh01062a.
(25) Röttger, M.; Domenech, T.; Van Der Weegen, R.; Breuillac, A.; Nicolaÿ, R.; Leibler, L. High-Performance Vitrimers from Commodity Thermoplastics through Dioxaborolane Metathesis. *Science (80-.).* **2017**, *356* (6333), 62–65. https://doi.org/10.1126/science.aah5281.
(26) Wölfel, B.; Seefried, A.; Allen, V.; Kaschta, J.; Holmes, C.; Schubert, D. W. Recycling and Reprocessing of Thermoplastic Polyurethane Materials towards Nonwoven Processing. *Polymers (Basel).* **2020**, *12* (9), 1–13. https://doi.org/10.3390/POLYM12091917.
(27) Demongeot, A.; Groote, R.; Goossens, H.; Hoeks, T.; Tournilhac, F.; Leibler, L. Cross-Linking of Poly(Butylene Terephthalate) by Reactive Extrusion Using Zn(II) Epoxy-Vitrimer Chemistry. *Macromolecules* **2017**, *50* (16), 6117–6127. https://doi.org/10.1021/acs.macromol.7b01141.
(28) Ishibashi, J. S. A.; Kalow, J. A. Vitrimeric Silicone Elastomers Enabled by Dynamic Meldrum's Acid-Derived Cross-Links. *ACS Macro Lett.* **2018**, *7* (4), 482–486. https://doi.org/10.1021/acsmacrolett.8b00166.
(29) Yang, Z.; Duan, C.; Sun, Y.; Wang, T.; Zhang, X.; Wang, Q. Utilizing

Polyhexahydrotriazine (PHT) to Cross-Link Polyimide Oligomers for High-Temperature Shape Memory Polymer. *Industrial and Engineering Chemistry Research*. 2019, pp 10599–10608. https://doi.org/10.1021/acs.iecr.9b01405.

(30) Martinez, A. M.; Cox, L. M.; Killgore, J. P.; Bongiardina, N. J.; Riley, R. D.; Bowman, C. N. Permanent and Reversibly Programmable Shapes in Liquid Crystal Elastomer Microparticles Capable of Shape Switching. *Soft Matter* **2021**, *17* (3), 467–474. https://doi.org/10.1039/d0sm01836h.

(31) Taplan, C.; Guerre, M.; Du Prez, F. E. Covalent Adaptable Networks Using β-Amino Esters as Thermally Reversible Building Blocks. *J. Am. Chem. Soc.* **2021**, *143* (24), 9140–9150. https://doi.org/10.1021/jacs.1c03316.

(32) Denissen, W.; Rivero, G.; Nicolaÿ, R.; Leibler, L.; Winne, J. M.; Du Prez, F. E. Vinylogous Urethane Vitrimers. *Adv. Funct. Mater.* **2015**, *25* (16), 2451–2457. https://doi.org/10.1002/adfm.201404553.

(33) Ying, H.; Zhang, Y.; Cheng, J. Dynamic Urea Bond for the Design of Reversible and Self-Healing Polymers. *Nat. Commun.* **2014**, *5*. https://doi.org/10.1038/ncomms4218.

(34) Reutenauer, P.; Buhler, E.; Boul, P. J.; Candau, S. J.; Lehn, J. M. Room Temperature Dynamic Polymers Based on Diels-Alder Chemistry. *Chem. - A Eur. J.* **2009**, *15* (8), 1893–1900. https://doi.org/10.1002/chem.200802145.

(35) Oehlenschlaeger, K. K.; Guimard, N. K.; Brandt, J.; Mueller, J. O.; Lin, C. Y.; Hilf, S.; Lederer, A.; Coote, M. L.; Schmidt, F. G.; Barner-Kowollik, C. Fast and Catalyst-Free Hetero-Diels-Alder Chemistry for on Demand Cyclable Bonding/Debonding Materials. *Polym. Chem.* **2013**, *4* (16), 4348–4355. https://doi.org/10.1039/c3py00476g.

(36) Sijbesma, R. P.; Beijer, F. H.; Brunsveld, L.; Folmer, B. J. B.; Hirschberg, J. H. K. K.; Lange, R. F. M.; Lowe, J. K. L.; Meijer, E. W. Reversible Polymers Formed from Self-Complementary Monomers Using Quadruple Hydrogen Bonding. *Science (80-.).* **1997**, *278* (5343), 1601–1604. https://doi.org/10.1126/science.278.5343.1601.

(37) Park, H. Y.; Kloxin, C. J.; Abuelyaman, A. S.; Oxman, J. D.; Bowman, C. N. Stress Relaxation via Addition-Fragmentation Chain Transfer in High T g, High Conversion Methacrylate-Based Systems. *Macromolecules* **2012**, *45* (14), 5640–5646. https://doi.org/10.1021/ma300228z.

(38) Li, L.; Chen, X.; Jin, K.; Torkelson, J. M. Vitrimers Designed Both to Strongly Suppress Creep and to Recover Original Cross-Link Density after Reprocessing: Quantitative Theory and Experiments. *Macromolecules* **2018**, *51* (15), 5537–5546. https://doi.org/10.1021/acs.macromol.8b00922.

(39) Hiemenz, P. C.; Lodge, T. P. *Polymer Chemistry Second Edition*; CRC Press Taylor & Francis Group, 2007. https://doi.org/10.1201/9781420018271-4.

(40) Wojtecki, R. J.; Jones, G. O.; Yuen, A. Y.; Chin, W.; Boday, D. J.; Nelson, A.; García, J. M.; Yang, Y. Y.; Hedrick, J. L. Developments in Dynamic Covalent Chemistries from the Reaction of Thiols with Hexahydrotriazines. *J. Am. Chem. Soc.* **2015**, *137* (45), 14248–14251. https://doi.org/10.1021/jacs.5b08815.

(41) Chen, J.; Zhang, X. F.; Kort, M. E.; Huth, J. R.; Sun, C.; Miesbauer, L. J.; Cassar, S. C.; Neelands, T.; Scott, V. E.; Moreland, R. B.; Reilly, R. M.; Hajduk, P. J.; Kym, P. R.; Hutchins, C. W.; Faltynek, C. R. Molecular Determinants of Species-Specific Activation or Blockade of TRPA1 Channels. *J. Neurosci.* **2008**, *28* (19), 5063–5071. https://doi.org/10.1523/JNEUROSCI.0047-08.2008.

(42) Boday, D. J.; García, J. M.; Hedrick, J. L.; Wojtecki, R. J. POLY (THIOAMINAL) PROBE

BASED LITHOGRAPHY. US 9 , 862 , 802 B2, 2018.
(43) Hogg, N. The Kinetics of S-Transnitrosation - A Reversible Second-Order Reaction. *Anal. Biochem.* **1999**, *272* (2), 257–262. https://doi.org/10.1006/abio.1999.4199.
(44) Worrell, B. T.; Mavila, S.; Wang, C.; Kontour, T. M.; Lim, C. H.; McBride, M. K.; Musgrave, C. B.; Shoemaker, R.; Bowman, C. N. A User's Guide to the Thiol-Thioester Exchange in Organic Media: Scope, Limitations, and Applications in Material Science. *Polym. Chem.* **2018**, *9* (36), 4523–4534. https://doi.org/10.1039/c8py01031e.
(45) Love, D. M.; Kim, K.; Goodrich, J. T.; Fairbanks, B. D.; Worrell, B. T.; Stoykovich, M. P.; Musgrave, C. B.; Bowman, C. N. Amine Induced Retardation of the Radical-Mediated Thiol-Ene Reaction via the Formation of Metastable Disulfide Radical Anions. *J. Org. Chem.* **2018**, *83* (5), 2912–2919. https://doi.org/10.1021/acs.joc.8b00143.
(46) Love, D. M.; Fairbanks, B. D.; Bowman, C. N. Evaluation of Aromatic Thiols as Photoinitiators. *Macromolecules* **2020**, *53* (13), 5237–5247. https://doi.org/10.1021/acs.macromol.0c00757.
(47) Winne, J. M.; Leibler, L.; Du Prez, F. E. Dynamic Covalent Chemistry in Polymer Networks: A Mechanistic Perspective. *Polym. Chem.* **2019**, *10* (45), 6091–6108. https://doi.org/10.1039/c9py01260e.
(48) Chao, A.; Zhang, D. Investigation of Secondary Amine-Derived Aminal Bond Exchange toward the Development of Covalent Adaptable Networks. *Macromolecules* **2019**, *52* (2), 495–503. https://doi.org/10.1021/acs.macromol.8b02654.
(49) Snyder, R. L.; Lidston, C. A. L.; De Hoe, G. X.; Parvulescu, M. J. S.; Hillmyer, M. A.; Coates, G. W. Mechanically Robust and Reprocessable Imine Exchange Networks from Modular Polyester Pre-Polymers. *Polym. Chem.* **2020**, *11* (33), 5346–5355. https://doi.org/10.1039/c9py01957j.
(50) Hakkarainen, M.; Xu, Y.; Odelius, K. Photocurable, Thermally Reprocessable, and Chemically Recyclable Vanillin-Based Imine Thermosets. *ACS Sustain. Chem. Eng.* **2020**, *8* (46), 17272–17279. https://doi.org/10.1021/acssuschemeng.0c06248.
(51) Hernandez, J. J.; Dobson, A. L.; Carberry, B. J.; Kuenstler, A. S.; Shah, P. K.; Anseth, K. S.; White, T. J.; Bowman, C. N. Controlled Degradation of Cast and 3-D Printed Photocurable Thioester Networks via Thiol–Thioester Exchange. *Macromolecules* **2022**, *55*, 1376–1385. https://doi.org/10.1021/acs.macromol.1c02459.
(52) Huang, S.; Sinha, J.; Podgórski, M.; Zhang, X.; Claudino, M.; Bowman, C. N. Mechanistic Modeling of the Thiol-Michael Addition Polymerization Kinetics: Structural Effects of the Thiol and Vinyl Monomers. *Macromolecules* **2018**, *51* (15), 5979–5988. https://doi.org/10.1021/acs.macromol.8b01264.
(53) Guo, Y.; Zhang, D.; Wang, J.; Lu, H.; Pu, S. Luminescent Probe Based on Photochromic Cyclometalated Iridium(III) Complex for High Selectivity Detection of Thiophenol. *Dye. Pigment.* **2020**, *175* (November 2019), 108191. https://doi.org/10.1016/j.dyepig.2020.108191.
(54) Burkersroda, F. Von; Schedl, L.; Göpferich, A. Why Degradable Polymers Undergo Surface Erosion or Bulk Erosion. *Biomaterials* **2002**, *23* (21), 4221–4231. https://doi.org/10.1016/S0142-9612(02)00170-9.
(55) Metters, A. T.; Bowman, C. N.; Anseth, K. S. Verification of Scaling Laws for Degrading PLA-b-PEG-b-PLA Hydrogels. *AIChE J.* **2001**, *47* (6), 1432–1437. https://doi.org/10.1002/aic.690470619.
(56) Saggiomo, V.; Velders, A. H. Simple 3D Printed Scaffold-Removal Method for the

Fabrication of Intricate Microfluidic Devices. *Adv. Sci.* **2015**, *2* (9), 1–5. https://doi.org/10.1002/advs.201500125.

(57) Carberry, B. J.; Hernandez, J. J.; Dobson, A.; Bowman, C. N.; Anseth, K. S. Kinetic Analysis of Degradation in Thioester Cross-Linked Hydrogels as a Function of Thiol Concentration, p Ka, and Presentation. *Macromolecules* **2022**, *55* (6), 2123–2129. https://doi.org/10.1021/acs.macromol.1c02396.

(58) Ghobril, C.; Charoen, K.; Rodriguez, E. K.; Nazarian, A.; Grinstaff, M. W. A Dendritic Thioester Hydrogel Based on Thiol-Thioester Exchange as a Dissolvable Sealant System for Wound Closure. *Angew. Chemie - Int. Ed.* **2013**, *52* (52), 14070–14074. https://doi.org/10.1002/anie.201308007.

5.8 Supporting Information

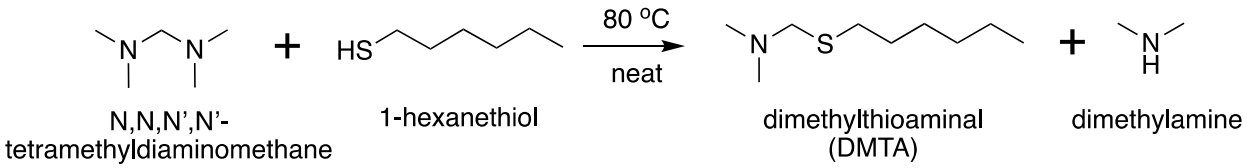

Scheme S5.1. Synthesis of dimethylthioaminal.

N,N,N',N'-Tetramethyldiaminomethane (25 mmol) and 1-hexanethiol (25 mmol) were mixed in an oven dried 50 mL round bottom flask and the resulting mixture was heated at 80 ºC (neat) for 16 hrs, following reported literature.[1] The crude was purified by silica column chromatography (0 % → 5 % EtOAc / Hexanes) to obtain dimethylthioaminal as clear oil (yield ~70 %).

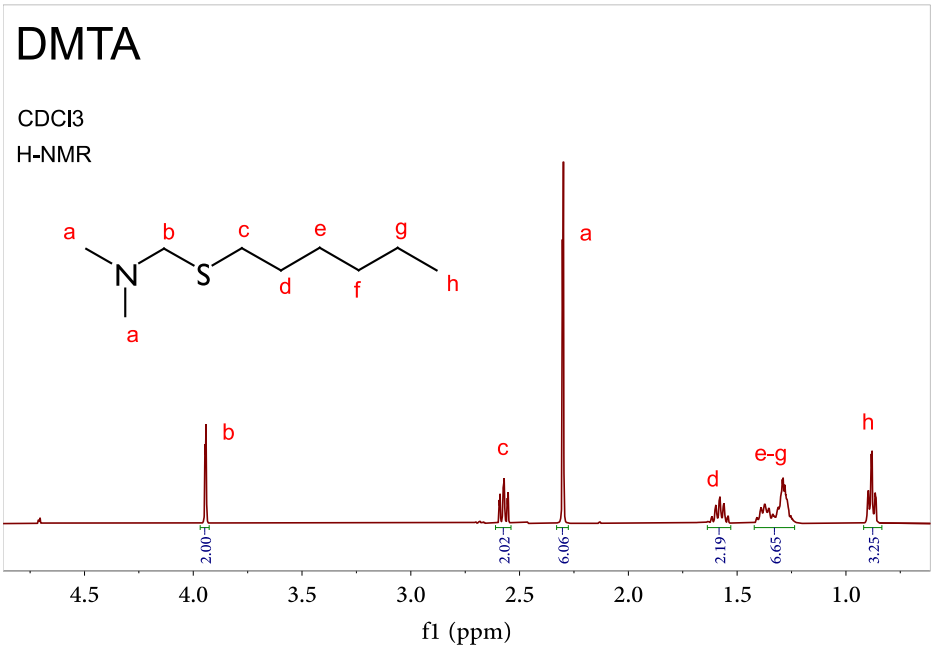

Figure S5.1. ^{1}H NMR spectra of DMTA. ^{1}H NMR (400 MHz, $CDCl_3$) δ 3.94 (s, 2H), 2.57 (t, *J* = 1.6 Hz, 2H), 2.30 (s, 6H), 1.57 (q, 2H), 1.43 – 1.33 (m, 2H), 1.33 – 1.27 (m, 2H), 1.30 – 1.23 (m, 2H), 0.88 (t, *J* = 1.5 Hz, 3H).

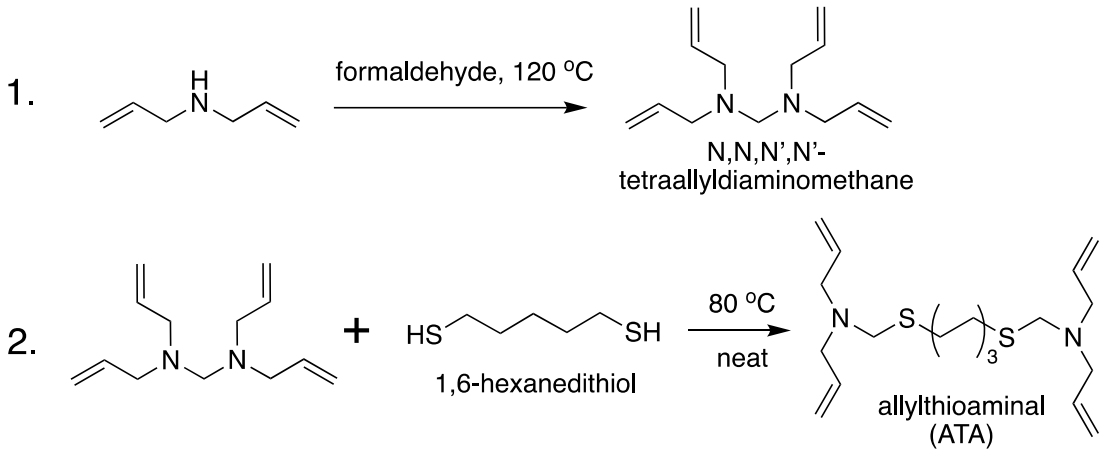

Scheme S5.2. Synthesis of allylthioaminal.

Required N,N,N',N'-Tetraallyldiaminomethane was synthesized according to the reported literature procedure.[2] Diallylamine (220 mmol) was placed in an oven dried 100 mL two-neck RBF and ice-cold formaldehyde (8.928g, 110 mmol, Formalin) was dripped in via addition funnel. The reaction mixture was refluxed at 120ºC and spun for 2 hrs. The reaction mixture was cooled and allowed to phase separate at room temperature. The top organic layer was collected, washed with KOH pellets, and the product was then purified by column chromatography (0 % → 5 % → 10 % EtOAc / Hexanes), dried under vacuum to yield the required N,N,N',N'-Tetraallyldiaminomethane as clear oil (71 % yield).

Above synthesized N,N,N',N'-Tetraallyldiaminomethane (65 mmol) and 1,6-Hexanedithiol (26 mmol) were mixed in an oven dried 100 mL RBF, and refluxed for 48 hrs at 80ºC. The crude reaction mixture was purified by column chromatography (0 % → 5 % → 10 % EtOAc / Hexanes), and solvent was removed under reduced pressure. The compound was dried at 50ºC under high vacuum for 24 hrs to yield the required allylthioamina (ATA) as a clear oil in 68 % yield.

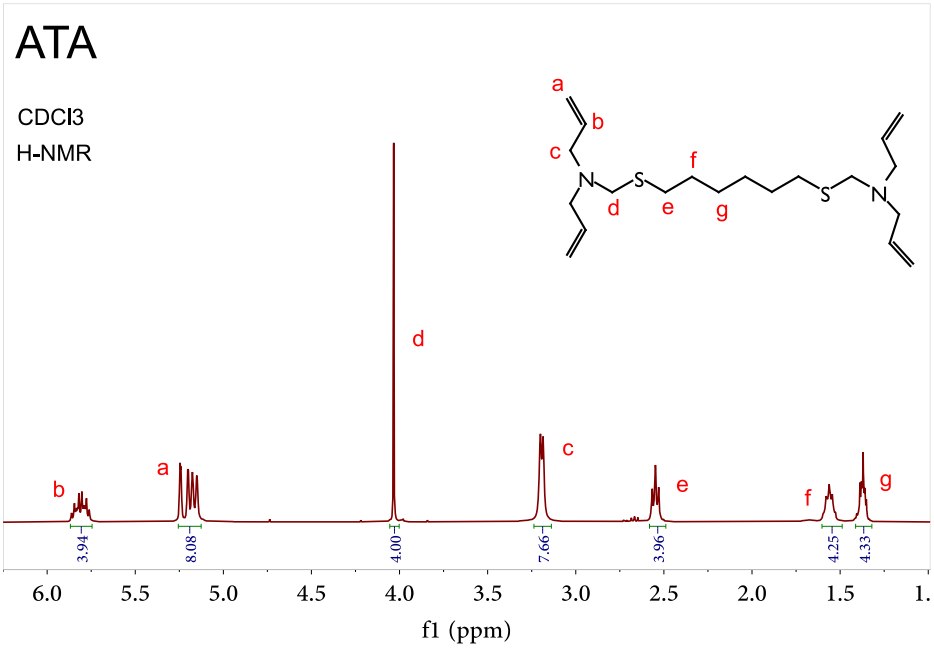

Figure S5.2. ^{1}H NMR spectra of ATA. ^{1}H NMR (400 MHz, $CDCl_3$) δ 5.88 – 5.74 (m, 4H), 5.27 – 5.12 (m, 8H), 4.03 (s, 4H), 3.19 (d, J = 6.4 Hz, 8H), 2.55 (t, J = 7.3 Hz, 4H), 1.62 – 1.50 (m, 4H), 1.44 – 1.33 (m, 4H).

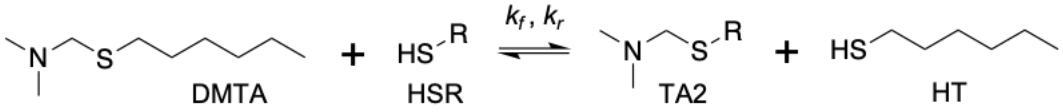

$$[DMTA] = \frac{P[DMTA]_\infty([DMTA]_0 + [DMTA]_\infty + Q) + ([DMTA]_0 - [DMTA]_\infty)([DMTA]_\infty + Q)}{P([DMTA]_0 + [DMTA]_\infty + Q) - ([DMTA]_0 - [DMTA]_\infty)}$$

$$P = \exp\left(\frac{k_f(2t[DMTA]_\infty(K-1) + Q(K-1))}{K}\right)$$

$$Q = \frac{K([HSR]_0 - [DMTA]_0) + 2[DMTA]_0}{K-1}$$

$$[DMTA]_\infty = \left(\frac{1}{2(K-1)}\right)\left(\sqrt{(K([HSR]_0 - [DMTA]_0) + 2[DMTA]_0)^2 + 4[DMTA]_0^2(K-1)} - (K([HSR]_0 - [DMTA]_0) + 2[DMTA]_0)\right)$$

$$K = \frac{k_f}{k_r}$$

$$[TA2] = [DMTA]_0 - [DMTA]$$

Scheme S5.3. Modeling reversible 2nd order reaction for thiol-thioaminal exchange.[3]

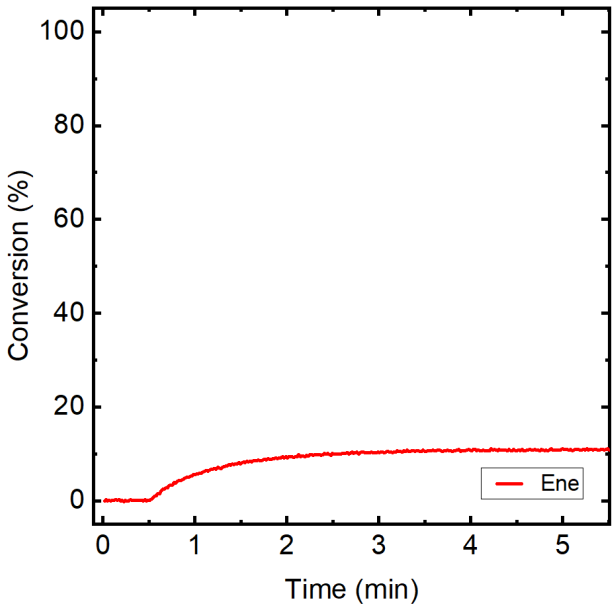

Figure S5.3. Homopolymerization of allylthioaminal (ATA) when mixed with 1 mol % I819 and exposed to 400-500 nm light at 30 mW/cm^2 starting at 0.5 minutes. Conversion measured by real-time FTIR.

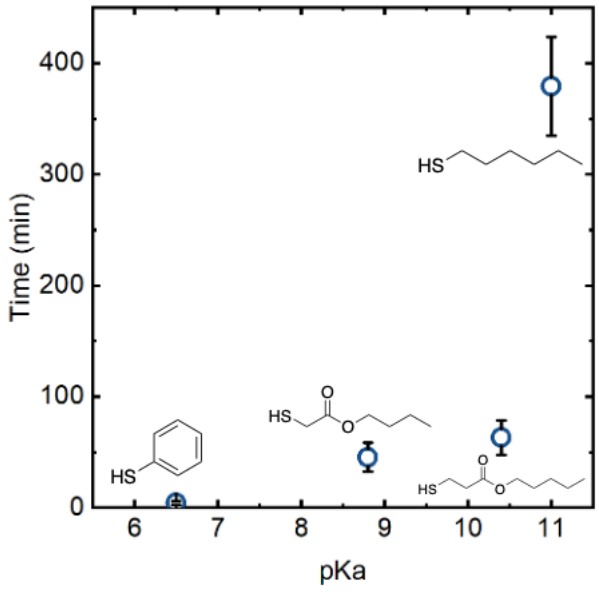

Figure S5.4. Degradation time of thioaminal networks when submerged in various thiols.

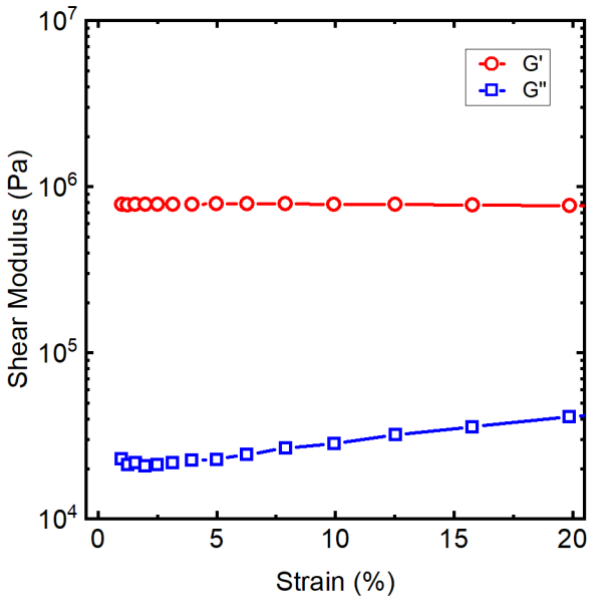

Figure S5.5. Shear strain sweep experiment for the ATA-HDT-I819 formulation, with a frequency of 1 Hz. All rheology experiments were subsequently conducted at 10 % shear strain.

5.8.1 References

(1) Wojtecki, R. J.; Jones, G. O.; Yuen, A. Y.; Chin, W.; Boday, D. J.; Nelson, A.; García, J. M.; Yang, Y. Y.; Hedrick, J. L. Developments in Dynamic Covalent Chemistries from the Reaction of Thiols with Hexahydrotriazines. *J. Am. Chem. Soc.* **2015**, *137* (45), 14248–14251. https://doi.org/10.1021/jacs.5b08815.

(2) Chao, A.; Zhang, D. Investigation of Secondary Amine-Derived Aminal Bond Exchange toward the Development of Covalent Adaptable Networks. *Macromolecules* **2019**, *52* (2), 495–503. https://doi.org/10.1021/acs.macromol.8b02654.

(3) Hogg, N. The Kinetics of S-Transnitrosation - A Reversible Second-Order Reaction. *Anal. Biochem.* **1999**, *272* (2), 257–262. https://doi.org/10.1006/abio.1999.4199.

Chapter 6: Radical-Mediated Scission of Thioaminals for On-Demand Construction-then-Destruction of Crosslinked Polymer Networks

This chapter to be submitted as a manuscript to Macromolecules with the following coauthors: Juan J. Hernandez, Gopal Reddy Sama, Yunfeng Hu, Shafer Soars, Claire E. Niemet, Cassandra M. Sanchez, Christopher N. Bowman

6.1 Abstract

Two-stage polymerizing-then-degrading networks were achieved under a single near UV light source, by sequentially performing thiol-ene photopolymerization and radical-mediated thioaminal scission. Synthesis of model thioaminal small molecules showed photo-activated thioaminal scission produced thioamide moieties, identifiable by distinct NMR singlets at 3.29 and 3.26 ppm and an FTIR peak around 1530 cm^{-1}. The scission process is proposed to occur via ß-scission of the carbon next to the sulfur atom and was found to be influenced by thiol substitution on the thioaminal, leading to scission conversion increasing from 5 ± 1% to 39 ± 3 % and scission time decreasing from 6 to 2 min as thiols were progressively more substituted. Thioaminal scission occurred semi-orthogonally with radical-mediated thiol-ene reactions; the thiol-ene reaction achieved near quantitative yield within the first 0.5 min while thioaminal scission required a further 5 – 15 min of exposure. This semi-orthogonality was exploited to create two-stage polymerizing-then-degrading networks, with both regimes dependent on total light dose and the transition occurring around 2 J/cm^2 under these exposure and polymerization conditions. This work establishes thioaminals as a new photo-mediated scission chemistry and a means to create multi-stage, light-activated networks.

6.2 Introduction

Light-responsive chemical reactions enable ways to process materials that are otherwise unachievable by traditional means. Unlike traditional chemical reactions which activate materials with stimuli such as redox,[1–3] pH,[4,5] temperature,[6,7] or mechanical agitation,[8] the use of light provides spatiotemporal control[9] and the irradiation parameters required to define the light-process, such as light intensity, exposure time, and wavelength, are readily tuned to manipulate the desired process kinetics and characteristics.[10] By means of light exposure, materials have been adapted to create self-propelled actuators,[11] multi-stage drug release capsules,[12] and micron-scale 3-D structures.[13]

Of the many light-responsive reactions available, photodegradation reactions are of particular interest. Within polymers, photodegradation reduces the degree of connectivity between chemical groups,[14] leading to polymer breakdown, and this has been used to create lithography micropatterning,[15] burst-release capsules,[16] and selective cell harvesting.[17] Photodegradation may occur as a result of either reversible photoreactions, such as those using azobenzenes,[18] coumarins,[19] and other cyclo-addition reactions,[20] or irreversible photoreactions, such as scission caused by ortho-nitrobenzyl esters,[15,21] vinyl ketones,[22] radical formation,[9] and high-power ablation.[14] Of the irreversible reaction types, scission leads to photodegradation by either directly cleaving the bonds to result in degradation, or by deprotecting reactive groups which initiate a secondary reaction that results in degradation.[9,23]

Here, spatiotemporal control over the entire material life-cycle is achieved by combining photodegradation with photopolymerization techniques, in ways unattainable by methods that only use light for one process.[24–26] Separation of the polymerization and degradation processes has been established by a number of means, including using different wavelengths to activate radical-

mediated polymerization of one group followed by direct photoscission of another,[27,28] using different wavelengths to activate separate polymerization and scission stages within the same functional group,[22] or using competing reactions with vastly different kinetics.[29] Of these methods, using different kinetic rates gives the added benefit of controlling the two processes with one light source,[30] and the ability to tune the timescale of each reaction by changing light intensity, relative absorptivity or relative quantum yields.[31] While past work on acyclic benzylidine acetals has opened this field,[29] there is much room left to explore. To that end, this work sought to explore the potential of thioaminal groups as a new photo-mediated scission chemistry which facilitates separate photopolymerization and photodegrading regimes simply by varying reaction kinetics, as shown in **Scheme 6.1**.

Thioaminals, also referred to as *N,S*-acetal[32] or thiomethylamine[33,34] groups, are the *N,S* analogue of acetals and consist of a nitrogen-carbon-sulfur moiety. While chemically similar to acetals and their variants, the increased nucleophilic difference between the *N,S* atoms and the available p-orbital electrons afford this group an alternate reactivity scheme.[35,36] This alternate scheme has been used to establish new organic syntheses,[37] enhance drug activity,[38] and mediate hydrolysis.[39] Thioaminals may also undergo thiol-thioaminal exchange, which has been used to alter biologically-active molecules[40] and synthesize dynamic linear polymers.[41] While photo-mediated scission of thioaminals has not been explored to these authors' knowledge, photo-mediated scission of acetals and their variants have been shown to occur.[17,29,42,43] As thioaminals are chemically similar to acetals, it is reasonable to consider that thioaminals may also undergo photo-mediated scission, and due to their altered reactivity may grant another method of control over scission.

This work explored thioaminals as a new photo-mediated scission chemistry, and its possible use as a novel polymerizing-then-degrading polymer system that is controlled via different reaction kinetic regimes. A model system of thioaminal small molecules was developed to study the possible thioaminal scission reaction, with NMR and FTIR used to quantify the speed and extent of scission. Four different functional groups were synthesized in the small molecules to investigate the effects of electronics and resonance. The kinetics of thioaminal scission were then compared to a competing thiol-ene polymerization reaction, which was done by synthesizing a monomer than contained both reactive thioaminal and thiol-ene functional groups. These experiments characterized how the thioaminal and thiol-ene reactions competed within small molecules and bulk polymer networks analyzed via photorheology. Everything culminated in the formation of light-programmable polymer network, which could be polymerized and degraded on cue by controlling the competing thioaminal scission and thiol-ene polymerization reactions via total light dose incident on the network. This research expands the chemical library available to create light-controlled materials and shows that by properly tuning kinetic rates there are still several advances to be made in material life-cycle design.

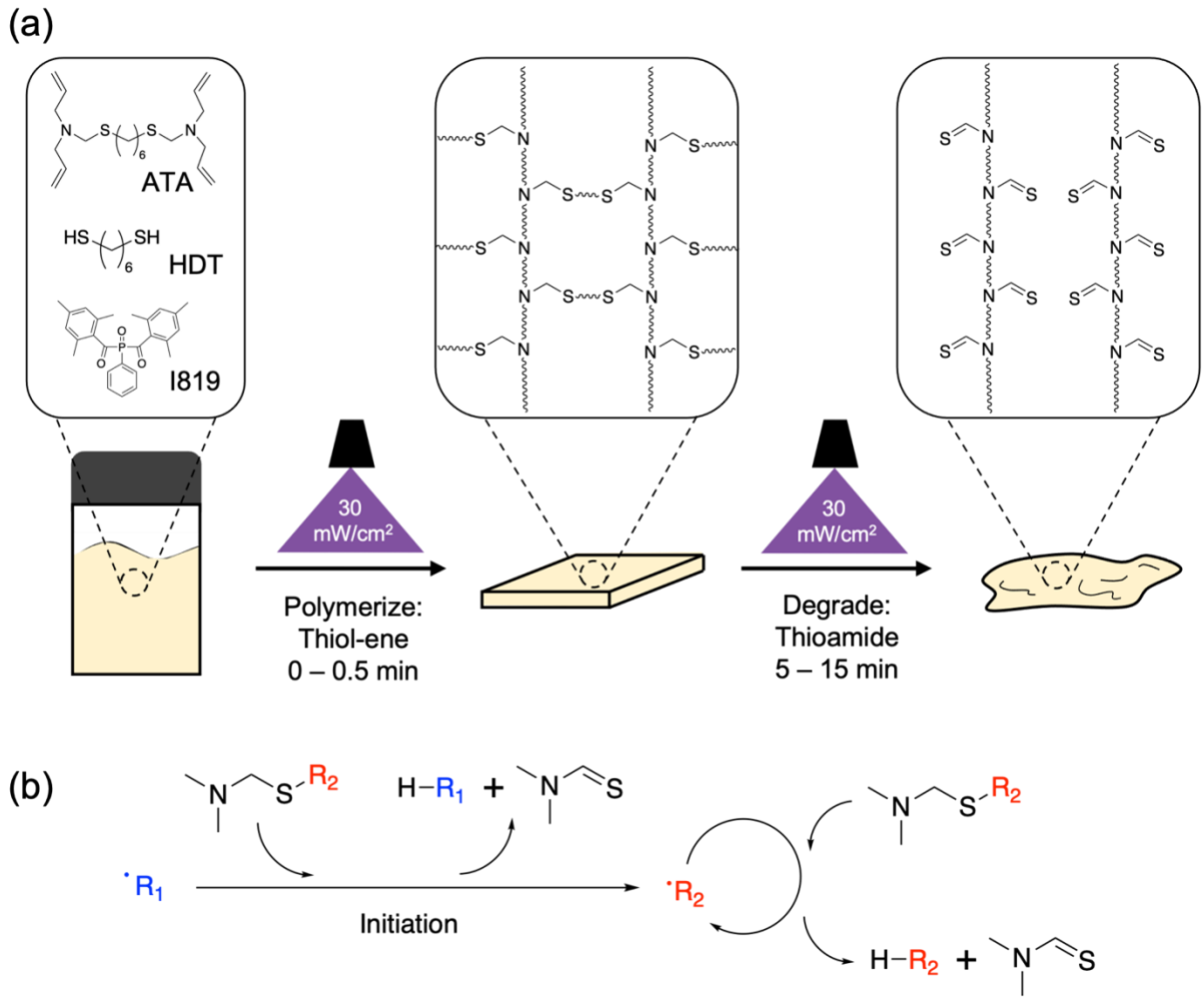

Scheme 6.1. On-demand polymerizing-then-degrading networks were created by combining the thiol-ene polymerization reaction with radical-mediated thioaminal scission. (a) Thioaminal and thiol-ene monomers investigated (*left*), the polymerized network (*middle*), and the degraded network (*right*). (b) Proposed thioaminal scission process used to control network degradation, where the R_2 group on the thioaminal becomes a radical.

6.3 Materials and Experimental Methods

6.3.1 Materials

Thioaminal small molecules (1°TA, 2°TA, 3°TA) and allylthioaminal (ATA) were synthesized according to procedures described in the Supporting Information **Scheme S6.1** and **Scheme S6.2**. All other materials were purchased commercially and used without further purification. 1-

hexanethiol (HT), 1,6-hexanedithiol (HDT), 1-butanethiol, 2-butanethiol, diallylamine, formaldehyde, and tert-Butyl mercaptan were purchased from Sigma Aldrich. N,N,N',N'-tetramethyldiaminomethane was purchased from TCI America and Irgacure 819 (I819) from IGM Resins.

6.3.2 Small Molecule Scission

The scission of three thioaminal small molecules (1^oTA, 2^oTA, 3^oTA) was investigated. Each small molecule was mixed neat in a 1 thioaminal : 0.01 I819 ratio without solvent, placed between glass slides separated by 25 μm spacers, and exposed to 400-500 nm light at 30 mW/cm^2 for 15 min. NMR of the mixtures was taken before and after light exposure using an Avance III, 400 MHz NMR under ambient conditions. Samples were compared to a dimethylsulfone internal standard (singlet at 3.00 ppm) with a concentration of 20 mM in $CDCl_3$.

6.3.3 NMR Conversion

Assuming a 1 : 1 conversion of thioaminals into thioamides via thioaminal scission, the following equation was used to determine scission conversion,

$$Conversion = \frac{Int_{TD}*\frac{1}{6}}{Int_{TD}*\frac{1}{6}+Int_{TA}*\frac{1}{2}} \quad (1)$$

Here, Int_{TD} is the total integral value of the two thioamide singlets at 3.26 and 3.29 ppm, Int_{TD} is the integral value of the thioaminal peak around 3.9 ppm, and the fractions come from the number of protons per integral site.

6.3.4 Fourier Transform Infrared Spectroscopy

Fourier Transform Infrared (FTIR) spectroscopy of small molecules and polymers used a Nicolet 6700 FTIR instrument from Thermo Scientific. Samples were placed between KOH plates under ambient conditions and exposed to 400-500 nm light at 30 mW/cm^2 for up to 10 min. Small molecule samples were mixed neat in a ratio of 1 thioaminal : 0.01 I819 without solvent, while polymeric samples were mixed neat in a ratio of 0.7 thiol : 1 ene : 0.005 I819.

6.3.5 Photorheology

Photorheology of samples was run using an Ares-G2 Rheometer from TI Instruments under ambient conditions. A solution of 0.7 thiol : 1 ene : 0.005 I819 was made from molecules ATA, HDT, and I819 and placed between transparent 8 mm quartz parallel plates with a 25 μm gap. Shear storage modulus was recorded in real time using 10 % shear strain and a frequency of 1 Hz. 0.5 min after the test started a 400-500 nm light was turned on, with intensity ranging from 1 to 30 mW/cm^2.

6.3.6 Curing and Degrading Polymer Films

Polymer films were cured by mixing a solution of 0.7 thiol : 1 ene : 0.005 I819 using molecules ATA, HDT, and I819. The solution was placed between glass slides coated with RainX and separated by 100 μm spacers. The slides were exposed to 400-500 nm light at 30 mW/cm^2 for 34 s, to reach a dose of 1 J/cm^2. The glass was then peeled apart to isolate the cured film.

Degradation proceeded by exposing cured films to 400-500 nm light for 120 s at 100 mW/cm^2, adding a dose of 12 J/cm^2. The films were then lightly washed with a solvent mixture of 35 : 65

dichloromethane : hexanes, by volume, to remove degraded material. At times, photomasks were used to pattern the cured and degraded regions.

6.4 Results and Discussion

As mentioned previously, this work sought to determine if photo-mediated thioaminal scission may occur as has been reported in other acetal-adjacent chemistries.[17,29,42,43] To the best of the authors' knowledge, no prior work has investigated the radical-mediated scission of thioaminals and doing so will expand the breadth of chemistries available to achieve completely light-controlled polymerizing-then-degrading systems. To begin, a small molecule model was developed to investigate the thioaminal scission process, its mechanism, and the extent to which scission can be controlled.

6.4.1 Small Molecule Thioaminal Scission

Three small molecule thioaminals were synthesized from butanethiol isomers and N,N,N',N'-tetramethyldiaminomethane according to the procedures described in **Scheme S6.1**. A primary (1-butanethiol), secondary (2-butanethiol), and tertiary (tertbutylthiol) butanethiol were chosen to probe the impact of radical stability on the possible thioaminal scission process, and created the three thioaminal molecules 1ºTA, 2ºTA, and 3ºTA, respectively, **Figure 6.1a**. Each molecule was mixed with 1 mol % I819, placed between glass slides, and exposed to 400-500 nm light for 15 min at 30 mW/cm^2.

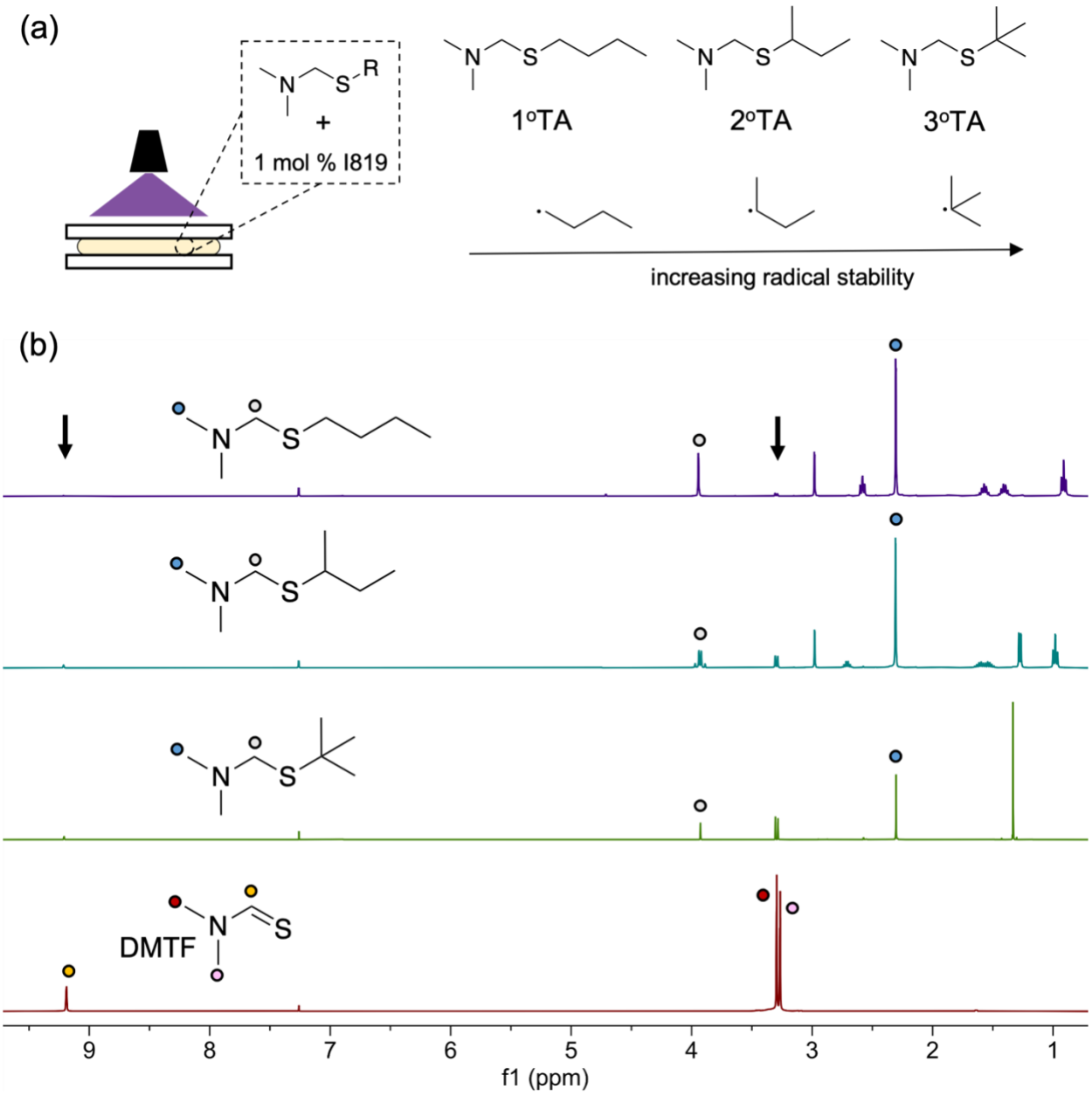

Figure 6.1. Photo-mediated thioaminal scission was found to occur, with radicals catalyzing the reaction to form thioamides. (a) Small molecule reaction used to investigate thioaminal scission, where thioaminal molecules 1°TA, 2°TA, or 3°TA were mixed with photoinitiator and exposed to 400-500 nm light at 30 mW/cm^2 for 15 min. (b) NMR spectra of each thioaminal molecule after exposure to photo-generated radicals, showing the presence of thioaminals (grey dots) and the formation of new peaks (black arrows) as thiol substitution increased. The newly formed peaks matched the spectra for commercially-sourced dimethylthioformamide (DMTF; red, pink, and orange dots).

It was found that thioaminal scission did occur upon exposure to photo-generated radicals.

Figure 6.1b shows the NMR spectra of each thioaminal molecule after it was mixed with

photoinitiator and exposed to near-UV light. All molecules displayed methylene singlets at 3.93 ppm (grey dots) and methyl singlets at 2.30 ppm (blue dots), confirming the presence of thioaminals. All samples also displayed singlets at 9.21, 3.29, and 3.26 ppm (orange, red, and pink dots) as indicated by the black arrows. These three peaks did not appear in the NMR spectra of the neat thioaminal molecules (**Figures S6.1**, **S6.2**, and **S6.3)**, nor did they appear when the thioaminals were exposed to near-UV without a photoinitiator present. Furthermore, all three peaks matched the NMR spectra of commercially sourced dimethylthioformamide (DMTF, **Figure 6.1b** *bottom*). These data indicate that in the presence of the photo-generated radicals, the thioaminal molecules formed DMTF. Following the scission mechanisms proposed in other acetal-adjacent chemistry,[29,42] it is likely that the photo-generated radicals interacted with the thioaminal methylene carbon, causing β-scission of the carbon on the other side of the sulfur and resulting in DMTF, as illustrated in the *Initiation* step of **Scheme 6.1b**.

Greater thiol substitution within thioaminal molecules resulted in a greater extent of scission for otherwise identical doses. In **Figure 6.1b**, as thiol substitution increased, so too did the height and integration values for the DMTF NMR peaks. This increase occurred despite a fixed photoinitiator concentration of 1 mol % in all samples, indicating the photoinitiator served as a catalyst for a secondary reaction. It is likely that once the thioaminal scission *Initiation* step completed it led to a cyclic loop, where the radical produced during *Initiation* ($\cdot R_2$) then reacted with another thioaminal, leading to more scission, **Scheme 6.1b**. To investigate better the conversion of thioaminal groups into thioamide groups, the thioaminal scission experiment was repeated in a round bottom flask, with aliquots removed at 15 min intervals to track the concentration of all components via quantitative NMR. By using the internal standard dimethylsulfone (singlet at 3.0 ppm), NMR spectra showed a near 1 : 1 ratio of the loss of the thioaminal to the formation of the

thioamide which supported the theory that photoinitiator served as a catalyst, and further indicated a 1 : 1 conversion of thioaminal to thioamide groups, **Figure S6.7**. Equation 1 was developed following the 1 : 1 relationship and was used to quantify scission of the 1°TA, 2°TA, and 3°TA molecules from the NMR spectra of **Figure 6.1b**. As thiol substitution increased for constant dose exposures, scission conversion increased from 5 ± 1, to 16 ± 1, and to 39 ± 3 %. This increase in conversion lines up with the increased stability of the resulting radicals formed by thioaminal scission, which suggests that the radical electronics impact the scission reaction.

Inclusion of an aromatic group on the sulfur was observed to hinder thioaminal scission. Phenylthioaminal (PTA) scission was also tested as a means to investigate the effect that a resonance-stabilized radical has on thioaminal scission. PTA was mixed with 1 mol % I819 and exposed to near-UV light; however, in this scenario no thioamide peak formation was observed in the NMR spectra, **Figure S6.8**. This behavior suggests the aromatic group inhibited thioaminal scission, which may have been caused by excessive delocalization of the radical on the aromatic ring, thereby decreasing the chances of the propagation reaction.[44]

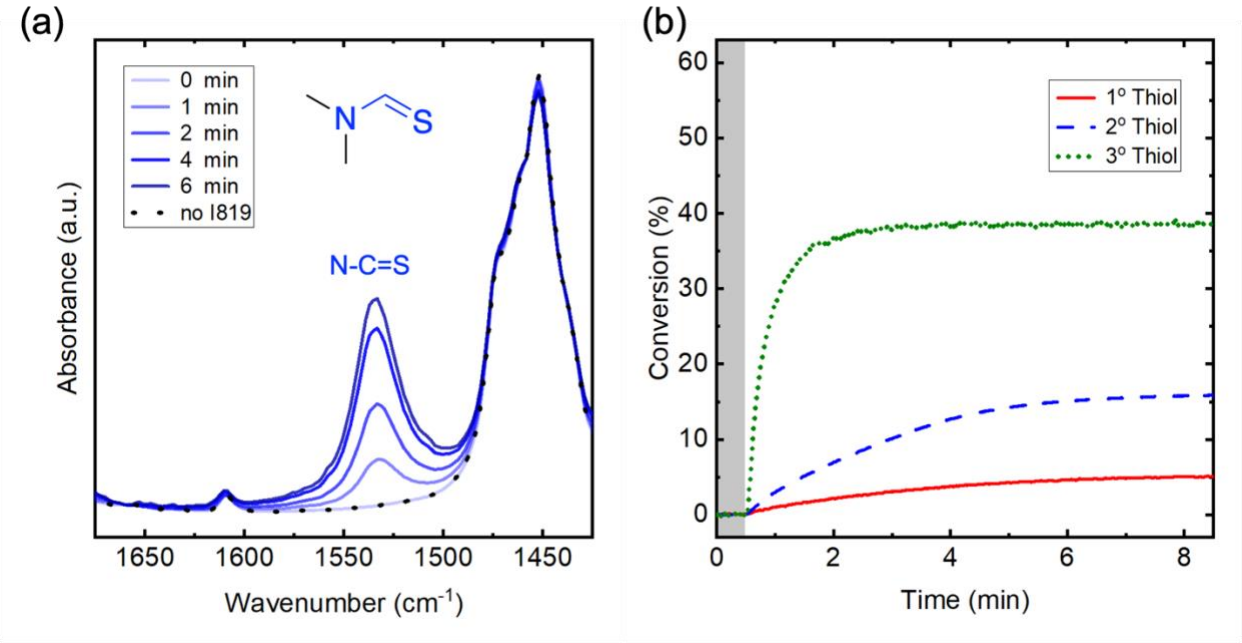

Figure 6.2. Real-time transmission FTIR showed thioaminal scission occurred within minutes and resulted in distinct DMTF peaks. (a) FTIR spectra of 2°TA mixed with 1 mol % I819 (solid lines), and neat 2°TA (dashed line) before and after exposure to 400-500 nm light. The peak forming at 1530 cm^{-1} corresponds to a N-C=S vibration. (b) Conversion profiles for each thioaminal molecule plotted as a function of illumination time, with the light turned on at 0.5 min. Conversion was tracked by peak formation at 1530 cm^{-1} and verified by combining ^{1}H NMR data with equation 1.

Real-time transmission FTIR of the thioaminal molecules further supported the claim that thioaminal scission formed thioamides. **Figure 6.2** shows a representative FTIR spectra of the three thioaminal molecules investigated, and how their scission conversions changed when the thioaminals were mixed with 1 mol % I819 and exposed to a 400-500 nm light. **Figure 6.2a** shows the FTIR spectra of thioaminal 2°TA. After exposure to photo-generated radicals, a new peak formed at 1530 cm^{-1}, indicating the formation of a complex N-C=S vibration,[45] which is also characteristic of commercial DMTF, **Figure S6.14**. This 1530 cm^{-1} peak did not form when 2°TA was exposed to light in the absence of a photoinitiator, **Figure 6.2a** *dashed line*. Repeating the experiment with 1°TA and 3°TA confirmed that photo-generated radicals were required to form the 1530 cm^{-1} peak, and the full spectra for all thioaminals are displayed in **Figures S6.11**, **S6.12**, and **S6.13**.

Kinetic analysis of thioaminal scission using FTIR found that thiol substitution also controlled the scission rate. **Figure 6.2b** shows conversion as a function of illumination time for the thioaminal molecules studied, where the reaction was monitored by tracking the 1530 cm^{-1} peak in FTIR and conversions were confirmed by ^{1}H NMR. All thioaminals reached final conversion within 8 min, with the tertiary thiol substitution achieving the highest conversion (39 ± 3 %) within the shortest reaction time (2 min). As substitution decreased from tertiary to primary, the final conversion dropped to 5 ± 1 % and the time to plateau increased to 6 min. A clear trend developed in which increased radical stability on the propagating carbon center resulted in increased rates and higher overall conversions.

6.4.2 Semi-Orthogonal Radical Reactions

Having established that thioaminals undergo on-demand photo-mediated scission, this work envisioned incorporating this moiety with a photo-mediated polymerization reaction, as a step toward creating on-demand construction and destruction of materials. The thiol-ene polymerization reaction was chosen as it is highly selective, insensitive to oxygen, and may be tuned to achieve rapid kinetics simply by changing the light intensity or other initiation conditions.[46,47] Thiol-ene polymerization is a radical-mediated reaction (with the radicals often resulting from a photoinitiator and light) coupling a thiol group to an ene group. As both thioaminal scission and thiol-ene polymerization are radical-mediated, differences in their kinetics may lead to semi-orthogonal processes. To investigate these reactions, the monomer allylthioaminal (ATA), which contains both thioaminal scission and thiol-ene polymerization active groups, was synthesized. ATA was found to achieve non-trivial homopolymerization, ~10 % when mixed with 1 mol % I819 (**Figure S6.15**), and as such was used in off-stoichiometric ratios in future

experiments to ensure complete thiol and ene consumption. To investigate the competing thioaminal scission and thiol-ene polymerization reactions, ATA was mixed with 1-hexanethiol (HT) and I819 in a mole ratio of 0.7 thiol : 1 ene : 0.005 I819, a non-stoichiometric ratio, **Figure 6.3a**.

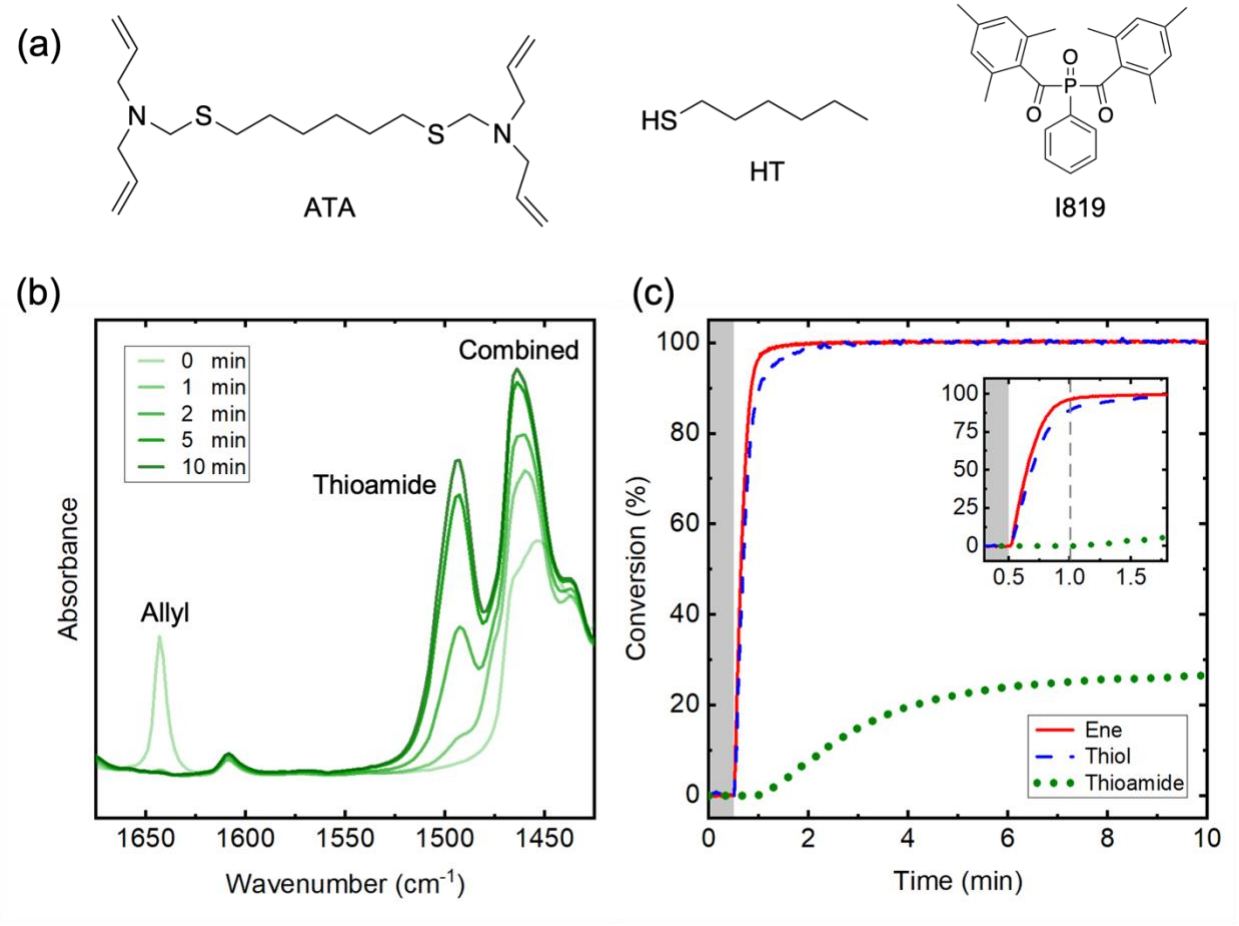

Figure 6.3. Incorporating thioaminal groups into a thiol-ene polymerization system showed thioaminal scission occurred on a tenfold slower time scale, enabling semi-orthogonal control between the polymerization and scission reactions. (a) Monomers and photoinitiator used to compare the kinetics of thiol-ene polymerization versus thioaminal scission. (b) FTIR spectra of a 0.7 thiol : 1 ene : 0.005 I819 mole ratio of the ATA, HT, and I819 components, before and after 400-500 nm light exposure. The allyl stretch peak at 1640 cm^{-1} disappeared while the N-C=S vibration (thioamide) peak formed at 1500 cm^{-1}. (c) Conversion profiles are for the thiol, ene, and thioamide peaks plotted as a function of illumination time, with the light turned on at 0.5 min. Conversion was verified using ^{1}H NMR data and equation 1.

Upon illumination, the thiol-ene and thioaminal scission reactions occurred simultaneously but at differing rates. In early stages of the reaction, nearly quantitative conversion of thiols and enes was observed, followed by the onset of thioaminal scission (**Figure 6.3**), effectively achieving a semi-orthogonal polymerizing-then-cleaving system. **Figure 6.3b** shows the FTIR spectra of the ATA-HT-I819 mixture before and after being exposed to a 400-500 nm light source for 10 min. During the exposure the allyl C=C stretch peak (1640 cm^{-1}) disappeared while an N-C=S vibration peak (1500 cm^{-1}) formed. Peak changes occurred at different rates; the allyl peak disappeared within 0.5 min, while the thioamide peak formed over 9.5 min. The allyl C-H stretch peak (3080 cm^{-1}) and the thiol S-H peak (2550 cm^{-1}) supported this observation of rapid thiol-ene polymerization, as these peaks also disappeared within 0.5 min, **Figure S6.16**. Aside from thiol-ene and thioamide peak formation, another peak formed at 1460 cm^{-1} although in two distinct stages: the peak first increased proportionally to allyl consumption during the initial 0.5 min after light exposure, then slowed down and increased proportionally to thioamide formation during the last 9.5 min. This behavior suggests the 1460 cm^{-1} is likely a convolution of two or more peaks, affected by both the thiol-ene polymerization and thioaminal scission reactions.

The polymerization and scission reactions showed clearer semi-orthogonality when conversion was plotted by using the area under the curve of the FTIR peaks. **Figure 6.3c** shows conversion for the allyl, thiol, and thioamide functional groups as illumination time increased after the light source was turned on at 0.5 min. As in **Figure 6.2b**, the reaction was monitored by tracking the relevant peak in FTIR, and conversions were confirmed by ^{1}H NMR. The ally and thiol peaks reached near quantitative conversion (94 % allyl, 80 % thiol) within 0.5 min of light exposure, i.e. 1 min on the x-axis, while the thioamide peak only started forming afterwards, supporting the observations made in **Figure 6.3b**. The near 100 % consumption of allyl groups within 0.5 min

was likely due to allyl homopolymerization, and suggests that the remaining 20 % of thiol reacted via a non-thiol-ene polymerization process.

It was interesting to note that the thioaminal ATA achieved a higher extent of scission than the previous thioaminals studied. **Figure 6.3c** shows ATA scission reached 28%, much greater than scission of 1°TA (5 ± 1 %), even though both thioaminal molecules had primary thiol substitution. This increased scission was likely due to the limited mobility of the carbon-centered radicals formed by ATA scission. When scission occurred on a thioaminal group of ATA, the resulting radical was still attached to half of the molecule. Furthermore, since thiol-ene polymerization had preceded scission, most ATA molecules were extended with HT connections, meaning the radical formed after scission was attached to a 463 g/mol moiety. This larger pendant group may have inhibited radical mobility, making these radicals less likely to terminate via recombination and thus increased scission.[48] Another explanation for why scission in ATA exceeded that of 1°TA is the 20 % unreacted thiols remaining at the 1 min time point may have assisted in propagating thioaminal scission, leading to higher final conversion.

As mentioned previously, the thioaminal scission reaction effectively began after thiol-ene polymerization was largely completed. This delay may have occurred due to photo-generated radicals preferentially interacting with allyl groups. When the photoreaction began, I819 radicals preferentially formed thiyl radicals due to sulfur's low bond dissociation energy.[49] These thiyl radicals may then propagate across an allyl carbon or abstract a hydrogen from a thioaminal methylene carbon. To test which group could more readily donate a proton, FTIR spectra of the ATA homopolymerization reaction (1 ATA : 0.01 I819) were inspected, and showed allyl groups outcompeted thioaminal groups for I819 radical interactions, **Figure S6.17**. After exposing the mixture to 10 min of 400-500 nm light, ~10 % of ally FTIR peak was consumed while trivial

thioamide peak formation occurred. This outcome implies that within the ATA-HT-I819 system radical species formed during the photoreaction (I819, thiyl, carbon-centered) also preferentially interacted with allyl groups, causing thiol-ene polymerization to occur first. The thioaminal scission reaction could only commence once most of the allyl groups were consumed.

6.4.3 Two-Stage Polymer Networks

With the thiol-ene polymerization and thioaminal scission reactions having been shown to achieve on-demand, semi-orthogonal reactivity with approximately tenfold different timescales, this work turned to investigate how these reactions' interplay could be incorporated into bulk materials to develop light-mediated polymerizing-then-degrading polymer networks. The first step was to investigate how the polymerization and scission reactions competed in networks. A 0.7 thiol : 1 ene : 0.005 I819 mixture of ATA, 1,6-hexanedithiol (HDT), and I819 was exposed to 400-500 nm light at various light intensities for up to 30 min. The resulting polymer structure contained backbone strands composed of hydrocarbons, thioethers, and tertiary amines and contained crosslink bridges connected by two thioaminal groups, **Figure 6.4a**.

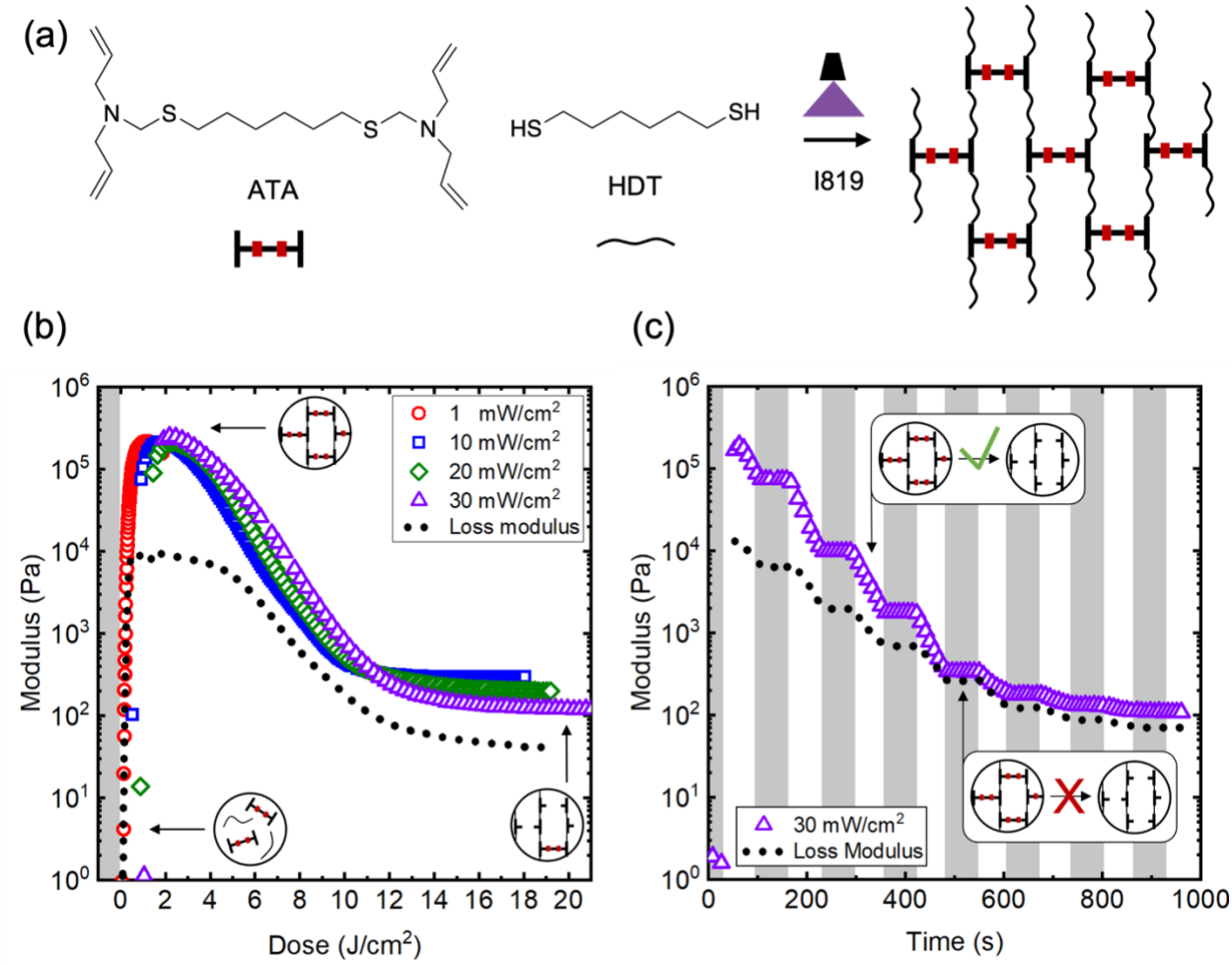

Figure 6.4. Control between the polymerization and scission reactions was expanded into polymer networks, where multifunctional thioaminal monomers were used to create on-demand polymerizing-then-degrading materials using a single 400-500 nm light source. (a) Monomers used to create the thioaminal-containing network, consisting of a non-degradable backbone (*curves*) connected by two cleavable thioaminal units (*red blocks*). (b) Photorheology plot of the thioaminal network, comparing storage (G', markers) and loss (G'', black dotted line) moduli as a function of 400-500 nm light dose. At 2 J/cm^2 the network transitioned from polymerizing to degrading. (c) Photorheology plot showing storage (markers) and loss (black dotted line) moduli as a function of time as the light source was turned on (*white*) and off (*grey*).

Exposing the thioaminal-containing mixture to light confirmed that this material could both undergo polymerization and degradation from a single, near-UV light source. **Figure 6.4b** shows how shear storage (G') and loss (G'') moduli changed as light dose, *i.e.* exposure time at a fixed intensity, increased, and this experiment was repeated for various light intensities from 1 to 30

mW/cm^2. Light dose was calculated using the equation $dose\left[\frac{J}{cm^2}\right] = intensity\left[\frac{W}{cm^2}\right] \times time\,[s]$. These photorheology curves show the material first exhibited a polymerization region from 0 to 2 J/cm^2, with G' increasing to 3 x 10^5 Pa, followed by a degradation region from 3 to 20 J/cm^2, with G' dropping to ~100 Pa. Furthermore, all samples followed a single representative G' and G'' curve where moduli depended on total light dose and not on the light intensity used during exposure. These data indicate that similar to the small molecule study in **Figure 6.3**, the material first underwent thiol-ene polymerization and then underwent thioaminal scission and degraded.

While degradation was achieved, no crossover point for the storage and loss moduli was observed. In **Figure 6.4b**, G' values (markers) never dropped below G'' values (black dotted line), even after both moduli plateaued at 14 J/cm^2. This indicates that degradation only resulted in partial cleavage, allowing part of the network to remain intact. ATA homopolymerization and incomplete thioaminal scission may have both contributed to incomplete network cleavage. As in the **Figure 6.3** study, ATA homopolymerization consumed allyl groups and an off-stoichiometric ratio of 0.7 thiol : 1 ene was required to ensure total consumption of both thiol and ene functionalities. Since allyl homopolymerization occurs via chain-growth[50] and consumed ~30 % of the allyl groups available, it is possible the allyl groups formed a separate network that could not be degraded via thioaminal scission. Incomplete thioaminal scission may have inhibited a crossover point when considering the fraction of ATA crosslink bridges left intact. ^{1}H NMR spectra of the degraded ATA-HDT-I819 material showed that 40 % of thioaminal groups had undergone scission, **Figure S6.19**. Using this scission conversion, and the structure of the ATA crosslink bridges, the equation $F_{cleaved} = 1 - (1 - C)^2$ was derived, where $F_{cleaved}$ is the fraction of ATA bridges cleaved, C is the thioaminal scission conversion, and the full derivation is shown in **Figure S6.20**. For a scission

conversion of 40 %, $F_{cleaved}$ equals 0.64, meaning 36 % of ATA bridges remained intact throughout the degradation process and may have also contributed to the lack of a crossover point.

Despite the lack of a crossover point, submerging the degraded polymer in dichloromethane (DCM) resulted in complete dissolution of the material. Glass slides containing the polymer were exposed to 20 J/cm^2 of light dose to ensure degradation. Rinsing the polymer on these slides with DCM into a 100 mL RBF showed no insoluble material was left on the glass or could be seen within the flask. Repeating this procedure with polymers that had been exposed to less light, only 2 J/cm^2, resulted in an insoluble film that remained on the slide. This experiment showed that for practical applications, thioaminal-containing networks could be completely degraded via thioaminal scission. Researchers seeking to improve this breakdown of polymer networks via thioaminal scission may consider increasing the concentration of photoinitiator used as a catalyst for scission,[29] designing another network where every connection contains cleavable thioaminal units,[51] or using tertiary thiol substitution within thioaminal groups.

As with the initial ATA molecule study, the extent of thioaminal scission within bulk material exceeded that of scission within thioaminal small molecules. ^{1}H NMR tests showed different extents of thioaminal scission for the ATA-HDT system (40 %), the ATA-HT system (28 %), and the 1^{o}TA system (5 $\pm$ 1 %) even though all thioaminals had primary thiol substitution. This difference was likely due to mobility limitations of the carbon-centered radicals formed by thioaminal scission in all three systems, where decreased mobility limited radical termination by recombination and led to higher scission conversion.[48] Furthermore, in the bulk material system this limited mobility increased the chances the scission-induced radicals interacted with nearby thioaminal groups, further propagating scission, as opposed to interacting with mobile I819 or thiyl radicals, leading to termination.

Exposing the ATA-HDT-I819 system to a variable light source that turned on and off found that degradation required illumination and would not proceed in the dark. **Figure 6.4c** shows how G' and G'' changed as a near-UV light sourced was flipped on and off every 60 s. When the light was on (white regions) both G' and G'' changed immediately, while when the light was off (gray regions) both G' and G'' plateaued immediately. As before, G' dropped until it plateaued at ~100 Pa, at which point total illumination time was 450 s, and this time equaled a light dose of 13.5 J/cm^2 which was consistent with the plateau region exhibited in **Figure 6.4b**. These data showed that thioaminals not only enable photodegradation of polymer networks, but that this degradation may take place over an arbitrary number of illumination stages, allowing multi-stage processing of these materials with control over the entire polymerization and degradation regimes. Furthermore, these results imply analog control could be achieved over both the modulus and shape of thioaminal-containing networks, as light dose may be 3-D patterned into these polymers.

6.4.4 Interchangeable Photoresists

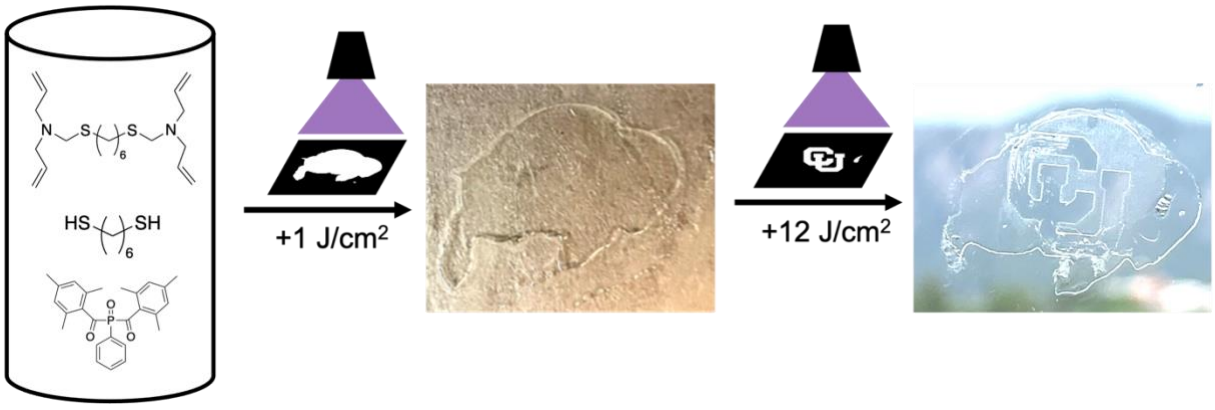

Figure 6.5. On-demand construction and destruction of thioaminal networks was used to create a material that behaved as both a positive and negative photoresist under a single light source. Shining 1 J/cm^2 of 400-500 nm light onto a thioaminal mixture using a photomask cured a buffalo

(positive photoresist, *middle*), while an additional 12 J/cm^2 of light using a second photomask etched out a CU logo (negative photoresist, *right*).

A benefit of achieving photo-mediated spatiotemporal control over both polymerization and degradation via different reaction rates is the ability to command construction and destruction of a material using a single light source. To that end, this work culminated in the creation of thioaminal-containing networks that could be used as both a positive and negative photoresist by controlling exposure to near-UV light. This concept was explored by using photolithography masks as shown in **Figure 6.5**. A solution of 0.7 thiol : 1 ene : 2 I819 was mixed using ATA, HDT, and I819. The mixture was placed between glass slides, exposed to 1 J/cm^2 of light under a buffalo mask, and lightly rinsed with DCM. In this scenario the material demonstrated its potential as a positive photoresist, leaving behind the cured image of a buffalo on the slide. After that, the image was exposed to an additional 12 J/cm^2 of light under a CU mask and rinsed again with DCM. This time the material demonstrated potential as a negative photoresist, dissolving the illuminated CU logo and leaving a patterned hole in the buffalo. This proof-of-concept experiment shows the potential for thioaminal networks to serve as a multi-stage material for photolithography applications,[27] 3-D printing,[28] or volumetric additive manufacturing.[52] Should other researchers seek to expand the use of multi-stage thioaminal networks they may consider investigating the effect of multiple wavelengths,[53] or two-photon polymerization to achieve greater spatial control.[13]

6.5 Conclusions

In this work, the thioaminal scission reaction was established as a new photolabile chemistry, and was combined with the thiol-ene polymerization reaction to create multi-stage tunable materials from a single light source. Thioaminal scission was found to occur by radical-mediated β-scission of the carbon adjacent to the thioaminal sulfur. NMR and FTIR studies confirmed

thioaminal molecules 1ºTA, 2ºTA, and 3ºTA all cleaved to form DMTF, although to different extents. Increasing thiol substitution increased scission conversion from 5 ± 1 % up to 39 ± 3 %, while aromatic thiol substitution inhibited scission. Investigations of the monomer ATA, which contained both thioaminal and thiol-ene active groups, showed these two radical-activated reactions may occur in a semi-orthogonal fashion. Under the conditions used here, the thiol-ene polymerization proceeded first, within 0.5 min, and thioaminal scission proceeded second, taking 9.5 min after the consumption of allyl groups. A polymer network created using ATA showed two semi-orthogonal stages and could be used to create the aforementioned polymerizing-then-degrading material. This material changed modulus at different light exposure doses, polymerizing up to G' of 0.3 MPa when the dose reached 2 J/cm^2 and degrading down to G' of 100 Pa when the dose exceeded 14 J/cm^2. Lastly, a proof-of-concept experiment showed the thioaminal network could be used as both a positive and negative photoresist material by first curing a buffalo and then etching away a CU logo. While this work has laid the foundation for the thioaminal scission reaction, it did not attempt to take an in-depth approach to identifying the detailed mechanism. This research has broadened the chemical library of photolabile reactions, and may be used to create new on-demand multi-stage materials.

6.6 Acknowledgements

This work was made possible by funding from the Graduate Assistance in Areas of National Need (GAANN) and a National Science Foundation's Grant DMR 1809841.

6.7 References

(1) Theato, P.; Sumerlin, B. S.; O'reilly, R. K.; Epp, T. H. Stimuli Responsive Materials. *Chem. Soc. Rev.* **2013**, *42* (17), 7055–7056. https://doi.org/10.1039/c3cs90057f.

(2) Gao, S.; Tang, G.; Hua, D.; Xiong, R.; Han, J.; Jiang, S.; Zhang, Q.; Huang, C. Stimuli-Responsive Bio-Based Polymeric Systems and Their Applications. *J. Mater. Chem. B* **2019**, *7* (5), 709–729. https://doi.org/10.1039/c8tb02491j.

(3) Roth, P. J.; Lowe, A. B. Stimulus-Responsive Polymers. *Polym. Chem.* **2017**, *8* (1), 10–11. https://doi.org/10.1039/c6py90169g.

(4) Xu, Z.; Liang, Y.; Ma, X.; Chen, S.; Yu, C.; Wang, Y.; Zhang, D.; Miao, M. Recyclable Thermoset Hyperbranched Polymers Containing Reversible Hexahydro-s-Triazine. *Nat. Sustain.* **2020**, *3* (1), 29–34. https://doi.org/10.1038/s41893-019-0444-6.

(5) Lazzari, S.; Codari, F.; Storti, G.; Morbidelli, M.; Moscatelli, D. Modeling the PH-Dependent PLA Oligomer Degradation Kinetics. *Polym. Degrad. Stab.* **2014**, *110*, 80–90. https://doi.org/10.1016/j.polymdegradstab.2014.08.012.

(6) McMurry, J. *Organic Chemistry*, Eighth Edi.; Cengage Learning, 2012.

(7) Hiemenz, P. C.; Lodge, T. P. *Polymer Chemistry Second Edition*; CRC Press Taylor & Francis Group, 2007. https://doi.org/10.1201/9781420018271-4.

(8) Soars, S.; Kamps, J.; Fairbanks, B.; Bowman, C. Stimuli-Responsive Depolymerization of Poly(Phthalaldehyde) Copolymers and Networks. *Macromol. Chem. Phys.* **2021**, *222* (17), 1–7. https://doi.org/10.1002/macp.202100111.

(9) Chatani, S.; Kloxin, C. J.; Bowman, C. N. The Power of Light in Polymer Science: Photochemical Processes to Manipulate Polymer Formation, Structure, and Properties. *Polym. Chem.* **2014**, *5* (7), 2187–2201. https://doi.org/10.1039/c3py01334k.

(10) Bertrand, O.; Gohy, J. F. Photo-Responsive Polymers: Synthesis and Applications. *Polym. Chem.* **2017**, *8* (1), 52–73. https://doi.org/10.1039/c6py01082b.

(11) Zuo, B.; Wang, M.; Lin, B. P.; Yang, H. Visible and Infrared Three-Wavelength Modulated Multi-Directional Actuators. *Nat. Commun.* **2019**, *10* (1). https://doi.org/10.1038/s41467-019-12583-x.

(12) Liu, C.; Ewert, K. K.; Yao, W.; Wang, N.; Li, Y.; Safinya, C. R.; Qiao, W. A Multifunctional Lipid Incorporating Active Targeting and Dual-Control Release Capabilities for Precision Drug Delivery. *ACS Appl. Mater. Interfaces* **2020**, *12* (1), 70–85. https://doi.org/10.1021/acsami.9b14470.

(13) Adzima, B. J.; Kloxin, C. J.; Deforest, C. A.; Anseth, K. S.; Bowman, C. N. 3D Photofixation Lithography in Diels-Alder Networks. *Macromol. Rapid Commun.* **2012**, *33* (24), 2092–2096. https://doi.org/10.1002/marc.201200599.

(14) Pasparakis, G.; Manouras, T.; Argitis, P.; Vamvakaki, M. Photodegradable Polymers for Biotechnological Applications. *Macromol. Rapid Commun.* **2012**, *33* (3), 183–198. https://doi.org/10.1002/marc.201100637.

(15) Li, L.; Deng, X. X.; Li, Z. L.; Du, F. S.; Li, Z. C. Multifunctional Photodegradable Polymers for Reactive Micropatterns. *Macromolecules* **2014**, *47* (14), 4660–4667. https://doi.org/10.1021/ma501019c.

(16) Han, D.; Tong, X.; Zhao, Y. Fast Photodegradable Block Copolymer Micelles for Burst Release. *Macromolecules* **2011**, *44* (3), 437–439. https://doi.org/10.1021/ma102778d.

(17) Pasparakis, G.; Manouras, T.; Selimis, A.; Vamvakaki, M.; Argitis, P. Laser-Induced Cell Detachment and Patterning with Photodegradable Polymer Substrates. *Angew. Chemie*

2011, *123* (18), 4228–4231. https://doi.org/10.1002/ange.201007310.
(18) Russew, M. M.; Hecht, S. Photoswitches: From Molecules to Materials. *Adv. Mater.* **2010**, *22* (31), 3348–3360. https://doi.org/10.1002/adma.200904102.
(19) Trenor, S. R.; Shultz, A. R.; Love, B. J.; Long, T. E. Coumarins in Polymers: From Light Harvesting to Photo-Cross-Linkable Tissue Scaffolds. *Chem. Rev.* **2004**, *104* (6), 3059–3077. https://doi.org/10.1021/cr030037c.
(20) Houck, H. A.; Blasco, E.; Du Prez, F. E.; Barner-Kowollik, C. Light-Stabilized Dynamic Materials. *J. Am. Chem. Soc.* **2019**, *141* (31), 12329–12337. https://doi.org/10.1021/jacs.9b05092.
(21) Romano, A.; Roppolo, I.; Rossegger, E.; Schlögl, S.; Sangermano, M. Recent Trends in Applying Ortho-Nitrobenzyl Esters for the Design of Photo-Responsive Polymer Networks. *Materials (Basel).* **2020**, *13* (12), 1–26. https://doi.org/10.3390/ma13122777.
(22) Reeves, J. A.; Allegrezza, M. L.; Konkolewicz, D. Rise and Fall: Poly(Phenyl Vinyl Ketone) Photopolymerization and Photodegradation under Visible and UV Radiation. *Macromol. Rapid Commun.* **2017**, *38* (13), 1–5. https://doi.org/10.1002/marc.201600623.
(23) Worrell, B. T.; McBride, M. K.; Lyon, G. B.; Cox, L. M.; Wang, C.; Mavila, S.; Lim, C. H.; Coley, H. M.; Musgrave, C. B.; Ding, Y.; Bowman, C. N. Bistable and Photoswitchable States of Matter. *Nat. Commun.* **2018**, *9*, 1–7. https://doi.org/10.1038/s41467-018-05300-7.
(24) Stubbs, C. J.; Khalfa, A. L.; Chiaradia, V.; Worch, J. C.; Dove, A. P. Intrinsically Re-Curable Photopolymers Containing Dynamic Thiol-Michael Bonds. *J. Am. Chem. Soc.* **2022**. https://doi.org/10.1021/jacs.2c03525.
(25) Wang, C.; Goldman, T. M.; Worrell, B. T.; McBride, M. K.; Alim, M. D.; Bowman, C. N. Recyclable and Repolymerizable Thiol-X Photopolymers. *Mater. Horizons* **2018**, *5* (6), 1042–1046. https://doi.org/10.1039/c8mh00724a.
(26) Chen, Z.; Yang, M.; Ji, M.; Kuang, X.; Qi, H. J.; Wang, T. Recyclable Thermosetting Polymers for Digital Light Processing 3D Printing. *Mater. Des.* **2021**, *197*, 109189. https://doi.org/10.1016/j.matdes.2020.109189.
(27) Romano, A.; Angelini, A.; Rossegger, E.; Palmara, G.; Castellino, M.; Frascella, F.; Chiappone, A.; Chiadò, A.; Sangermano, M.; Schlögl, S.; Roppolo, I. Laser-Triggered Writing and Biofunctionalization of Thiol-Ene Networks. *Macromol. Rapid Commun.* **2020**, *41* (10), 1–7. https://doi.org/10.1002/marc.202000084.
(28) Batchelor, R.; Messer, T.; Hippler, M.; Wegener, M.; Barner-Kowollik, C.; Blasco, E. Two in One: Light as a Tool for 3D Printing and Erasing at the Microscale. *Adv. Mater.* **2019**, *31* (40). https://doi.org/10.1002/adma.201904085.
(29) Walker, W. D.; Sandoz, M. J.; Roland, S.; Buster, T. M.; Newman, J. K.; Patton, D. L. Command-Destruct Thermosets: Via Photoinduced Thiol-Catalyzed β-Scission of Acyclic Benzylidene Acetals. *Polym. Chem.* **2020**, *11* (43), 6873–6878. https://doi.org/10.1039/d0py01006e.
(30) Soars, S. M.; Bongiardina, N. J.; Fairbanks, B. D.; Podgórski, M.; Bowman, C. N. Spatial and Temporal Control of Photomediated Disulfide-Ene and Thiol-Ene Chemistries for Two-Stage Polymerizations. *Macromolecules* **2022**, *55* (5), 1811–1821. https://doi.org/10.1021/acs.macromol.1c02464.
(31) Wydra, J. W.; Cramer, N. B.; Stansbury, J. W.; Bowman, C. N. The Reciprocity Law Concerning Light Dose Relationships Applied to BisGMA/TEGDMA Photopolymers: Theoretical Analysis and Experimental Characterization. *Dent. Mater.* **2014**, *30* (6), 605–612. https://doi.org/10.1016/j.dental.2014.02.021.

(32) Junjappa, H.; Ila, H.; Asokan, C. V. α-Oxoketene-S,S-, N,S- and N,N-Acetals: Versatile Intermediates in Organic Synthesis. *Tetrahedron* **1990**, *46* (16), 5423–5506. https://doi.org/10.1016/S0040-4020(01)87748-6.

(33) Beifuss, U.; Ledderhose, S. Intermolecular Polar [4π+ + 2π] Cycloadditions of Cationic 2-Azabutadienes from Thiomethylamines: A New and Efficient Method for the Regio- and Diastereo-Selective Synthesis of 1,2,3,4-Tetrahydroquinolines. *J. Chem. Soc. Chem. Commun.* **1995**, *1* (20), 2137–2138. https://doi.org/10.1039/C39950002137.

(34) Kim, J. K.; Souma, Y.; Beutow, N.; Ibbeson, C.; Caserio, M. C. Alkylation and Sulfenylation of Amino Thioethers. Tetrahydro-l,3-Thiazine and Related Compounds. *J. Org. Chem.* **1989**, *54* (7), 1714–1720. https://doi.org/10.1021/jo00268a039.

(35) Fialho, D. M. Physical Organic Principles Governing the Spontaneous Prebiotic Emergence of Proto-Nucleic Acids, Georgia Institute of Technology, 2019.

(36) Zhang, L.; Dong, J.; Xu, X.; Liu, Q. Chemistry of Ketene N,S-Acetals: An Overview. *Chem. Rev.* **2016**, *116* (2), 287–322. https://doi.org/10.1021/acs.chemrev.5b00360.

(37) Cavaca, L. A. S.; Gomes, R. F. A.; Afonso, C. A. M. Preparation of Thioaminals in Water. *Molecules* **2022**, *27* (5). https://doi.org/10.3390/molecules27051673.

(38) Chang, H.-M.; Oakes, J.; Olsson, A.; Panaitescu, L.; Britt, B.; Kearney, C.; Kane, R. Synthesis and In Vitro Evaluation of Adenosine Deaminase Resistant N-6 Aminal and Thioaminal Prodrugs of Cordycepin. *Lett. Drug Des. Discov.* **2005**, *2* (2), 133–136. https://doi.org/10.2174/1570180053175151.

(39) Góngora-Benítez, M.; Basso, A.; Bruckdorfer, T.; Royo, M.; Tulla-Puche, J.; Albericio, F. Eco-Friendly Combination of the Immobilized PGA Enzyme and the s-Phacm Protecting Group for the Synthesis of Cys-Containing Peptides. *Chem. - A Eur. J.* **2012**, *18* (50), 16166–16176. https://doi.org/10.1002/chem.201201370.

(40) Chen, J.; Zhang, X. F.; Kort, M. E.; Huth, J. R.; Sun, C.; Miesbauer, L. J.; Cassar, S. C.; Neelands, T.; Scott, V. E.; Moreland, R. B.; Reilly, R. M.; Hajduk, P. J.; Kym, P. R.; Hutchins, C. W.; Faltynek, C. R. Molecular Determinants of Species-Specific Activation or Blockade of TRPA1 Channels. *J. Neurosci.* **2008**, *28* (19), 5063–5071. https://doi.org/10.1523/JNEUROSCI.0047-08.2008.

(41) Wojtecki, R. J.; Jones, G. O.; Yuen, A. Y.; Chin, W.; Boday, D. J.; Nelson, A.; García, J. M.; Yang, Y. Y.; Hedrick, J. L. Developments in Dynamic Covalent Chemistries from the Reaction of Thiols with Hexahydrotriazines. *J. Am. Chem. Soc.* **2015**, *137* (45), 14248–14251. https://doi.org/10.1021/jacs.5b08815.

(42) Kumhee, C. Acetal Copolymers: Synthesis, Chemical Modifications and Degradation Study, 1994.

(43) Feilding, A. J.; Franchi, P.; Roberts, B. P.; Smits, T. M. EPR and Computational Studies of the Formation and β-Scission of Cyclic and Acyclic Dialkoxyalkyl Radicals. *J. Chem. Soc. Perkin Trans. 2* **2002**, *2* (1), 155–163. https://doi.org/10.1039/b106140m.

(44) Pople, J. A.; Beveridge, D. L. Delocalization of Unpaired Electron Density of [Formula Omitted] Radicals into Substituent Phenyl Groups. *J. Chem. Phys.* **1968**, *49* (10), 4725–4726. https://doi.org/10.1063/1.1669945.

(45) Rao, C. N. R.; Venkataraghavan, R. The C=S Stretching Frequency and the "−N−C=S Bands" in the Infrared. *Spectrochim. Acta - Part A Mol. Spectrosc.* **1989**, *45* (1958), 299–305. https://doi.org/10.1016/S0584-8539(89)80280-6.

(46) Hoyle, C. E.; Bowman, C. N. Thiol-Ene Click Chemistry. *Angew. Chemie - Int. Ed.* **2010**, *49* (9), 1540–1573. https://doi.org/10.1002/anie.200903924.

(47) Love, D. M.; Kim, K.; Goodrich, J. T.; Fairbanks, B. D.; Worrell, B. T.; Stoykovich, M. P.; Musgrave, C. B.; Bowman, C. N. Amine Induced Retardation of the Radical-Mediated Thiol-Ene Reaction via the Formation of Metastable Disulfide Radical Anions. *J. Org. Chem.* **2018**, *83* (5), 2912–2919. https://doi.org/10.1021/acs.joc.8b00143.
(48) Hacioğlu, B.; Berchtold, K. A.; Lovell, L. G.; Nie, J.; Bowman, C. N. Polymerization Kinetics of HEMA/DEGDMA: Using Changes in Initiation and Chain Transfer Rates to Explore the Effects of Chain-Length-Dependent Termination. *Biomaterials* **2002**, *23* (20), 4057–4064. https://doi.org/10.1016/S0142-9612(02)00138-2.
(49) Dénès, F.; Pichowicz, M.; Povie, G.; Renaud, P. Thiyl Radicals in Organic Synthesis. *Chem. Rev.* **2014**, *114* (5), 2587–2693. https://doi.org/10.1021/cr400441m.
(50) Zubov, V. P.; Kumar, M. V.; Kabanov, V. A.; Faculty, C. C.; State, M. Reactivity of Allyl Monomers in Radical Polymerization. *J. Macromol. Sci. Part A* **1979**, *A13* (1), 111–131.
(51) Hernandez, J. J.; Dobson, A. L.; Carberry, B. J.; Kuenstler, A. S.; Shah, P. K.; Anseth, K. S.; White, T. J.; Bowman, C. N. Controlled Degradation of Cast and 3-D Printed Photocurable Thioester Networks via Thiol–Thioester Exchange. *Macromolecules* **2022**, *55*, 1376–1385. https://doi.org/10.1021/acs.macromol.1c02459.
(52) Cook, C. C.; Fong, E. J.; Schwartz, J. J.; Porcincula, D. H.; Kaczmarek, A. C.; Oakdale, J. S.; Moran, B. D.; Champley, K. M.; Rackson, C. M.; Muralidharan, A.; McLeod, R. R.; Shusteff, M. Highly Tunable Thiol-Ene Photoresins for Volumetric Additive Manufacturing. *Adv. Mater.* **2020**, *32* (47), 1–6. https://doi.org/10.1002/adma.202003376.
(53) De Beer, M. P.; Van Der Laan, H. L.; Cole, M. A.; Whelan, R. J.; Burns, M. A.; Scott, T. F. Rapid, Continuous Additive Manufacturing by Volumetric Polymerization Inhibition Patterning. *Sci. Adv.* **2019**, *5* (1). https://doi.org/10.1126/sciadv.aau8723.

6.8 Supporting Information

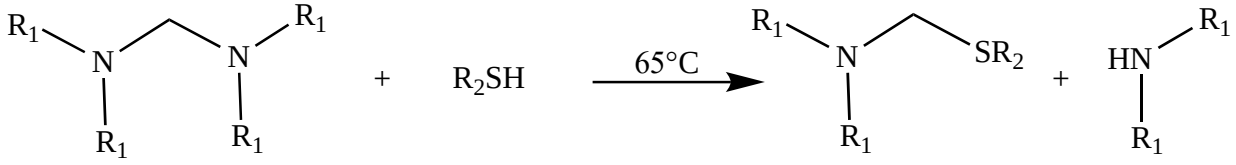

R_1 = Methyl or piperidine R_2= n-butyl, isobutyl, tert.butyl or phenyl

Scheme S6.1. Synthesis of thioaminal small molecules.

General procedure for synthesis of alkyl thioaminals

N,N,N',N'-Tetramethyldiaminomethane (25 mmol) and alkyl thiol (25 mmol; n-butanethiol, 2-butanethiol, or tert-butylthiol) were mixed in an oven dried 50 mL round bottom flask and the resulting mixture was heated at 65 ºC (neat) for 16 h, following reported literature.[1] For n-butanethiol and 2-butanethiol, the crude was purified by silica column chromatography (0 % → 5 % EtOAc / Hexanes) to obtain the required thioaminal as clear oil (yield ~70 %). For tert-butylthiol the crude was used without purification for FTIR and NMR studies due to high volatility of the product.

Synthesis of phenylthioaminal (PTA)

Dipiperidinomethane (DPPM) was synthesized following literature procedures,[2] giving a yield of 92 % and characterized prior to using it in the next step.

DPPM (11 mmol) and thiophenol (11 mmol) were mixed in an oven dried 25 mL RBF, and the resulting mixture was heated at 80 ºC for 16 hrs. The white precipitate formed during the reaction was removed by filtration. Crude reaction mixture was collected and the by-product piperidine was removed under reduced pressure to yield the required phenylthioaminal as a clear oil (yield ~10 %).

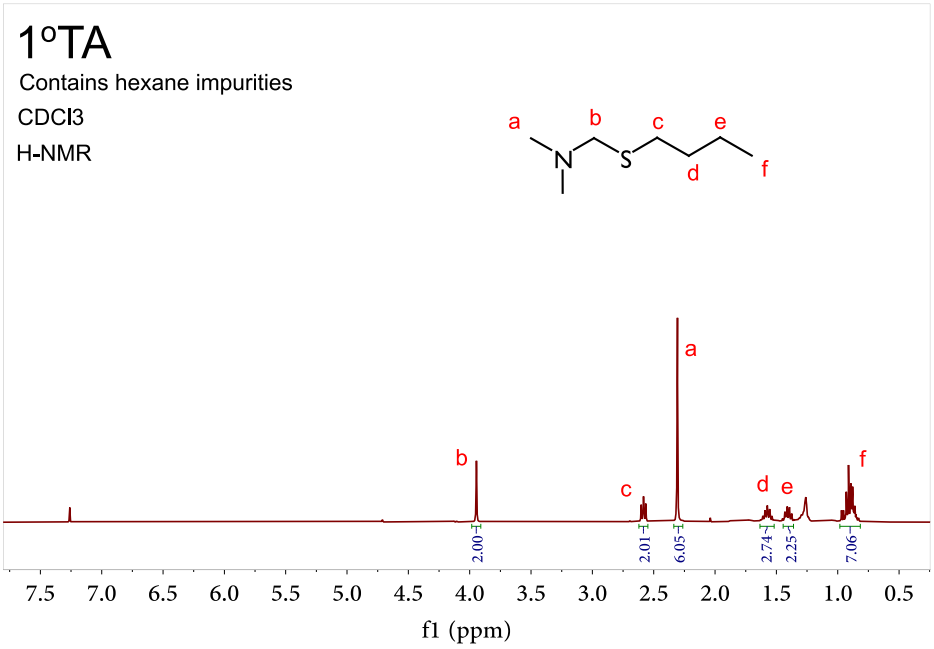

Figure S6.1. ^{1}H NMR spectra of 1°TA. ^{1}H NMR (400 MHz, $CDCl_3$) δ 3.94 (s, 2H), 2.58 (t, *J* = 1.4 Hz, 2H), 2.30 (s, 6H), 1.67 – 1.48 (m, 2H), 1.48 – 1.33 (m, 2H), 0.91 (t, 3H).

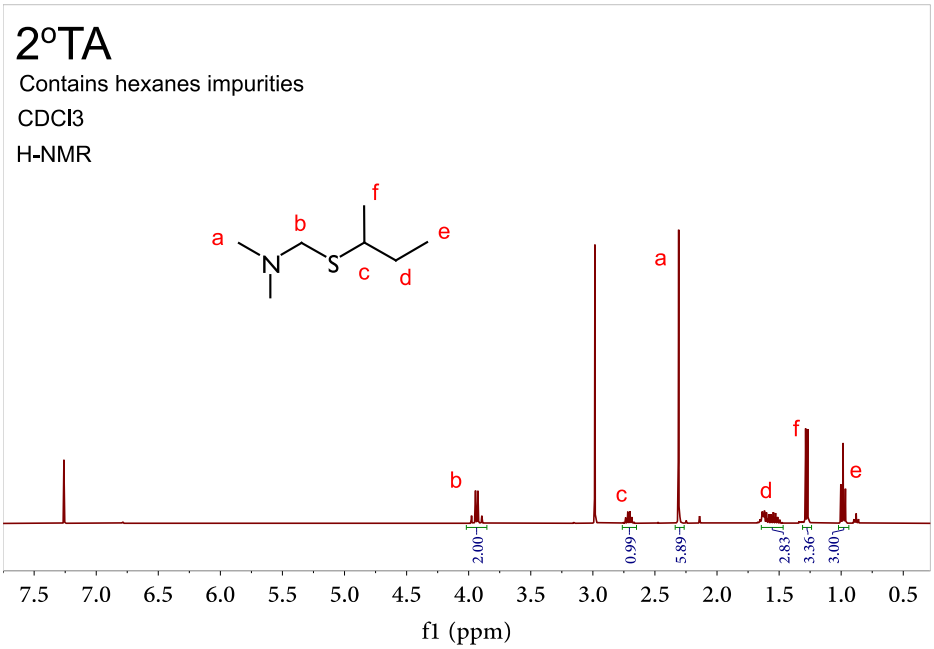

Figure S6.2. ^{1}H NMR spectra of 2°TA with internal standard dimethylsulfone (peak at 2.98 ppm). ^{1}H NMR (400 MHz, $CDCl_3$) δ 4.00 – 3.87 (m, 2H), 2.71 (h, *J* = 6.6 Hz, 1H), 2.31 (s, 6H), 1.69 – 1.45 (m, 2H), 1.28 (d, *J* = 1.0 Hz, 3H), 0.99 (t, *J* = 0.8 Hz, 3H).

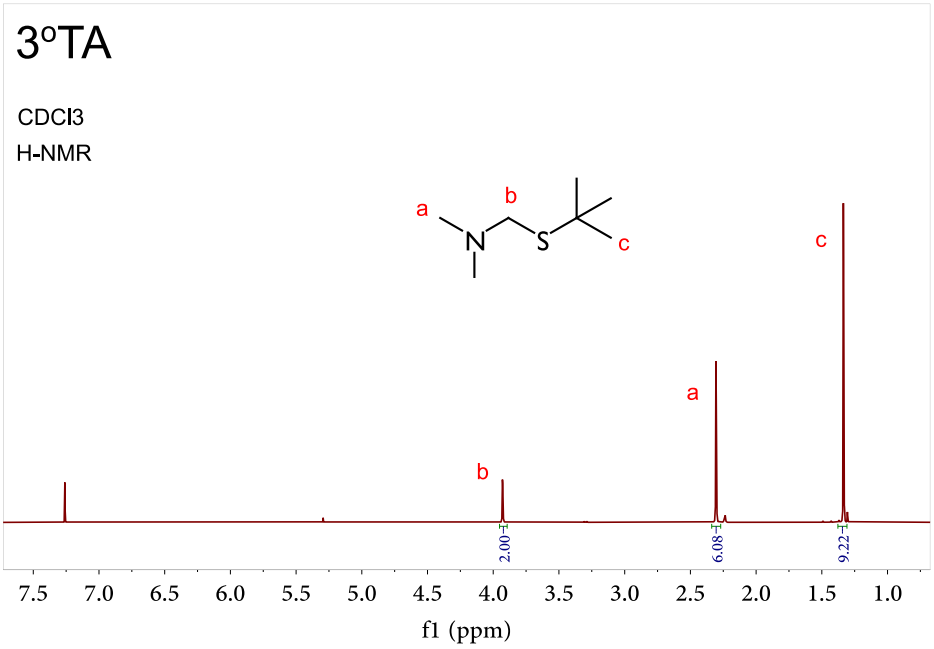

Figure S6.3. ^{1}H NMR spectra of 3°TA. ^{1}H NMR (400 MHz, $CDCl_3$) δ 3.93 (s, 2H), 2.31 (s, 6H), 1.33 (s, 9H).

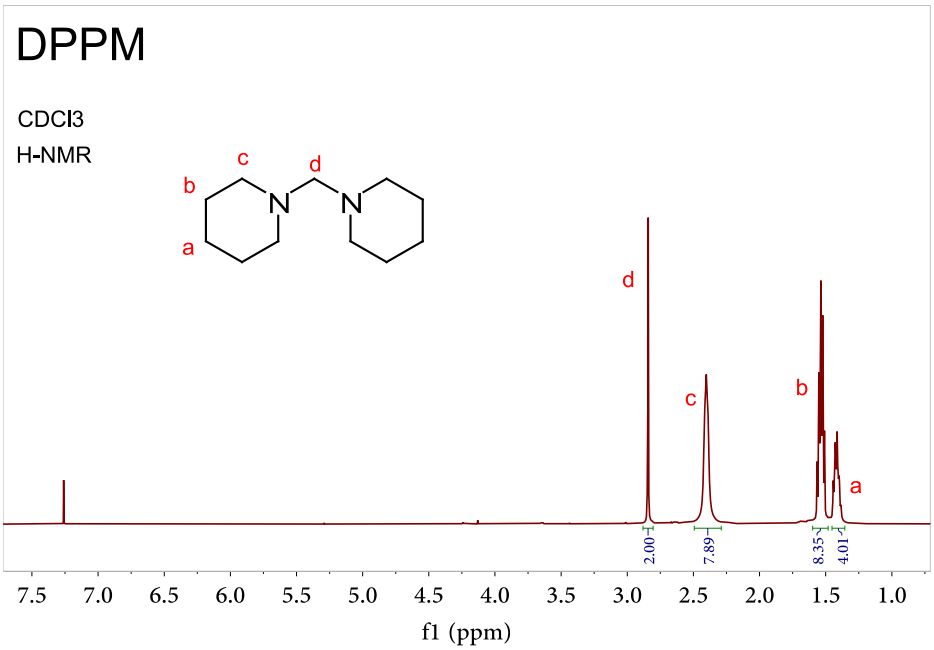

Figure S6.4. ^{1}H NMR spectra of dipiperidinomethane (DPPM). ^{1}H NMR (400 MHz, $CDCl_3$) δ 2.84 (s, 2H), 2.43 – 2.37 (m, 8H), 1.59 – 1.49 (m, 8H), 1.47 – 1.36 (m, 4H).

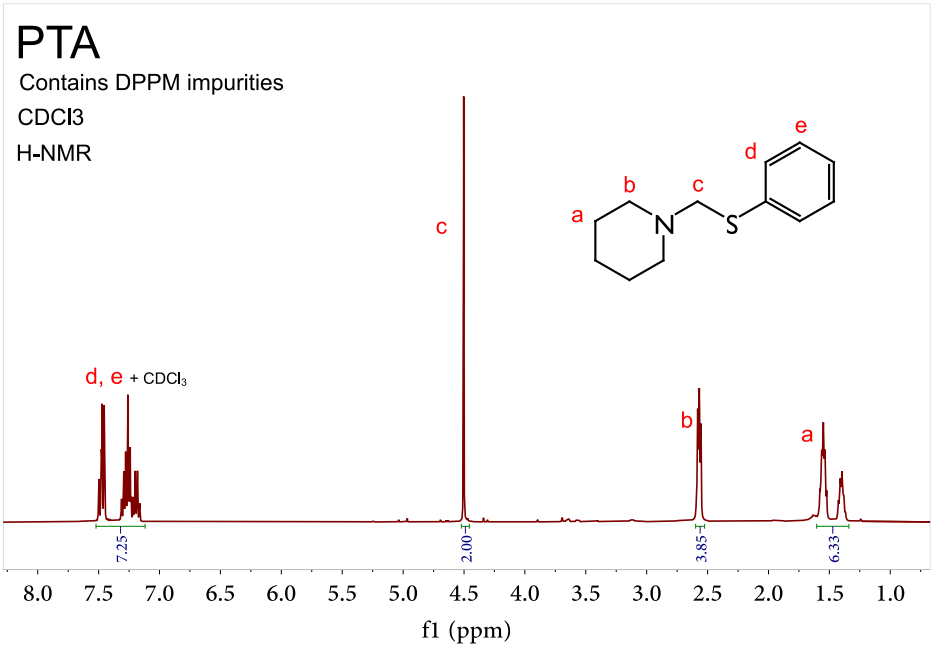

Figure S6.5. ^{1}H NMR spectra of PTA with some DPPM impurity. ^{1}H NMR (400 MHz, $CDCl_3$) δ 7.52 – 7.43 (m, 2H), 7.32 – 7.23 (m, 2H), 7.22 – 7.14 (m, 1H), 4.50 (s, 2H), 2.57 (t, 4H), 1.55 (q, 4H), 1.46 – 1.34 (m, 2H).

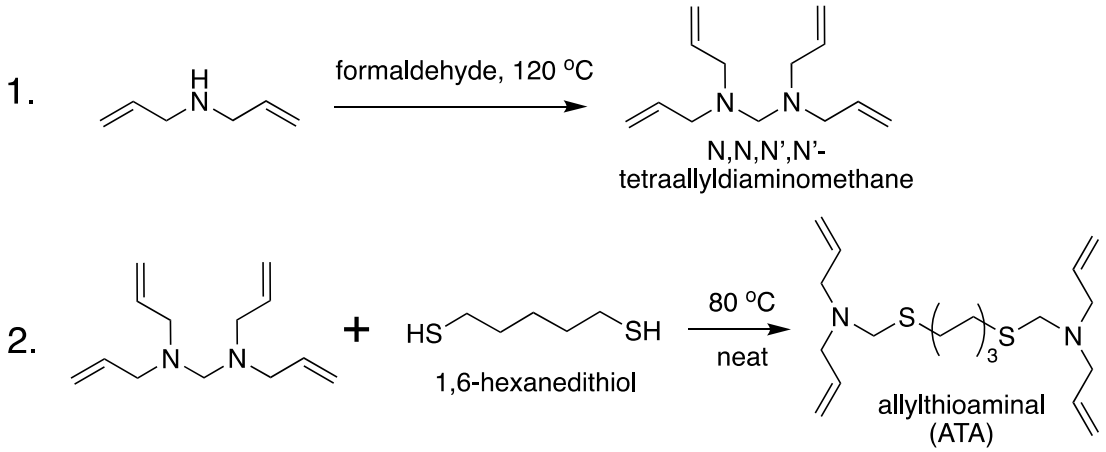

Scheme S6.2. Synthesis of allylthioaminal (ATA).

Required N,N,N',N'-Tetraallyldiaminomethane was synthesized according to the reported literature procedure.[2] Diallylamine (220 mmol) was placed in an oven dried 100 mL two-neck RBF and ice-cold formaldehyde (8.928g, 110 mmol, Formalin) was dripped in via addition funnel.

The reaction mixture was refluxed at 120ºC and spun for 2 hrs. The reaction mixture was cooled and allowed to phase separate at room temperature. The top organic layer was collected, washed with KOH pellets, and the product was then purified by column chromatography (0 % → 5 % → 10 % EtOAc / Hexanes), dried under vacuum to yield the required N,N,N',N'-Tetraallyldiaminomethane as clear oil (71 % yield).

Above synthesized N,N,N',N'-Tetraallyldiaminomethane (65 mmol) and 1,6-Hexanedithiol (26 mmol) were mixed in an oven dried 100 mL RBF, and refluxed for 48 hrs at 80ºC. The crude reaction mixture was purified by column chromatography (0 % → 5 % → 10 % EtOAc / Hexanes), and solvent was removed under reduced pressure. The compound was dried at 50ºC under high vacuum for 24 hrs to yield the required allylthioaminal as a clear oil in 68 % yield.

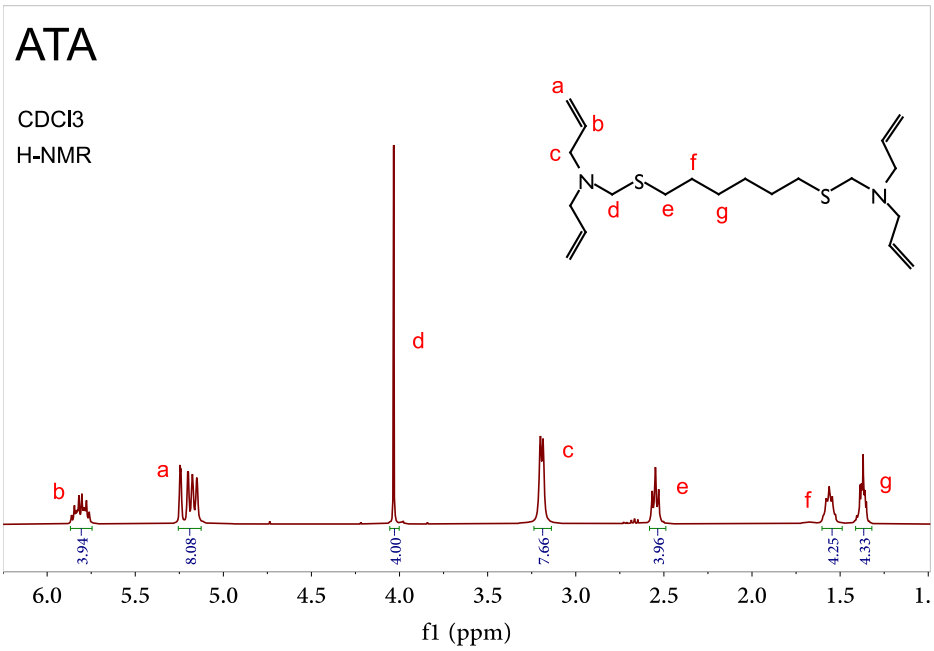

Figure S6.6. ^{1}H NMR spectra of ATA. ^{1}H NMR (400 MHz, $CDCl_3$) δ 5.88 – 5.74 (m, 4H), 5.27 – 5.12 (m, 8H), 4.03 (s, 4H), 3.19 (d, *J* = 6.4 Hz, 8H), 2.55 (t, *J* = 7.3 Hz, 4H), 1.62 – 1.50 (m, 4H), 1.44 – 1.33 (m, 4H).

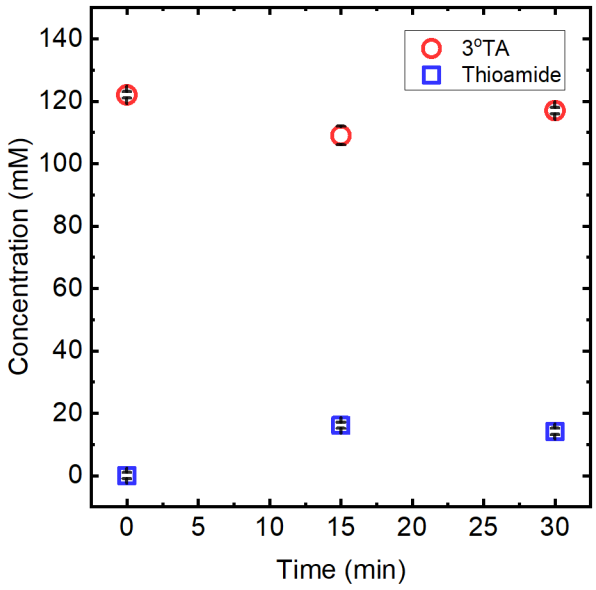

Figure S6.7. 3°TA consumption and resulting thioamide formation as a mixture of 1 thioaminal : 0.01 I819 was exposed to 400 – 500 nm light at 30 mW/cm^2. Concentrations quantified via qNMR using 20 mM dimethylsulfone in $CDCl_3$.

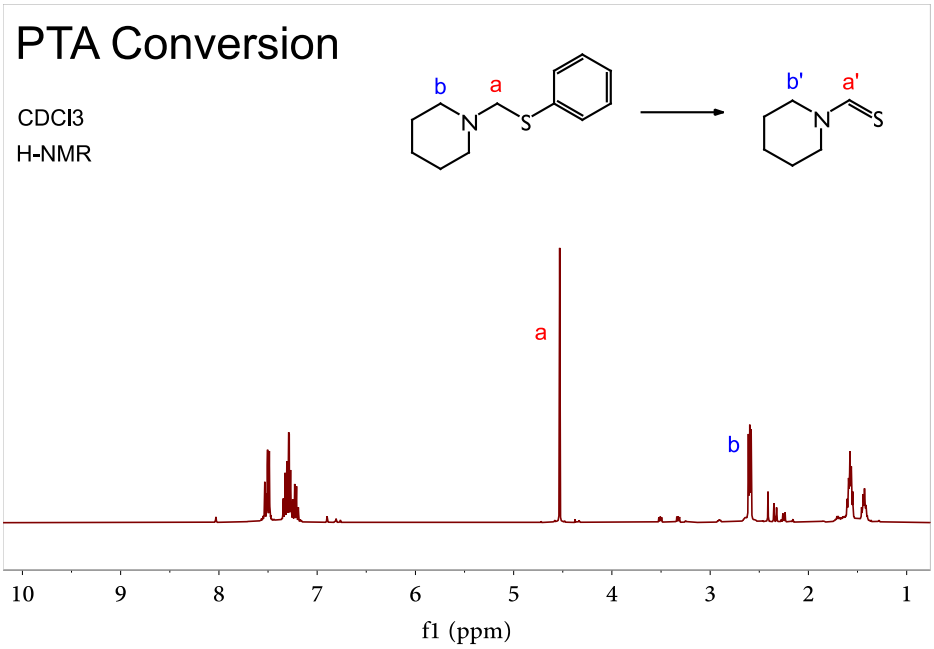

Figure S6.8. NMR spectra used to calculate conversion of thioaminal PTA. PTA was mixed with 2 mol % I819, exposed to 400 – 500 nm light at 30 mW/cm^2 for 10 min, and achieved a conversion of 0 % since no thioamide peaks (3.29 and 3.26 ppm) were observed.

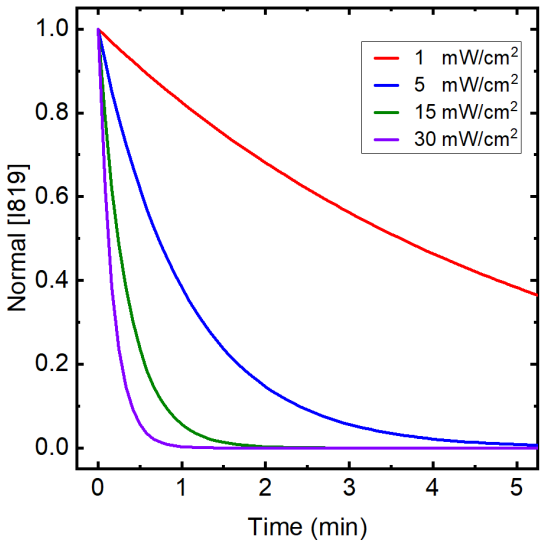

Figure S6.9. Theoretical calculation of [I819] as a function of illumination time under a 400 - 500 nm light source. The calculation used equation $[\mathbf{I819}] = [\mathbf{I819}]_0 \cdot e^{-\Phi \cdot \varepsilon_{405,\,Nap} \cdot \frac{I_{405}}{E_{405}} \cdot t}$, where $[I819]_o$ was the initial concentration of I819 (0.052 mM), $\boldsymbol{\Phi}$ the quantum yield (0.6), $\boldsymbol{\varepsilon_{405,\,Nap}}$ the molar absorptivity for I819 at 405 nm (696 L / mol / cm), I_{405} the light intensity (1 – 30 mW/cm^2), E_{405} the energy per mole of 405 nm photons (3 x 10^5 J / Einsteins), and t the illumination time.

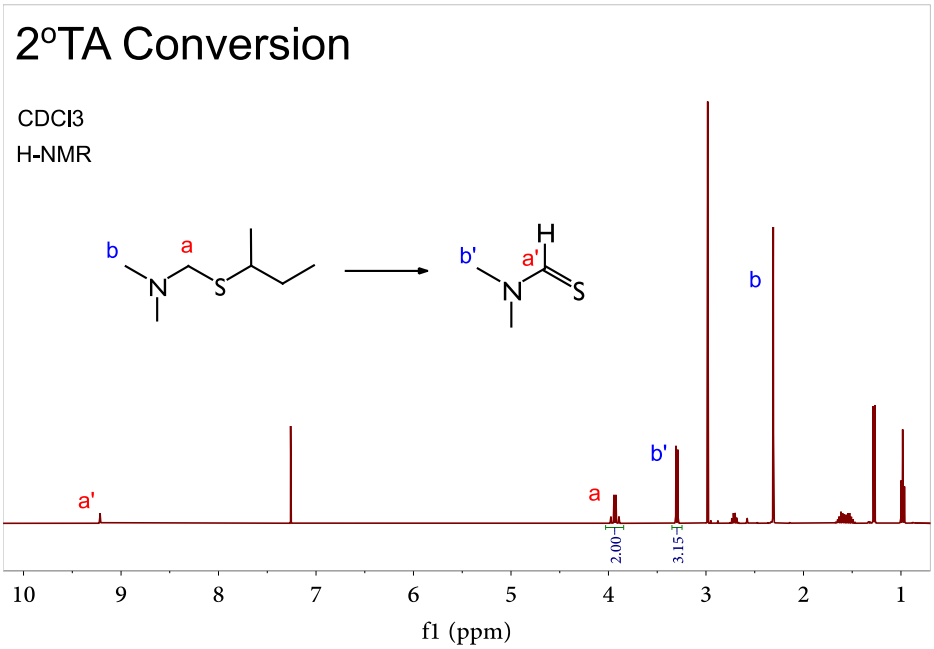

Figure S6.10. Representative comparison of thioaminal and thioamide NMR peak integrals used to calculate degradation conversion. Conversion was calculated using equation 1 of the paper, where Int_{TD} was the area of combined thioamide singlets at 3.29 and 3.26 ppm (location b'), Int_{TA}

the area of the thioaminal singlet at 3.93 ppm (location a), and the fractions account for number of protons per peak. This 2°TA sample was mixed with 1 mol % I819, exposed to 400 – 500 nm light at 30 mW/cm^2 for 10 min, and achieved a conversion of 34 %.

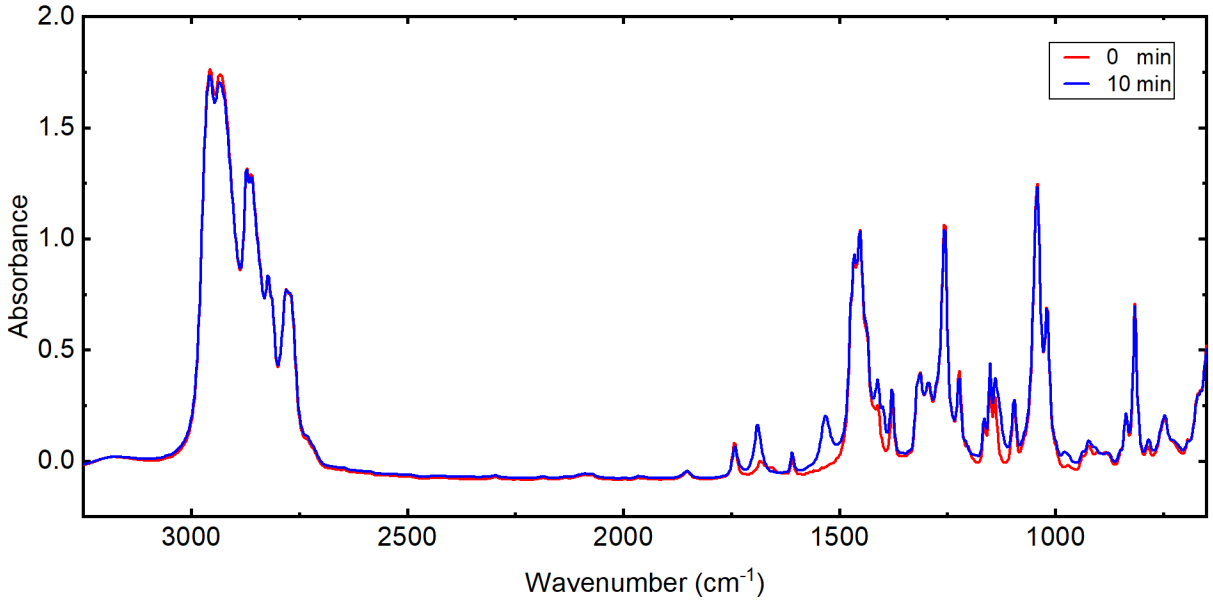

Figure S6.11. FTIR spectra for a 1 : 0.01 molar ratio of 1°TA and I819 exposed to 400 – 500 nm light for 10 min at 30 mW/cm^2.

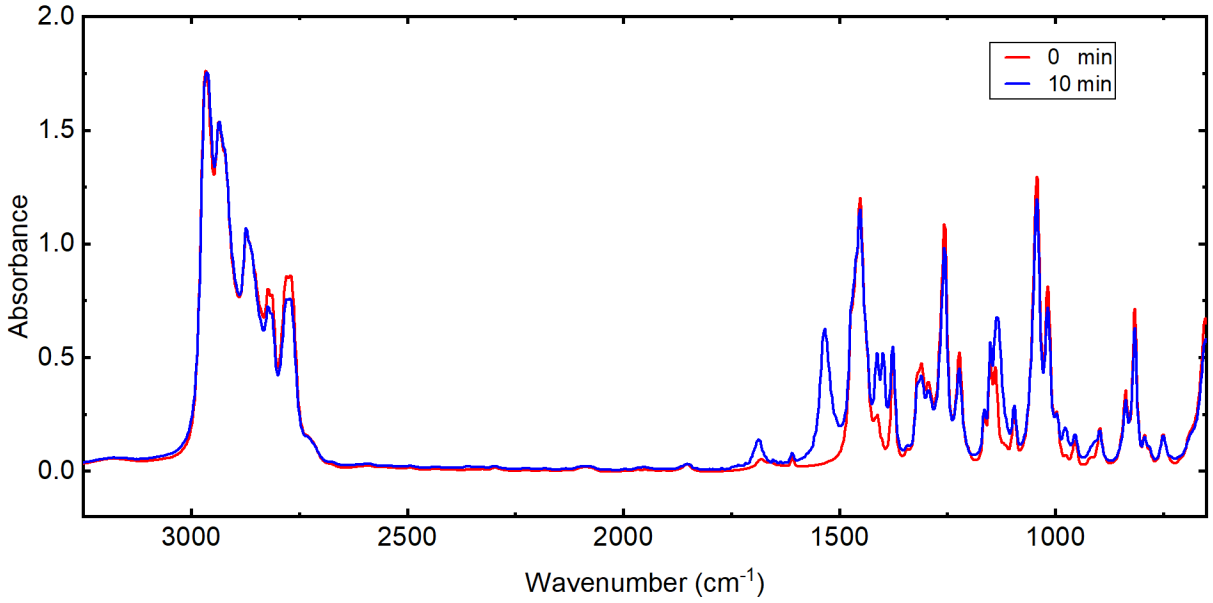

Figure S6.12. FTIR spectra for a 1 : 0.01 molar ratio of 2°TA and I819 exposed to 400 – 500 nm light for 10 min at 30 mW/cm^2.

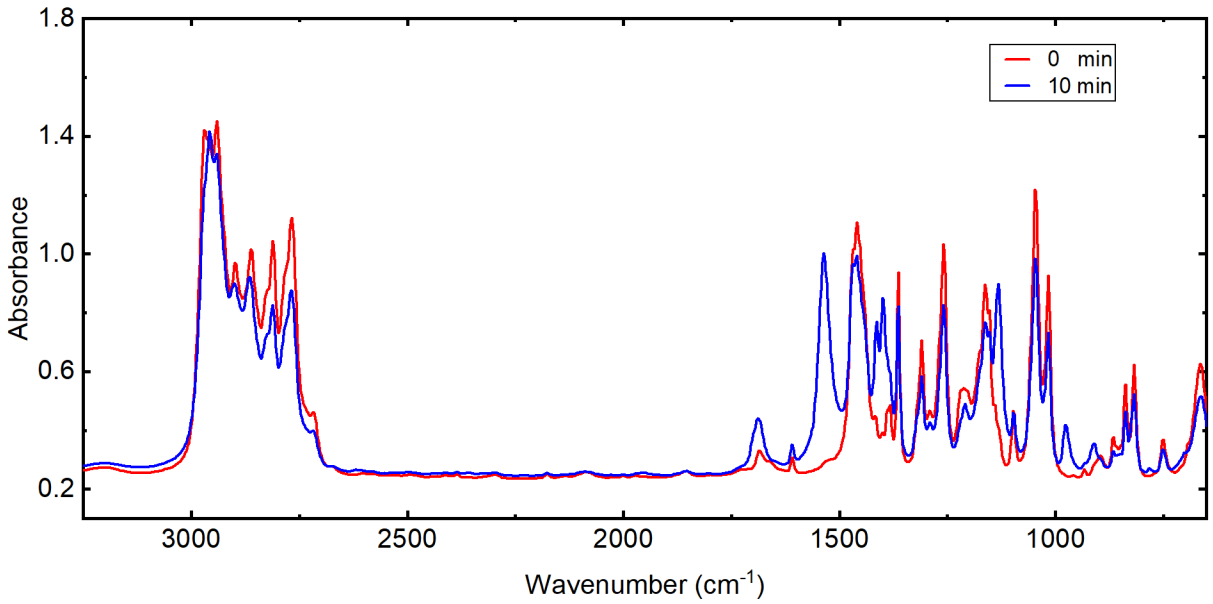

Figure S6.13. FTIR spectra for a 1 : 0.01 molar ratio of 3ºTA and I819 exposed to 400 – 500 nm light for 10 min at 30 mW/cm^2.

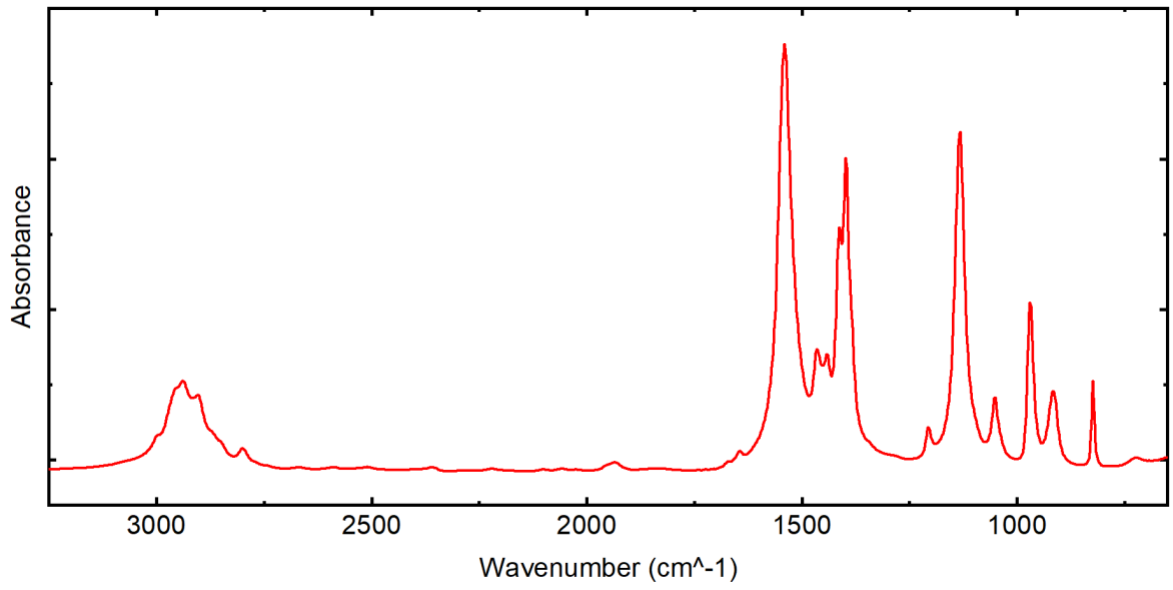

Figure S6.14. FTIR spectra of dimethylthioformamide (DMTF), showing a distinct peak near 1540 cm^{-1}.

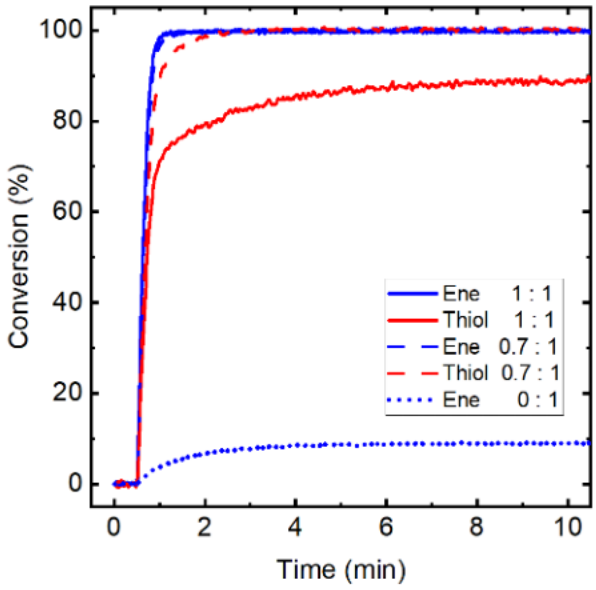

Figure S6.15. Thiol and ene conversions for ATA-HT-I819 solutions, mixed with varying thiol : ene ratios. All samples were mixed with 2 mol % of I819 and exposed to 400 - 500 nm light at 30 mW/cm^2 for 15 min. Ene, or allyl peaks, were tracked at 3080 cm^{-1} and thiol at 2500 cm^{-1}. A 0.7 thiol : 1 ene ratio resulted in near quantitative conversion for both thiol and ene groups. The 0 : 1 thiol to ene ratio represents the homopolymerization of ATA with I819.

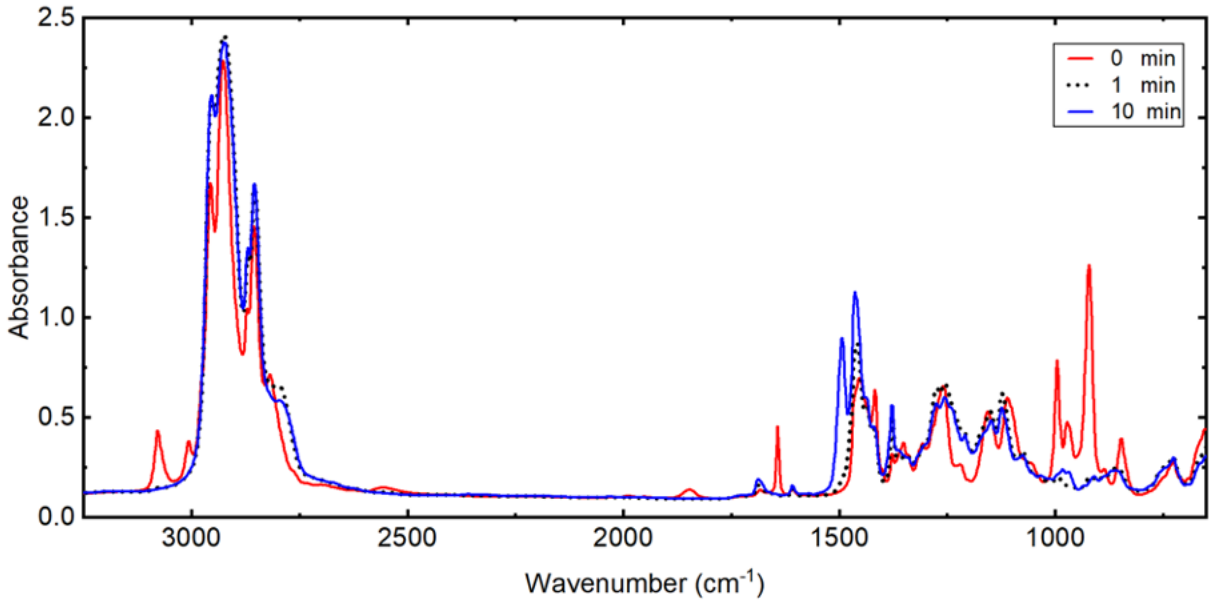

Figure S6.16. Full FTIR spectra of a thiol : ene : I819 (0.7: 1 : 0.005) mixture composed of ATA-HT-I819. Sample was exposed to a 400-500 nm light source at 30 mW/cm^2 for up to 10 min. After 1 minute exposure of the sample to the light, peaks corresponding to the ene (3080 cm^{-1}) and thiol (2550 cm^{-1}) both disappeared while gradually developing a peak at 1500 cm^{-1} indicating the formation of thioamide.

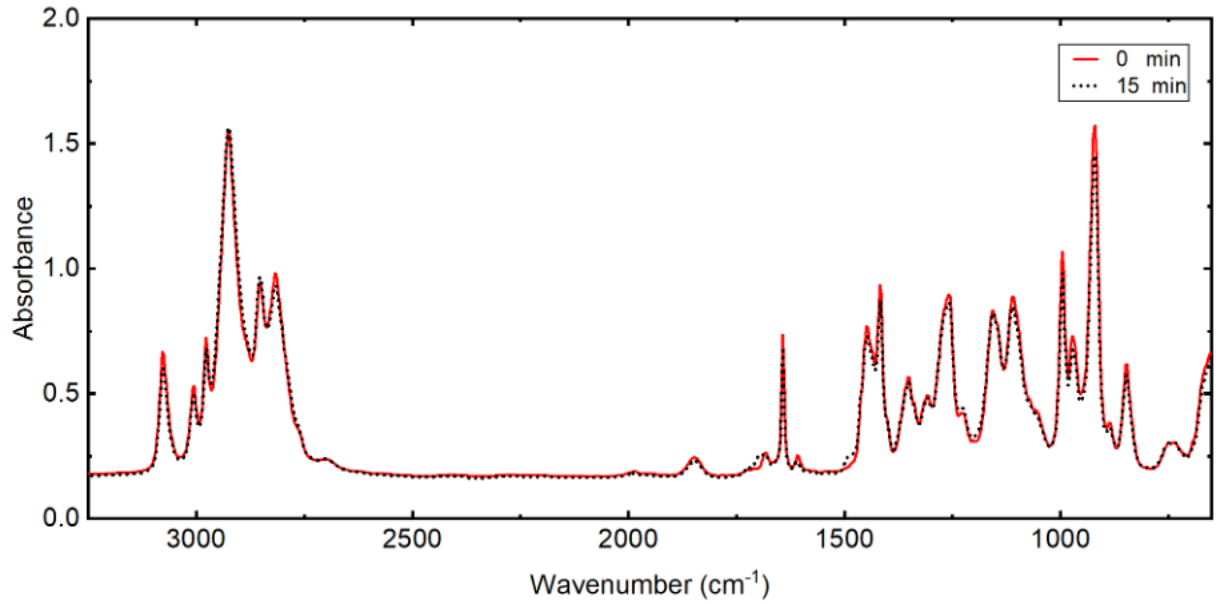

Figure S6.17. FTIR spectra of a 1 ATA : 0.01 I819 mixture before and after light exposure. The sample was exposed to 400 - 500 nm light at 30 mW/cm^2 for 15 min. Ene conversion dropped ~10 % (3120 cm^{-1}) while minimal thioamide formed (1500 cm^{-1}).

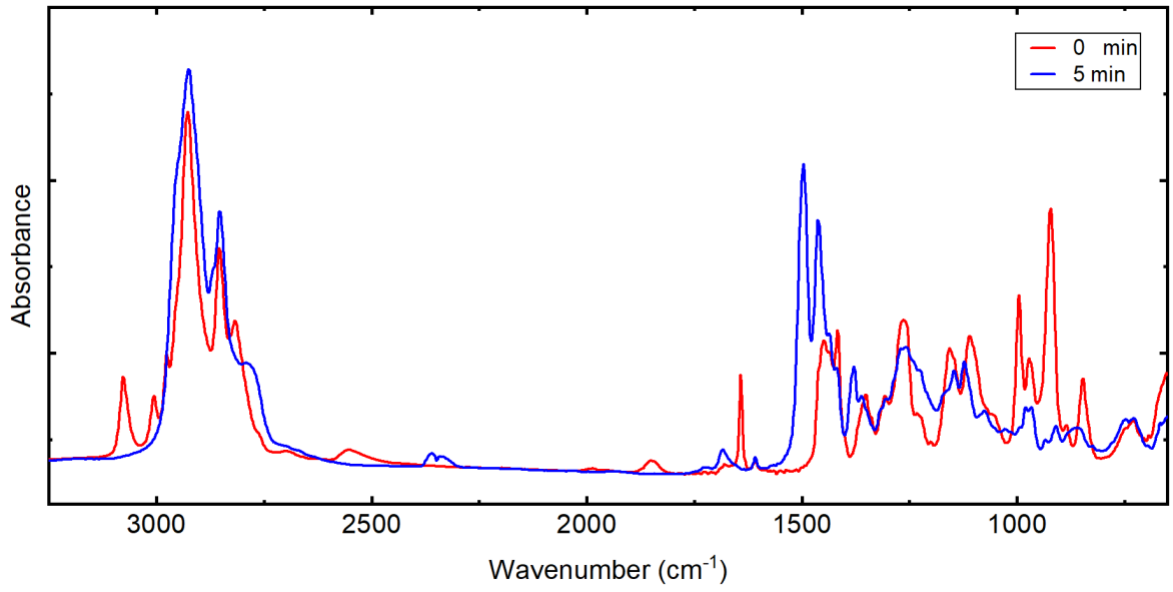

Figure S6.18. FTIR spectra of a 0.7 thiol : 1 ene : 0.005 I819 mixture composed of ATA, HDT, and I819 exposed to a 400 – 500 nm light for 5 min at 30 mW/cm^2.

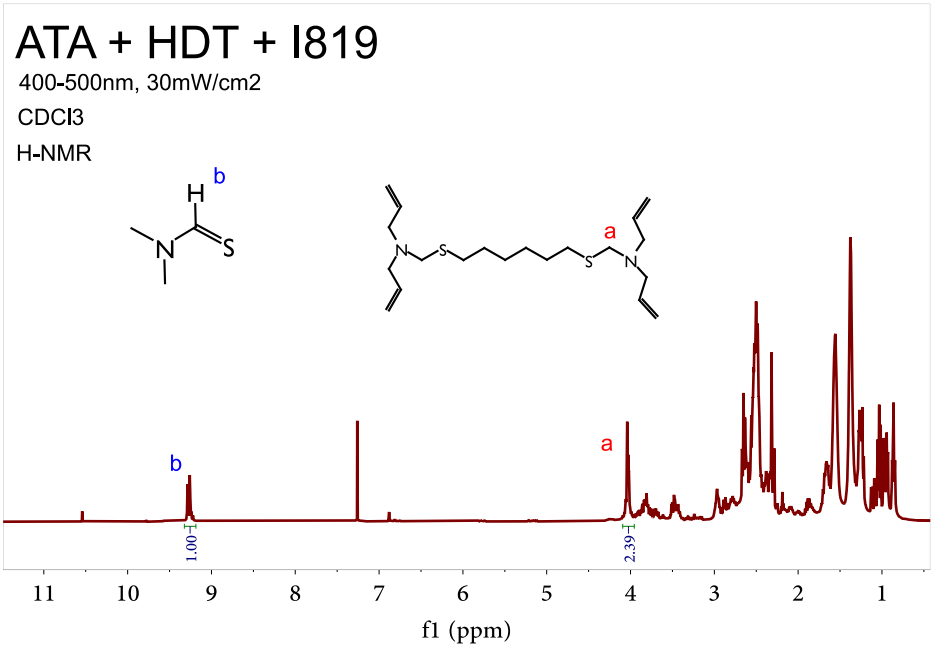

Figure S6.19. ^{1}H NMR spectra of degraded thioaminal network composed of 0.7 thiol : 1 ene : 0.005 I819. Comparing integral of thioamide peak (9.26 ppm) with thioaminal peak (4.03 ppm) and gave a conversion of $\boldsymbol{conversion} = \frac{\mathbf{1}*\frac{\mathbf{1}}{\mathbf{1}}}{\mathbf{1}*\frac{\mathbf{1}}{\mathbf{1}}+\mathbf{2.39}*\frac{\mathbf{1}}{\mathbf{2}}} = \sim\mathbf{40}\%$.

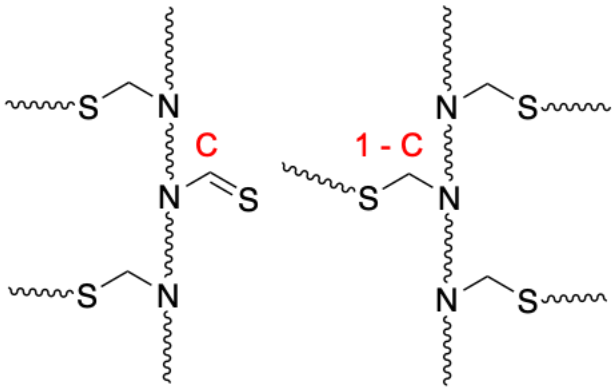

Figure S6.20. Degradation conversion of thioaminals was used to determine fraction of thioaminal crosslink bridges left intact. The fraction of cleaved crosslinks, $\boldsymbol{F_{cleaved}}$, can be said to be $\boldsymbol{F_{cleaved}} = \mathbf{1} - \boldsymbol{F_{connected}}$. Since each crosslink in ATA contained two thioaminal groups, $\boldsymbol{F_{connected}} = (\mathbf{1} - \boldsymbol{C})^{\mathbf{2}}$, where $\boldsymbol{C}$ was the thioaminal degradation conversion. For $\boldsymbol{C} = \mathbf{0.4}$ the fraction of cleaved ATA crosslinks became $\boldsymbol{F_{cleaved}} = \mathbf{1} - (\mathbf{1} - \mathbf{0.4})^{\mathbf{2}} = \mathbf{0.64}$. This shows 64 % of ATA crosslink bridges were cleaved, leaving 36 % of crosslinks intact to contribute to the network.

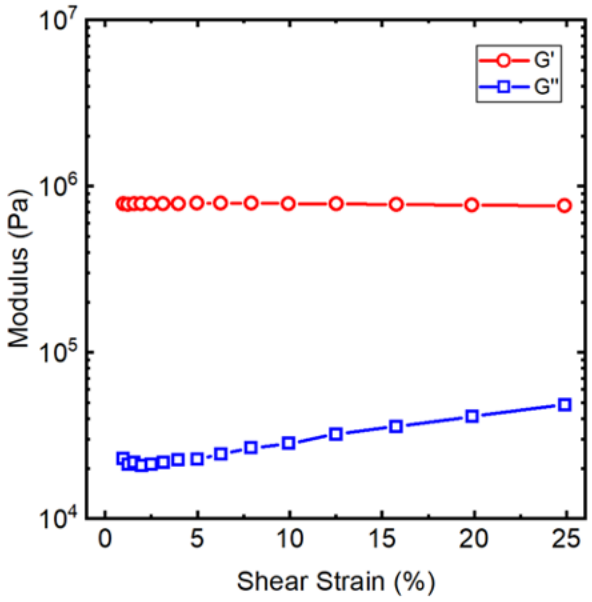

Figure S6.21. Representative plot of a strain sweep experiment on the rheometer for the ATA-HDT-I819 formulation, ranging from 0 to 25 % shear strain with a frequency of 1 Hz. Storage modulus only dropped 10 % when 25 % shear strain was reached. All rheology experiments were subsequently conducted at 10 % shear strain.

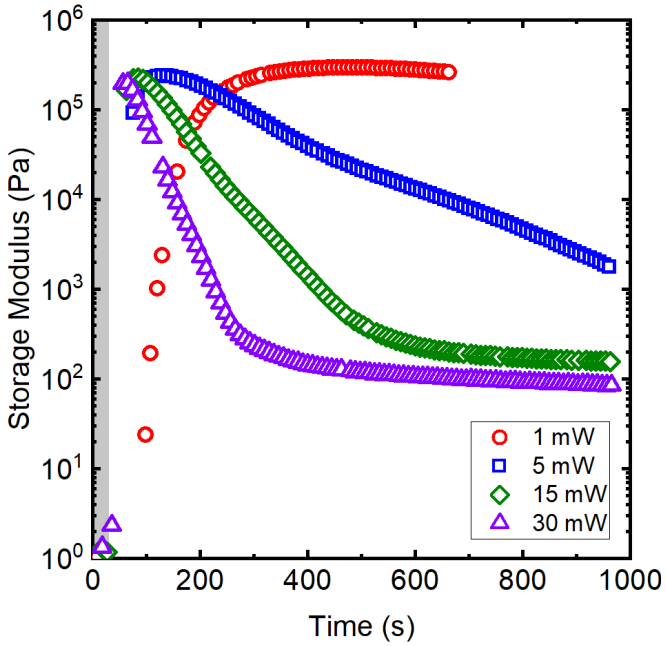

Figure S6.22. Photorheology of 25 μm thick thioaminal networks showing storage modulus at various light intensities.

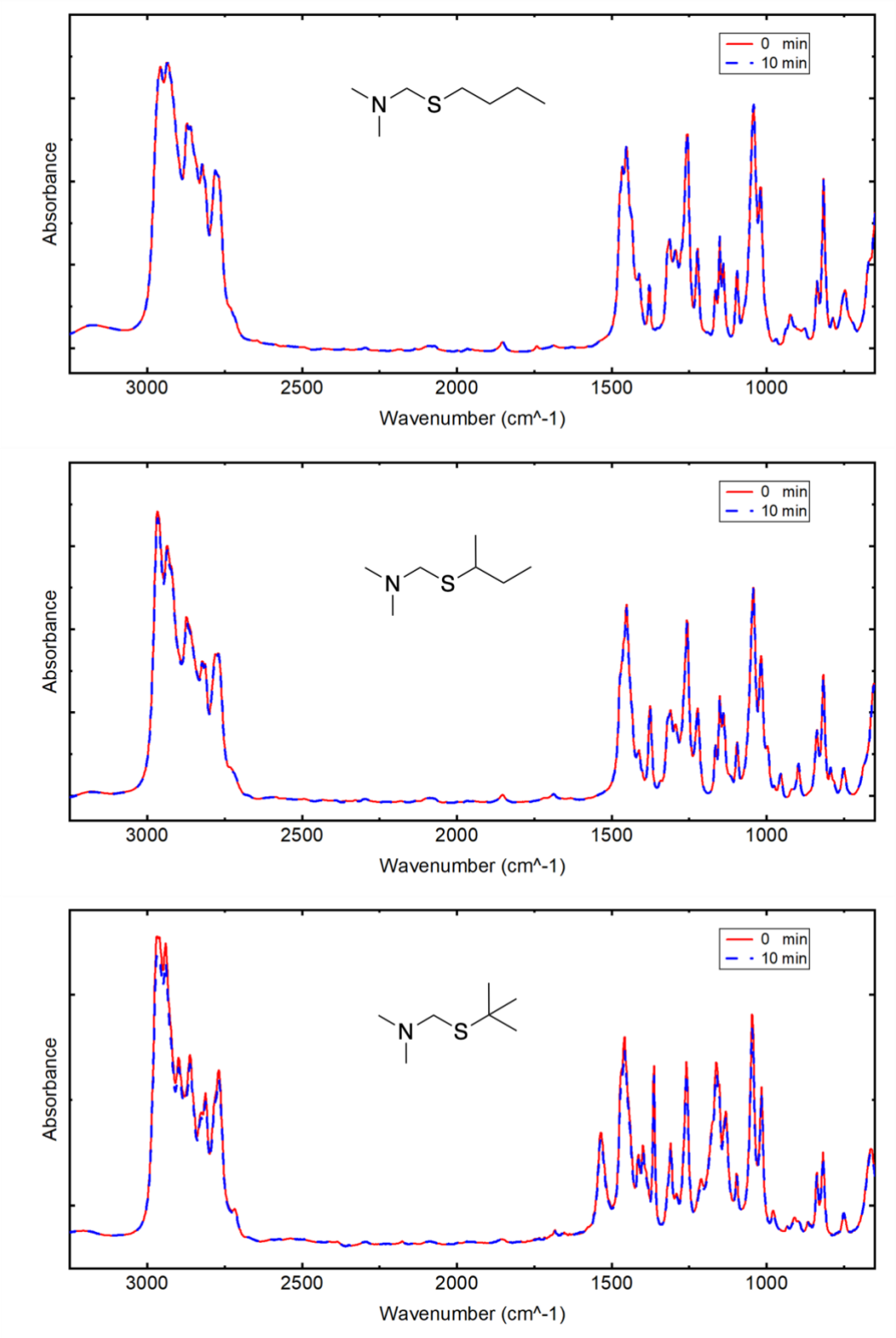

Figure S6.23. FTIR spectra of thioaminal small molecules after exposure to light without any I819 present. All molecules were exposed to 400 – 500 nm light at 30 mW/cm^2 for 10 min.

6.8.1 References

(1) Wojtecki, R. J.; Jones, G. O.; Yuen, A. Y.; Chin, W.; Boday, D. J.; Nelson, A.; García, J. M.; Yang, Y. Y.; Hedrick, J. L. Developments in Dynamic Covalent Chemistries from the Reaction of Thiols with Hexahydrotriazines. *J. Am. Chem. Soc.* **2015**, *137* (45), 14248–14251. https://doi.org/10.1021/jacs.5b08815.

(2) Chao, A.; Zhang, D. Investigation of Secondary Amine-Derived Aminal Bond Exchange toward the Development of Covalent Adaptable Networks. *Macromolecules* **2019**, *52* (2), 495–503. https://doi.org/10.1021/acs.macromol.8b02654.

Chapter 7: Conclusions and Future Recommendations

This thesis focused on the analysis, control, and design of polymer degradation within covalent adaptable networks (CANs), investigating how dynamic reactions within CANs induce mass loss. In the first part of this thesis, the thiol-thioester exchange reaction was investigated with an emphasis on how network structure and reaction kinetics could be coupled with theoretical models to precisely tune the degradation processes of thioester containing networks. In the second part of this thesis, thioaminals were investigated as a means to create new CANs through either the thiol-thioaminal exchange reaction or the photomediated thioaminal scission reaction, and in both studies the effects of functional groups and network structure were manipulated to tune degradation. The remainder of this thesis is dedicated to summarizing these results and proposing future work.

7.1 Thiol-Thioester Degradation

With the difficulty that arises from reprocessing traditional thermosets, recent work has turned toward CANs as a means to bridge the material property benefits of crosslinked networks with the reprocessability of thermoplastics. Degradation within reversible exchange CANs is different from that in traditional thermosets because polymer chains disconnect by means of reversible exchange reactions as opposed to irreversible scission reactions. As the majority of degradation models have been developed for irreversible scission reactions and not for reversible exchange reactions, barring some recent work on transesterification[1–3] and boronic ester exchange,[4] there was a need to improve the quantitative models available in the field.

Aim 1 of this thesis sought to develop quantitative models for CANs degradation by focusing on the thiol-thioester reaction as a model system. Specifically, Aim 1 investigated how small molecule thiol-thioester exchange reactions translate into macroscopic degradation within

thioester CANs and is discussed within Chapter 3 of this thesis. A statistical kinetic model that took into consideration the network structure and the thiol-thioester exchange kinetics was developed and compared to experimental mass loss data for step-growth thioester networks. These thioester CANs were degraded by submerging films in a solution of the thiol butyl 3-mercaptopropionate, the base triethylamine, and acetone to trigger the base-catalyzed exchange. A single fitting parameter, the reaction rate constant *k* which only varied from 0.0039 to 0.0051 $M^{-1}min^{-1}$, could accurately match model predictions to experimental mass loss and confirmed the accuracy of the model. Increasing the concentration of the thiol, the base, or decreasing crosslink density resulted in faster degradation with timescales that tuned from 2.5 h to theoretical infinity. Degradation of 3-D printed thioester networks showed that these materials transitioned from bulk to surface degradation profiles when part thickness exceeded 3 mm and also showed that exchange within thioester composites selectively degrades the matrix but allows 91 % recovery of the composite filler.

Proposed future work building off the findings in Aim 1 consist of:

1) Transposing the model towards other exchange chemistries. The structural components of the developed model are chemistry agnostic. By simply adjusting the kinetic equation to reflect another exchange reaction, this model may readily describe bulk degradation in other reversible exchange chemistry systems such as transesterification or vinylogous-urethane exchange.

2) Exploring situations where the model fails. A crucial assumption of this model is detached polymer segments rapidly diffuse out of the network. Work by Carberry *et. al.*[5] has shown detached segments in PEG-thioester network have long diffuse times and break this assumption, exhibiting a linear mass loss profile more akin to surface degradation.

3) Applying the derived mass gain equations to described self-replicating networks. Past work has focused on creating expanding polymer networks, either through the use of solvent[6] or by inducing self-replication.[7,8] This self-replication is caused by the by addition of monomers into the network, a process which mimics the mass gain observed during the degradation of reversible exchange CANs. As such, the mass gain equations developed in Aim 1 offer a unique opportunity to characterize the self-replication process and guide future polymer expansion design.

Aim 2 of this thesis continued to improve the quantitative models developed for CAN degradation by focusing on tuning degradation via oligomer structure. Specifically, Aim 2 investigated how oligomer structure impacts the degradation of thioester CANs via the base-catalyzed thiol-thioester exchange reaction and is discussed in Chapter 4 of this thesis. The statistical kinetic model from Chapter 1 was evolved to consider the impact of the number of thioester linkages within oligomers (N) and the dispersity profiles of these oligomers. Model predictions matched experimental mass loss studies for step-growth thioester networks, showing that increasing the number of thioester linkages from 1 – 4 decreased mass loss time from 25 – 4 h. Mass loss experiments were achieved by submerging thioester CAN films in a solution of 1 M butyl 3-mercaptopropionate, 0.3 M triethylamine, and acetone to trigger the base-catalyzed thiol-thioester exchange reaction. Once again a single fitting parameter, the reaction rate constant k could match model and experiment results and this variable only varied from 0.0024 to 0.0040 $M^{-1}min^{-1}$. Controlled mass release studies using Nile Red within thioester networks then confirmed oligomer structure enabled quantifiable mass release from 4 – 25 h via the Beer-Lambert law.

Proposed future work for Aim 2 includes:

1) Transposing the model towards other exchange chemistries. As before, the structural components of the models developed are chemistry agnostic, being readily adapted towards other exchange reactions and other oligomer-containing networks.

2) Modelling degradation of tailored oligomer distributions. Aim 2 found the degradation profiles of blended CANs, produced by mixing oligomers together, were accurately predicted by merely adding the mass loss components of each oligomer weighted by their relevant molar fraction. This implies the model may be used to describe a variety of precisely defined oligomer dispersity profiles,[9] which has been shown to impacts properties such as self-assembly[10] and optical clarity.[11]

3) Decoupling the effects of diffusion versus additional exchange that contribute to mass loss. Diffusion of detached polymer segments out of CANs is convoluted by several competing factors including dynamic mesh sizes,[12] detached polymer segments reattaching into the network via additional exchange reactions,[5] and detached polymers segments further cleaving into smaller pieces via additional exchange reactions.[3] The relative contributions from these processes may be investigated by comparing CANs that undergo reversible exchange reactions versus CANs that only undergo irreversible reactions. A promising first experiment would be to degrade the thioester networks from Aim 2 in a solution of methanol plus butyl 3-mercaptopropionate and compare that mass loss to the networks submerged in methanol plus 1-hexanethiol. As the 1-hexanethiol reaction should be more irreversible (K_{eq} of 1.37 versus 1)[13] its deviations from the mass loss model should be due to diffusion and not additional exchange reactions.

7.2 Thiol-Thioaminal Covalent Adaptable Networks

Compared to reversible addition CANs, the crosslink density of reversible exchange CANs does not change with temperature and as such these materials have improved dimensional stability and solvent resistance. However, this constant crosslinking density also makes reprocessing more

difficult which is why there has been a push to design reversible exchange CANs that rearrange fast enough for reprocessing by thermoplastic techniques. Past chemical reactions that fit this criteria require elevated temperatures (above 100 °C) and typically require exogenous catalyst, showing these was a need for an exchange chemistry that could be triggered under near-ambient conditions.

Aim 3a of this thesis sought to fulfill this need by investigating the thiol-thioaminal exchange reaction and is captured in Chapter 5 of this thesis. A model system studied thiol-thioaminal exchange between small molecules, extracting 4 kinetic constants (k_f, k_r, K_{eq}, $t_{1/2,eq}$) and discovering the choice of thiol in the exchange most impacted the reverse reaction rate constant, k_r. Stress relaxation of step-growth thioaminal networks found these networks rearranged rapidly, within 5 s at 95 °C, and with % excess thiol and temperature resulting in faster relaxation. Coupling stress relaxation with frequency sweep experiments confirmed thiol-thioaminal exchange proceeded through a reversible exchange type mechanism with activation energies ranging from 97 – 112 kJ/mol. Submerging thioaminal CAN films in solutions of excess thiols showed thiol-thioaminal exchange could rapidly degrade thioaminal networks, with the choice of thiol controlling degradation time from 4 – 379 min.

Proposed future work for Aim 3 includes:

1) Exploring thiol-thioaminal exchange within sacrificial substrates. The ~100x control over degradation timescale (4 – 379 min) and the ability to define surface or bulk degradation all by the appropriate choice of thiol makes thioaminal networks ideal sacrificial substrates.

2) Expanding thiol-thioaminal exchange into biological media. Enabling selective exchange under mild conditions is a requirement for biologically relevant chemical reactions. As past work has

shown thiol-thioaminal exchange readily occurs with cysteine,[14] the exchange may be applied towards other thiol-rich biological media such as hydrogels.[15]

7.3 Photomediated Thioaminal Scission

Combining photopolymerization with photodegradation techniques grants unique control over the entire life-cycle of a material. While this has been achieved by using different wavelengths to mediate the two stages, few works have investigated using vastly different reaction kinetics to control the two processes. Furthermore, using these different kinetic rates gives the added benefit of controlling the two processes with one light source. As such, there was a need to explore new photomediated reactions that could grant this type of temporal control.

Aim 3b of this thesis investigated the thioaminal scission reaction as a means to achieve radical-mediated polymer degradation and is detailed in Chapter 6 of this thesis. A model system studied thioaminal scission in molecules with increasing degrees of substitution (1^o – 3^o), showing that thioaminal scission is a radical-mediated process that forms thioamide molecules in a 1 : 1 molar ratio. Increasing the thiol substitution from primary to tertiary resulted in the extent of scission also increasing from 5 – 39 %. As scission was found to occur semi-orthogonally to the thiol-ene polymerization reaction, a two-stage polymerizing-then-degrading network was developed with polymerization and degradation regimes switched at 2 J/cm^2 and plateaued at 13 J/cm^2. These networks were then designed to create single materials that served as both positive and negative photoresists.

Lastly, proposed future work for Aim 4 includes:

1) Identifying the precise mechanism for the thioaminal scission reaction. While a general degradation process was established for how thioaminal scission yields thioamides, the particular steps and energy levels that occur along the way were not explored. Researchers interested in

pursuing this path may consider isolating the proposed carbon-centered radical, calculating the reaction rate constant, and determining the rate limiting step.

2) Exploring the impact of radical initiator. Aim 3b found that the thioaminal scission reaction requires radical-initiation, but the impacts of this initiating species on the overarching scission reaction was not well explored. Researchers interested in studying the initiating radical may consider investigating the impact of radical chemistry and the impact of radical concentrations on the speed of scission and the extent of scission.

3) Designing thioaminal holograms. Holographic photopolymers enable data storage by means of encoding 3-D optical patterns in polymers via changes in the refractive index.[16,17] As opposed to traditional holograms, which used a binding matrix and writing monomers to create this refractive index change,[18,19] using a photodegradable network would enable the erosion of polymer at these small length scales, creating a refractive index difference between polymer matrix and air, a Δn value much larger than typically recorded.

7.4 References

(1) Yang, H.; Yu, K.; Mu, X.; Shi, X.; Wei, Y.; Guo, Y.; Qi, H. J. A Molecular Dynamics Study of Bond Exchange Reactions in Covalent Adaptable Networks. *Soft Matter* **2015**, *11* (31), 6305–6317. https://doi.org/10.1039/c5sm00942a.

(2) Hamel, C. M.; Kuang, X.; Chen, K.; Qi, H. J. Reaction-Diffusion Model for Thermosetting Polymer Dissolution through Exchange Reactions Assisted by Small-Molecule Solvents. *Macromolecules* **2019**, *52* (10), 3636–3645. https://doi.org/10.1021/acs.macromol.9b00540.

(3) Yu, K.; Yang, H.; Dao, B. H.; Shi, Q.; Yakacki, C. M. Dissolution of Covalent Adaptable Network Polymers in Organic Solvent. *J. Mech. Phys. Solids* **2017**, *109*, 78–94. https://doi.org/10.1016/j.jmps.2017.08.006.

(4) Marco-Dufort, B.; Willi, J.; Vielba-Gomez, F.; Gatti, F.; Tibbitt, M. W. Environment Controls Biomolecule Release from Dynamic Covalent Hydrogels. *Biomacromolecules* **2021**, *22* (1), 146–157. https://doi.org/10.1021/acs.biomac.0c00895.

(5) Carberry, B. J.; Hernandez, J. J.; Dobson, A.; Bowman, C. N.; Anseth, K. S. Kinetic Analysis of Degradation in Thioester Cross-Linked Hydrogels as a Function of Thiol Concentration, p Ka, and Presentation. *Macromolecules* **2022**, *55* (6), 2123–2129. https://doi.org/10.1021/acs.macromol.1c02396.

(6) Chen, F.; Tillberg, P. W.; Boyden, E. S. Expansion Microscopy. *Science (80-.).* **2015**, *347* (6221), 543–548. https://doi.org/10.1126/science.1260088.

(7) Chen, M.; Gu, Y.; Singh, A.; Zhong, M.; Jordan, A. M.; Biswas, S.; Korley, L. T. J.; Balazs, A. C.; Johnson, J. A. Living Additive Manufacturing: Transformation of Parent Gels into Diversely Functionalized Daughter Gels Made Possible by Visible Light Photoredox Catalysis. *ACS Cent. Sci.* **2017**, *3* (2), 124–134. https://doi.org/10.1021/acscentsci.6b00335.

(8) Xue, L.; Xiong, X.; Krishnan, B. P.; Puza, F.; Wang, S.; Zheng, Y.; Cui, J. Light-Regulated Growth from Dynamic Swollen Substrates for Making Rough Surfaces. *Nat. Commun.* **2020**, *11* (1), 1–9. https://doi.org/10.1038/s41467-020-14807-x.

(9) De Neve, J.; Haven, J. J.; Harrisson, S.; Junkers, T. Deconstructing Oligomer Distributions: Discrete Species and Artificial Distributions. *Angew. Chemie - Int. Ed.* **2019**, *58* (39), 13869–13873. https://doi.org/10.1002/anie.201906842.

(10) Das, A.; Petkau-Milroy, K.; Klerks, G.; Van Genabeek, B.; Lafleur, R. P. M.; Palmans, A. R. A.; Meijer, E. W. Consequences of Dispersity on the Self-Assembly of ABA-Type Amphiphilic Block Co-Oligomers. *ACS Macro Lett.* **2018**, *7* (5), 546–550. https://doi.org/10.1021/acsmacrolett.8b00168.

(11) van Genabeek, B.; Lamers, B. A. G.; Hawker, C. J.; Meijer, E. W.; Gutekunst, W. R.; Schmidt, B. V. K. J. Properties and Applications of Precision Oligomer Materials; Where Organic and Polymer Chemistry Join Forces. *J. Polym. Sci.* **2021**, *59* (5), 373–403. https://doi.org/10.1002/pol.20200862.

(12) Meng, Y.; Fenoli, C. R.; Aguirre-Soto, A.; Bowman, C. N.; Anthamatten, M. Photoinduced Diffusion Through Polymer Networks. *Adv. Mater.* **2014**, *26* (37), 6497–6502. https://doi.org/10.1002/adma.201402097.

(13) Worrell, B. T.; Mavila, S.; Wang, C.; Kontour, T. M.; Lim, C. H.; McBride, M. K.; Musgrave, C. B.; Shoemaker, R.; Bowman, C. N. A User's Guide to the Thiol-Thioester Exchange in Organic Media: Scope, Limitations, and Applications in Material Science. *Polym. Chem.* **2018**, *9* (36), 4523–4534. https://doi.org/10.1039/c8py01031e.

(14) Chen, J.; Zhang, X. F.; Kort, M. E.; Huth, J. R.; Sun, C.; Miesbauer, L. J.; Cassar, S. C.; Neelands, T.; Scott, V. E.; Moreland, R. B.; Reilly, R. M.; Hajduk, P. J.; Kym, P. R.; Hutchins, C. W.; Faltynek, C. R. Molecular Determinants of Species-Specific Activation or Blockade of TRPA1 Channels. *J. Neurosci.* **2008**, *28* (19), 5063–5071. https://doi.org/10.1523/JNEUROSCI.0047-08.2008.

(15) Brown, T. E.; Carberry, B. J.; Worrell, B. T.; Dudaryeva, O. Y.; McBride, M. K.; Bowman, C. N.; Anseth, K. S. Photopolymerized Dynamic Hydrogels with Tunable Viscoelastic Properties through Thioester Exchange. *Biomaterials* **2018**, *178*, 496–503. https://doi.org/10.1016/j.biomaterials.2018.03.060.

(16) Kowalski, B. A.; McLeod, R. R. Design Concepts for Diffusive Holographic Photopolymers. *J. Polym. Sci. Part B Polym. Phys.* **2016**, *54* (11), 1021–1035. https://doi.org/10.1002/polb.24011.

(17) Gambogi, Jr., W. J.; Weber, A. M.; Trout, T. J. Advances and Applications of DuPont Holographic Photopolymers. *Hologr. Imaging Mater.* **1994**, *2043* (January 1994), 2. https://doi.org/10.1117/12.165557.

(18) Alim, M. D.; Glugla, D. J.; Mavila, S.; Wang, C.; Nystrom, P. D.; Sullivan, A. C.; McLeod, R. R.; Bowman, C. N. High Dynamic Range (Δn) Two-Stage Photopolymers via Enhanced Solubility of a High Refractive Index Acrylate Writing Monomer. *ACS Appl. Mater. Interfaces* **2018**, *10* (1), 1217–1224. https://doi.org/10.1021/acsami.7b15063.

(19) Hu, Y.; Kowalski, B. A.; Mavila, S.; Podgórski, M.; Sinha, J.; Sullivan, A. C.; McLeod, R. R.; Bowman, C. N. Holographic Photopolymer Material with High Dynamic Range (Δ n) via Thiol-Ene Click Chemistry. *ACS Appl. Mater. Interfaces* **2020**, *12* (39), 44103–44109. https://doi.org/10.1021/acsami.0c08872.

Bibliography

Adzima, B. J., Kloxin, C. J., Deforest, C. A., Anseth, K. S., & Bowman, C. N. (2012). *Macromolecular Rapid Communications*, *33*(24), 2092–2096.

Alim, M. D., Glugla, D. J., Mavila, S., Wang, C., Nystrom, P. D., Sullivan, A. C., McLeod, R. R., & Bowman, C. N. (2018). *ACS Applied Materials and Interfaces*, *10*(1), 1217–1224.

Ambulo, C. P., Burroughs, J. J., Boothby, J. M., Kim, H., Shankar, M. R., & Ware, T. H. (2017). *ACS Applied Materials and Interfaces*, *9*(42), 37332–37339.

Arie, M. A., Shooshtari, A. H., Tiwari, R., Dessiatoun, S. V., Ohadi, M. M., & Pearce, J. M. (2017). *Applied Thermal Engineering*, *113*, 575–584.

Armstrong, R. D., Jenkins, A. T. A., & Johnson, B. W. (1995). *Corrosion Science*, *37*(10), 1615–1625.

Bagheri, A., Ling, H., Bainbridge, C. W. A., & Jin, J. (2021). *ACS Applied Polymer Materials*, *3*(6), 2921–2930.

Barba, A. A., d'Amore, M., Chirico, S., Lamberti, G., & Titomanlio, G. (2009). *European Journal of Pharmaceutical Sciences*, *36*(2–3), 359–368.

Barnes, D. K. A., Galgani, F., Thompson, R. C., & Barlaz, M. (2009). *Philosophical Transactions of the Royal Society B: Biological Sciences*, *364*(1526), 1985–1998.

Batchelor, R., Messer, T., Hippler, M., Wegener, M., Barner-Kowollik, C., & Blasco, E. (2019). *Advanced Materials*, *31*(40).

Beifuss, U., & Ledderhose, S. (1995). *Journal of the Chemical Society, Chemical Communications*, *1*(20), 2137–2138.

Bertrand, O., & Gohy, J. F. (2017). *Polymer Chemistry*, *8*(1), 52–73.

Boday, D. J., García, J. M., Hedrick, J. L., & Wojtecki, R. J. (2018).

Bongiardina, N. J., Long, K. F., Podgórski, M., & Bowman, C. N. (2021). *Macromolecules*, *54*(18), 8341–8351.

Bracher, P. J., Snyder, P. W., Bohall, B. R., & Whitesides, G. M. (2011). *Origins of Life and Evolution of Biospheres*, *41*(5), 399–412.

Brown, T. E., Carberry, B. J., Worrell, B. T., Dudaryeva, O. Y., McBride, M. K., Bowman, C. N., & Anseth, K. S. (2018). *Biomaterials*, *178*, 496–503.

Browne, M. A., Crump, P., Niven, S. J., Teuten, E., Tonkin, A., Galloway, T., & Thompson, R. (2011). *Environmental Science and Technology*, *45*(21), 9175–9179.

Burkersroda, F. Von, Schedl, L., & Göpferich, A. (2002). *Biomaterials*, *23*(21), 4221–4231.

Byambaa, B., Konno, T., & Ishihara, K. (2013). *Colloids and Surfaces B: Biointerfaces*, *103*, 489–495.

CAMMARATA, P. S., & COHEN, P. P. (1950). *The Journal of Biological Chemistry*, *187*(1), 439–452. http://www.ncbi.nlm.nih.gov/pubmed/14794729

Capelot, M., Unterlass, M. M., Tournilhac, F., & Leibler, L. (2012). *ACS Macro Letters*, *1*(7), 789–792.

Carberry, B. J., Hergert, J. E., Yavitt, F. M., Hernandez, J. J., Speckl, K. F., Bowman, C. N., McLeod, R. R., & Anseth, K. S. (2021). *Biofabrication*, *13*(4).

Carberry, B. J., Hernandez, J. J., Dobson, A., Bowman, C. N., & Anseth, K. S. (2022). *Macromolecules*, *55*(6), 2123–2129.

Cargoët, M., Diemer, V., Snella, B., Desmet, R., Blanpain, A., Drobecq, H., Agouridas, V., & Melnyk, O. (2018). *Journal of Organic Chemistry*, *83*(20), 12584–12594.

Cavaca, L. A. S., Gomes, R. F. A., & Afonso, C. A. M. (2022). *Molecules*, *27*(5).

Chang, H.-M., Oakes, J., Olsson, A., Panaitescu, L., Britt, B., Kearney, C., & Kane, R. (2005). *Letters in Drug Design & Discovery*, *2*(2), 133–136.

Chao, A., Negulescu, I., & Zhang, D. (2016). *Macromolecules*, *49*(17), 6277–6284.

Chao, A., & Zhang, D. (2019). *Macromolecules*, *52*(2), 495–503.

Chatani, S., Kloxin, C. J., & Bowman, C. N. (2014). *Polymer Chemistry*, *5*(7), 2187–2201.

Chen, F., Tillberg, P. W., & Boyden, E. S. (2015). *Science*, *347*(6221), 543–548.

Chen, J. S., Ober, C. K., Poliks, M. D., Zhang, Y., Wiesner, U., & Cohen, C. (2004). *Polymer*, *45*(6), 1939–1950.

Chen, J., Zhang, X. F., Kort, M. E., Huth, J. R., Sun, C., Miesbauer, L. J., Cassar, S. C., Neelands, T., Scott, V. E., Moreland, R. B., Reilly, R. M., Hajduk, P. J., Kym, P. R., Hutchins, C. W., & Faltynek, C. R. (2008). *Journal of Neuroscience*, *28*(19), 5063–5071.

Chen, M., Gu, Y., Singh, A., Zhong, M., Jordan, A. M., Biswas, S., Korley, L. T. J., Balazs, A. C., & Johnson, J. A. (2017). *ACS Central Science*, *3*(2), 124–134.

Chen, Z., Yang, M., Ji, M., Kuang, X., Qi, H. J., & Wang, T. (2021). *Materials and Design*, *197*, 109189.

Cook, C. C., Fong, E. J., Schwartz, J. J., Porcincula, D. H., Kaczmarek, A. C., Oakdale, J. S., Moran, B. D., Champley, K. M., Rackson, C. M., Muralidharan, A., McLeod, R. R., &

Shusteff, M. (2020). *Advanced Materials*, *32*(47), 1–6.

Cordes, E. H., & Bull, H. G. (1974). *Chemical Reviews*, *74*(5), 581–603.

Cui, C., An, L., Zhang, Z., Ji, M., Chen, K., Yang, Y., Su, Q., Wang, F., Cheng, Y., & Zhang, Y. (2022). *Advanced Functional Materials*, *32*(29), 1–9.

Das, A., Petkau-Milroy, K., Klerks, G., Van Genabeek, B., Lafleur, R. P. M., Palmans, A. R. A., & Meijer, E. W. (2018). *ACS Macro Letters*, *7*(5), 546–550.

Davidson, E. C., Kotikian, A., Li, S., Aizenberg, J., & Lewis, J. A. (2020). *Advanced Materials*, *32*(1), 1–6.

De Alwis Watuthanthrige, N., Ahammed, B., Dolan, M. T., Fang, Q., Wu, J., Sparks, J. L., Zanjani, M. B., Konkolewicz, D., & Ye, Z. (2020). *Materials Horizons*, *7*(6), 1581–1587.

De Beer, M. P., Van Der Laan, H. L., Cole, M. A., Whelan, R. J., Burns, M. A., & Scott, T. F. (2019). *Science Advances*, *5*(1).

De Neve, J., Haven, J. J., Harrisson, S., & Junkers, T. (2019). *Angewandte Chemie - International Edition*, *58*(39), 13869–13873.

Decker, C., & Zahouily, K. (1999). *Polymer Degradation and Stability*, *64*, 293–304.

Demongeot, A., Groote, R., Goossens, H., Hoeks, T., Tournilhac, F., & Leibler, L. (2017). *Macromolecules*, *50*(16), 6117–6127.

Dénès, F., Pichowicz, M., Povie, G., & Renaud, P. (2014). *Chemical Reviews*, *114*(5), 2587–2693.

Denissen, W., Rivero, G., Nicolaÿ, R., Leibler, L., Winne, J. M., & Du Prez, F. E. (2015). *Advanced Functional Materials*, *25*(16), 2451–2457.

Denissen, W., Winne, J. M., & Du Prez, F. E. (2016). *Chemical Science*, *7*(1), 30–38.

Deye, J. F., Berger, T. A., & Anderson, A. G. (1990). *Analytical Chemistry*, *62*(14), 1552.

Di, C., Genua, A., Rymarczyk, M., Dobbels, C., Malburet, S., Graillot, A., & Mija, A. (2021). *Composites Science and Technology*, *205*(September 2020), 108678.

Doss, G. A., & Baillie, T. A. (2006). *Drug Metabolism Reviews*, *38*(4), 641–649.

El-Zaatari, B. M., Ishibashi, J. S. A., & Kalow, J. A. (2020). *Polymer Chemistry*, *11*(33), 5339–5345.

Fairbanks, B. D., Scott, T. F., Kloxin, C. J., Anseth, K. S., & Bowman, C. N. (2009). *Macromolecules*, *42*(1), 211–217.

Farah, S., Anderson, D. G., & Langer, R. (2016). *Advanced Drug Delivery Reviews*, *107*, 367–392.

Feilding, A. J., Franchi, P., Roberts, B. P., & Smits, T. M. (2002). *Journal of the Chemical Society, Perkin Transactions 2*, *2*(1), 155–163.

Fialho, D. M. (2019). Georgia Institute of Technology.

Fife, T. H. (1972). *Accounts of Chemical Research*, *5*(8), 264–272.

Fila, K., Goliszek, M., Podkościelna, B., & Podgórski, M. (2020). *European Polymer Journal*, *136*(August), 109918.

Flory, P. J. (1941). *Journal of the American Chemical Society*, *63*(11), 3083–3090.

Fortman, D. J., Brutman, J. P., Cramer, C. J., Hillmyer, M. A., & Dichtel, W. R. (2015). *Journal of the American Chemical Society*, *137*(44), 14019–14022.

Gambogi, Jr., W. J., Weber, A. M., & Trout, T. J. (1994). *Holographic Imaging and Materials*, *2043*(January 1994), 2.

Gao, S., Tang, G., Hua, D., Xiong, R., Han, J., Jiang, S., Zhang, Q., & Huang, C. (2019). *Journal of Materials Chemistry B*, *7*(5), 709–729.

García, J. M., Jones, G. O., Virwani, K., Mccloskey, B. D., Boday, D. J., Huurne, G. M., Horn, H. W., Coady, D. J., Bintaleb, A. M., Alabdulrahman, A. M. S., Alsewailem, F., Almegren, H. A. A., & Hedrick, J. L. (2014). *Science*, *13073*(May), 732–735.

Garrido-González, J. J., Sánchez-Santos, E., Habib, A., Cuevas Ferreras, Á. V., Sanz, F., Morán, J. R., & Fuentes de Arriba, Á. L. (2022). *Angewandte Chemie - International Edition*, *61*(35).

Gharde, S., & Kandasubramanian, B. (2019). *Environmental Technology and Innovation*, *14*, 100311.

Ghobril, C., Charoen, K., Rodriguez, E. K., Nazarian, A., & Grinstaff, M. W. (2013). *Angewandte Chemie - International Edition*, *52*(52), 14070–14074.

Ghosh, S., Ingerman, L. A., Frye, A. G., Lee, S. J., Gagné, M. R., & Waters, M. L. (2010). *Organic Letters*, *12*(8), 1860–1863.

Góngora-Benítez, M., Basso, A., Bruckdorfer, T., Royo, M., Tulla-Puche, J., & Albericio, F. (2012). *Chemistry - A European Journal*, *18*(50), 16166–16176.

Göpferich, A. (1996). *The Biomaterials: Silver Jubilee Compendium*, *17*(2), 117–128.

Göpferich, A. (1997). *Macromolecules*, *30*(9), 2598–2604.

Guerre, M., Taplan, C., Winne, J. M., & Du Prez, F. E. (2020). *Chemical Science*, *11*(19), 4855–4870.

Guo, Y., Zhang, D., Wang, J., Lu, H., & Pu, S. (2020). *Dyes and Pigments*, *175*(November 2019),

108191.

Hacioğlu, B., Berchtold, K. A., Lovell, L. G., Nie, J., & Bowman, C. N. (2002). *Biomaterials*, *23*(20), 4057–4064.

Hakkarainen, M., Xu, Y., & Odelius, K. (2020). *ACS Sustainable Chemistry and Engineering*, *8*(46), 17272–17279.

Hamel, C. M., Kuang, X., Chen, K., & Qi, H. J. (2019). *Macromolecules*, *52*(10), 3636–3645.

Han, D., Tong, X., & Zhao, Y. (2011). *Macromolecules*, *44*(3), 437–439.

Han, X., & Pan, J. (2011). *Acta Biomaterialia*, *7*(2), 538–547.

Hawkins, W. L. (1984). Springer Berlin Heidelberg.

Hernandez, J. J., Dobson, A. L., Carberry, B. J., Kuenstler, A. S., Shah, P. K., Anseth, K. S., White, T. J., & Bowman, C. N. (2022). *Macromolecules*, *55*, 1376–1385.

Hiemenz, P. C., & Lodge, T. P. (2007). In *Polymer Chemistry*. CRC Press Taylor & Francis Group.

Hogg, N. (1999). *Analytical Biochemistry*, *272*(2), 257–262.

Holloway, J. L., Ma, H., Rai, R., & Burdick, J. A. (2014). *Journal of Controlled Release*, *191*, 63–70.

Hopfenberg, H. B. (1976). In *Am Chem Soc Div Org Coat Plast Chem Prepr* (Vol. 36, Issue 1, pp. 26–32).

Houck, H. A., Blasco, E., Du Prez, F. E., & Barner-Kowollik, C. (2019). *Journal of the American Chemical Society*, *141*(31), 12329–12337.

Houk, J., & Whitesides, G. M. (1987). *Journal of the American Chemical Society*, *109*(22), 6825–6836.

Hoyle, C. E., & Bowman, C. N. (2010). *Angewandte Chemie - International Edition*, *49*(9), 1540–1573.

Hu, L., Zhang, Q., Li, X., & Serpe, M. J. (2019). *Materials Horizons*, *6*(9), 1774–1793.

Hu, Y., Kowalski, B. A., Mavila, S., Podgórski, M., Sinha, J., Sullivan, A. C., McLeod, R. R., & Bowman, C. N. (2020). *ACS Applied Materials and Interfaces*, *12*(39), 44103–44109.

Huang, S., Sinha, J., Podgórski, M., Zhang, X., Claudino, M., & Bowman, C. N. (2018). *Macromolecules*, *51*(15), 5979–5988.

Ishibashi, J. S. A., & Kalow, J. A. (2018). *ACS Macro Letters*, *7*(4), 482–486.

Jaque, D., Martínez Maestro, L., Del Rosal, B., Haro-Gonzalez, P., Benayas, A., Plaza, J. L., Martín Rodríguez, E., & García Solé, J. (2014). *Nanoscale*, *6*(16), 9494–9530.

Javed, M., Tasmim, S., Abdelrahman, M. K., Ambulo, C. P., & Ware, T. H. (2020). *Crystals*, *10*(5).

Jin, Y., Lei, Z., Taynton, P., Huang, S., & Zhang, W. (2019). *Matter*, *1*(6), 1456–1493.

Jørgensen, M., Norrman, K., & Krebs, F. C. (2008). *Solar Energy Materials and Solar Cells*, *92*(7), 686–714.

Junjappa, H., Ila, H., & Asokan, C. V. (1990). *Tetrahedron*, *46*(16), 5423–5506.

Kalathimekkad, S., Missinne, J., Schaubroeck, D., Mandamparambil, R., & Van Steenberge, G. (2015). *IEEE Sensors Journal*, *15*(1), 76–81.

Kaminker, R., Callaway, E. B., Dolinski, N. D., Barbon, S. M., Shibata, M., Wang, H., Hu, J., & Hawker, C. J. (2018). *Chemistry of Materials*, *30*(22), 8352–8358.

Käpylä, E., Delgado, S. M., & Kasko, A. M. (2016). *ACS Applied Materials and Interfaces*, *8*(28), 17885–17893.

Kazemi, M., Faisal Kabir, S., & Fini, E. H. (2021). *Resources, Conservation and Recycling*, *174*(April), 105776.

Khawam, A., & Flanagan, D. R. (2006). *Journal of Physical Chemistry B*, *110*(35), 17315–17328.

Kim, J. K., Souma, Y., Beutow, N., Ibbeson, C., & Caserio, M. C. (1989). *Journal of Organic Chemistry*, *54*(7), 1714–1720.

Kim, J. S., Ho, P. K. H., Murphy, C. E., Seeley, A. J. A. B., Grizzi, I., Burroughes, J. H., & Friend, R. H. (2004). *Chemical Physics Letters*, *386*(1–3), 2–7.

Klajn, R. (2014). *Chemical Society Reviews*, *43*(1), 148–184.

Klose, D., Siepmann, F., Elkharraz, K., & Siepmann, J. (2008). *International Journal of Pharmaceutics*, *354*(1–2), 95–103.

Kloxin, C. J., & Bowman, C. N. (2013). *Chemical Society Reviews*, *42*(17), 7161–7173.

Kohrs, N. J., Liyanage, T., Venkatesan, N., Najarzadeh, A., & Puleo, D. A. (2019). In *Encyclopedia of Biomedical Engineering* (Vols. 1–3). Elsevier.

Konetski, D., Mavila, S., Wang, C., Worrell, B., & Bowman, C. N. (2018). *Chemical Communications*, *54*(58), 8108–8111.

Kowalski, B. A., & McLeod, R. R. (2016). *Journal of Polymer Science, Part B: Polymer Physics*, *54*(11), 1021–1035.

Kuang, X., Roach, D. J., Wu, J., Hamel, C. M., Ding, Z., Wang, T., Dunn, M. L., & Qi, H. J. (2019). *Advanced Functional Materials*, *29*(2), 1–23.

Kuang, X., Shi, Q., Zhou, Y., Zhao, Z., Wang, T., & Qi, H. J. (2018). *RSC Advances*, *8*(3), 1493–1502.

Kuang, X., Zhou, Y., Shi, Q., Wang, T., & Qi, H. J. (2018). *ACS Sustainable Chemistry and Engineering*, *6*(7), 9189–9197.

Kumhee, C. (1994). In *Dissertation*.

Layer, R. W. (1963). *Chemical Reviews*, *63*(5), 489–510.

Lazzari, S., Codari, F., Storti, G., Morbidelli, M., & Moscatelli, D. (2014). *Polymer Degradation and Stability*, *110*, 80–90.

Le Neindre, M., & Nicolaÿ, R. (2014). *Polymer International*, *63*(5), 887–893.

Lee, D. W., Park, Y. M., & Lee, K. Y. (2009). *Catalysis Surveys from Asia*, *13*(2), 63–77.

Li, L., Deng, X. X., Li, Z. L., Du, F. S., & Li, Z. C. (2014). *Macromolecules*, *47*(14), 4660–4667.

Li, Q., Ma, S., Wang, S., Yuan, W., Xu, X., Wang, B., Huang, K., & Zhu, J. (2019). *Journal of Materials Chemistry A*, *7*(30), 18039–18049.

Li, X., Yu, R., He, Y., Zhang, Y., Yang, X., Zhao, X., & Huang, W. (2019). *ACS Macro Letters*, *8*(11), 1511–1516.

Liu, B., & Thayumanavan, S. (2020). *Cell Reports Physical Science*, *1*(12), 100271.

Liu, C., Ewert, K. K., Yao, W., Wang, N., Li, Y., Safinya, C. R., & Qiao, W. (2020). *ACS Applied Materials and Interfaces*, *12*(1), 70–85.

Liu, C., Qin, H., & Mather, P. T. (2007). *Journal of Materials Chemistry*, *17*(16), 1543–1558.

Liu, J., Li, J., Luo, Z., & Zhou, Y. (2023). *Chemical Engineering Journal*, *452*(P3), 139452.

Liu, Y., Wang, W., Yang, J., Zhou, C., & Sun, J. (2013). *Asian Journal of Pharmaceutical Sciences*, *8*(3), 159–167.

Long, T. R., Elder, R. M., Bain, E. D., Masser, K. A., Sirk, T. W., Yu, J. H., Knorr, D. B., & Lenhart, J. L. (2018). *Soft Matter*, *14*(17), 3344–3360.

Love, D. M., Fairbanks, B. D., & Bowman, C. N. (2020). *Macromolecules*, *53*(13), 5237–5247.

Love, D. M., Kim, K., Goodrich, J. T., Fairbanks, B. D., Worrell, B. T., Stoykovich, M. P., Musgrave, C. B., & Bowman, C. N. (2018). *Journal of Organic Chemistry*, *83*(5), 2912–2919.

Lu, L., Garcia, C. A., & Mikos, A. G. (1999). *Journal of Biomedical Materials Research*, *46*(2), 236–244.

Lv, C., Wang, Z., Wang, P., & Tang, X. (2012). *Langmuir*, *28*(25), 9387–9394.

Ma, S., & Webster, D. C. (2018). *Progress in Polymer Science*, *76*, 65–110.

Mabey, W., & Mill, T. (1978). *Journal of Physical and Chemical Reference Data*, *7*(2), 383–415.

Macosko, C. W., & Miller, D. R. (1976). *Macromolecules*, *9*(2), 199–206.

Manouras, T., & Vamvakaki, M. (2017). *Polymer Chemistry*, *8*(1), 74–96.

Mao, Y., Ding, Z., Yuan, C., Ai, S., Isakov, M., Wu, J., Wang, T., Dunn, M. L., & Qi, H. J. (2016). *Scientific Reports*, *6*(January), 1–13.

Marco-Dufort, B., Willi, J., Vielba-Gomez, F., Gatti, F., & Tibbitt, M. W. (2021). *Biomacromolecules*, *22*(1), 146–157.

Martens, P., Metters, A. T., Anseth, K. S., & Bowman, C. N. (2001). *Journal of Physical Chemistry B*, *105*(22), 5131–5138.

Martinez, A. M., Cox, L. M., Darabi, A., Bongiardina, N. J., & Bowman, C. N. (2022). *ACS Applied Materials & Interfaces*, *14*(23), 27177–27186.

Martinez, A. M., Cox, L. M., Killgore, J. P., Bongiardina, N. J., Riley, R. D., & Bowman, C. N. (2021). *Soft Matter*, *17*(3), 467–474.

Martinez, V., & Henary, M. (2016). *Chemistry - A European Journal*, *22*(39), 13764–13782.

Mavila, S., Culver, H. R., Anderson, A. J., Prieto, T. R., & Bowman, C. N. (2022). *Angewandte Chemie - International Edition*, *61*(1), 1–5.

Mavila, S., Worrell, B. T., Culver, H. R., Goldman, T. M., Wang, C., Lim, C. H., Domaille, D. W., Pattanayak, S., McBride, M. K., Musgrave, C. B., & Bowman, C. N. (2018). *Journal of the American Chemical Society*, *140*(42), 13594–13598.

McBride, R. A., & Gillies, E. R. (2013). *Macromolecules*, *46*(13), 5157–5166.

McMurry, J. (2012). In *Physical Chemistry* (Eighth Edi). Cengage Learning.

Melchor Bañales, A. J., & Larsen, M. B. (2020). *ACS Macro Letters*, *9*(7), 937–943.

Meng, Y., Fenoli, C. R., Aguirre-Soto, A., Bowman, C. N., & Anthamatten, M. (2014). *Advanced Materials*, *26*(37), 6497–6502.

Metters, A., & Hubbell, J. (2005). *Biomacromolecules*, *6*(1), 290–301.

Metters, A. T., Anseth, K. S., & Bowman, C. N. (2000). *Polymer*, *41*(11), 3993–4004.

Metters, A. T., Anseth, K. S., & Bowman, C. N. (2001). *Journal of Physical Chemistry B*, *105*(34), 8069–8076.

Metters, A. T., Bowman, C. N., & Anseth, K. S. (2000). *Journal of Physical Chemistry B*, *104*(30), 7043–7049.

Metters, A. T., Bowman, C. N., & Anseth, K. S. (2001). *AIChE Journal*, *47*(6), 1432–1437.

Min, Y., Huang, S., Wang, Y., Zhang, Z., Du, B., Zhang, X., & Fan, Z. (2015). *Macromolecules*, *48*(2), 316–322.

Moorhoff, C. M., Cook, W. D., & Braybrook, C. (2013). *Monatshefte Fur Chemie*, *144*(6), 891–902.

Nimmo, C. M., Owen, S. C., & Shoichet, M. S. (2011). *Biomacromolecules*, *12*(3), 824–830.

Oehlenschlaeger, K. K., Guimard, N. K., Brandt, J., Mueller, J. O., Lin, C. Y., Hilf, S., Lederer, A., Coote, M. L., Schmidt, F. G., & Barner-Kowollik, C. (2013). *Polymer Chemistry*, *4*(16), 4348–4355.

Orrillo, A. G., & Furlan, R. L. E. (2022). *Angewandte Chemie - International Edition*, *61*(26).

Pasparakis, G., Manouras, T., Argitis, P., & Vamvakaki, M. (2012). *Macromolecular Rapid Communications*, *33*(3), 183–198.

Pasparakis, G., Manouras, T., Selimis, A., Vamvakaki, M., & Argitis, P. (2011). *Angewandte Chemie*, *123*(18), 4228–4231.

Peng, X., & Wang, H. (2018). *Journal of Polymer Science, Part B: Polymer Physics*, *56*(19), 1314–1324.

Pickering, S. J. (2006). *Composites Part A: Applied Science and Manufacturing*, *37*(8), 1206–1215.

Pietrocola, F., Galluzzi, L., Bravo-San Pedro, J. M., Madeo, F., & Kroemer, G. (2015). *Cell Metabolism*, *21*(6), 805–821.

Podgórski, M., Fairbanks, B. D., Kirkpatrick, B. E., McBride, M., Martinez, A., Dobson, A., Bongiardina, N. J., & Bowman, C. N. (2020). *Advanced Materials*, *32*(20), 1–26.

Podgórski, M., Huang, S., & Bowman, C. N. (2021). *ACS Applied Materials and Interfaces*, *13*(11), 12789–12796.

Podgórski, M., Mavila, S., Huang, S., Spurgin, N., Sinha, J., & Bowman, C. N. (2020). *Angewandte Chemie - International Edition*, *59*(24), 9345–9349.

Pople, J. A., & Beveridge, D. L. (1968). *The Journal of Chemical Physics*, *49*(10), 4725–4726.

Ramon, E., Sguazzo, C., & Moreira, P. M. G. P. (2018). *Aerospace*, *5*(4).

Rao, C. N. R., & Venkataraghavan, R. (1989). *Spectrochimica Acta - Part A Molecular Spectroscopy*, *45*(1958), 299–305.

Raquez, J. M., Deléglise, M., Lacrampe, M. F., & Krawczak, P. (2010). *Progress in Polymer*

Science (Oxford), *35*(4), 487–509.

Reeves, J. A., Allegrezza, M. L., & Konkolewicz, D. (2017). *Macromolecular Rapid Communications*, *38*(13), 1–5.

Reichardt, C. (1994). *Chemical Reviews*, *94*(8), 2319–2358.

Reutenauer, P., Buhler, E., Boul, P. J., Candau, S. J., & Lehn, J. M. (2009). *Chemistry - A European Journal*, *15*(8), 1893–1900.

Romano, A., Angelini, A., Rossegger, E., Palmara, G., Castellino, M., Frascella, F., Chiappone, A., Chiadò, A., Sangermano, M., Schlögl, S., & Roppolo, I. (2020). *Macromolecular Rapid Communications*, *41*(10), 1–7.

Romano, A., Roppolo, I., Rossegger, E., Schlögl, S., & Sangermano, M. (2020). *Materials*, *13*(12), 1–26.

Rosales, A. M., & Anseth, K. S. (2016). *Nature Reviews Materials*, *1*(2), 1–15.

Roth, P. J., & Lowe, A. B. (2017). *Polymer Chemistry*, *8*(1), 10–11.

Röttger, M., Domenech, T., Van Der Weegen, R., Breuillac, A., Nicolaÿ, R., & Leibler, L. (2017). *Science*, *356*(6333), 62–65.

Russew, M. M., & Hecht, S. (2010). *Advanced Materials*, *22*(31), 3348–3360.

Rydholm, A. E., Reddy, S. K., Anseth, K. S., & Bowman, C. N. (2006). *Biomacromolecules*, *7*(10), 2827–2836.

Rydholm, A. E., Reddy, S. K., Anseth, K. S., & Bowman, C. N. (2007). *Polymer*, *48*(15), 4589–4600.

Sackett, C. K., & Narasimhan, B. (2011). *International Journal of Pharmaceutics*, *418*(1), 104–114.

Saggiomo, V., & Velders, A. H. (2015). *Advanced Science*, *2*(9), 1–5.

Saiz, C., Wipf, P., Manta, E., & Mahler, G. (2009). *Organic Letters*, *11*(15), 3170–3173.

Scheutz, G. M., Lessard, J. J., Sims, M. B., & Sumerlin, B. S. (2019). *Journal of the American Chemical Society*, *141*(41), 16181–16196.

Schneiderman, D. K., & Hillmyer, M. A. (2017). *Macromolecules*, *50*(10), 3733–3749.

Scott, T. F., Schneider, A. D., Cook, W. D., & Bowman, C. N. (2005). *Science*, *308*(5728), 1615–1617.

Shi, Q., Yu, K., Kuang, X., Mu, X., Dunn, C. K., Dunn, M. L., Wang, T., & Jerry Qi, H. (2017). *Materials Horizons*, *4*(4), 598–607.

Shih, H., & Lin, C. C. (2012). *Biomacromolecules*, *13*(7), 2003–2012.

Sijbesma, R. P., Beijer, F. H., Brunsveld, L., Folmer, B. J. B., Hirschberg, J. H. K. K., Lange, R. F. M., Lowe, J. K. L., & Meijer, E. W. (1997). *Science*, *278*(5343), 1601–1604.

Singh, B., & Sharma, N. (2008). *Polymer Degradation and Stability*, *93*(3), 561–584.

Snyder, R. L., Lidston, C. A. L., De Hoe, G. X., Parvulescu, M. J. S., Hillmyer, M. A., & Coates, G. W. (2020). *Polymer Chemistry*, *11*(33), 5346–5355.

Soars, S., Kamps, J., Fairbanks, B., & Bowman, C. (2021). *Macromolecular Chemistry and Physics*, *222*(17), 1–7.

Soars, S. M., Bongiardina, N. J., Fairbanks, B. D., Podgórski, M., & Bowman, C. N. (2022). *Macromolecules*, *55*(5), 1811–1821.

Soars, S. M., Kirkpatrick, B. E., Fairbanks, B. D., Kamps, J. T., Anseth, K. S., & Bowman, C. N. (2022). *Polymer International*, *71*(7), 906–911.

Stille, J. K. (1981). *Journal of Chemical Education*, *58*(11), 862–866.

Stubbs, C. J., Khalfa, A. L., Chiaradia, V., Worch, J. C., & Dove, A. P. (2022). *Journal of the American Chemical Society*.

Sun, X. H., Yu, H. Z., Pei, S. Q., & Dang, Z. M. (2015). *Chinese Chemical Letters*, *26*(10), 1259–1264.

Taplan, C., Guerre, M., & Du Prez, F. E. (2021). *Journal of the American Chemical Society*, *143*(24), 9140–9150.

Taplan, C., Guerre, M., Winne, J. M., & Du Prez, F. E. (2020). *Materials Horizons*, *7*(1), 104–110.

Taynton, P., Ni, H., Zhu, C., Yu, K., Loob, S., Jin, Y., Qi, H. J., & Zhang, W. (2016). *Advanced Materials*, *28*(15), 2904–2909.

Theato, P., Sumerlin, B. S., O'reilly, R. K., & Epp, T. H. (2013). *Chemical Society Reviews*, *42*(17), 7055–7056.

Trenor, S. R., Shultz, A. R., Love, B. J., & Long, T. E. (2004). *Chemical Reviews*, *104*(6), 3059–3077.

Um, I. H., Lee, J. Y., Bae, S. Y., & Buncel, E. (2005). *Canadian Journal of Chemistry*, *83*(9), 1365–1371.

Uygun, M., Tasdelen, M. A., & Yagci, Y. (2010). *Macromolecular Chemistry and Physics*, *211*(1), 103–110.

van Genabeek, B., Lamers, B. A. G., Hawker, C. J., Meijer, E. W., Gutekunst, W. R., & Schmidt, B. V. K. J. (2021). *Journal of Polymer Science*, *59*(5), 373–403.

Van Herck, N., Maes, D., Unal, K., Guerre, M., Winne, J. M., & Du Prez, F. E. (2020). *Angewandte Chemie - International Edition*, *59*(9), 3609–3617.

Vitaku, E., & Dichtel, W. R. (2017). *Journal of the American Chemical Society*, *139*(37), 12911–12914.

Vohlidal, J. (2021). *Chemistry Teacher International*, *3*(2), 213–220.

Vu, D. T., Kolah, A. K., Asthana, N. S., Peereboom, L., Lira, C. T., & Miller, D. J. (2005). *Fluid Phase Equilibria*, *236*(1–2), 125–135.

Walker, W. D., Sandoz, M. J., Roland, S., Buster, T. M., Newman, J. K., & Patton, D. L. (2020). *Polymer Chemistry*, *11*(43), 6873–6878.

Wang, C., Goldman, T. M., Worrell, B. T., McBride, M. K., Alim, M. D., & Bowman, C. N. (2018). *Materials Horizons*, *5*(6), 1042–1046.

Wang, C., Mavila, S., Worrell, B. T., Xi, W., Goldman, T. M., & Bowman, C. N. (2018). *ACS Macro Letters*, *7*(11), 1312–1316.

Wang, H. C., Zhang, Y., Possanza, C. M., Zimmerman, S. C., Cheng, J., Moore, J. S., Harris, K., & Katz, J. S. (2015). *ACS Applied Materials and Interfaces*, *7*(12), 6369–6382.

Whitesides, G. M. (2018). In *Angewandte Chemie - International Edition* (Vol. 57, Issue 16, pp. 4258–4273).

Winne, J. M., Leibler, L., & Du Prez, F. E. (2019). *Polymer Chemistry*, *10*(45), 6091–6108.

Wojtecki, R. J., Jones, G. O., Yuen, A. Y., Chin, W., Boday, D. J., Nelson, A., García, J. M., Yang, Y. Y., & Hedrick, J. L. (2015). *Journal of the American Chemical Society*, *137*(45), 14248–14251.

Wölfel, B., Seefried, A., Allen, V., Kaschta, J., Holmes, C., & Schubert, D. W. (2020). *Polymers*, *12*(9), 1–13.

Worrell, B. T., Mavila, S., Wang, C., Kontour, T. M., Lim, C. H., McBride, M. K., Musgrave, C. B., Shoemaker, R., & Bowman, C. N. (2018). *Polymer Chemistry*, *9*(36), 4523–4534.

Worrell, B. T., McBride, M. K., Lyon, G. B., Cox, L. M., Wang, C., Mavila, S., Lim, C. H., Coley, H. M., Musgrave, C. B., Ding, Y., & Bowman, C. N. (2018). *Nature Communications*, *9*, 1–7.

Wydra, J. W., Cramer, N. B., Stansbury, J. W., & Bowman, C. N. (2014). *Dental Materials*, *30*(6),

605–612.

Xu, Z., Liang, Y., Ma, X., Chen, S., Yu, C., Wang, Y., Zhang, D., & Miao, M. (2020). *Nature Sustainability*, *3*(1), 29–34.

Xue, L., Xiong, X., Krishnan, B. P., Puza, F., Wang, S., Zheng, Y., & Cui, J. (2020). *Nature Communications*, *11*(1), 1–9.

Yang, H., Yu, K., Mu, X., Shi, X., Wei, Y., Guo, Y., & Qi, H. J. (2015). *Soft Matter*, *11*(31), 6305–6317.

Yang, J., Chen, L., Zhu, M., Ishaq, M. W., Chen, S., & Li, L. (2022). *Macromolecules*.

Yang, P., Zhou, Q., Yuan, X. X., Van Kasteren, J. M. N., & Wang, Y. Z. (2012). *Polymer Degradation and Stability*, *97*(7), 1101–1106.

Yang, Z., Duan, C., Sun, Y., Wang, T., Zhang, X., & Wang, Q. (2019). In *Industrial and Engineering Chemistry Research* (Vol. 58, Issue 24, pp. 10599–10608).

Ying, H., Zhang, Y., & Cheng, J. (2014). *Nature Communications*, *5*.

Yousif, E., & Haddad, R. (2013). *SpringerPlus*, *2*(1), 1–32.

Yu, K., Shi, Q., Dunn, M. L., Wang, T., & Qi, H. J. (2016). *Advanced Functional Materials*, *26*(33), 6098–6106.

Yu, K., Xin, A., Du, H., Li, Y., & Wang, Q. (2019). *NPG Asia Materials*, *11*(1).

Yu, K., Yang, H., Dao, B. H., Shi, Q., & Yakacki, C. M. (2017). *Journal of the Mechanics and Physics of Solids*, *109*, 78–94.

Zakrevskii, V. A., Sudar, N. T., Zaopo, A., & Dubitsky, Y. A. (2003). *Journal of Applied Physics*, *93*(4), 2135–2139.

Zhang, B., Kowsari, K., Serjouei, A., Dunn, M. L., & Ge, Q. (2018). *Nature Communications*, *9*(1).

Zhang, L., Dong, J., Xu, X., & Liu, Q. (2016). *Chemical Reviews*, *116*(2), 287–322.

Zhang, X., Chen, G., Collins, A., Jacobson, S., Morganelli, P., Dar, Y. L., & Musa, O. M. (2009). *Journal of Polymer Science Part A: Polymer Chemistry*, *47*(4), 1073–1084.

Zhang, Y., Zhang, L., Yang, G., Yao, Y., Wei, X., Pan, T., Wu, J., Tian, M., & Yin, P. (2021). *Journal of Materials Science and Technology*, *92*, 75–87.

Zheng, P., & McCarthy, T. J. (2012). *Journal of the American Chemical Society*, *134*(4), 2024–2027.

Zhu, Y., Romain, C., & Williams, C. K. (2016). *Nature*, *540*(7633), 354–362.

Zivic, N., Kuroishi, P. K., Dumur, F., Gigmes, D., Dove, A. P., & Sardon, H. (2019). *Angewandte Chemie - International Edition*, *58*(31), 10410–10422.

Zubov, V. P., Kumar, M. V., Kabanov, V. A., Faculty, C. C., & State, M. (1979). *Journal of Macromolecular Science: Part A*, *A13*(1), 111–131.

Zuo, B., Wang, M., Lin, B. P., & Yang, H. (2019). *Nature Communications*, *10*(1).